

**Studies on the interaction of antimicrobial peptides
and protein with phospholipid membranes**

**Thesis Submitted to the Jadavpur University
for the Degree of
Doctor of Philosophy (Science)**

by

Animesh Halder

Supervisor: Prof. Sanat Karmakar

2022



Department of Physics

Jadavpur University

Kolkata – 700032

India



যাদবপুর বিশ্ববিদ্যালয়
JADAVPUR UNIVERSITY

Prof. (Dr.) Sanat Karmakar
Professor
Department of Physics

CERTIFICATE FROM THE SUPERVISOR

This is to certify that the thesis entitled “**Studies on the interaction of antimicrobial peptides and protein with phospholipid membranes**” submitted by **Sri Animesh Halder** who got his name registered on 29.09.2014 for the award of Ph.D. (Science) degree of Jadavpur University, is absolutely based upon his own work under the supervision of Prof. Sanat Karmakar and that neither this thesis nor any part of it has been submitted for either any degree/diploma or any other academic award anywhere before.

Sanat Karmakar 02/06/2022

Prof. Sanat Karmakar

(Signature of the Supervisor, date with official seal)



Prof. Sanat Karmakar
Department of Physics
Jadavpur University
Kolkata-700032, India

*Dedicated to
Ma and Baba*

DECLARATION

I hereby declare that the work reported in this thesis is entirely original. This thesis is composed independently by me at Jadavpur University under the supervision of Prof. Sanat Karmakar. I further declare that the subject matter presented in this thesis has not previously formed the basis for the award of any degree, diploma, membership, associateship, fellowship or any other similar title of any university or institution.

Sanat Karmakar
(Prof. Sanat Karmakar) 02/06/2022

Animesh Halder
(Animesh Halder)

Soft matter and Biophysics Laboratory

Department of physics

Jadavpur University

Kolkata-700032

INDIA

ACKNOWLEDGEMENT

I want to take the opportunity to sincerely thank the people who supported me throughout my research journey and shared with me unforgettable moments.

First and foremost, I would like to acknowledge my indebtedness and render my warmest thanks to my supervisor, prof. Sanat Karmakar for giving me the opportunity to work under his supervision. His friendly guidance and expert advice have been invaluable throughout all stages of the work.

I am very grateful to my collaborators Dr. Krishnananda Chattopadhyay and his scholar Achinta Sannigrahi at CSIR-IICB, Kolkata, for his extended discussions and valuable suggestions. I am extremely thankful to Dr. Gopinatha Suresh Kumar and his scholar Baisakhi Saha at CSIR-IICB, Kolkata, for allowing me to use his laboratory and instruments whenever required. I owe particular thanks to Dr. Deepak Kumar Sinha at IACS, Kolkata, for his keen interest of my work.

I would also wish to express my sincere thanks to prof. Kalyan Kumar Chattopadhyay, Head of the Department of physics, Prof. Sukhen Das, Prof Argha Deb, Prof Ruma Roy and other faculty members of the Department of physics, Jadavpur University. I am thankful to the staff of this department for their help. I also thank everyone in the administrative department.

My heartfelt thanks goes to my senior Pabitra Maity for his invaluable help, constant support and many academic and non-academic discussions.

I would like to thank to my friends Rahul, Tanmoy, Jnan, Mehebab, Biswajit, Wahida, Amrita Di, Prakriti, Sujoy, Ansar, Surojit, Kalyan for their company.

I am extremely grateful to Jadavpur University for giving me the opportunity to undertake my doctoral degree and providing the facilities for my research. My sincere thanks to all security personnel, library staff, canteen staff and everyone at Jadavpur University for making my stay enjoyable.

I thank the UGC, New Delhi for my fellowship and contingency grants.

My warmest thanks goes to my family. I want to thank my sister Susmita Halder, my uncle Sanjay Mandal and my beloved wife Soumita Pal Halder for their unconditional love, support and encouragement. I must extend my deepest respect to my father in law Mr. Swapan Kumar Pal for his valuable suggestions.

To the two most important people in my life, Baba and Ma, thank you for encouraging me to follow my dreams, for accompanying me through every choice, success and difficulty.

Last but not the least, I thank all my friends, teachers, relatives and well-wishers for their support, whom I could not mention by name.

Contents

Chapter 1: Introduction

1.1	Motivation	1
1.2	Amphiphilic molecules and their basic properties	2
1.3	Lipids	3
1.4	Self-assembly of amphiphilic molecules	5
1.5	Phase behavior of lipid bilayer (Lipid+water)	8
1.6	Lipid bilayer as model system of biological membranes	10
1.7	Influence of cholesterol on lipid membrane and membrane raft	12
1.8	Antimicrobial peptides and their classifications	13
1.9	Physico-chemical properties of antimicrobial peptides	15
1.10	Mechanism of antimicrobial activity on lipid membrane	16
1.10.1	Toroidal pore model	17
1.10.2	Barrel stave model	17
1.10.3	Carpet model	18
	References	19

Chapter 2: Experimental Techniques

2.1 Introduction	24
2.2 Preparation of large unilamellar vesicle	24
2.3 Preparation of giant unilamellar vesicle	25
2.4 Preparation of small unilamellar vesicle	27
2.5 Characterization of Vesicles	
2.5.1 Size Measurement using Dynamic Light Scattering	27
2.5.2 Zeta potential	30
2.6 Fluorescence spectroscopy	
2.6.1 Steady state fluorescence measurement	33
2.6.2 Fluorescence lifetime	34
2.6.3 Steady state fluorescence Anisotropy	35
2.7 Isothermal titration calorimetry	38
2.7.1 Surface partition model	38
2.8 Phase contrast microscopy	40
References	43

Chapter 3: Interaction of an antimicrobial peptide NK-2 with Phospholipid

Membrane: Evidence of pores in the membrane

3.1 Introduction	45
3.2 Earlier studies	46
3.3 Experimental results	

3.3.1 The membrane-membrane interaction induced by NK-2	48
3.3.2 Binding affinity of NK-2 with negatively charged membrane as envisaged from zeta potential	50
3.3.3 Binding affinity of NK-2 with model membranes measured from ITC	54
3.3.4 Observation of trans-membrane pores (Microscopy results)	60
3.4 Discussions	64
3.5 Conclusions	69
References	70

Chapter 4: Interaction of antimicrobial peptide, magainin 2 with phospholipid membrane: effect of cholesterol

4.1 Introduction	75
4.2 Earlier studies	76
4.3 Experimental results and discussions	
4.3.1 Size distributions of LUV	77
4.3.2 Zeta potential of LUV	78
4.3.3 Binding study of magainin 2 with model membrane: Isothermal Titration Calorimetry	80
4.3.4 Observation of trans-membrane pores: Phase contrast Microscopy	82
4.3.5 Effect of cholesterol on the pore formation	87
4.3.6 Fluorescence spectroscopy and anisotropy measurement	88
4.3.7 Membrane permeabilization experiments	90

4.4 Conclusion	91
Reference	93

Chapter 5: Formation of transmembrane pores in anionic phospholipid membranes induced by kinetoplastid membrane protein-11 (KMP-11): Effect of Cholesterol

5.1 Introduction	96
5.2 Earlier studies	97
5.3 Experimental results and discussion	
5.3.1 Interaction of KMP-11 with Phospholipid LUV	99
5.3.2 Charge distribution of the protein KMP-11	103
5.3.3 Formation of trans-membrane pores induced by KMP-11	
5.3.3.1 KMP-11 induced leakage in phospholipid membrane	104
5.3.3.2 KMP-11 induced pore formation as evidenced from the phase contrast Micrographs of GUV	106
5.3.3.3 Effect of cholesterol on the pore formation	110
5.3.3.4 A conjecture on the mechanism of parasite entry and implications in leishmaniasis	113
5.4 Conclusion	114
References	116

Chapter 6: Use of spectroscopic properties of lipophilic dye, Nile red to understand the physico-chemical properties of lipid bilayer: Effect of chain saturation and cholesterol.

6.1 Introduction	120
6.2 Earlier studies	121
6.3 Experimental results and discussions	
6.3.1 Effect of different phospholipids on the emission spectra of Nile red	122
6.3.2 Effect of cholesterol on the emission spectra of Nile Red in the presence of different phospholipids	127
6.3.3 Red edge excitation shift (REES) of Nile red in DOPC vesicles containing Cholesterol	130
6.3.4 Rotational dynamics of lipid bilayers as revealed from steady state fluorescence anisotropy	131
6.3.5 Lifetime of Nile red in phospholipid vesicles: effect of cholesterol	133
6.4 Conclusions	135
References	136

List of Publications

Reprints of papers

Preface

This thesis deals with the studies on the interaction of antimicrobial peptides/protein with phospholipid membranes. Antimicrobial peptides (AMPs) are promising novel antibiotics due to their antimicrobial activity against invading pathogens, such as viruses, fungi, bacteria etc. These molecules have been found in organisms ranging from prokaryotes to human innate immune system. The overuse of antibiotics promotes antibiotic resistance which is a serious threat to the mankind. The resistance to conventional antibiotics have led to a new possibility in the development of AMP as human therapeutics. Today we need a proper understanding of the complex interaction between antimicrobial peptides and biological membranes for the development of suitable antimicrobial peptide for clinical use. Biological membranes are complex, regulated by various membrane components. Therefore, it is often useful to study model membranes to understand more complex lipid-peptide interactions and hence to get some insight into the structure and functions of the membranes induced by AMP.

We have studied the interaction of various antimicrobial peptides/protein with unilamellar vesicles using a variety of experimental techniques, such as, dynamic light scattering, zeta potential, isothermal titration calorimetry (ITC), fluorescence spectroscopy and phase contrast microscopy. In contrast to classical antibiotics, antimicrobial peptides target bacterial membranes and disintegrate the membrane. The major constituents of bacterial membranes are phosphatidylethanolamine (PE) and phosphatidyl-glycerol (PG) (~4:1). Therefore, in our present study, we have chosen model systems, composed of dioleoyl phosphatidylglycerol (DOPG) and mixtures of DOPG with dioleoyl phosphatidylethanolamine (DOPE) and dioleoyl phosphatidylcholine (DOPC). These lipids also show fluid phase at room temperature (25⁰ C). The electrostatic behavior as well as the size distribution of the membranes in the presence of antimicrobial peptide was systematically characterized using ζ potential and DLS, respectively. Thermodynamics of the interaction of this system have been thoroughly investigated using ITC study. We have determined the binding affinity of antimicrobial peptide with negatively charged phospholipid membranes. Binding free energy and other interaction parameter have been delineated using theoretical ansatz. Giant unilamellar vesicles (GUVs) made from binary lipid-cholesterol mixtures were also studied using phase contrast microscopy. We have estimated the value of rate constant obtained from the fit to exponential decay function. The membrane sensitive

lipophilic fluorescence probe, Nile red, was used to study how physico-chemical properties of lipid bilayer get altered due to interaction of AMP. We have also measured the lifetime and steady state anisotropy of the Nile red in order to get some insight into the nature of peptide-lipid membrane interactions.

In chapter 1, we give a brief introduction to lipids and to the various lamellar phases exhibited by them in aqueous solutions. A summary of earlier studies on the influence of cholesterol on lipid membranes and a brief introduction to membrane rafts are also given. Also we provide a brief introduction of antimicrobial peptide and their classification on the basis of their charge, hydrophobicity and amphipathicity. Mechanism of the antimicrobial peptide on the lipid membrane also described here.

Amphiphiles in aqueous solution form a variety of self-assembled structures. Lipid bilayer is the basic building block of all biological membranes. In general, lipids are amphiphilic molecules, consisting of two parts; a polar hydrophilic head and a nonpolar hydrophobic hydrocarbon chains. All lipids have a transition temperature (T_m) above which they undergo a transition from gel phase to liquid phase. As model membrane, unilamellar vesicles are classified into three categories according to their average size range. They are small unilamellar vesicles (SUV), large unilamellar vesicles (LUV) and giant unilamellar vesicles (GUV). Cholesterol is also an essential constituent of plasma membranes. Cholesterol enhances the rigidity of the plasma membranes. Incorporation of cholesterol into lipid membranes leads to the progressive decrease in main- and pre-transition temperatures. It indicates that cholesterol transforms the gel phase into a fluid phase.

Antimicrobial peptides (AMPs) are the unique and diverse group of molecules which are part of innate immune response found in all animal and human body. They are the host defense peptides and work against invading pathogens, such as viruses, fungi, bacteria etc. Peptide charge, hydrophobic residue and amphipathicity play an important role on the antimicrobial activity. There are four categories of antimicrobial peptides based on their structural characteristics including linear α -helical peptides, β -sheet peptides, linear extension structure, and both α -helix and β -sheet peptides. Due to intermolecular disulfide bonds, β -sheet peptides are more rigid structures than α -helical peptides. AMPs commonly possess amphipathic structures and cationic in nature which strongly bind to the bacterial membranes via electrostatic interactions. An important property of AMP is the specificity of bacterial targets and excludes the killing of most eukaryotic cells. They

create defects, such as trans-membrane pores which eventually rupture the essential cellular contents by disintegrating lipid organization. There are several proposed mechanisms that AMP uses to destroy the cellular membrane reported in literatures such as toroidal pore model, barrel-stave pore model and carpet model. The essential and common feature of these mechanisms is the formation of trans-membrane pores.

In chapter 2, we describe experimental techniques employed by us for studying peptide-membrane interaction. The basic principles of experimental techniques and detailed methodology are also discussed.

We have prepared large unilamellar vesicles (LUV) from extrusion method. The size distribution of the LUVs was confirmed by dynamic light scattering measurement. The zeta potential is used to estimate the surface charge, surface potential of the vesicles. The fluorescence spectroscopy technique is widely used to determine the structure and dynamics of the lipid membrane. We have also measured fluorescence anisotropy and lifetime to investigate the local environment in which a fluorophore is localized. The thermodynamics of lipid-peptide interaction and binding kinetics of peptide have been investigated using ITC. The nature of interaction in terms of exothermic or endothermic can directly be envisaged from ITC heat flow. Now the integrated heat flow at injection provides the isotherm which can be fitted to an appropriate model in order to obtain binding parameters, such as k , ΔH , ΔS etc. One site binding model provided by microcal origin does not fit well the experimental binding curve. Therefore, we adopt a partition model to fit the data.

In this chapter we also describe electroformation of giant unilamellar vesicles (GUVs) made from lipid-cholesterol mixtures. Electroformation is a protocol to prepare GUVs of 10-100 μm size, which can be easily observed under a phase contrast or fluorescence microscope. Vesicles form when the lipid is in the fluid (L_α) phase.

In chapter 3, We have systematically studied the interaction of NK-2 with phospholipid membranes to obtain insights into the antimicrobial activity. As bacteria mimicking membranes, we have chosen large unilamellar vesicles (LUVs) composed of negatively charged phospholipid and neutral phospholipids. The binding affinity of NK-2 to the negatively charged membranes, PG, as well as the neutral phospholipids PC and PE was determined using ITC and ζ potential.

ITC and ζ potential results show the stronger binding affinity of NK-2 to negatively charged membranes than to neutral membranes. We compare binding affinity of NK-2 to PG, PE, and PC as $PG \gg PE > PC$.

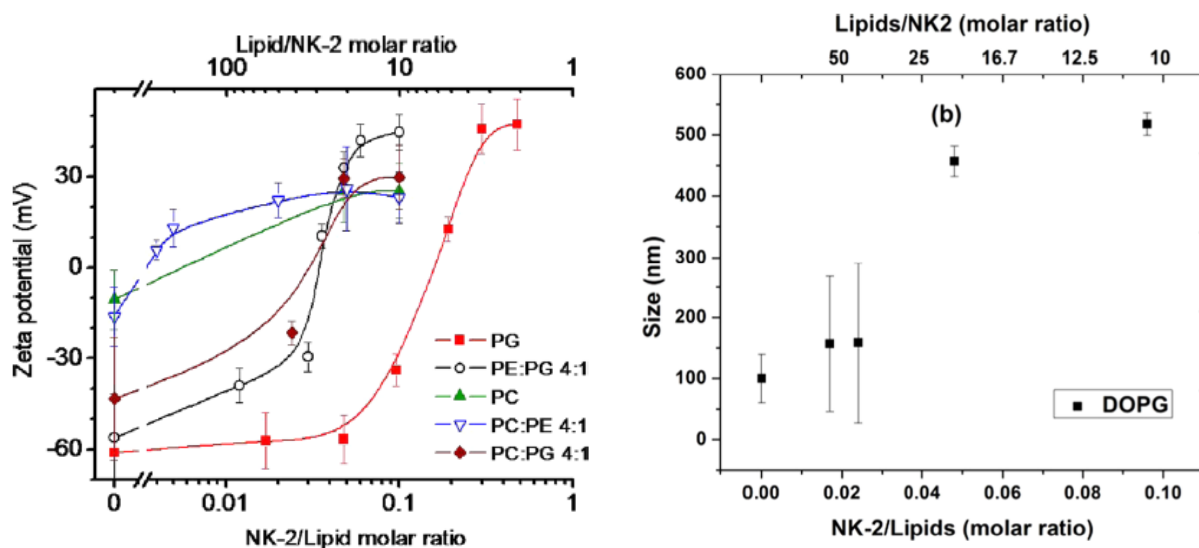


Figure 1: (a) ζ Potential of phospholipid LUV at various NK-2 to lipid molar ratios. Solid lines are intended only as guides to the points. Error bars indicate the width of the distribution profile of ζ potential. (b) Size distribution of LUV composed of DOPG in the presence of NK-2. Error bar is the standard deviation and was obtained from the width of the distribution.

The size distribution of negatively charged LUV in the presence of NK-2 was found to increase drastically, indicating the presence of large aggregates. Such a large aggregate has not been observed in neutral membranes, which supports the ITC and ζ potential results. The binding free energy, effective surface charge due to release of counter ion have been estimated from the minimal and maximal zeta potential. We have also determined the intrinsic binding constant from ITC Experiment Using the Surface Partition Model. Phase contrast optical microscopy experiment on GUV reveals the formation of trans-membrane pores which implies antimicrobial activity of NK-2. We compare pore formation in negatively charged membrane with neutral membrane.

In chapter 4, We have studied the interaction of magainin 2 with various phospholipid membranes to obtain insights into the antimicrobial activity. The size distribution of LUV composed of different phospholipid and lipid mixture increases with increasing concentration of magainin 2.

Results on zeta potential of LUV clearly infer that the presence of magainin 2, charge neutralization happens at much higher value for negatively charged membrane than neutral membrane. These differences are due to the fact that charge compensation occurs with respect to charge lipids. The thermodynamics of binding of the antibacterial peptide magainin 2 to phospholipid membrane has been studied with isothermal titration calorimetry (ITC). The binding of magainin 2 is caused essentially by electrostatic forces. We have also determined the binding constant and other thermodynamic parameters from ITC experiment using the one site binding model. Phase contrast microscopy on GUV has been performed in order to visualize directly the antimicrobial activity of Magainin 2.

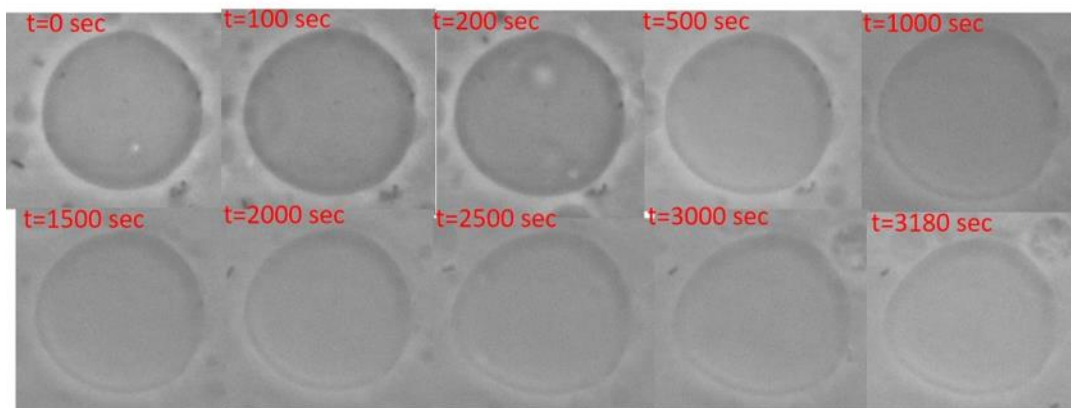


Figure 2: Phase contrast images of GUVs composed of DOPC–DOPG (4:1), exposed to 4.16 μM Magainin 2. The diameter of the vesicle is $\sim 35 \mu\text{m}$.

Change in the difference of the gray value (I_{ptp}) in the halo region with time DOPC-DOPG (4:1) GUV, as shown in Figs. 3 indicate leakage of internal fluid, leading to the loss of contrast. I_{ptp} decreases until GUV completely loses its contrast in the halo region. We have determined the value of rate constant for different concentration of peptide.

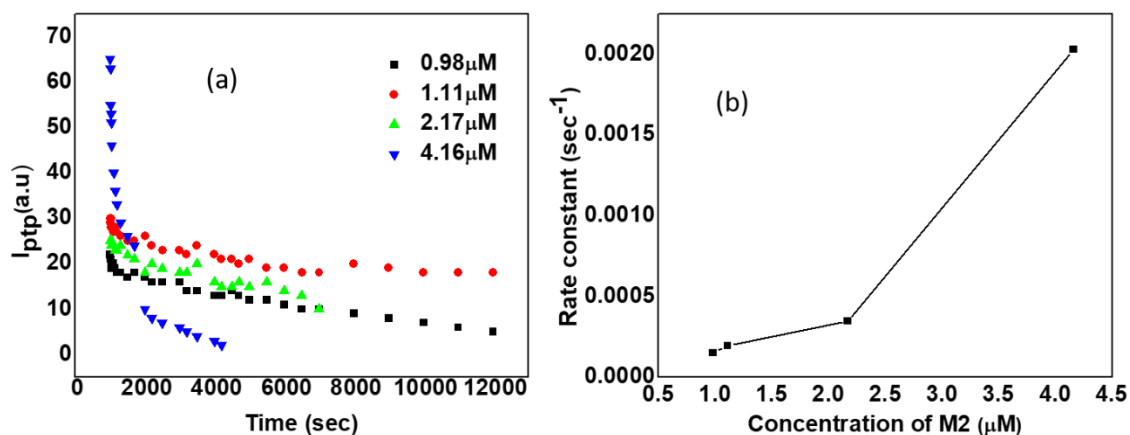


Figure 3: (a) shows profile of contrast decay of GUV made from DOPC: DOPG (4:1) with increasing concentration of magainin 2. (b) shows decay constant vs concentration of magainin 2.

However, we did not observe any significant decrease of I_{ptp} of vesicle made of DOPC when exposed to magainin 2. We also explored the pore-forming activity of magainin 2 on the membrane containing cholesterol. The fluorescence leakage experiment showing the leakage of entrapped calcein from the LUV composed of DOPC: DOPG (4:1) indicating the formation of transmembrane pores. We have observed the fluorescence intensity of Nile red in presence of phospholipid membrane with increasing peptide concentration. We also measured the anisotropy value of the bacterial membrane which increases with the increasing peptide concentration but remain same for neutral membrane.

In chapter 5, A systematic investigation on the interaction of KMP-11 with anionic phospholipid membranes reveals, for the first time, that KMP-11 is able to induce pores in the anionic phospholipid membrane. KMP-11 is a small protein which is considered a potential candidate for leishmaniasis vaccine. KMP-11 is found on the membrane surface of the parasite. Although the biological function of KMP-11 is unknown, we hypothesize from its sequence analysis that it may interact with the macrophage membrane and may influence the entry process of the parasite into the host cell. To validate this hypothesis, we have investigated the interaction of KMP-11 with unilamellar anionic phospholipid vesicles and explored its pore-forming activity. The decrease in negative ζ -potential of the vesicles and reduction in the fluorescence intensity of membrane-bound

dye DiI C-18 suggest a strong association of KMP-11 with the membrane. Both the calcein release fluorescence assay of large unilamellar vesicles and phase contrast microscopy of giant unilamellar vesicles have been employed to show the leakage of internal fluid and exchange of fluids, suggesting the formation of transmembrane pores in an anionic membrane.

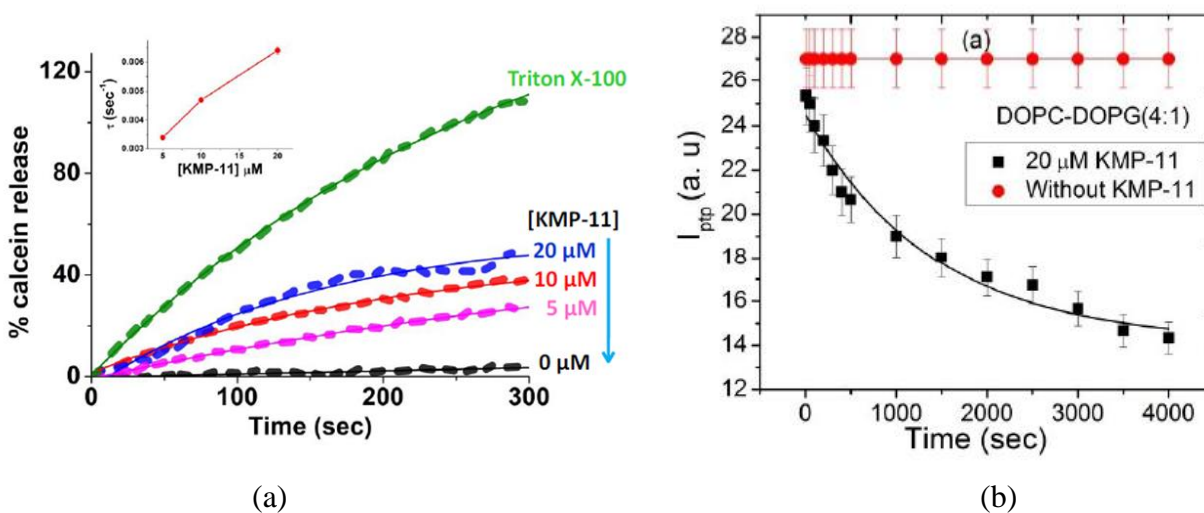


Figure 4: (a) Calcein release assay showing the leakage of entrapped calcein from the LUV composed of PC:PG (4:1). (b) The decay of (peak to peak intensity) with time for DOPC-DOPG GUVs. The solid line represents the fit, which was obtained from a single exponential decay. The decay rate constant (τ) was found to be $(0.7 \pm 0.06) \times 10^{-3} \text{ sec}^{-1}$.

Incorporation of cholesterol into the membrane has been found to inhibit pore formation induced by KMP-11, suggesting an important role of cholesterol in leishmaniasis. Interestingly, vesicles containing only neutral phospholipid do not exhibit any tendency toward pore formation.

In chapter 6, We have discussed the importance to study how physico-chemical properties of lipid bilayer get altered due to interaction of AMP. Nile red is environment sensitive lipophilic dye. Its spectroscopy properties can be used to probe the change in the properties of lipid bilayer. We have studied the effect of composition and the phase state of phospholipid membranes on the emission spectrum, anisotropy and lifetime of a lipophilic fluorescence probe nile red. Fluorescence spectrum of nile red in membranes containing cholesterol has also been investigated in order to

get insights into the influence of cholesterol on the phospholipid membranes. Maximum emission wavelength (λ_{em}) of Nile red in the fluid phase of saturated and unsaturated phospholipids was found to differ by ~ 10 nm. The λ_{em} was also found to be independent of chain length and charge of the membrane. However, the λ_{em} is strongly dependent on the temperature in the gel phase.

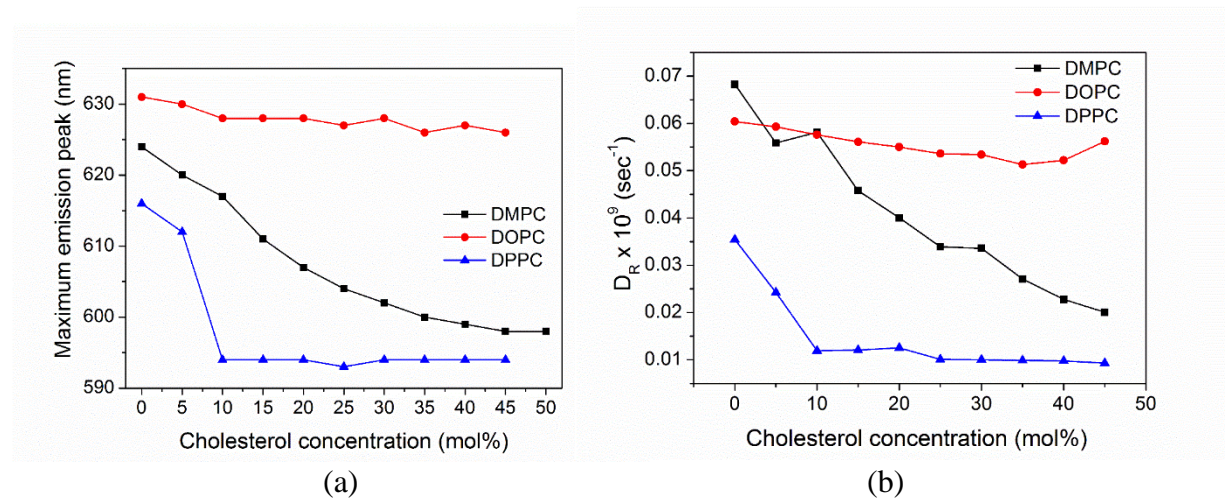


Figure 5: (a) Variation of maximum emission peak of Nile red obtained from different phospholipids at 25°C for different cholesterol concentration. (b) Rotational rate of Nile red in the presence of three different lipid vesicles.

The λ_{em} and rotational diffusion rate decrease, whereas the anisotropy and lifetime increase markedly with increasing cholesterol concentration for saturated phospholipids, such as, dimyristoyl phosphatidylcholine (DMPC) in the liquid ordered phase. However, these spectroscopic properties do not alter significantly in case of unsaturated phospholipids, such as, dioleoyl phosphatidylcholine (DOPC) in liquid disordered phase. Interestingly, red edge excitation shift (REES) in the presence of lipid-cholesterol membranes is the direct consequences of change in rotational diffusion due to motional restriction of lipids in the presence of cholesterol. This study provides correlations between the membrane compositions and fluorescence spectral features which can be utilized in a wide range of biophysical fields as well the cell biology.

Chapter 1

Introduction

Lipid bilayer is the basic building block of all biological membranes in which cholesterol, proteins and other bio-active molecules are embedded in it (1). Asymmetric distributions of lipids between outer and inner leaflets of the membrane plays an important role in many cellular functions such as cell signaling (2). Phosphatidylcholine (PCs) lipids are the major constituent in the outer leaflet, while the inner leaflet is mostly composed of phosphatidylethanolamines (PEs). Prokaryotic membranes contain negatively charged lipids namely phosphatidylglycerol, cardiolipin and phosphatidylserine while the eukaryotic membranes are rich in zwitterionic or neutral sphingomyelin and phosphatidylcholine.

Biological membranes are complex and regulated by various proteins and cholesterol. Therefore, it is often useful to study the artificial lipid bilayer as bio-mimetic system in order to gain insights into the structure and functions of the membranes. The interaction between antimicrobial peptide and phospholipid membrane were investigated in terms of lipid head group variation and role of cholesterol as well as peptide composition and structure. The interactions were studied on the model membranes in the form of liposomes through a combination of dynamic light scattering, zeta potential, fluorescence spectroscopy, phase contrast microscopy, isothermal titration calorimetry experiments. The precise sequence and mechanism of action of these peptides is still under investigation due to their potential significance in food, health and agriculture applications. One focus of the present work is further investigation the mechanism on the different lipid phase.

1.1 Motivation

The introduction of antibiotics into clinical use to fight against infectious diseases was revolutionary in the 20th century. Antimicrobial peptides (AMPs) are promising novel antibiotics which works against invading pathogens, such as viruses, fungi, bacteria etc. (3,4). They are the unique and diverse group of molecules which are part of innate immune response found in all

animal and human body. There are diverse applications of AMP include as anti-infective agents, anticancer agents, drug delivery and nonviral gene transfer (2,5). A major problem that has impeded in the development of drug design is the toxicity. The overuse of antibiotics leads antibiotic resistance which is a serious threat to the mankind. The resistance to conventional antibiotics have led to a new possibility in the development of AMP as human therapeutics. Therefore, there is a need of developing alternative antibiotics which will act directly to the bacterial membrane without interacting with the specific receptor. Antimicrobial peptide can be an emerging material to use as a therapeutics drug, such as peptide antibiotics. Therefore, studies on the interaction of AMP with lipid membranes have drawn a lot of attention due to their potential biomedical applications. Our aim is to understand their mechanism of action, membrane selectivity and to promote the reduction of the cellular toxicity, make them more stable.

1.2 Amphiphilic molecules and their basic properties

Amphiphilic molecules, such as surfactants, consist of a polar head group attached to a nonpolar part consisting of one or more hydrocarbon (saturated or unsaturated) chains. Polar head group possesses a high affinity to polar solvent such as water, and nonpolar part shows a strong affinity to nonpolar solvent such as ethers, hydrocarbons and esters. Polar head group usually called hydrophilic head group can be either ionic or nonionic. Due to surface activity, when amphiphilic molecules interact with water, its hydrophobic part try to minimize contact with water whereas hydrophilic part try to separate from each other as far as possible. Amphiphilic molecules are called surface active agents (i.e. surfactant) due to their ability to reduce the interfacial tension. These surfactant molecules are extensively used as emulsifiers, detergents, cleaning products, food, cosmetics etc. (6,7).

Many biological compounds are amphiphilic in nature such as phospholipids, cholesterol, glycolipids, fatty acid, proteins etc. An example of an artificial double chain cationic surfactant is Didodecyldimethylammonium bromide (DDAB) and dipalmitoyl phosphatidylcholine (DPPC) is a lipid found in biomembranes.

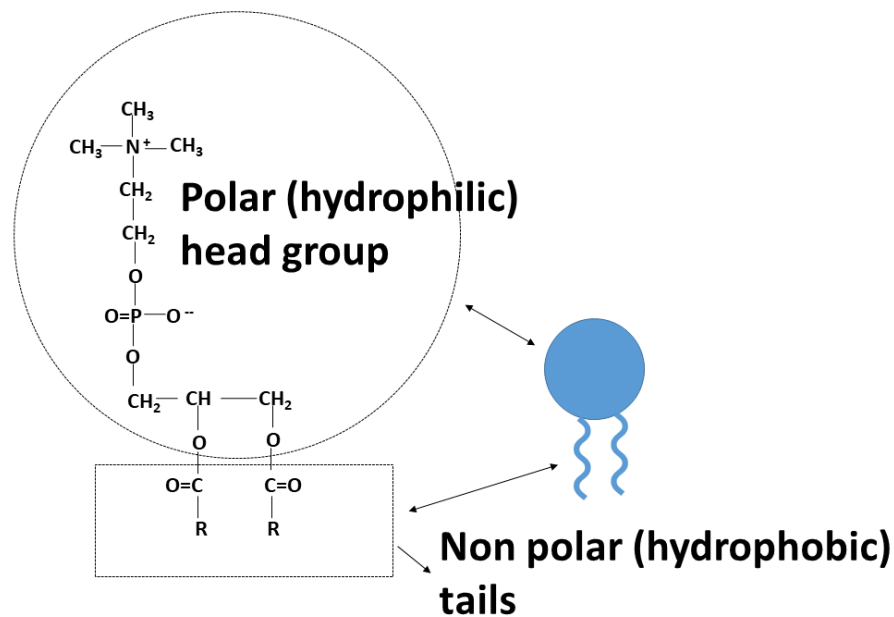


Figure 1.1: Chemical structure of DPPC ($\text{R} = (\text{CH}_2)_{14}-\text{CH}_3$)

1.3 Lipids

Lipids are amphiphilic molecules of biological origin. Lipids tend to be hydrophobic, nonpolar, and made up mostly of hydrocarbon chains. Lipids are fatty acid (consists of a long hydrocarbon chain attached to a carboxyl group) and their derivatives that are the essential building block of all biological membrane. Fatty acid chains may differ in length and most fatty acid contains carbon atoms from 4 to 28. There are two different type of fatty acids, saturated and unsaturated. If there are only single bonds between neighboring carbons in the hydrocarbon chain, a fatty acid is said to be saturated (Fig. 1.2 a) and when the hydrocarbon chain has a double bond, the fatty acid is said to be unsaturated. If there is just one double bond in a fatty acid, it is monounsaturated, while if there are multiple double bonds, it is polyunsaturated. The double bond in unsaturated fatty acid can exist in either a *cis* or a *trans* configuration. In the *cis* configuration (Fig. 1.2 b), the two hydrogens associated with the bond are on the same side and generates a kink or bend in the fatty acid. In the *trans* configuration (Fig. 1.2 c), hydrogens are on opposite sides.

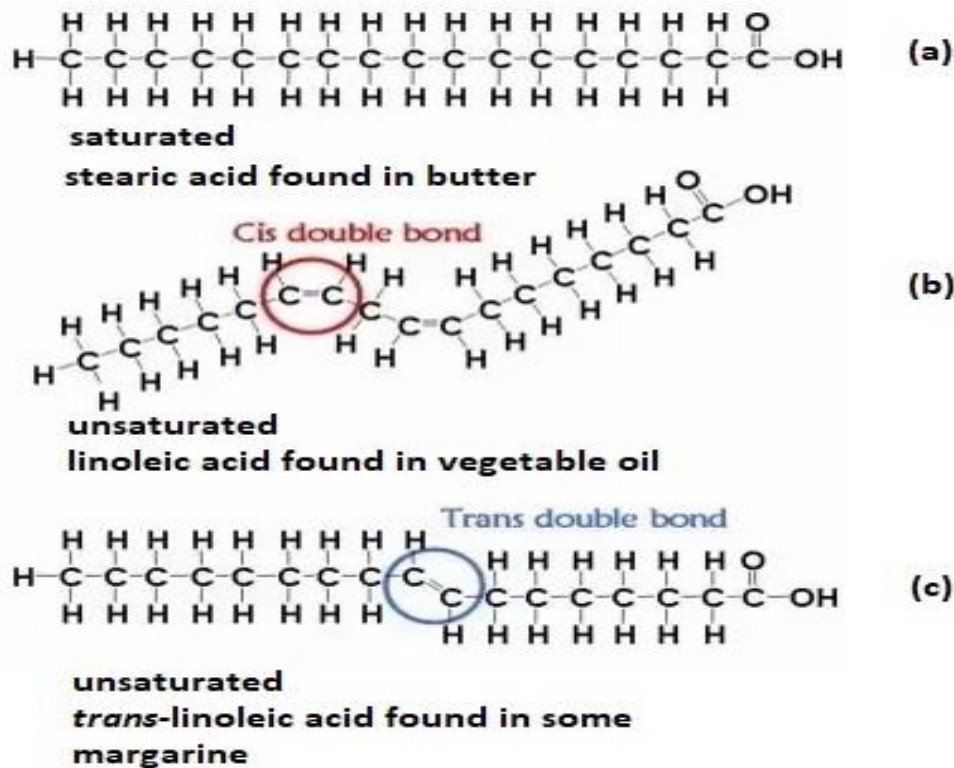


Figure 1.2: Structure of saturated and unsaturated lipid.

Saturated fatty acids tails are straight, so fat molecules with fully saturated tails can pack tightly against one another. This tight packing results in fats that are solid at room temperature. The tails of the unsaturated fatty acid in *cis* configuration are bent due to the *cis* double bond. This makes it hard for fat molecules with one or more *cis*-unsaturated fatty acid tails to pack tightly. So, fats with unsaturated tails tend to be liquid at room temperature.

The different varieties of lipids have different structures, and correspondingly diverse roles in organisms. The functions of lipids include storing energy, signaling and acting as structural components of cell membrane (8). Lipids have applications in the cosmetic and food industries as well as in nanotechnology. Cells are surrounded by a structure called the plasma membrane, which serves as a barrier between the inside of the cell and its surroundings. Phospholipids are major components of the plasma membrane. They are composed of fatty acid chains attached to a backbone of glycerol. Instead having three fatty acid tails, however, phospholipids generally have just two, and the third carbon of the glycerol backbone is occupied by a modified phosphate group.

Different phospholipids have different modifiers on the phosphate group, with choline (a nitrogen-containing compound) and serine (an amino acid) being common examples. Different modifiers give phospholipids different properties and roles in a cell.

Phospholipids are classified into several groups depending on the chemical structure of the head group. Phosphatidylcholines (PCs), phosphatidylethanolamines (PEs) and phosphatidylserines (PSs) are common phospholipids found in the plasma membranes. Among sphingolipids, sphingomyelin, sphingosine and gangliosides are the major classes. These lipids may be charged or neutral. Neutral lipids which possess dipole moments in aqueous solution are known as zwitterionic.

1.4 Self-assembly of amphiphilic molecules

Amphiphilic molecules can associate into a variety of structure (micelles and bilayers) in aqueous solution by spontaneous self-association. The main forces behind the self-association are hydrogen bonding, hydrophobic effects, electrostatic interaction, and van der Waals forces. The strength of total forces (5 kJ/mole to 120 kJ/mole) are much less than that of the covalent or ionic bonds (400 kJ/mole) but strong enough to maintain the stability of amphiphiles into solution (9,10). When amphiphilic molecules self-aggregate there is an enthalpic gain in solvation due to formation of hydrogen bond and entropic gain of the bulk water due to hydrophobic effect. Hydrogen bonds are critical for the structure and interaction of biological macromolecules. Together with the hydrogen bonds, the hydrophobic effect leads to the self-assembly of amphiphiles which plays an important role in many biological phenomena such as formation of lipid membrane, protein folding etc. Unlike hydrophobic part of the amphiphilic molecules does not form hydrogen bond with water molecule whereas the hydrophilic part forms hydrogen bond. Therefore, due to strong hydrophobic interaction the hydrophobic parts leads to minimize the contact area with water molecule by self-assembly.

The aggregates of various structure can transform from one to another by changing the solution conditions such as electrolyte or lipid concentration, pH or temperature. At very low concentration, amphiphilic molecules form a monolayer at air water interface. Above a certain concentration,

called critical micellar concentration (CMC), amphiphilic molecules are aggregate into a variety of structures like rods, disc, spherical, cylindrical, bilayers and vesicle shown in table 1.1





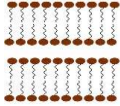
Packing parameter	Structure name	Structure
• $<1/3$	spherical micelles	
• $1/3-1/2$	cylindrical micelles	
• $1/2-1$	vesicles	
• $1/3-1/2$	hexagonal phase	
• ~ 1	lamellar phase	

Table 1.1 summary of the aggregate structures that can be predicted from the critical packing parameter.

The different aggregates of amphiphilic molecules are in thermodynamical equilibrium. This equilibrium claims that the chemical potential (μ) of all identical amphiphiles have to be same in all aggregates, i.e $\mu_1 = \mu_2 = \dots = \mu_N$. This may be written as

$$\mu = \mu_1^0 + kT \log X_1 = \mu_2^0 + \frac{kT}{2} \log \frac{X_2}{2} = \mu_3^0 + \frac{kT}{3} \log \frac{X_3}{3}$$

$$\mu_N = \mu_N^0 + \frac{kT}{N} \log \left(\frac{X_N}{N} \right) = \text{Constant}$$

where, $N = 1,2,3 \dots$ represent monomers, dimers and trimers and so on. μ_N is the mean chemical potential of a molecule in an aggregate of aggregation number N , μ_N^0 is the standard chemical potential corresponding to the interaction free energy per molecule in aggregates of aggregation number N , X_N is the total concentration of amphiphile in aggregate of size N . The second term in

the equation 1.2 arises from entropy of mixing. The total concentration (X) of the system considered to be small, i.e.

$$X = \sum_{N=1}^{\alpha} X_N \ll 1$$

From $\mu_N = \mu_1$, we get

$$X_N = N[X_1 \exp\{(\mu_1^0 - \mu_N^0)/KT\}]^N = N(X_1 e^{\alpha})^N$$

Where $\alpha = \frac{\mu_1^0 - \mu_N^0}{KT}$. The essential condition for the formation of aggregates of size N is $\mu_N^0 < \mu_1^0$. When $X_1 \ll 1$, $X_1 e^{\alpha} < 1$ and we must have $X_N \ll X_1$ for sufficiently low monomer concentrations. Therefore, $X \approx X_1$ and the isolated monomers in solution will be the favoured state. As X_1 is increased $X_1 e^{\alpha}$ approaches unity. Since $X_1 < 1$, X_1 never exceed a value of the order of $e^{-\alpha}$. Therefore, the monomer concentration should not increase the value of the order of $e^{-\alpha}$, beyond this concentration aggregation starts. This concentration is known as the critical micellar concentration (CMC). It is given by

$$CMC = (X)_c \approx (X)_1 \approx e^{-(\mu_1^0 - \mu_N^0)/KT}$$

The CMC is measured experimentally by many microscopic and macroscopic techniques such as conductivity and surface tension. The typical value of CMC of CTAB surfactant is $\sim 10^{-3}$ M and for DPPC lipid, it is $\sim 10^{-12}$ M. usually the CMC decreases with increasing length of the hydrocarbon chain (11).

According to Israelachvili (9) the structure of the aggregate can be predicted from the critical packing parameter (p). The dimensionless parameter (p) is defined as

$$p = \frac{v}{a_0 l_c}$$

where v is the effective volume occupied by hydrophobic chains in the aggregate core, l_c is the critical acyl chain length and a_0 is the effective hydrophilic head group surface area at the aggregate-solution interface.

1.5 Phase behavior of lipid bilayer (Lipid +water)

Phospholipids are the main constituents of plasma membranes and they form the structural basis of these membranes. Phospholipid molecules spontaneously form bilayers when placed in water. Due to hydrophobic effect, phospholipid molecule reorients in such a way that their head groups towards water and shield their fatty acid tails from water. Fluidity i.e. relative mobility of individual lipid molecules is important property for lipid bilayers. This relative mobility is greatly influenced by the temperature. As the temperature changes mobility of the lipid molecule also changes. This response is known as the phase behavior of the lipid bilayer. Self-assembly of lipids in an aqueous solution above critical micellar concentration leads to the formation of lamellar phases, consisting of a stack of bilayers separated by water. Depending upon the nature of the head group and temperature they exhibit a variety of lamellar phases (12). The lipid bilayer is a thermodynamic system. Like other thermodynamic systems, the lipid bilayer exists in phases. Lipid bilayer are usually in fluid phase at high temperatures, whose structure is shown in Fig. 1.3 In this phase, known as L_α phase, the hydrocarbon chains are completely molten and disordered. Head groups of lipid molecule in the liquid phase are loosely packed with rotational freedom and the acyl chain tails are not rigid.

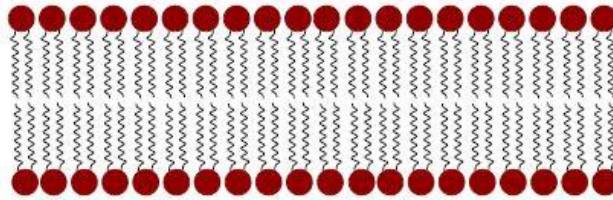


Figure 1.3: Schematic representation of the fluid phase of lipid bilayer

Typical lateral diffusion constant and bilayer bending modulus in this phase are $\sim 10^{-11} \text{m}^2 \text{s}^{-1}$ and $\sim 10^{-19} \text{J}$ ($\sim 10\text{-}20 \text{kT}$), respectively. Water can penetrate deep into the membranes due to the flexible bilayer in this phase.

The temperature (T_m) above which the fluid phase occurs in the membrane is known as the main transition temperature and is different for different lipids. T_m is dependent on the number of carbon atoms, number of double bonds in the hydrocarbon chain, and also on the nature of the head group. The position of the double bond and its conformational (*cis/trans*) state in the hydrocarbon chain

change the transition temperature drastically. For example, in the case of DOPC, T_m reduces from 41°C to -18.3°C as the position of the double bond changes from the 2nd to the 9th carbon atom (starting from the ester group) in the chain. At a given position of the double bond, *cis* configuration has a considerably lower transition temperature compared to *trans*. Typical enthalpy change during the main transition is about 5-10 kcal/mole for phospholipids (13). T_m of a few lipids are listed in table 1.2 (13).

Table 1.2 List of lipids used in the studies presented in this thesis. All these lipids have two identical chains. The numbers of carbon atoms in the chains and the number of double bonds are also given. The position of the double bond along the chain (starting from the ester group) and its conformation are indicated in the bracket. T_m is the main transition temperature.

Lipids	Abbreviation	Charge	Lipid chains	T_m (°C)
1,2-dioleoyl-sn-glycero-3-phosphocholine	DOPC	Zwitterionic	18:1(cis-9)	-18.3
1,2-dioleoyl-sn-glycero-3-phospho-(1'-rac-glycerol)	DOPG	Negative	18:1(cis-9)	-18
1,2-dioleoyl-3-trimethylammonium-propane	DOTAP	Positive	18:1(cis-9)	-11.9
1,2-dimyristoyl-sn-glycero-3-phosphocholine	DMPC	Zwitterionic	14:0	24
1,2-dipalmitoyl-sn-glycero-3-phosphocholine	DPPC	Zwitterionic	16:0	42

At temperatures below T_m , the lipid bilayer enters from the relatively disordered liquid phase to the relatively ordered gel phase where hydrocarbon chains are predominantly in the fully stretched all *trans* conformation. In this phase, the lipid head groups and the lipid acyl chain tails become more tightly packed. There are two types of gel phases found in lipids. The L_β phase is exhibited by lipids, such as PE, where hydrocarbon chains are parallel to the bilayer normal (zero tilt). Some lipids with larger head groups, such as PC, exhibit the $L_{\beta'}$ phase where chains are tilted with respect to bilayer normal as shown in Fig. 1.4

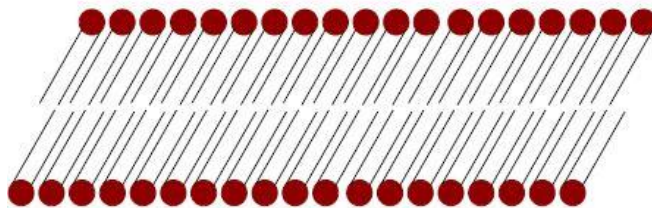


Figure 1.4: Schematic representation of the $L_{\beta'}$ phase.

Ripple phase $P_{\beta'}$ (fig 1.5) is formed in between L_{α} and $L_{\beta'}$ at high hydration. The $P_{\beta'} \rightarrow L_{\beta'}$ transition is known as pre-transition. This transition is absent for lipids such as PE.

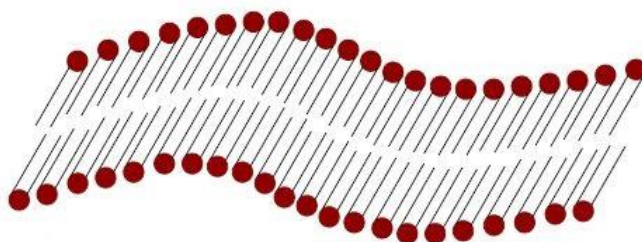


Figure 1.5: Schematic representation of the $P_{\beta'}$ phase.

Apart from these three phases, lipids exhibit another phase, known as the L_C phase, at temperatures below the gel phase. In general, the L_C phase occurs after long incubation at low temperatures, typically 4°C . L_C is a highly ordered phase where hydrocarbon chains as well as head groups are ordered.

1.6 Lipid bilayer as model system of biological membranes

Biological membrane is very complex due to many active process occurring on the membrane surface. So lipid bilayer can be used as model system of all biological membranes. Therefore, it is often useful to study the artificial lipid bilayer as bio-mimetic system in order to gain insights into the structure and functions of the membranes. Lipid bilayer can be made with mixtures of several synthetic or natural lipids. There are many different types of lipid bilayers such as black lipid membranes (BLM), supported lipid bilayers (SLB), tethered bilayer lipid membranes (t-BLM), unilamellar vesicles, droplet interface bilayers, micelles etc. Each lipid bilayers have some experimental advantages and disadvantages. In our study we use unilamellar vesicles to investigate

the fundamental properties of biological membrane at physiological condition. Besides the model system of biological membranes, these vesicles can be used as micro reactors for enzymatic RNA synthesis (14) and also to form Nano particle of control size distributions (15). Vesicles are also extensively used as carriers of bioactive agents, including drugs, vaccines and cosmetics (16). When a small amount of dehydrated lipid is dissolved into water and vortex then multilamellar vesicles are formed. To make unilamellar vesicle there are so many methods such as sonication, extrusion through a membrane and electro formation. Depending to their average size, unilamellar vesicles are classified into three categories. Vesicles have diameter between 10-100 nm called small unilamellar vesicle (SUV), between 100-250 nm called large unilamellar vesicle (LUV) and between 5-50 μm called giant unilamellar vesicle (GUV). SUV can usually be prepared by high energy (power >150 watt) probe sonication method and LUV are made by the extrusion method which are discussed in chapter 2. Both the size of SUV and LUV are confirmed by dynamic light scattering measurement. GUVs are prepared from the electro formation first described by Angelova et al (17). Owing to their large size these vesicles can be observed under phase contrast or fluorescence microscopy. Therefore, any morphological change of GUV can directly be envisaged using optical microscopy. Figure 1.6 represents different forms of bilayers depending on their environment.

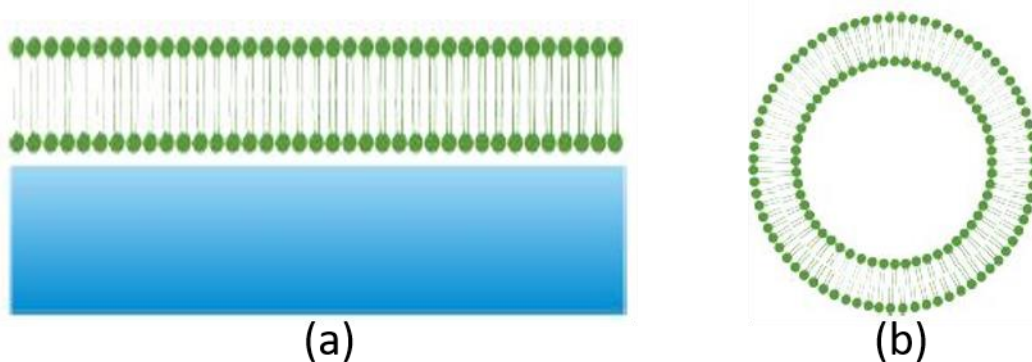


Figure 1.6: (a) Planar lipid bilayer on a glass support.

(b) Spherical closed lipid bilayer in aqueous environment.

1.7 Influence of cholesterol on lipid membrane and membrane raft

Cholesterol is an essential and major sterol component of all animal cell membranes. The structure of cholesterol is shown in Fig 1.7. It plays an important role in maintaining the membrane structure and physical–chemical properties necessary for correct cell functioning. Cholesterol is an amphipathic molecule like phospholipids and form a hydrogen bond with neighbouring lipid molecule especially with sphingomyelin. Cholesterol provides rigidity and integrity to the plasma membrane and helps to maintain its fluidity. The presence of cholesterol is believed to be responsible for lateral organization of lipids in the membranes in sub-micrometer domains, called rafts, and is known to regulate the activities of certain membrane proteins (18). Lipid rafts influences membrane fluidity, membrane protein trafficking and signal transduction, especially in hematopoietic cells.

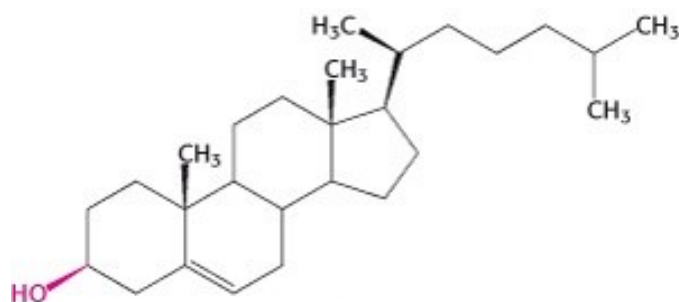


Figure 1.7: Structure of cholesterol

Cholesterol is present in bio membranes of all animal cells, but its content varies in different parts of organisms. In particular, a high content of cholesterol can be found in the brain, which contains about 25% of the whole cholesterol of a human body (1).

Cholesterol influences the main transition temperature (T_m) and the pre transition temperature (T_p) of lipid bilayer. These temperatures (T_m, T_p) of lipid bilayers has been determined by DSC experiments. The main transition temperature decreases with increasing concentration of cholesterol indicating that cholesterol transforms the gel phase into a fluid phase (19,20). In the cholesterol containing membrane, bilayer thickness depends only on the chain length and phase state of the lipid. Bilayer thickness is increased in the gel phase of PC bilayers for chain length

from 12 to 16 carbons, as cholesterol is known to remove the chain tilt. However, for longer chain lengths, the bilayer thickness is decreased in the gel phase (21). Bilayer thickness of fluid phase of cholesterol containing membrane also increases but at low cholesterol concentration this effect is not significant (22). Cholesterol induces non-lamellar phases in lipids, such as PEs and unsaturated PCs (23,24). Cholesterol also facilitates the formation of the L_C phase in PE bilayers (25) which in general occurs after long incubation at 4⁰ C. At a particular concentration of cholesterol (~ 20 mole %) below T_m , liquid ordered phase (L_O) is formed which indicates that coexistence of the gel ($L_{\beta'}/L_{\beta}$) with a cholesterol-rich phase (26). Above T_m it transform into the coexistence of with another fluid phase, known as liquid disordered phase (L_d) (27). At higher cholesterol concentration typically > 20 mole %, the main transition completely disappears and the gel phase replaced by the L_O phase. Lipid diffusion or mobility is decreased in the fluid phase and increased in the gel phase, as cholesterol concentration is increased (28). In general, cholesterol has greater affinity for saturated lipids than for unsaturated ones. This is due to the fact that cholesterol cannot pack efficiently in the lipid bilayers if the molecules possess a *cis*-double bond, creating a kink in the chain. Among phospholipids, affinity for cholesterol increases in order of PC > PS >PE (19). However, sphingomyelin has more affinity for cholesterol than PC (29). This could be due to the ability of the -OH group of cholesterol to form hydrogen bond with the neighbouring sphingomyelin molecules. Rafts probably exist in membrane in the liquid order (L_O) phase. The coexistence of the cholesterol-rich liquid-ordered (L_O) phase and cholesterol-poor liquid-disordered (L_d) phase below the transition temperature (T_m) of the saturated lipid, is believed to be relevant for the formation of rafts in plasma membranes.

1.8 Antimicrobial peptides and their classifications

Antimicrobial peptides (AMPs) are the unique and diverse group of molecules which are part of innate immune response found in all animal and human body (3). They are the host defense peptides and works against invading pathogens, such as viruses, fungi, bacteria etc. (30,31). The number of amino acid residues of antimicrobial peptide is between 10 and 60. Antimicrobial peptides are classified on the basis of source, activity, structural characteristics and amino acid composition. Source based AMPs are found in mammals (human, cattle, sheep), amphibians, microorganism and insects. Cathelicidins and defensins are the main families of mammalian

antimicrobial peptides. Human host defense peptides (HDPs) can protect human from microbial infections. Antimicrobial peptides derived from amphibians play an important role in the protection of amphibians from the pathogens. Frogs are the main source of amphibian AMPs and the most famous AMP from frogs is magainin; the skin secretions of frogs from genera *Xenopus*. Cecropin is the most famous family of AMPs from insects, and it can be found in guppy silkworm, bees, drosophila. Cecropin A shows activity against different inflammatory diseases and cancers. The activity of AMPs can be divided into several categories such as antibacterial, antiviral, antifungal, antiparasitic, anti-human immunodeficiency virus (HIV), and anti-tumor peptides. According to their different amino acid rich, antimicrobial peptides are classified into four categories: proline-rich antimicrobial peptides, Tryptophan- and Arginine-Rich Antimicrobial Peptides and Histidine-Rich antimicrobial peptides, Glycine-Rich Antimicrobial Peptides. Proline is a non-polar amino acid. They enter bacterial cytoplasm by the inner membrane transporter SbmA instead of killing bacteria through membrane destruction. Proline rich antimicrobial peptides mainly kill Gram-positive bacteria. Example of proline rich antimicrobial peptide is pPR-AMP1, which is identified from crab, exhibits antimicrobial activity against Gram-positive and Gram-negative bacteria. Tryptophan (Trp) also a non-polar amino acid which plays a remarkable role on the interface region of lipid bilayer. Indolicidin and Triptropicin are famous antimicrobial peptides that rich in Arg and Trp residues. Octa 2 (RRWWRWWR) is a Trp- and Arg-rich AMP that prevents the growth of microorganisms. Histidine is a common basic amino acid. HV2 is an example of histidine-rich AMP which increases the permeability of bacterial cell membranes to cause cell membrane rupture and death. Glycine-Rich Antimicrobial Peptides contain 14% to 22% glycine residues which have an important effect on the tertiary structure of the peptide. There are four categories of antimicrobial peptides based on their structural characteristics including linear α -helical peptides, β -sheet peptides, linear extension structure, and both α -helix and β -sheet peptides. Among these, α -helical peptides are well studied group of antimicrobial peptides (32). These peptides are usually unstructured in aqueous solution and only fold into helical conformation upon partitioning into phospholipid bilayers. The prominent example of the α -helical antimicrobial peptides are mellitin, magainin 2, human antimicrobial peptide LL 37. β -sheet antimicrobial peptides represent another large conformational group. Due to intermolecular disulfide bonds the β -sheet peptides are more rigid structures than α -helical peptides (33).

1.9 Physico-chemical properties of antimicrobial peptides

Physico-chemical properties are the intrinsic physical and chemical characteristics of the peptide. These include charge, hydrophobicity and amphipathicity etc. If one of these parameter has changed, antimicrobial activity of the peptide also affected.

The net charge of most antimicrobial peptides are between +2 to +9 (34). Many reports suggest that net peptide charge plays an important role on the antimicrobial activity. If hydrophobicity, helicity and amphipathicity were kept constant then increasing the net charge of magainin 2 amide analogues from +3 to +5 lead to an increase in antibacterial activity against *Escherichia coli* and *Bacillus subtilis* (35). It should be noted that cationicity do not always affect antimicrobial activity. For example, if four lysine residues added to the N-terminal of the magainin 2 then its activity will decrease against bacteria *Escherichia coli*, *Pseudomonas aeruginosa*, and *Staphylococcus aureus* (36). Increasing the net charge of the peptide will often not only change the antimicrobial activity of a given peptide but also the selectivity of that peptide. So there is an optimum net charge at which antimicrobial selectivity is maximal. However anionic antimicrobial peptides with a charge of -1 to -7 do also exist (37). These peptides are rich in glutamic and aspartic acids.

The hydrophobic residues of antimicrobial peptide play an important role for antimicrobial activity when peptide interacts with biological membrane. Actually hydrophobicity is the measurement of the percentage of the hydrophobic residues in a peptide. About 50 % hydrophobic amino acid residues are present in naturally occurring antimicrobial peptides (34). These hydrophobic residues can often be seen to appear in a pattern of 1-2 every 3-4 residues. Many experiments suggest that hydrophobicity is an important parameter for hemolytic activity (37). Hemolytic and antimicrobial activity of AMP can be affected if threshold value of hydrophobicity changing. Higher hydrophobicity was correlated with stronger hemolytic activity. Both hemolytic and antimicrobial activity of four different magainin 2 analogues increasing as a function of hydrophobicity against *Escherichia coli* when other physicochemical parameters were kept constant (38). Peptide with higher hydrophobicity have the tendency of stronger self-association and aggregation compared to those with lower hydrophobicity (39).

The distribution of hydrophobic and hydrophilic residues in AMPs is usually called amphipathicity which is measured by the sum of hydrophobic moment of individual amino acid. Several in vitro experiments have also found amphipathicity to be an important parameter for antimicrobial

activity and cell toxicity. If charge and hydrophobicity were kept constant, then antimicrobial activity and hemolytic activity as a function of increasing hydrophobic moment (40).

Apart from these characteristic, antimicrobial activity of the peptide depends on the length of amino acids of the antimicrobial peptide. Disruption of bacterial membrane in barrel stave model, minimum 22 amino acids required for an AMP to form an α -helical structure and 8 amino acids to form a β -sheet (41). The hemolytic and antimicrobial activities of the peptides also increased with increasing chain length. Primary sequence of the AMPs also has the influence on the antimicrobial activity. Glycine (Gly) residue is the most favoured in position 1 in the N-terminal region of α -helical AMPs (42). The presence of positively charged residues in AMPs are responsible for electrostatic interactions between the cationic AMPs and negatively charged bacterial membrane. Tryptophan (Trp) residue plays a vital role on the interaction between the peptide and the bacterial membrane (43).

1.10 Mechanism of antimicrobial activity on lipid membrane

The antimicrobial mechanisms of AMPs on lipid bilayer are very diverse and complex. Understanding the peptide activity on the membrane surface, a details studies on the interactions between peptide and membrane are needed. To elucidate how the peptide interacts with lipid membranes, a lot of parameters are responsible for which antimicrobial peptides prefer to bind with bacterial membrane but not to eukaryotic membrane. Bacterial membranes are usually negatively charged due to presence of anionic lipid phosphatidylglycerol (DOPG). Therefore, it is believed that interaction of positively charged AMP with the bacterial membranes initiates with the electrostatic attraction (44,45). Membrane potential is also an important parameter that differs between bacterial membrane and eukaryotic membrane. Membrane potential for bacterial membrane is -130 mV to -150 mV whereas for eukaryotic membrane it is -90 mV to -110 mV (46). This potential difference might promote the activity of antimicrobial peptide to bacterial membrane (47). Previous studies have shown that the membrane bound peptide concentration is supposed to be activated above a threshold peptide to lipid molar ratio (it varies from 0.05 to 0.1) (48). This threshold seems to be different for different peptide.

Different AMP uses a different mechanism to disrupt the bacterial membranes (49), which indeed depend on effective charge, hydrophobicity and length of the AMP. Due to the high level of complexity of the biological membrane, it is often useful to study model membranes in order to understand the mechanism of cellular damage induced by AMP (50). As model membranes, large unilamellar vesicles (LUV) and giant unilamellar vesicles (GUV) are an excellent model system to study the membrane-AMP interaction (51,52). The pore forming ability of AMP is determined by measuring the fluorescence intensity of calcein-loaded LUV with time (52). Valuable insights into antimicrobial peptide-induced membrane permeabilization of GUV have been visualized by phase contrast microscopy. Antimicrobial peptides can permeabilize lipid bilayers by formation of transmembrane pore. Peptides accumulate and orientate in a parallel manner onto the lipid bilayer at very low peptide/lipid ratios (53). When this ratio increased, the peptides start to re-orientate perpendicularly, insert into the bilayer and form trans-membrane pores. There are several proposed mechanisms of antimicrobial action reported in literatures. Three such major models are summarised below:

1.10.1 Toroidal pore model:

Matsuzaki et al. first proposed this model for magainin (54). This model is also known as the wormhole model. In this model, peptides are inserted vertically into the lipid head group region and to form a ring hole with diameter of 1-2 nm by simultaneously increasing membrane tension (55). Magainin 2 and melittin can induce this type of pore (56).

1.10.2 Barrel-stave pore model:

This mechanism describes the formation of transmembrane pores by antimicrobial peptides such that their hydrophobic surfaces interact with the lipid core of the membrane and their hydrophilic surfaces form the interior region of the pore. Alamethicin performs its pore-forming activity by using this model (53,57).

1.10.3 carpet model:

Pouny et al. proposed this model for describing the interaction of dermaseptin peptide with phospholipid membranes. In the carpet model, antimicrobial peptides accumulate on the bilayer surface in a carpet-like manner (58). The hydrophilic domain of the peptides is facing the phospholipid head groups or water molecules and hydrophobic domains are oriented towards the acyl chain core of the bilayers. For this pore forming mechanism, the required concentration of antimicrobial peptides should be high. Antimicrobial peptides such as dermaseptin, cecropin, caerin and Human cathelicidin LL-37 exhibit its activity through this mechanism.

Reference

- (1) B. Alberts, D. Bray, J. Lewis, M. Raft, K. Roberts and J. D. Watson, *Molecular Biology of the Cell*, (Garland Publishing, 1361, 1994).
- (2) Y. Ma, K. Poole, J. Goyette, K. Gaus, Introducing Membrane Charge and membrane potential to T cell signaling, *Front. Immunol.* 2017, 8:1513.
- (3) M. Zasloff, Antimicrobial peptides of multicellular organisms. *Nature* 2002, 415, 389–395.
- (4) N. Stempel, J. Strehmel, J. Overhage, Potential application of antimicrobial peptides in the treatment of bacterial biofilm infections. *Curr. Pharm. Des.* 2015, 21, 67–84.
- (5) J. Bankovic, J. Andra, N. Todorovic, A. Podolski-Renic, Z. Milosevica, D. Miljkovic, J. Krause, S. Ruzdijic, N. Tanic, M. Pesic, The elimination of P-glycoprotein over-expressing cancer cells by antimicrobial cationic peptide NK-2: The unique way of multi-drug resistance modulation. *Exp. Cell Res.* 2013, 319, 1013–1027.
- (6) K. Holmberg, B. Jonsson, B. Kronberg, and B. Lindman, *Surfactants and Polymers in Aqueous Solution*, (John Wiley & Sons, Chichester, UK, 2nd edition, 2002).
- (7) M. J. Rosen, *Surfactants and Interfacial Phenomena*, (Wiley, New York, NY, USA, 2nd edition, 1989).
- (8) D. J. Murphy, Structure, function and biogenesis of storage lipid bodies and oleosins in plants, *Progress in Lipid Research*, **32**, 247-280 (1993).
- (9) J. N. Israelachvili, *Intermolecular and Surface Forces*, (Academic Press, New York, NY, USA, 2nd edition, 1992).
- (10) X. Cui, S. Mao, M. Liu, H. Yuan, and Y. Du, “Mechanism of surfactant micelle formation,” *Langmuir*, 2008, 24(19), 10771–10775.
- (11) C. J. Marzocco, B. Peterson, The Effect of Hydrocarbon Chain Length on the Critical Micelle Concentration of Cationic Surfactants: An Undergraduate Physical Chemistry Experiment, *The Chemical Educator*, 2007, 12, 80-84.
- (12) K. John, et al., Transbilayer Movement of Phospholipids at the Main Phase Transition of Lipid Membranes: Implications for Rapid Flip-Flop in Biological Membranes. *Biophysical Journal*, 2002, 83(6), 3315-3323.
- (13) R. Koynova and M. Caffrey, Phases and phase transitions of the phosphatidylcholines, *Biochim. Biophys. Acta*, 1998, 1376, 91-145.

- (14) A. Fischer, A. Franco, T. Oberholzer, Giant Vesicles as Microreactors for Enzymatic mRNA Synthesis, *Chem biochem*, 2002, 3, 409-417.
- (15) P. Yang, R. Lipowsky, R. Dimova. Nanoparticle Formation in Giant Vesicles: Synthesis in Biomimetic Compartments, *Small*, 2009, x, 1-5.
- (16) V. P. Torchilin, Recent advances with liposomes as pharmaceutical carriers, *Nat. Rev. Drug Discovery*, 2005, 4, 145-160.
- (17) M. I. Angelova, S. Soleau, P. Meleard, J.F. Faucon and P. Bothorel, Preparation of giant vesicles by external AC electric fields. Kinetics and applications, *Progress in Colloid & Polymer Science*, 1992, 89, 127-131.
- (18) L. Finegold, ed. Cholesterol in Membrane Models (CRC press, Boca Raton, FL, 1993).
- (19) T. P. W. McMullen and R. N. McElhaney, Differential scanning calorimetric studies of the interaction of cholesterol with distearoyl and dielaidoyl molecular species of phosphatidylcholine, phosphatidylethanolamine, and phosphatidylserine, *Biochemistry*, 1997, 36, 4979-86.
- (20) T. P. McMullen, R. N. Lewis, and R. N. McElhaney, Differential scanning calorimetric study of the effect of cholesterol on the thermotropic phase behavior of a homologous series of linear saturated phosphatidylcholines, *Biochemistry*, 1993, 32, 516-22.
- (21) T. J. McIntosh, The effect of cholesterol on the structure of phosphatidylcholine bilayers, *Biochim. Biophys. Acta*, 1978, 513, 43-58.
- (22) S. W. Hui and N. B. He, Molecular organization in cholesterol-lecithin bilayers by x-ray and electron diffraction measurements, *Biochemistry*, 1983, 22, 1159-64.
- (23) R. M. Epand, D. W. Hughes, B. G. Sayer, N. Borochoy, D. Bach, and E. Wachtel, Novel properties of cholesterol-dioleoylphosphatidylcholine mixtures, *Biochim. Biophys. Acta*, 2003, 1616, 196-208.
- (24) H. Takahashi, K. Sinoda, and I. Hatta, Effects of cholesterol on the lamellar and the inverted hexagonal phases of dielaidoylphosphatidylethanolamine, *Biochim. Biophys. Acta*, 1996, 1289, 209-16.
- (25) T. P. McMullen, R. N. Lewis, and R. N. McElhaney, Calorimetric and spectroscopic studies of the effects of cholesterol on the thermotropic phase behavior and organization of a homologous series of linear saturated phosphatidylethanolamine bilayers, *Biochim. Biophys. Acta*, 1999, 1416, 119-34.

- (26) K. Mortensen, W. Pfeiffer, E. Sackmann and W. Knoll, Structural properties of a phosphatidylcholine-cholesterol system as studied by small-angle neutron scattering: ripple structure and phase diagram, *Biochim. Biophys. Acta*, 1988, 945, 221-245.
- (27) T.E. Thompson, M.B. Sankaram, Interaction of cholesterol with various glycerophospholipids and sphingomyelin, *Biochemistry*, 1990, 29, 10670-5.
- (28) A. Filippov, G. Oradd, G. Lindblom, Lipid Lateral Diffusion in Ordered and Disordered Phases in Raft Mixtures, *Biophys. J.*, 2004, 86, 891–896.
- (29) M. B. Sankaram and T. E. Thompson, *Biochemistry* 29, 10670 (1990).
- (30) J. Wiesner, A. Vilcinskas. Antimicrobial peptides: the ancient arm of the human immune system. *Virulence*, 2010, 1(5), 440-64.
- (31) M. Hirano, C. Saito, H. Yokoo, C. Goto, R. Kawano, T. Misawa, Y. Demizu. Development of Antimicrobial Stapled Peptides Based on Magainin 2 Sequence., 2021, *Molecules* 2021, 26, 444.
- (32) M. Pasupuleti, A. Schmidtchen, and M. Malmsten. Antimicrobial peptides: key components of the innate immune system. *Crit. Rev. Biotechnol.*, 2012, 32, 143–171.
- (33) J. P. S. Powers and R. E. W. Hancock. The relationship between peptide structure and antibacterial activity. *Peptides*, 2003, 24, 1681–1691.
- (34) M. R. Yeaman and N. Y. Yount. Mechanisms of antimicrobial peptide action and resistance. *Pharmacol. Rev.*, 2003, 55, 27–55.
- (35) M. Dathe, H. Nikolenko, J. Meyer, M. Beyermann, and M. Bienert. Optimization of the antimicrobial activity of magainin peptides by modification of charge. *FEBS Lett.*, 2001, 501, 146–150.
- (36) R. Bessalle, H. Haas, A. Gorla, I. Shalit, and M. Fridkin. Augmentation of the antibacterial activity of magainin by positive-charge chain extension. *Antimicrob. Agents Chemother.*, 1992, 36, 313–317.
- (37) V. Teixeira, M. J. Feio, and M. Bastos. Role of lipids in the interaction of antimicrobial peptides with membranes. *Prog. Lipid Res.*, 2012, 51, 149–177.
- (38) T. Wieprecht, M. Dathe, M. Beyermann, E. Krause, W. L. Maloy, D. L. MacDonald, and M. Bienert. Peptide hydrophobicity controls the activity and selectivity of magainin 2 amide in interaction with membranes. *Biochemistry*, 1997, 36, 6124–6132.

- (39) LM Yin, MA Edwards, J Li, CM Yip, CM Deber. Roles of hydrophobicity and charge distribution of cationic antimicrobial peptides in peptide-membrane interactions. *Journal of Biological Chemistry*, 2012, 287, 7738-7745.
- (40) H. T. Chou, T. Y. Kuo, J. C. Chiang, M. J. Pei, W. T. Yang, H. C. Yu, S. B. Lin, and W. J. Chen. Design and synthesis of cationic antimicrobial peptides with improved activity and selectivity against *Vibrio* spp. *Int. J. Antimicrob. Agents*, 2008, 32, 130–138.
- (41) HV Westerhoff, D Juretic, RW Hendler, M Zasloff. Magainins and the disruption of membrane-linked free-energy transduction. *Proceedings of the National Academy of Sciences of the United States of America*, 1989, 86, 6597-6601.
- (42) A Tossi, L Sandri, A Giangaspero. Amphipathic, α -helical antimicrobial peptides. *Biopolymers - Peptide Science Section*, 2000, 55, 4-30.
- (43) DI Chan, EJ Prenner, HJ Vogel. Tryptophan- and arginine-rich antimicrobial peptides: structures and mechanisms of action. *Biochimica et Biophysica Acta*, 2006, 1758, 1184-1202.
- (44) HW Huang. Action of antimicrobial peptides: Two-state model. *Biochemistry*, 2000, 39, 8347-8352.
- (45) Z Jiang, AI Vasil, JD Hale, REW Hancock, ML Vasil, RS Hodges. Effects of net charge and the number of positively charged residues on the biological activity of amphipathic α -helical cationic antimicrobial peptides. *Biopolymers - Peptide Science Section*, 2008, 90, 369-383.
- (46) M. R. Yeaman and N. Y. Yount. Mechanisms of antimicrobial peptide action and resistance. *Pharmacol. Rev.*, 2003, 55, 27–55.
- (47) K. Matsuzaki, K. Sugishita, N. Fujii, and K. Miyajima. Molecular basis for membrane selectivity of an antimicrobial peptide, magainin 2. *Biochemistry*, 1995 34, 3423–3429.
- (48) M. N. Melo, R. Ferre, and M. A. R. B. Castanho. Antimicrobial peptides: linking partition, activity and high membrane-bound concentrations. *Nat. Rev. Microbiol.*, 2009, 7, 245–250.
- (49) H.M Chen, K.W Leung, N Thakur, A Tan, R.W Jack. Distinguishing between different pathways of bilayer disruption by the related antimicrobial peptides cecropin B, B1 and B3. *Eur. J. Biochem*, 2003, 270, 911-920.

- (50) L. Zhang, A. Rozek, R. E. Hancock, Interaction of cationic antimicrobial peptides with model membranes, *J. Biol. Chem.*, 2001, 276, 35714-35722.
- (51) S. Karmakar, P. Maity, A. Halder, Charge-Driven Interaction of Antimicrobial Peptide NK-2 with Phospholipid Membranes, *ACS Omega*, 2018, 2, 8859-8867.
- (52) A Halder, A Sannigrahi, N De, K Chattopadhyay, S Karmakar. Kinetoplastid Membrane Protein-11 Induces Pores in Anionic Phospholipid Membranes: Effect of Cholesterol. *Langmuir* 2020, 36, 3522-5330.
- (53) L Yang, TA Harroun, TM Weiss, L Ding, HW Huang. Barrel-stave model or toroidal model? A case study on melittin pores. *Biophysical Journal*, 2001, 81, 1475-1485.
- (54) K Matsuzaki, O Murase, N Fujii, K Miyajima. An antimicrobial peptide, magainin 2, induced rapid flip-flop of phospholipids coupled with pore formation and peptide translocation. *Biochemistry*, 1996, 35, 11361-11368.
- (55) H. W. Huang, F. Y. Chen, and M. T. Lee. Molecular mechanism of peptide-induced pores in membranes. *Phys. Rev. Lett.*, 2004, 92, 198304.
- (56) K Brogden. Antimicrobial peptides: pore formers or metabolic inhibitors in bacteria? *Nature Reviews Microbiology*, 2005, 3, 238-250.
- (57) M K Mathew, P Balaram. A helix dipole model for alamethicin and related transmembrane channels. *FEBS Letters*, 1983, 157, 1-5.
- (58) E. Gazit I. R. Miller, Phil C. Biggin, M. S. P. Sansom, and Y. Shai. Structure and orientation of the mammalian antibacterial peptide cecropin P1 within phospholipid membranes. *J. Mol. Biol.*, 1996, 258, 860–870.

Chapter 2

Experimental Techniques

2.1 Introduction:

In this chapter, we have described briefly the experimental techniques which are used to study the interaction of antimicrobial peptide with phospholipid membrane. Section 2.2 describes the extrusion technique used to prepare to large unilamellar vesicle. In section 2.3 we have discussed the electroformation method for preparation of giant unilamellar vesicles. The preparation of small unilamellar vesicles using sonication method is described in section 2.4. The average size of the lipid vesicles was confirmed by dynamic light scattering measurement and principle of zeta potential are discussed in section 2.5. Section 2.6 describes the fluorescence spectroscopy techniques, including fluorescence lifetime and fluorescence anisotropy. In this section we discuss the Perrin's equation and rotational diffusion rate. We discuss isothermal titration calorimetry and surface partition model with electrostatic contribution in section 2.7. Phase contrast microscopy was used to observe morphological changes in giant unilamellar vesicles (GUVs). Basic principles of phase contrast microscopy are illustrated in section 2.8.

2.2 Preparation of large unilamellar vesicle (LUV):

The most convenient and widely used method for preparation of large unilamellar vesicle is extrusion method. During the preparation of vesicles, it is important to keep the temperature above the chain melting transition temperature (T_m) of lipid i.e. vesicles form only in the fluid lamellar phase of the hydrated lipid film. In the gel phase, the membranes are rigid and stiff. It cost more energy to bend the bilayer and hence it prevents the formation of vesicles. Large unilamellar vesicles were prepared using an extrusion technique as described by Hope et al (1). Various

phospholipids and phospholipid-cholesterol mixtures have been used for vesicle preparation. An appropriate amount of lipid or lipid-cholesterol mixture in chloroform was transferred to a 5 ml glass vial. Chloroform solvent was removed by gently passing dry nitrogen gas. The traces of the solvent were then removed by keeping the sample in a vacuum desiccator for a couple of hours. Milli Q water was added to the dried lipid film so that the final desired concentration (1mM) was obtained. Vortexing of hydrated lipid film for about 30min produces multilamellar vesicles (MLV). MLV suspensions were extruded through polycarbonate membranes of pore diameters 100 nm. This results in a formation of fairly monodispersed LUV (average diameter ~100 nm).

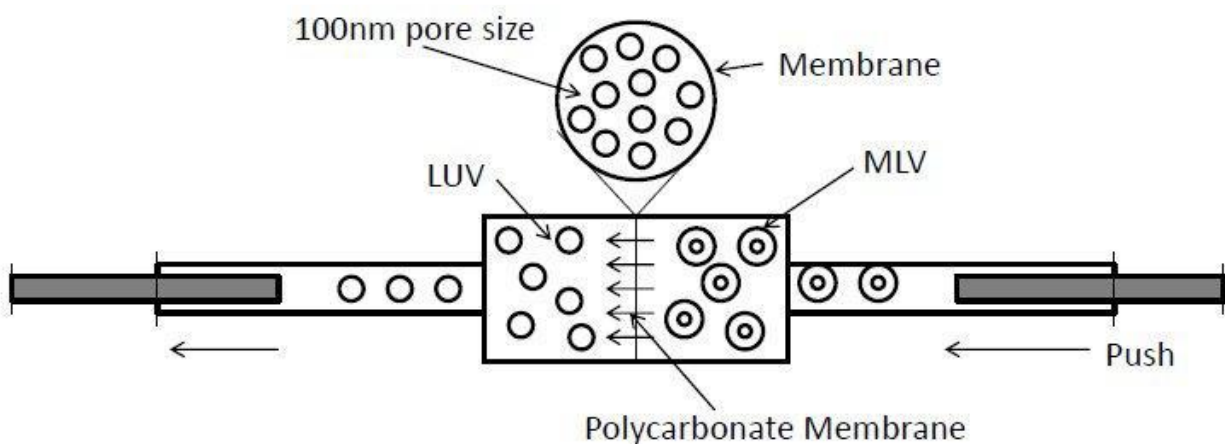


Figure 2.1: Schematic diagram of extruder which showing the formation of MLV to LUV.

Size distribution and the Polydispersity index were measured using, dynamic light scattering. LUV solution was degassed prior to all measurements to eliminate the artifacts caused by the air bubble formation.

2.3 Preparation of giant unilamellar vesicle (GUV):

GUVs were prepared in 0.1 M sucrose in 1 mM N-(2-hydroxyethyl) piperazine-N-ethanesulfonic acid (HEPES) (pH 7.4) buffer using electro formation, as described by Pott et al (2). Briefly, 20 μ L of a 1 mM lipid solution in chloroform was spread onto the surfaces of two conductive indium

tin oxide (ITO) glasses. The coated lipid solutions were then allowed to dry overnight in a closed chamber containing saturated solution of NaCl. This is to avoid complete drying of the droplets. The hydration of these droplets facilitates the electro formation process. The electro formation chamber was prepared using a Teflon spacer of ~ 2 mm thickness. This electro swelling chamber was filled with 0.1 M sucrose solution, and an alternating voltage of 1.5 V and frequency of 15 Hz were applied for 2 h at room temperature ($22 - 25$ °C).

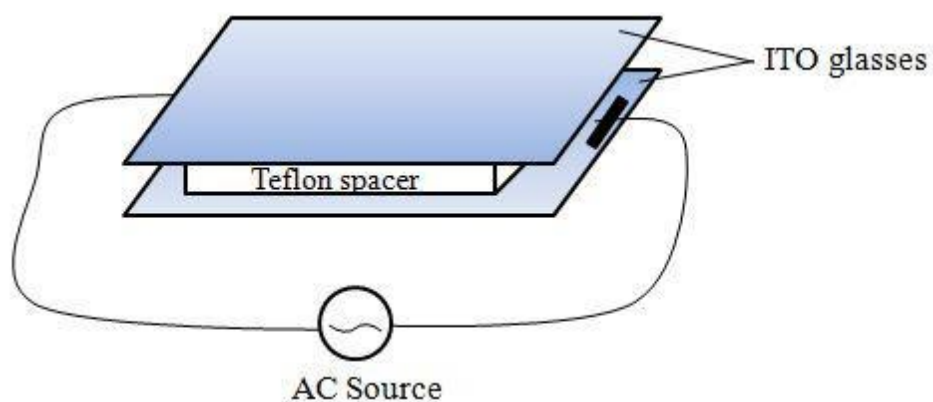


Figure 2.2: Schematic diagram of electroformation chamber.

The vesicle solution was then carefully transferred to an Eppendorf vial and kept at rest at 4 °C before use. The average diameter of the GUV obtained was $10 - 100$ μm . GUVs were diluted in 0.1 M glucose, prepared in 1 mM HEPES (pH 7.4), for observation. A typical observation experiment, using an inverted microscope, was made in an observation chamber by mixing 30 μL of the GUV solution with 100 μL of a 0.1 M glucose solution. The slight density difference between the inner and outer solutions drives the vesicles to settle at the bottom of the slide and provides better contrast while observing under phase contrast.

2.4 Preparation of small unilamellar vesicle (SUV):

Small unilamellar vesicles can be prepared by two ways. One of them is extrusion method and another way is sonication method. Extrusion technique is same as the LUV preparation which described in previous section 2.2. In this case, the pore diameter of the polycarbonate membrane was taken as 50 nm. MLV suspension successively was extruded through polycarbonate membrane of 50 nm pore diameter and the mean size of the SUVs obtained less than 100 nm which was confirmed by DLS experiment. The size of the SUV was around 60 nm. In this method we could not reduce the size below 60 nm. Sonication method is a useful technique for the preparation of different sizes of SUV (3). Same procedure was followed to prepare MLV as discussed for LUV. For the formation of SUV, the MLV was sonicated gently using probe tip sonicator, QSONICA-SONICATORS (125W, 20 kHz). Probe tip sonicator deliver high energy into the lipid suspension. Power delivery was controlled as percentage amplitude (20%, 30% & 40%). After the sonication at 30°C (above the chain melting transition temperature of the lipid) for 30 min, a clear suspension of SUVs was obtained. We extruded the sonicated vesicles one-time through 100 nm polycarbonate membrane as a filtration step. Also, due to the high degree of curvature of these membranes, SUV are inherently unstable and will spontaneously fuse to form larger vesicles when stored below their phase transition temperature.

2.5 Characterization of Vesicles

2.5.1 Size Measurement using Dynamic Light Scattering

The method of dynamic light scattering (DLS) is the most common measurement technique for particle size analysis in the nanometer range. To determine the average size of the LUV/SUV, DLS technique is very useful (4-6). Dynamic light scattering (DLS) is based on the Brownian motion of dispersed particles. When particles are dispersed in a liquid they move randomly in all directions. The principle of Brownian motion is that particles are constantly colliding with solvent molecules. These collisions cause a certain amount of energy to be transferred, which induces particle movement. The energy transfer is more or less constant and therefore has a greater effect on smaller particles. As a result, smaller particles are moving at higher speeds than larger particles. If all other parameters are known which have an influence on particle movement, we can determine

the hydrodynamic diameter by measuring the speed of the particles. In a typical experimental setup, scattered light can be detected at both 90° as well as 173° scattering angle. The backscattered light intensity (173°) is better than 90° scattered for more accuracy of size measurement. This is because the scattered light from unwanted big particles or dust particles in the solution can be minimized by the backscattered mechanism since there are known to scattered by the dust particle in forward direction (7). It is also important that the rotational diffusion coefficient can be ignored when the scattered light is detected at 173° compared to the detection at 90°. Therefore, by detecting the back scattered light, the translational diffusion D can be obtained. The back scattered light is detected and sent to digital signal processing correlator. The scattering wave vector (\vec{q}) is defined as

$$|\vec{q}| = |\vec{k}_s - \vec{k}_i| = \frac{4\pi \sin\theta/2}{\lambda} \quad (2.1)$$

where \vec{k}_i and \vec{k}_s are the incident and scattering vector respectively.

The intensity fluctuations measured at two different time t and t + τ , where τ is the correlation time of the measured intensities that time is much smaller than the characteristic time of fluctuation. The correlation function is defined as

$$G(\tau) = \langle I(t) I(t + \tau) \rangle = \lim_{T \rightarrow \infty} \left\{ \frac{1}{T} \int_0^T I(t) I(t + \tau) dt \right\} \quad (2.2)$$

The translational diffusion coefficient (D) of the particles can be determined from autocorrelation by fitting the equation

$$G(\tau) \sim e^{-q^2 D \tau} \quad (2.3)$$

The hydrodynamic radius (R_H) of the vesicles can be determined from the diffusion coefficient using the Stokes-Einstein relation.

$$R_H = \frac{k_B T}{6\pi\eta D} \quad (2.4)$$

Where k_B is Boltzmann constant, T is absolute temperature, η is the viscosity of the medium in which LUV are dispersed D is the diffusion constant and other symbols have their usual meaning. Hydrodynamic radius (R_H) refers to the radius of the sphere that diffuses with the same velocity

as that of the particle. The major assumption in DLS is that we assume the spherical shape of LUV. Therefore, the information of shape change or fluctuations of the vesicles does not determine by the DLS experiment i.e. it always consider the spherical shape during the measurement (8). DLS measures the hydrodynamic radius which includes both solvent (hydro) and shape (dynamic) effects. Polydispersity index (PDI) is a measure of dispersion or the standard deviation of size distribution. PDI indicates the extent of Polydispersity of the size distribution. The slope of the correlogram and width of the size distribution provide the idea of Polydispersity of the sample. Smooth exponential decay of intensity correlation curve indicates no aggregation or coagulation process occurring in the system. It is known that $PDI > 0.7$ usually indicates that sample is highly polydisperse and probably not suitable for the DLS measurement. $PDI < 0.05$ is purely monodisperse.

Using dynamic light scattering (DLS), the size distribution was measured at room temperature ($\sim 25^{\circ}\text{C}$) with Zetasizer Nano ZS (Malvern Instruments, UK). Zetasizer Nano uses 4 mW He Ne Laser of wavelength 632.8 nm and power 2 – 4 mW. A transparent quartz cuvette was used for the size measurement. In each measurement, we have performed 10-100 consecutive runs. The disposable zeta cuvette is also used to measure size distribution. Typical size distribution of LUV has been shown in Fig. 2.3

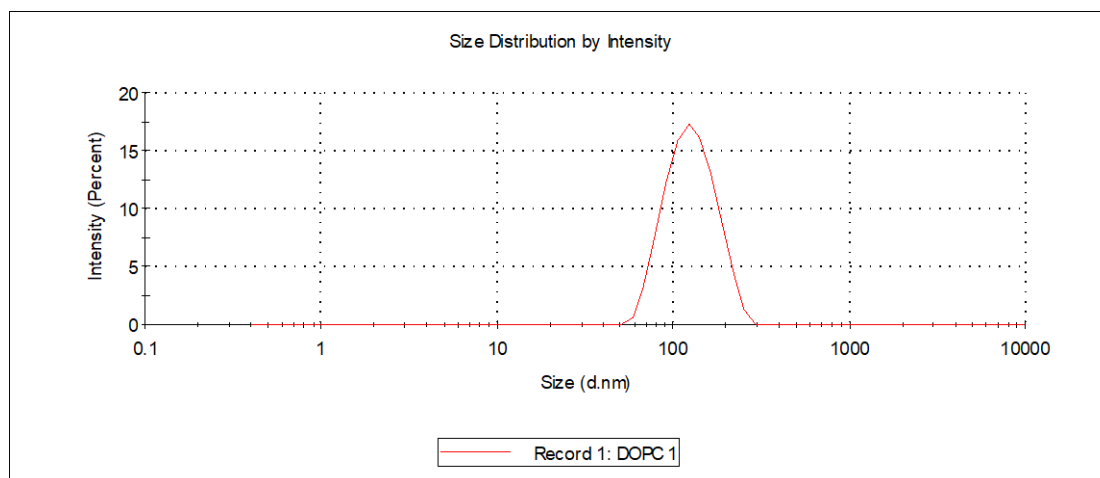


Figure 2.3: Size distribution of LUV made from DOPC.

2.5.2 Zeta potential:

The scientists Derjaguin, Verwey, Landau and Overbeek developed a theory in the 1940s which dealt with the stability of colloidal systems. DVLO theory suggests that the stability of a particle in solution is dependent upon its total potential energy function V_T .

$$V_T = V_A + V_R + V_S \quad (2.5)$$

V_S is the potential energy due to the solvent. V_A and V_R , these are the attractive and repulsive contributions. They potentially are much larger and operate over a much larger distance.

$$V_A = -A/12\pi D^2 \quad (2.6)$$

where A is the Hamaker constant and D is the particle separation. The repulsive potential V_R is a far more complex function.

$$V_R = 2\pi\epsilon a\zeta^2 \exp(-\kappa D) \quad (2.7)$$

where a is the particle radius, π is the solvent permeability, κ is a function of the ionic composition and ζ is the zeta potential.

DVLO theory suggests that the stability of a colloidal system is determined by the sum of these van der Waals attractive (V_A) and electrical double layer repulsive (V_R) forces that exist between particles as they approach each other due to the Brownian motion they are undergoing. If the particles have a sufficiently high repulsion, the dispersion will resist flocculation and the colloidal system will be stable. However, if a repulsion mechanism does not exist then flocculation or coagulation will eventually take place.

Zeta potential is a physical property which is exhibited by any particle in suspension, macromolecule or material surface. It can be used to optimize the formulations of suspensions and protein solutions and also predict the interaction with the surfaces. This technique is widely used to estimate the surface charge, surface potential of the particle and to determine the electrophoretic mobility, isoelectric point of charge system. When charged LUVs are embedded in aqueous solution containing ions, the oppositely charged ions form electrostatic double layer around the LUV. Thus electrostatic double layer exists around each vesicle. Ions are strongly bound

surrounding the vesicles and form the first liquid layer is called stern layer. From the stern layer ions are loosely bound with the vesicles and free to diffuse and form diffuse layer. The boundary of the diffuse layer is called shear or slipping plane. When the vesicle moves, ion within the boundary of slipping plane move with it. The electrostatic potential that exists in the shear or slipping plane is known as zeta potential. Therefore, zeta potential can be a good approximation of the surface potential of LUV.

The ζ -potential was measured from the electrophoretic mobility by laser Doppler velocimetry using the Helmholtz-Smoluchowski equation.

$$\zeta = \frac{3\mu\eta}{2\epsilon f(\kappa a)} \quad (2.8)$$

where η and ϵ are the coefficient of viscosity and the permittivity of the aqueous medium, respectively. $f(\kappa a)$ is the Henry function, which depends on the inverse Debye length (κ) and the radius (a) of the vesicle, the change in the size distribution of the vesicles does not alter the zeta potential significantly. This is due to the fact that zeta potential depends on the formation of electrostatic double layer. In Smoluchowski approximation, the maximum value of the function $f(\kappa a)$ is equal to 1.5 when particles are in aqueous media (9). However, when the particles are suspended in a nonaqueous medium, the value of $f(\kappa a)$ would be 1 (Huckel approximation). we have used $f(\kappa a) = 1.5$ to calculate the ζ -potential from measured electrophoretic mobility. The average ζ -potential was obtained using three successive measurements. Each measurement included 10 – 100 runs.

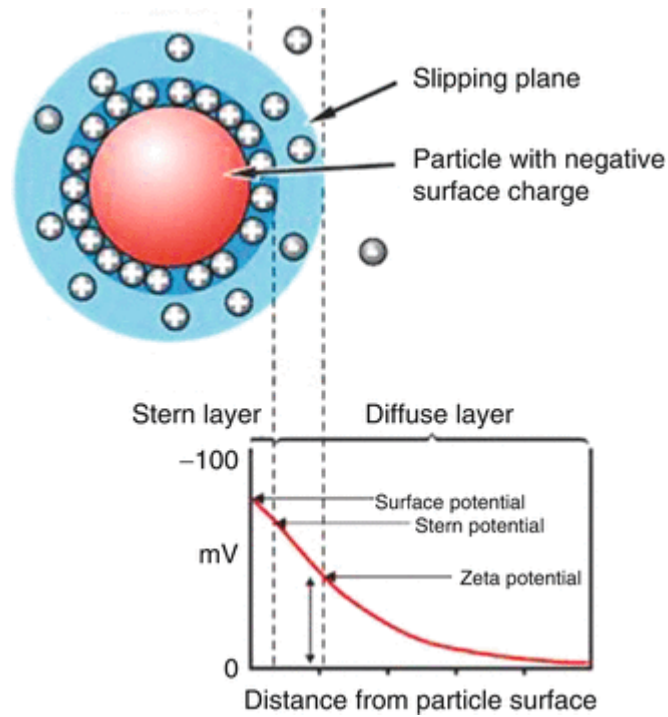


Figure 2.4: Formation of electric double layer due to charged vesicles and zeta potential measures at the slipping plane.

Effective charge, Q_{eff} of the vesicles has also been estimated from the measured electrophoretic mobility according to equation

$$\mu = \frac{Q_{eff}}{6\pi\eta a_{eff}} \quad (2.9)$$

a_{eff} is the effective radius of the vesicle including stern layer and can be obtained from dynamic light scattering.

In this study, the average ζ potential and size were obtained from 3 to 4 successive measurements. The same cuvette is used for both ζ potential and DLS measurements. All experiments were performed at 25 °C. Typical zeta potential distribution curve of LUV has been shown in Fig. 2.5

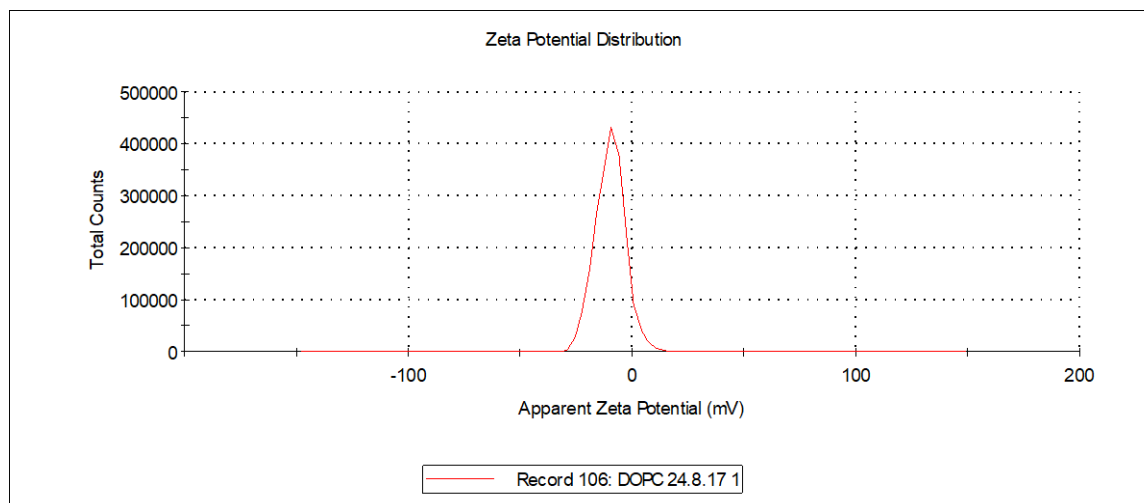


Figure 2.5: Zeta potential distribution of LUV made from DOPC

2.6 Fluorescence spectroscopy:

2.6.1 Steady state fluorescence measurement:

Fluorescence spectroscopy analyzes fluorescence from a molecule based on its fluorescent properties. Fluorescence spectroscopy uses a beam of light that excites the electrons in molecules of certain compounds and causes them to emit light. That light is directed towards a filter and onto a detector for measurement to identify the molecule or change in the molecule. When molecules are excited by a constant source of light i.e. fixed wavelength, emit fluorescence detected as a function of wavelength called steady state fluorescence spectra. A fluorescence emission spectrum is when the excitation wavelength is fixed and the emission wavelength is scanned to get a plot of intensity emission wavelength. Typically, the emission spectrum occurs at higher wavelength (lower energy) than the excitation spectrum. These two spectrum are used to see how a sample is changing. The spectral intensity or peak wavelength may change with the changing of temperature, concentration or interaction with other molecules. Some fluorophores are sensitive to solvent environment properties such as pH, polarity and ion concentration. Some intrinsically fluorescent molecules are chlorophyll and amino acid residue tryptophan (Trp) phenylalanine (Phe) and

tyrosine (Tyr). Others synthesized molecules used as stable organic dyes to tag non-fluorescent system.

The fluorescence spectroscopy technique is widely used to determine the structure and dynamics of the lipid membrane (10,11). Nile red (9-diethylamino-5H-benzo(α) phenoxazine-5-one), is one such environment sensitive probe and is widely used to monitor the membrane organization and dynamics (12). It emits fluorescence in the presence of lipid membrane (13). However, its fluorescence is significantly quenched in the aqueous or polar environment. Therefore, the Nile red is used on living cells as a fluorescence stain for the detection of intracellular lipid droplets if the proper spectral condition is chosen.

We have measured the steady state fluorescence emission intensity of Nile red labeled large unilamellar vesicles composed of various lipids and lipid-cholesterol mixtures. Fluorescence measurements were carried out using a PTI Quantamaster 400 spectrofluorimeter (Horiba-PTI, Canada). We have measured the absorption spectrum of Nile red and optimum excitation wavelength was found to be at 550 nm. Therefore, excitation wavelength has been kept fixed at 550 nm and emission spectra of Nile red were monitored for different lipids and at different cholesterol concentration. We have kept the emission and excitation band pass filters at 5 nm for all measurements. Spectra were also observed at different cholesterol concentration at temperatures below and above the chain melting transition for saturated lipids. The effect of temperature on the emission spectrum has also been investigated.

2.6.2 Fluorescence lifetime:

Fluorescence lifetime serves as a reliable indicator of the local environment in which a fluorophore is localized. Fluorescence lifetime measurement was carried out using time-correlated single photon counting set up from Horiba Jobin-Yvon. The luminescence decay data were collected on a Hamamatsu MCP Photomultiplier (R3809) and were analyzed using IBH DAS6 software.

The decay of the excited state of a molecule to the ground state can be expressed as;

$$I(t) = I_0 \exp(-t/\tau) \quad (2.10)$$

Where I_0 is the intensity at time zero (upon excitation) and τ is the lifetime. This is defined as the time for the intensity to drop by $1/e$ or to $\sim 37\%$. In terms of rate constant, the lifetime can be written as below

$$\tau = \frac{1}{k_r + k_{nr}} \quad , \quad \phi = \frac{k_r}{k_r + k_{nr}} \quad (2.11)$$

where k_r and k_{nr} are the radiative and non-radiative rate constant respectively. Φ is quantum yield.

Fluorescence lifetime is an absolute measurement. It is an intrinsic molecular property. It is concentration independent which means if the concentration of the sample change, lifetime value will not change. Fluorescence decay take places on the nanosecond timescale and it can be influenced by molecular process occurring on the nanometer range. The emission of the fluorophore can be highly influenced by its environment or the presence of other interacting molecules which can affect k_{nr} . The decay of fluorescence intensity is measured using Time Correlated Single Photon Counting (TCSPC) technique. t represents the value of lifetime. Using Eq. 2.21, the best fit was evaluated from the χ^2 value to find out the lifetime. In this thesis, all lifetime values were determined by the best fit using single exponential equation. The range of χ^2 value was 0.95 to 1.12.

2.6.3. Steady state fluorescence Anisotropy:

Fluorescence anisotropy is widely used to characterize the angular displacement of the fluorophore by the extent of linear polarization of fluorescence emission. This angular displacement is dependent upon the rate and extent of rotational diffusion during the lifetime of the excited state. The rate of rotational diffusion of fluorophore gives idea about the change of environment of the fluorophore. Fluorescence anisotropy was obtained using the Hitachi F4010 spectrofluorimeter (Hitachi, Tokyo, Japan). Membrane level probe Nile red was used as a fluorophore to measure the anisotropy. Nile red was excited at 550 nm with a vertically polarized light. The intensity of emission was then measured at 630 nm through a polarizer/analyzer at crossed (I_{vh}) and parallel (I_{vv}) positions of the analyzer with respect to polarized excitation. Steady state polarization anisotropy (r) is defined as

$$r = \frac{I_{vv} - GI_{vh}}{I_{vv} + 2GI_{vh}} \quad (2.12)$$

Polarization represents same phenomena but is calculated with a different equation (14).

$$P = \frac{I_{vv} - GI_{vh}}{I_{vv} + GI_{vh}} \quad (2.13)$$

Polarization and anisotropy are interrelated. Fluorescence Polarization is commonly used in clinical medicine for measurement of biomarkers, while fluorescence anisotropy is used mechanistic studies and drug discovery. G is an instrument and a wavelength dependent correction factor to compensate for the polarization bias of the detection system and for the ratio $\frac{I_{hv}}{I_{hh}}$. The I_{vv} , I_{vh} , I_{hv} and I_{hh} represents the excitation and emission fluorescence signal with the polarizer positions set at $(0^0, 0^0)$, $(0^0, 90^0)$, $(90^0, 0^0)$ and $(90^0, 90^0)$ respectively.

If we consider a single fluorophore with a fixed position (θ) of its transition dipole moment, then I_{vv} and I_{vh} can be written as $I_{vv} \approx \cos^2\theta$

$$I_{vh} \approx \sin^2\theta \sin^2\varphi$$

For ensemble of molecules with random values of φ i.e. the average over φ

$$\langle \sin^2\varphi \rangle = \frac{\int_0^{2\pi} \sin^2\varphi d\varphi}{\int_0^{2\pi} d\varphi} = 1/2$$

$$I_{vh} \approx 1/2 \sin^2\theta$$

The anisotropy (r) can be express from equation Eq. 2.30 as

$$r = \frac{3\cos^2\theta - 1}{2} \quad (2.14)$$

Now assume the dipole moments of fluorophores are oriented randomly and have to take average over θ in Eq. 2.31.

$$r = \frac{3\langle \cos^2\theta \rangle - 1}{2} \quad (2.15)$$

$$\text{Where } \langle \cos^2\theta \rangle = \frac{\int_0^{\pi/2} \cos^2\theta f(\theta) d\theta}{\int_0^{\pi/2} f(\theta) d\theta} = \frac{\int_0^{\pi/2} \cos^4\theta \sin\theta d\theta}{\int_0^{\pi/2} \cos^2\theta \sin\theta d\theta} = \frac{3}{5}$$

$f(\theta)$ is the probability density function of finding an excited molecule with a dipole under the angle θ , $f(\theta) = \sin\theta\cos^2\theta$

From Eq. 2.32 the maximum value of anisotropy (r_0) is 0.4 when the absorption and emission dipole are collinear. However, in general the absorption (D_a) and emission (D_e) dipole are not collinear. The displacement of the dipoles by an angle α results the loss of anisotropy due to the photo selection. Therefore, the fundamental anisotropy of a fluorophore is given by

$$r = \frac{2}{5} \left(\frac{3\cos^2\alpha - 1}{2} \right) \quad (2.16)$$

The perrin equation:

The time resolved decay of anisotropy due to rotation is

$$r(t) = r_0 \exp(-t/\theta) = r_0 \exp(-6Dt) \quad (2.17)$$

For a spherical molecule $\theta = \frac{\eta V}{RT} = \frac{1}{6D}$

where θ is the rotational correlation time; D is the rotational diffusion coefficient and η is the coefficient of viscosity. The steady state anisotropy can be calculated from an average of the anisotropy decay, $r(t)$, over the intensity decay, $I(t)$:

$$r = \frac{\int_0^\infty I(t)r(t)dt}{\int_0^\infty I(t)dt} = \frac{\int_0^\infty I_0 r_0 \exp\left(-\frac{t}{\tau} - \frac{t}{\theta}\right) dt}{\int_0^\infty I_0 \exp\left(-\frac{t}{\tau}\right) dt} = r_0 \frac{1}{1 + \frac{\theta}{\tau}} \quad (2.18)$$

Where τ is the lifetime and the value of r_0 was considered to be 0.4 in this thesis work.

2.7 Isothermal titration calorimetry:

Isothermal Titration Calorimetry (ITC) is widely used to investigate the thermodynamics of binding kinetics by measuring heat of reaction between ligand and macromolecules (15). The thermodynamical parameters such as binding constant (K), reaction stoichiometry (N), binding enthalpy (ΔH), Gibbs energy and entropy (ΔS) are quantitatively determined from the ITC and provides the mechanism of interaction between biomolecules.

The binding affinity of peptide to the lipids was measured using a VP-ITC micro calorimeter produced by Microcal Inc. (Northampton, USA) at fixed temperature as per the requirement. In all experiments, the injection syringe was filled with degassed LUV suspension. The sample cell of volume 1.414 ml contains various concentrations of peptide dissolved in 1 mM HEPES buffer (pH 7.4). The reference cell is filled with HEPES buffer only. All solutions were degassed prior to filling the syringe and ITC cells to eliminate air bubble formation under vacuum (140 mbar, 8 min) using the Microcal's thermovac unit. The rotating speed of syringe was maintained at 300 rpm. A series of 28 injections, each of 8 μL , was introduced into the sample cell at 300 s intervals. All experiments were performed at 25 °C. Each injection produces a characteristic heat signal, arising from the released or absorbed heat from the system, leading to exothermic or endothermic peaks. Heat of dilution was measured by injecting LUV into the buffer. Net heat per injection was obtained by subtracting the heat of dilution from the actual measurement. Although The heat of dilution was found to be small as compared to the actual measurement. ITC data have been analyzed without altering the lipid concentration. This would ensure that the peptides interact with both monolayers of the membrane. All dilution measurements show exothermic signal. The binding constant (K) and binding enthalpy (ΔH) and Gibbs free energy ($\Delta G = -RT \ln K$) and entropic contributions ($T\Delta S = \Delta H - \Delta G$) of the binding kinetics can be obtained from the model, as described by Domingues et al.(16). A summary of the model is described below.

2.7.1 Surface partition model:

In a typical ITC experiment, when LUVs are injected into the peptide solution, the total concentration of the peptide is the sum of the concentration of bound peptides and the free peptides. The apparent binding constant K_{app} is defined as $X_b = K_{app} C_f$, where X_b is the extent of peptide

binding per mole of lipid and C_f is the free peptide concentration of the solution. When the charged peptide adsorbs, the membrane becomes charged. Hence, further adsorption of peptide onto the membrane is restricted by the electrostatic repulsion. Therefore, K_{app} is no longer a constant but rather changes with C_f . Therefore, the most relevant binding parameter would be the intrinsic binding constant K_{int} ($X_b = K_{int} C_M$), which is assumed to be directly proportional to the surface concentration of the peptide in the membrane. The model essentially calculates X_b and C_M for each injection of the ITC experiment. As the C_M of the peptide is governed by the electrostatic contribution, it is determined by the Boltzmann distribution.

$$C_M = C_f e^{-z_p F \psi_0 / RT} \quad (2.19)$$

where z_p is the effective peptide charge. The maximum charge of NK-2 is +10. F is the Faraday constant (= charge of 1 mole of electron = electronic charge \times Avogadro's number = 96 485 C/mol). ψ_0 is the surface potential. R is the universal gas constant and T is the absolute temperature. As the ψ_0 is related to surface charge density, σ , of the peptide, it can be estimated from the well-known Gouy – Chapman theory. As the ζ potential can be a good approximation to the surface potential, we have taken ψ_0 same as the ζ potential. Now we need to know the ζ potential for each peptide-to-lipid molar ratio obtained after every injection. However, we have measured the ζ potential for few peptide-to-lipid ratios. To obtain the ζ potential for all peptide-to-lipid ratios required for the calculation of C_M , we have fitted the ζ potential data to a Hill equation originally used to describe cooperative binding of ligand to macromolecules (17). Hence, we have obtained ζ potentials for all required concentrations from interpolation or extrapolation of the fitted curve. Now, for each data point, the concentration of the free peptide and ψ_0 have been determined. Once C_f and ψ_0 are known, C_M can be calculated. We now discuss briefly how X_b and C_f have been estimated from an ITC experiment.

In an ITC experiment (lipids into peptide injection), the X_b and the enthalpy change ΔH per mole of peptides can be measured directly. The ΔH has been estimated from the sum over all heat per injection divided by the number of moles of peptide in the calorimeter cell.

$$\Delta H = \frac{\sum_i \delta h_i}{C_p^0 V_{cell}} \quad (2.20)$$

where δh_i is the heat per injection in the ITC experiment. C_p^0 is the initial molar concentration of peptide in the ITC cell, and V_{cell} is the volume of the ITC cell. Now, the extent of peptide binding, X_b , per mole of lipid after completion of i^{th} is given by

$$X_b^i = \frac{\sum_k^i \delta h_k}{\Delta H i V_{inj} C_L} \quad (2.21)$$

where V_{inj} is the volume of each injection with lipid of concentration C_L . Now, the fraction of bound peptide after i th injection is given by

$$X_p^i = \frac{\sum_k^i \delta h_k}{\Delta H V_{cell} C_p^0} \quad (2.22)$$

where the free peptide concentration C_f can be obtained from

$$C_f = C_p^0 (1 - X_p^i) \quad (2.23)$$

Now, the K_{app} can be obtained from the X_b and C_f . Therefore, C_M and K_{int} can be estimated for each pair of X_b and C_f , obtained from experimental data.

2.8 Phase contrast microscopy:

A large number of living biological specimens are virtually transparent when observed in the optical microscope under bright field illumination. Earlier these biological structures were made visible by staining. Most of stains or staining procedures will kill the cell. But Phase contrast microscopy technique provides an excellent method of improving contrast in unstained biological specimens without significant loss in resolution. This technique is widely utilized to examine dynamic events in living cells, microorganisms, thin tissue slices, lithographic patterns and sub-cellular particles such as nuclei and other organelles. Phase contrast microscopy invented in 1934 by Dutch physicist Frits Zernike (18). The phase contrast microscopy is based on the principle that small phase changes in the light rays, induced by differences in the thickness and refractive index of the different parts of an object, can be transformed into differences in brightness or light intensity. Human eyes are not sensitive to detect the phase change in the sample whereas brightness

or light intensity can be easily detected by human eyes. Phase contrast microscopy converts invisible phase shift into visible differences of intensities. Unstained living cells absorb practically no light. Poor light absorption results in extremely small differences in the intensity distribution in the image. This makes the cells barely, or not at all, visible in a bright field microscope. When light passes through cells, small phase shifts occur, which are invisible to the human eye. In a phase contrast microscope, these phase shifts are converted into changes in amplitude, which can be observed as differences in image contrast. However, this label-free technique is strongly dependent on the correct alignment of components in the optical pathway. This alignment can be disturbed by the naturally occurring meniscus effect, causing weak phase contrast.

Phase contrast microscopy was performed with a DMI8 inverted microscope from Leica (Wetzlar, Germany). Observation chamber consists of a glass slide with rubber spacers. Appropriate amount of peptide solution from the 50 μM stock solution in HEPES buffer was added to 200 μl of Glucose and uniformly mixed. 10-20 μl of GUV suspension was added to the chamber. The chamber was then closed immediately for observation under phase contrast microscope. Typical phase contrast images of GUV are shown in fig. 2.6. In the present experiment, it is not possible to determine the exact peptide to lipid molar ratio. However, we can roughly estimate the peptide/lipid. For example, if we introduce 10 μl of diluted GUV solution (~ 0.1 mM) to the chamber containing 100 μl of 1 μM NK-2 solution, the final NK-2/lipid (molar ratio) becomes 0.1 (Number of moles = molar concentration \times volume in liter). Response of individual GUV when exposed to the peptide solution was continuously recorded with time using a CCD camera. Images were analyzed using image analysis software, ImageJ. A straight line was drawn across the GUV to obtain an intensity profile. Peak to peak intensity (I_{ptp}) across the halo region is calculated (shown in fig. 2.7). Average (I_{ptp}) is obtained from the several line profiles across the GUV. The time in second versus (I_{ptp}) was plotted in order to observe any significant change in the intensity profile of the GUV.

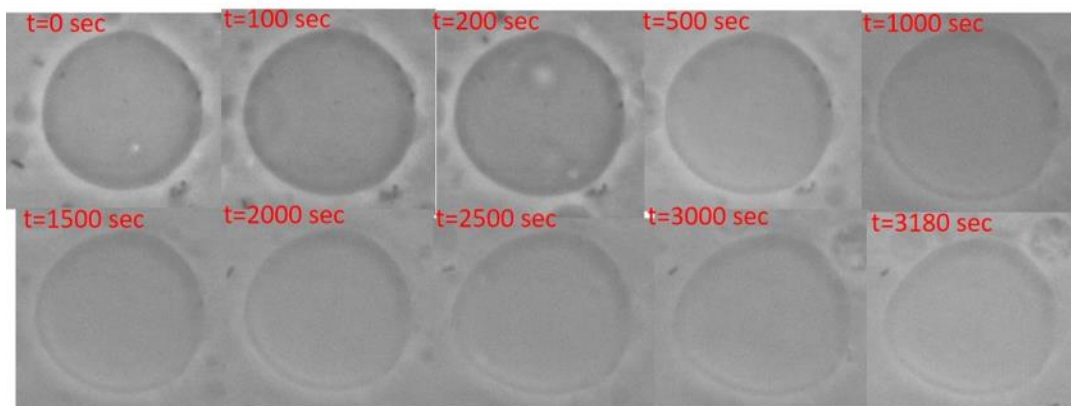


Figure 2.6: Phase contrast images of GUVs composed of DOPC–DOPG (4:1).

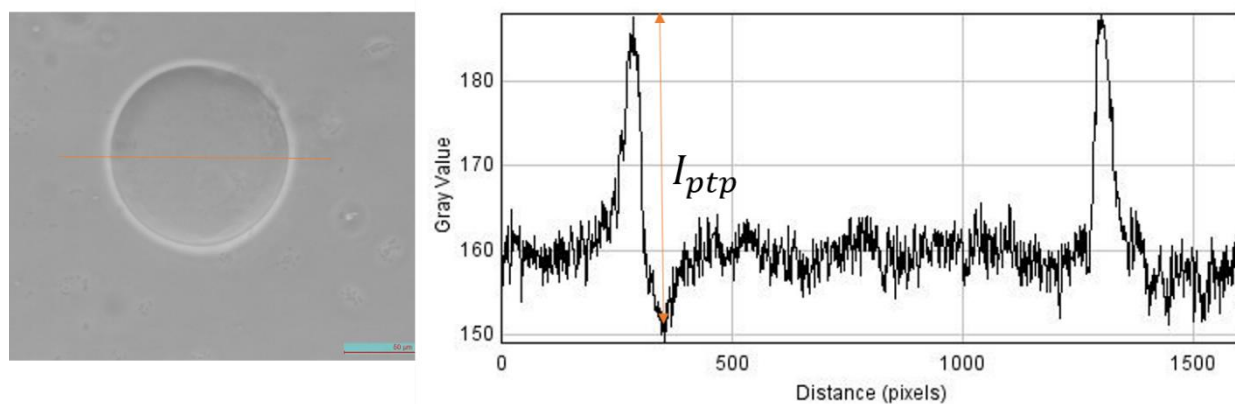


Figure 2.7: Estimation of the peak-to-peak intensity (gray value), I_{ptp} , across the halo region of the phase contrast micrograph of GUV.

References:

- (1) M.J. Hope, M.B. Bally, G.Webb, P.R. Cullis, Production of large unilamellar vesicles by a rapid extrusion procedure: characterization of size distribution, trapped volume and ability to maintain a membrane potential, *Biochim. Biophys. Acta*, 1985, 812, 55–65.
- (2) T Pott, H Bouvrais, P Méléard. Giant unilamellar vesicle formation under physiologically relevant conditions. *Chem. Phys. Lipids*, 2008, 154, 115 – 119.
- (3) N. J. Cho, L. Y. Hwang, J. J. R. Solandt, C. W. Frank, Comparison of Extruded and Sonicated Vesicles for Planar Bilayer Self-Assembly, *Materials*, 2013, 6, 3294-3308.
- (4) R. Pecora, Dynamic Light Scattering Measurement of Nanometer Particles in Liquids, *Journal of Nanoparticle Research*, 2000, 2, 123–131.
- (5) B. J. Frisken, Revisiting the method of cumulants for the analysis of dynamic light-scattering data, *Applied optics*, 2001, 40, 4087-4091.
- (6) K. S. Schmitz, *Dynamic light scattering by macromolecules*, (Academic press, 1990).
- (7) V. Patravale, P. Dandekar, R. Jain, Nanoparticulate drug delivery: perspectives on the transition from laboratory to market, (*nanoparticulate drug delivery*, 87–121, 2012).
- (8) E. Lau, size and shape fluctuations of Large Unilamellar Vesicles as investigated using light scattering. 1992.
- (9) P Maity, B Saha, G.S Kumar, S Karmakar, Binding of monovalent alkali metal ions with negatively charged phospholipid membranes. *Biochim. Biophys. Acta, Biomembr.* 2016, 1858, 706 – 714.
- (10) J. R. Lakowicz, *Principles of Fluorescence Spectroscopy*, (Springer, 1988).
- (11) M. Hof, V. Fidler, R. Hutterer. *Basics of Fluorescence Spectroscopy in Biosciences*, (Springer, 3-29, 2005).

- (12) O.A. Kucherak, S. Oncul, Z. Darwich, D.A. Yushchenko, Y. Arntz, P. Didier, Y.Mely, A.S. Klymchenko, Switchable Nile red-based probe for cholesterol and lipid order at the outer leaflet of biomembranes, *J. Am. Chem. Soc.* 2010, 132, 4907–4916.
- (13) A. Halder, B. Saha, P. Maity, G. S. Kumar, D. K. Sinha and S. Karmakar, Lipid chain saturation and the cholesterol in the phospholipid membrane affect the spectroscopic properties of lipophilic dye Nile red, *Spectrochim. Acta, Part A*, 2018, 191, 104 —110.
- (14) J.R. Lakowicz, *Principles of Fluorescence Spectroscopy*, Kluwer-Plenum Press, New York, 1999.
- (15) M. R. Duff Jr, J. Grubbs, E. E. Howell, Isothermal titration calorimetry for measuring macromolecule-ligand affinity, *Journal of Visualized Experiments*, 2011, 55, 1- 4.
- (16) T.M Domingues, B Mattei, J Seelig, K.R Perez, A Miranda, K.A Riske. Interaction of the Antimicrobial Peptide Gomesin with Model Membrane: A calorimetric Study. *Langmuir* 2013, 29, 8609 – 8618.
- (17) A Sannigrahi, P. Maity, S Karmakar, K Chattopadhyay. Interaction of KMP-11 with Phospholipid Membranes and Its Implications in Leishmaniasis: Effects of Single Tryptophan, Mutation and Cholesterol. *J. Phys. Chem. B*, 2017, 121, 1824 – 1834.
- (18) Frits Zernike. "Phase contrast, a new method for the microscopic observation of transparent objects part I". *Physica*. 1942, 9 (7), 686–698.

Chapter 3

Interaction of an antimicrobial peptide NK-2 with Phospholipid Membrane: Evidence of pores in the membrane

3.1 Introduction

As discussed in chapter 1, Antimicrobial peptides (AMPs) have a wide range of inhibitory effects against bacteria, fungi, parasites and viruses. NK-2, derived from a cationic core region of NK-lysin, displays antimicrobial activity toward negatively charged bacterial membranes. The major component of phospholipids in cell membrane is phosphatidylcholine (PC). The major constituents of bacterial membranes are phosphatidylethanolamine (PE) and phosphatidyl-glycerol (PG) (~4:1). Therefore, in our present study, we have chosen model systems, composed of dioleoyl phosphatidylglycerol (DOPG) and mixtures of DOPG with dioleoyl phosphatidylethanolamine (DOPE) and dioleoyl phosphatidylcholine (DOPC). These lipids also show fluid phase at room temperature (25 °C). As model membranes, we have used large unilamellar vesicles (LUVs) to study the interaction of NK-2 with different phospholipids using isothermal titration calorimetry (ITC), ζ potential, and dynamic light scattering (DLS).

This chapter deals with the binding affinity of NK-2 with negatively charged phospholipid membranes. The electrostatic behavior as well as the size distribution of the membranes in the presence of NK-2 was systematically characterized using ζ potential and DLS, respectively. Thermodynamics of the interaction of this system have been thoroughly investigated using ITC study. An evidence of trans-membrane pores in negatively charged phospholipid membranes in presence of nk-2 was seen using phase contrast microscopy. The Earlier studies are summarized in section 3.2. All experimental results have been discussed in section 3.3. We conclude this chapter in section 3.4.

3.2 Earlier studies

Antimicrobial peptides (AMPs) are an innate immune response in animal and human body against invading pathogens, such as viruses, fungi, bacteria, etc. (1,2). They target the bacterial membrane, especially negatively charged surface, and create defects, such as pores, leading to disruption of the membrane (3). An important property of AMP is the specificity of bacterial targets and excludes the killing of most eukaryotic cells (4). The resistance to conventional antibiotics and the natural cell lytic activity of many AMP and their unique mode of action have led to a new possibility in the development of AMP as human therapeutics (5). Therefore, studies on the interaction of AMP with lipid membranes have drawn a lot of attention due to their potential biomedical applications (1,6–8). Diverse applications of AMP include as anti-infective agents, anticancer agents, drug delivery and nonviral gene transfer (1,9). A major problem that has impeded the development of drug design is the toxicity. NK-2, an AMP, which is nontoxic and nonhemolytic to the human skin cells, can be a potential candidate for designing antibiotics (10). NK-2 is a water soluble linear amphipathic helical peptide (8). It is the highest density region of NK-lysin having cationic charge of +10 at physiological pH. The high positive charges within the NK-2 promote strong binding to the negatively charged membranes (11). The antimicrobial activity of NK-2 toward parasitic membranes involves the interaction with lipids in the membranes. A teleost NK-lysin peptide, NKLP27, is known to induce degradation of bacterial DNA and inhibits bacterial and viral infection (12). There have been a large number of studies of many AMP, using a variety of experimental techniques, such as optical microscopy (13–16), oriented circular dichroism (17), X ray and neutron scattering (18), isothermal titration calorimetry (ITC) (19), and differential scanning calorimetry (20). However, very little is known in the case of NK-2. NK-2 impels significant changes in cellular morphology of human cancer cells and eventually cells lose their cellular integrity until destruction (21). NK-2 intercalates and binds to the negatively charged membranes, such as 1,2-dipalmitoyl-sn-glycero-3-phosphoglycerol (DPPG) and 1,2-dioleoyl-sn-glycero-3-phospho-L-serine (DOPS), but does not interact with the phosphatidylcholine (PC) or sphingomyelin, as revealed by the fluorescence resonance energy transfer (21) and ζ potential (22). Conformational changes as well as the orientation of AMP play a vital role in the formation of transmembrane pores (7,21). Previous study of NK-2, dissolved in different aqueous solutions, has shown mainly α -helical conformation in the presence of negatively charged amphiphiles (8). Similar α -helical confirmation in the membrane environment has also

been found in other AMP, such as melittin (23) and Magainin 2 (24). However, NK-2 adopts an unoriented random coil structure in the buffer, including water and in the presence of cationic and neutral amphiphiles below their critical micellar concentration. The conformational transition from random coil to helix arises mainly due to electrostatic interaction of positively charged residues of the peptide with the negatively charged head group of amphiphiles (8). However, penetration of peptides into the hydrophobic core is a result of hydrophobic interaction between the hydrophobic chain of the amphiphiles and hydrophobic residues of the peptide.

Lipopolysaccharide (LPS), the major constituent of the outer membrane of gram negative bacteria, shows strong binding affinity to NK-2, as determined by various experimental techniques, such as small angle X-ray diffraction, ζ potential, and isothermal titration calorimetry (10). It is believed that the main pathway to disrupt the integrity of the cellular membrane is the formation of transmembrane pores. Different AMPs seem to follow different pathways to create transmembrane pores (25). Therefore, in spite of a large number of attempts, the mechanism of transmembrane pore formation is still under dispute (6,26). For example, molecular electroporation was proposed as the mechanism of membrane pore formation, induced by NK-lysin (27).

Biological membranes are complex, regulated by various membrane components. Therefore, it is often useful to study model membranes to understand more complex lipid-peptide interactions and hence to get some insight into the mechanism of cellular damage induced by AMP. Giant unilamellar vesicles (GUVs), made from lipid molecules, serve as an excellent model system to study many biological activities (28). For example, a kinetic process involving interaction of melittin and other AMP with PC vesicles have previously been demonstrated using the micropipette aspiration technique (13) and leakage assay using fluorescence spectroscopy (14,16). It was found from previous studies of various AMP that the activity of pore formation initiates above a threshold lipid to the peptide ratio (~ 70 for melittin) (13,17). This threshold seems to be different for different peptides. There have not been systematic studies on the interaction of NK-2 with phospholipid membranes. Therefore, there are several open questions which have not been addressed in the literature. Does NK-2 make pores on the membranes, as in the case of other AMPs? If NK-2 makes pores, what is the mechanism that NK-2 uses to form transmembrane pores? How does the size of pores depend on lipid composition and concentration of NK-2? Although there was a previous study on the interaction of NK-2 with LPS,11 the binding affinity

of NK-2 with negatively charged phospholipid is still not well understood. It is also important to know how the binding affinity of NK-2 with phospholipids depends on the head group charge and size of the head group. It would also be interesting to observe any morphological change induced by NK-2 in the model membrane.

The major constituents of bacterial membranes are phosphatidylethanolamine (PE) and phosphatidyl-glycerol (PG) (~4:1) (20). Therefore, in our present study, we have chosen model systems, composed of dioleoyl phosphatidylglycerol (DOPG) and mixtures of DOPG with dioleoyl phosphatidylethanolamine (DOPE) and dioleoyl phosphatidylcholine (DOPC). These lipids also show fluid phase at room temperature (25 °C). As model membranes, we have used large unilamellar vesicles (LUVs) to study the interaction of NK-2 with different phospholipids using isothermal titration calorimetry (ITC), ζ potential, and dynamic light scattering (DLS). In particular, the electrostatic behavior as well as the size distribution of the membranes in the presence of NK-2 was systematically characterized using ζ potential and DLS, respectively. Thermodynamics of the interaction of this system have been thoroughly investigated using ITC study. We have determined, for the first time, the binding affinity of NK-2 with negatively charged phospholipid membranes.

3.3 Experimental results

3.3.1. The membrane-membrane interaction induced by NK-2

Size distribution of LUV, made from different lipid and lipid mixture, has been measured before and after the interaction of NK-2 using dynamic light scattering (DLS). DLS technique can, in principle, provide the evidence of membrane-membrane interaction induced by NK-2. LUVs composed of pure DOPC and DOPG were found to be very stable, as no significant change in the size distribution was seen in DLS measurement even a couple of months later. The extrusion of MLV gives the average diameter of the vesicle ~ 100 nm. The average diameter of LUV at different NK-2/lipid ratios is presented in Figure 3.1. The error bars in Figure 3.1 represent the width of the distribution, which is a measure of polydispersity of LUV. This error is relevant for understanding the effect of NK-2 on the membranes. However, errors, obtained from different measurements, are

small and are not shown in the plot. Neutral LUVs, made from DOPC and a mixture of DOPC and DOPE, do not exhibit any significant change in their size distribution in the presence of NK-2 (Figure 3.1a). However, the average size of the negatively charged LUV increases with increasing Cnk2. Interestingly, LUVs made from pure DOPG show a dramatic increase in their average size in the presence of NK-2 (Figure 3.1b). The width of the size distribution (error bar in Figure 3.1), indicating polydispersity, also increases with the increase of C_{nk2} . In all samples containing DOPG, transparent LUV dispersion becomes turbid after ITC measurement. Therefore, as the NK-2/lipid ratio is increased, the sample exhibits a high value of size as well as high polydispersity and eventually shows large aggregates. After a couple of hours, the sample appears very turbid and hence the sample was not suitable for DLS measurement. This behavior clearly indicates that sample contains large aggregates induced by NK-2.

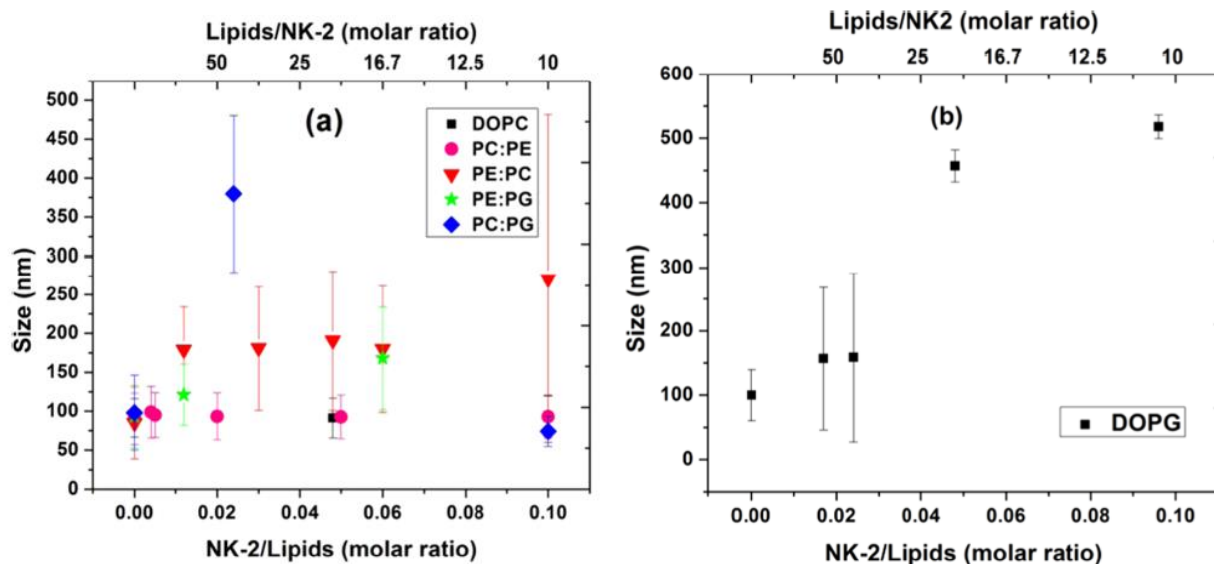


Figure 3.1: Size distribution of LUV made from various lipid compositions in the presence of NK-2. (a) LUV are composed of DOPC and other phospholipid mixtures, as indicated by the figure legend. (b) LUV composed of DOPG. Error bar is the standard deviation and was obtained from the width of the distribution.

3.3.2 Binding affinity of NK-2 with negatively charged membrane as envisaged from zeta potential:

The summary of results on ζ potential is illustrated in Figure 3.2. The ζ potential was measured in LUV dispersion, made from DOPC, DOPG, DOPE–DOPG (4:1) mixture, and mixtures of DOPC with DOPE and DOPG, before and after introducing peptides (i.e., before and after ITC measurements).

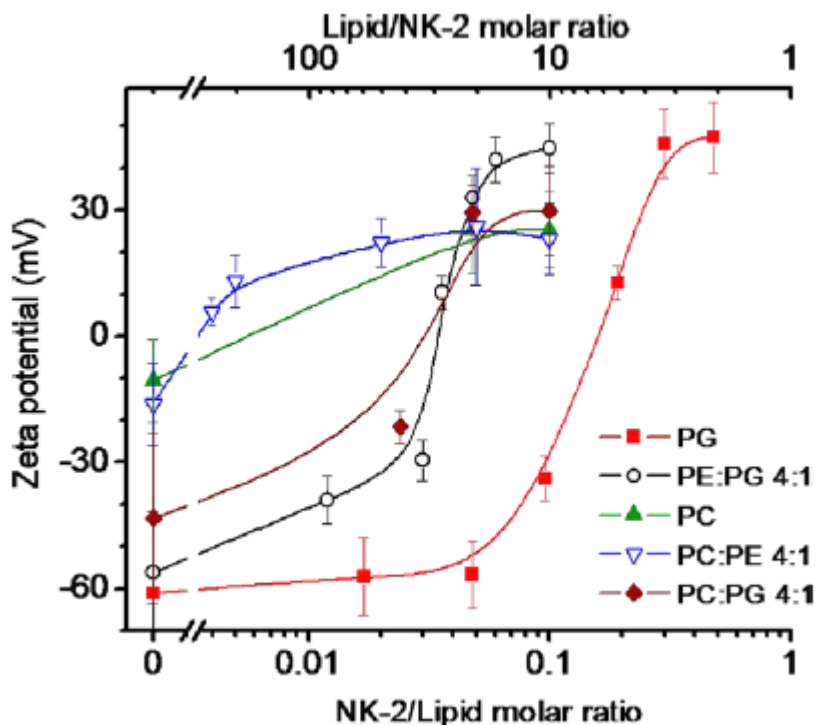


Figure 3.2: ζ Potential of phospholipid LUV at various NK-2 to lipid molar ratios. Solid lines are intended only as guides to the points. Error bars indicate the width of the distribution profile of ζ potential.

As shown in Figure 3.2, ζ potential increases with increasing NK-2 to lipid molar ratio (NK-2/L) and charge compensation occurs at different NK-2/L for different lipid mixtures. Although phospholipids, such as DOPC and a mixture of DOPC–DOPE, are neutral, they exhibit a low negative value. A small negative ζ potential gets neutralized at NK-2/L, $\sim 1:250$. In comparison, charge neutralization happens for DOPG at much higher NK-2/L (1:5). For DOPE–DOPG (4:1) mixtures, charge compensation occurs at intermediate NK-2/L (1:25). These differences are due

to the fact that charge compensation occurs with respect to charge lipids. Interestingly, the ζ potential shows its saturation value, indicating overcharge compensation at different NK-2/L for various lipid mixtures (Figure 3.2). The ζ potential of DOPG shows a saturation at a much higher NK-2/L (3:10) than that of DOPC and DOPC–DOPE (1:250), whereas the ζ potential for DOPE–DOPG and DOPC–DOPG mixtures shows this at intermediate NK-2/L (1:20). The above result clearly indicates that NK-2 has a stronger affinity toward the negatively charged lipids. This is indeed an essential requirement for an AMP to exhibit antimicrobial activity. We now present a theoretical description of the interaction in terms of binding free energy, binding constant and other binding parameters pertaining to the system. The minimal and maximal values of the zeta potentials were used to infer binding free energies for NK-2 using the following ansatz.

Theory: The overall binding free energy, ΔG_{app} denoted as apparent binding free energy for a given lipid composition, is given by

$$\Delta G_{app} = \Delta G_{el} + \Delta G_{int} \quad (1)$$

where, ΔG_{el} is the electrostatic and ΔG_{int} the intrinsic binding free energy. The intrinsic binding free energy presumably arises from the amphiphilic nature of the peptide and the lipids leading to binding affinity *via* the hydrophobic effect. The electrostatic binding free energy is given by

$$\Delta G_{el} = q_p \zeta \quad (2)$$

Where, ζ is the zeta potential and q_p be the effective peptide charge which is the charge of the bare peptide ($q_p = +10 e$) minus the charge of the counterions released upon peptide binding. Therefore, we require to reckon the effective peptide charge q_p . As ΔG_{el} and hence, ΔG_{app} , depend on ζ which varies with peptide concentration, c_p , both free energies also depend on c_p . As the liposomes are negatively charged and the peptide is cationic, the binding affinity will be highest in the limit of low peptide concentrations, that is, the values of ΔG_{el} and ΔG_{app} are lowest in the limit $c_p \rightarrow 0$. The value of ΔG_{app} in this limit denoted as $\Delta G_{app,0}$ obeys

$$\Delta G_{app,0} = q_p \zeta_0 + \Delta G_{int}. \quad (3)$$

This quantity is denoted as standard binding free energy. It is a measure for the affinity of NK-2 to membranes with a given lipid composition in the limit of low peptide concentrations where,

intermolecular interactions between different NK-2 molecules can be neglected (dilute peptide concentrations).

The experiments show that for increasing peptide concentrations, the zeta potential increases and eventually becomes positive. If $\zeta > 0$ also the electrostatic binding free energy is positive. The maximal surface coverage by the cationic peptides, indicated by the plateau in the zeta potential at the maximal value ζ_{max} is reached when $\Delta G_{app} = 0$, hence $q_p \zeta_{max} + \Delta G_{int} = 0$, i.e.

$$\Delta G_{int} = -q_p \zeta_{max} \quad (4)$$

This implies $\Delta G_{int} < 0$ as we indeed find in the present study. The maximal surface charge, σ_{max} is inferred *via* the Grahame or Gouy equation,

$$\sigma_{max} = \sqrt{8\varepsilon_w \varepsilon_0 R T C_{ion}} \sinh\left(\frac{e\zeta_{max}}{2K_B T}\right) \quad (5)$$

where $\varepsilon_w = 80$ denotes the relative dielectric permittivity (or dielectric constant) of water, ε_0 the relative dielectric permittivity of vacuum, R ($= 8.31 \text{ J} \cdot \text{K}^{-1} \cdot \text{Mol}^{-1}$) is the universal gas constant, K_B ($= 1.38 \times 10^{-23} \text{ J/K}$) is the Boltzmann constant, and $T = 300 \text{ K}$ the absolute temperature. C_{ion} being the concentration of ions present in the electrolyte. Here we approximate the surface potential by zeta potential. This is a good approximation at low peptide concentration. It is assumed that's surface charges are smeared uniformly over the entire membrane surface and solvent is treated as continuous medium of fixed dielectric constant. Although use of Gouy Chapman theory underestimates the membrane association for high peptide concentration and overestimate due to adsorption of multivalent ions on the membrane, we could estimate the order of magnitude of maximal surface charge (29,30). From σ_{max} the surface charge due to the membrane-bound peptides, σ_p is estimated from

$$\sigma_p = \sigma_{max} - \sigma_0. \quad (6)$$

Here, σ_0 is the surface charge at peptide-free conditions which is estimated from ζ_0 using equation 5, replacing σ_{max} by σ_0 and ζ_{max} by ζ_0 . From σ_0 , the surface charge from membrane-bound counterions, σ_I is estimated *via*

$$\sigma_I = \sigma_0 - \sigma_L \quad (7)$$

Here, σ_L denotes the surface charge from the lipids. For pure DOPG, σ_L is given by $\sigma_L = -\frac{e}{a_L}$ where a_L denotes the average area per lipid. The area per lipid for pure DOPC and DOPG was determined from the MD simulations (31), yielding $a_{L,PC} = 0.73 \text{ nm}^2$ for DOPC And $a_{L,PG} = 0.65$

nm² for DOPG (32). The average area per lipid for the 4:1 DOPC/DOPG mixture, $a_{L,mix}$ was determined from $a_{L,mix} = \frac{4 a_{L,PC} + a_{L,PG}}{5}$. The surface charge from membrane-bound counterions is $\sigma_I = \alpha \frac{e}{a_L}$, where α denotes the fraction of lipids binding a counterion, i.e, $\alpha = \frac{\sigma_0 - \sigma_L}{\sigma_L}$. Hence, the charge of counterions released upon peptide binding, q_I , is estimated *via*

$$q_I = \alpha e n_L \quad (8)$$

Here, n_L is the number of lipids covered by a membrane-bound peptide as determined from $n_L = \frac{a_P}{a_L}$, where a_P denotes the area of the peptide. To estimate a_P , we consider that NK-2 when bound to a membrane is α -helical and that an α -helix has a thickness of $d = 0.54$ nm and a length of $l = 0.15$ nm times the number of residues, N , which is $N=27$ here. Assuming that the helix is parallel to the membrane surface in agreement with the experimental observation by Olak et al.(33), the peptide thus covers a membrane area of $a_P = dlN = 2.2$ nm² From q_I , the effective peptide charge is obtained *via*

$$q_p = q_P - q_I \quad (9)$$

The results of our analyses for the two different lipid compositions are listed in Table-1. The relative standard binding free energy for DOPG is $\Delta\Delta G_{DOPG} = 35 (\pm) 13$ kJ/mol.

It is interesting to mention that no significant effect was found in the gel phase of DPPC as reported by Willumeit et al (34). Further, NK-2 has no considerable influence even on fluid phase of POPC as revealed by x-ray scattering and Fourier transform infra-red spectroscopy. NK-2 with membrane is primarily governed by electrostatic attraction, it is expected that NK-2 would have very little effect of no influence on the neutral membrane. Therefore, it is naive to compare earlier results on neutral membrane with our zeta potential of the anionic membranes. Our analysis of experimental results is in agreement with the simulation study by Knetch et al, where they showed the stronger affinity of negatively charged vesicles and also estimated the binding free energies of transfer of NK-2 on the membrane (35). The decrease in maximal surface charge membrane and concomitant decrease the free energy in DOPC-DOPG membrane suggests that presence of PC interaction becomes much weaker. Further previous study already established that NK-2 does not exhibit significant interaction with the DOPC membranes. This study implicates that NK-2 primarily interacts with the negatively charged membranes which is indeed the pre-requisite for antimicrobial activity. Therefore, the difference in composition of the membrane helps NK-2 to discriminate the bacterial membrane from the eukaryotic cells.

It is important to mention that besides electrostatic contribution, hydrophobic interaction as well as the increase in membrane tension due to adsorption of NK-2 on the membrane play a significant role in antimicrobial activity. Although we have not explored effect of hydrophobicity and membrane tension in this study, we could as well hypothesize that the role of these parameters in the context of antimicrobial activity of NK-2 would also be similar as in the case of other alpha helical cationic peptides (36,37).

Table–1: Minimal and maximal zeta potentials observed experimentally, ζ_0 and ζ_{max} , and quantities hence inferred. Given are the surface charge at peptide-free conditions, σ_0 , the maximum surface charge density σ_{max} , the effective peptide charge, q_p , the intrinsic binding free energy, ΔG_{int} , the total standard binding free energy, $\Delta G_{app,0}$.

Lipids	Zeta potential (mV)		Surface charge (C/m ²)		Effective peptide Charge q_p (e)	Binding free energies KJ/mol	
	ζ_0	ζ_{max}	σ_0	σ_{max}		ΔG_{int}	$\Delta G_{app,0}$
DOPG	-61±18	47±8	-5.5×10 ⁻³	3.8×10 ⁻³	6.69	-36	-75
DOPC/DOPG (4:1)	-43±20	30±11	-3.5 ×10 ⁻³	2.3×10 ⁻³	7	-20	-59

3.3.3 Binding affinity of NK-2 with model membranes measured from ITC.

NK-2 of various concentrations, C_{nk2} (100, 50, 40, 30, 25, and 10 μ M) was titrated with 4 mM of LUV made from the DOPE–DOPG (4:1) mixture. For first few injections, heat flow remains constant, then starts decreasing as less and less NK-2 is available for binding. Typical raw data of ITC measurement at $C_{nk2} = 50 \mu$ M are shown in Figure 3.3.

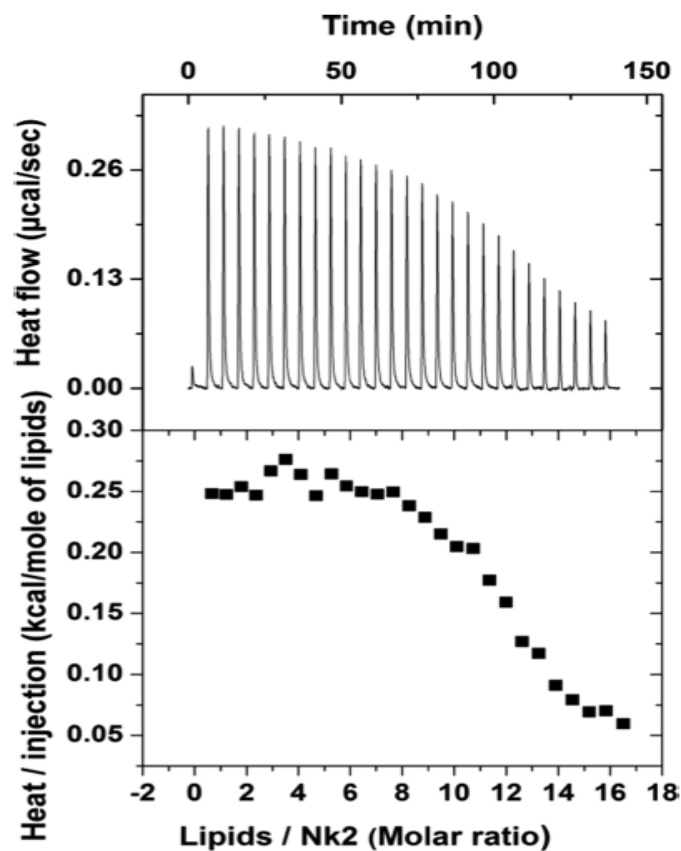


Figure 3.3: Titration calorimetry of 50 μM NK-2 with 4 mM DOPE–DOPG (4:1) LUV (top); normalized heat of injection/mole of lipids, obtained from the integration of the individual peak (bottom). Heat of dilution, obtained from injecting 4 mM LUV into buffer, was subtracted from the actual measurement. Here we assume, lipids from both monolayers interact with the NK-2.

The lipid to NK-2 (L/NK-2) ratio at which saturation of the heat flow occurs is $\sim 20:1$, taking into account all lipids (i.e., both monolayers of the LUV) interacting with the NK-2. The overall binding reaction was endothermic for all C_{nk2} . Interestingly, when the endothermic signal attains its saturation at $\sim L/NK-2 = 20$, further successive one to three injections show an exothermic signal and then successive injections contribute almost negligible heat (data not shown). This behavior is displayed in the raw ITC thermogram when lower C_{nk2} , typically $<40 \mu\text{M}$, was used. For these concentrations, saturation occurs before completing all injections of LUV. At the beginning of the titration, there are plenty of peptides to bind with lipids. Therefore, we have

analyzed the data taking into account only the initial part of the endothermic heat signals or the data where all injections of LUV have been finished before the exothermic peaks appear, i.e., for $C_{nk2} > 40 \mu\text{M}$. Although some of the isotherms can be fitted to one site binding model given by microcal origin, it gives us the apparent binding constant (K_{app}), which is expected to vary with concentrations of unbound or free NK-2 concentration. However, the order of magnitude of the K_{app} has been found to be consistent with the value obtained from the surface partition model. As the interaction of NK-2 with the negatively charged membranes is primarily driven by the surface charge of the membranes, it is desirable to fit the data taking into account the electrostatic contributions. Therefore, the more relevant parameter would be the intrinsic binding constant (K_{int}), where the surface concentration of peptide (C_M) is more relevant than the bulk or free peptide concentration (C_f).

The model parameters, such as the extent of peptide binding (X_b), C_f , C_M , K_{int} , etc, obtained numerically from experimental data, have been summarized in Table 2.

Table 2. Parameters obtained from each data point in an ITC experiment using the surface partition model including electrostatic contribution^a

Lipid+peptide	Lipid/NK-2	C_f (mM)	$C_M \times 10^{-6}$ (mM)	X_b	K_{int} (M^{-1})
DOPG (5 mM) + NK-2 (0.1 mM)	0.34	0.08	3.29	0.420	1.28×10^8
	0.62	0.07	2.86	0.414	1.45×10^8
	0.90	0.06	2.41	0.422	1.75×10^8
	1.19	0.05	1.97	0.422	2.14×10^8
	1.47	0.04	1.58	0.415	2.64×10^8
	1.76	0.03	1.20	0.407	3.41×10^8
	2.05	0.02	1.33	0.395	2.98×10^8
	2.34	0.01	1.07	0.381	3.56×10^8
	2.63	0.01	0.96	0.365	3.80×10^8

DOPE–DOPG (4:1-4 mM) + NK- 2 (0.05 mM)	1.79	0.047	16.2	0.121	7.52×10^6
	2.36	0.045	15.4	0.112	7.30×10^6
	2.93	0.042	14.6	0.110	7.56×10^6
	3.51	0.040	13.8	0.108	7.85×10^6
	4.09	0.038	13.0	0.109	8.41×10^6
	4.67	0.035	12.1	0.110	9.11×10^6
	5.26	0.032	11.3	0.110	9.79×10^6
	5.85	0.030	10.5	0.109	10.4×10^6

^a X_b : binding fraction; C_f : free peptide concentration; C_M : intrinsic peptide concentration, K_{int} : intrinsic binding constant. The lipid concentration used in the analysis is the total lipid concentration considering NK-2 interaction with both monolayers of the membrane (38).

In the case of DOPE–DOPG mixture, it is interesting to observe that C_M versus X_b behaves linearly for lower lipid/NK-2, corresponding to 9–10 injections. However, the tendency to increase the value of K_{int} is evident from Table 1. Above 10 injections, the K_{int} increases with increasing the number of injections. Therefore, we have presented only the linear part of the data to estimate the K_{int} . The possible reason for increasing the value of K_{int} at higher lipid/NK-2 has been discussed later. The estimated values of molar binding enthalpy, ΔH , K_{int} , and binding entropy ΔS , obtained from the surface partition model with electrostatic contribution, have been summarized in Table 3.

Table 3. Thermodynamical Parameters of Binding Kinetics of NK-2^{a,b}.

Lipids	ΔH (kcal/mol)	K_{int} (M^{-1})	ΔG (kcal/mol)	$T\Delta S$ (kcal/mol)
DOPG	0.8 ± 0.2	$2.5 \times 10^8 \pm 3.5 \times 10^7$	-13.8 ± 0.2	14.6 ± 0.4
DOPE – DOPG(4:1)	2.9 ± 0.8	$7.3 \times 10^6 \pm 4.5 \times 10^5$	-11.7 ± 0.6	14.6 ± 0.8

^aBinding enthalpy (ΔH), intrinsic binding constant K_{int} , entropy (ΔS), obtained numerically using surface partition model taking into account the electrostatic contribution (39). ^bHere, the K_{int} is the mean value calculated from Table 1. Here, we have assumed NK-2 interacts with both leaflets of the membrane (38). The heat of dilution has been subtracted from all data. ζ Potential in the absence of NK-2 is also shown. The effective charge, z_p , of the NK-2 when binding to the membrane has been taken as 5. Note that ΔH for DOPG was estimated from the first endothermic part (Figure 3.4) of the ITC thermogram.

Titration isotherm of DOPG is shown in Figure 3.4. Surprisingly, it shows few exothermic signals at L/NK-2 (4:1) between two regions of endothermic response. In this case, exothermic peaks begin at much lower L/NK-2 (~ 5). It is important to note that such an exothermic signal also occurs at a similar PG/NK-2 ratio for DOPE–DOPG (4:1) mixture. To understand the detailed behavior of two regions of the isotherm, 100 μM NK-2 was titrated with five different DOPG concentrations (10, 5, 2.5, 1.6, and 1 mM). The second region of the isotherm was accessed when two different C_{nk2} (50, 35 μM) were titrated with 10 mM DOPG LUV. At present, we are not able to fit the entire isotherm with the model available in the literature. However, we have determined the average thermodynamic parameters obtained from the first region using a partition model, taking into account the electrostatic contribution. The parameters obtained from the model have been presented in Table 2. In the model, we have reduced the effective charge of the NK-2 starting from the maximum charge +10 and found the linear relationship between X_b and C_M at $z_p = 5$. This can also be realized as L/NK-2 ~ 5 to neutralize the membrane.

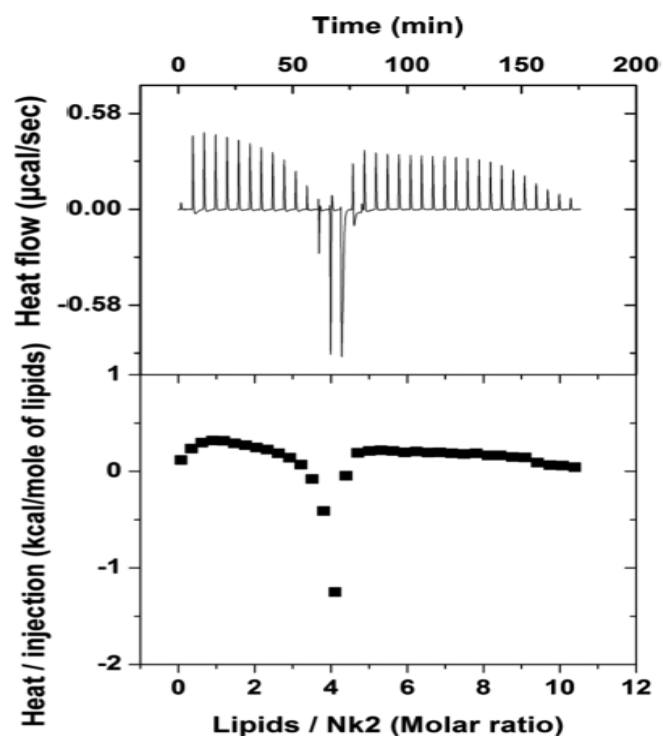


Figure 3.4: Raw titration calorimetry data of DOPG, where NK-2 of 100 μM is titrated with 5 mM of DOPG LUV (top); the corresponding normalized heat per injection obtained from the integration of the individual peak (bottom). Here, we have assumed NK-2 interacts with all lipids.

The large binding constants in the case of DOPG and DOPE–DOPG mixture, as shown in Table 2, suggest that NK-2 strongly binds to negatively charged membranes. Therefore, it is interesting to check the affinity of NK-2 with neutral lipids, such as DOPC and DOPE. Unfortunately, LUVs from DOPE alone are not formed using the extrusion method used here. This is because PE bilayers are more rigid than PCs in the fluid phase due to hydrogen bonding between the head groups (39). Therefore, bending of PE bilayers costs more energy, which in turn prevents the formation of unilamellar vesicles. Therefore, a mixture of DOPE–DOPC (4:1) was used to investigate the influence of PE in the binding isotherm. A 100 μM NK-2 was titrated with 10 mM DOPE–DOPC (4:1). For comparison, 10 mM of DOPE/DOPC (1:4) mixture was injected in to three different C_{nk2} (10, 100, and 200 μM). Similar experiments were done for DOPC. For DOPE–DOPC (4:1), the heat signal is stronger than that of DOPE–DOPC (1:4) but weaker than that of the DOPE–DOPG mixture. In all above mixtures, the binding reaction is endothermic, whereas the

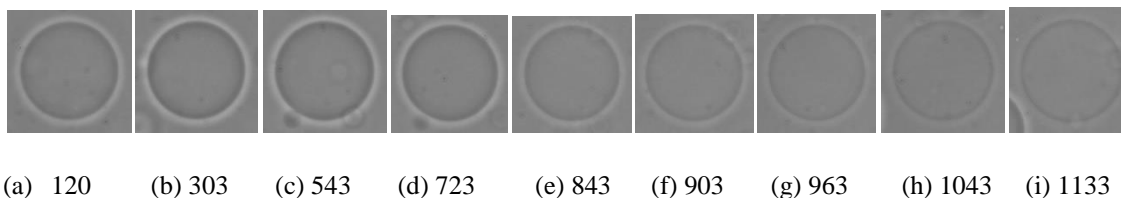
simple dilution experiment shows an exothermic response. The interaction of NK-2 with DOPC and DOPC–DOPE LUV is too weak to obtain a binding constant and other thermodynamic parameters. Considering all ITC results, we can easily conclude that the interaction of NK-2 with PE is stronger than with PC but weaker than with PG (PG \gg PE > PC).

3.3.4 Observation of trans-membrane pores (Microscopy results)

Phase contrast microscopy on GUV has been performed in order to visualize directly the antimicrobial activity of NK-2 and also to obtain complementary information on the results obtained from DLS and zeta potential measurements. Previous studies of some other AMP have reported the evidence of transmembrane pores using fluorescence leakage (40) and micro-pipette aspiration (41). We have avoided in incorporating any fluorescence dye into the membrane, as the interaction of AMP with membranes might be affected by fluorescence dye. GUV, made from DOPC and mixtures of DOPC with DOPG at 4:1, were observed with three different C_{nk2} (1.3, 0.9, 0.45 μ M). Pure DOPG did not seem to form GUV. The tendency to adhere the negatively charged lipid into the positive electrode might prevent the swelling of lipid film, which may not facilitate the formation of GUV (42). Therefore, we have not used pure DOPG for GUV formation. If NK-2 forms pores in the membranes, we would expect leakage of internal fluid through the pores. Therefore, halo regions are expected to disappear with time and GUV should look similar to that without diluting in glucose. Experiments on GUV, exposed to NK-2, show direct evidence of formation of trans-membrane pores. Change in the difference of the gray value (I_{ptp}) of the halo region with time for DOPC-DOPG (4:1) GUV, as shown in Figs. 3.5 (a-i), indicate leakage of internal fluid, leading to the loss of contrast. I_{ptp} decreases until GUV completely loses its contrast in the halo region. We have compared I_{ptp} between GUV, exposed to NK-2 and GUV without NK-2, but the interior and exterior regions contain the same glucose solution. (Fig. 3.5 j). This behavior is attributed to the fact that pores are large enough to permeate the sucrose and glucose molecules and fluids between the interior and exterior of the GUV, leading to loss of contrast in the halo region. Pores are found to be stable, as GUV remain stable with time. If it would have been transient pores, one would not expect such contrast loss due to exchange of fluids as time scale of pore fluctuations is much faster than rate of exchange or diffusion of large size molecules, like glucose or sucrose. Since we have looked at an average response of many GUV, exposed to

NK-2, it was not possible to determine the exact ratio of NK-2/L. However, rough estimation yields NK-2/L = 0.05 to 0.1 where, zeta potential already show saturation. Previous isothermal calorimetric study also exhibits saturation of heat signal at these NK-2/L. Different GUV seems to take different time to initiate pore formation. Therefore, we cannot precisely determine the time point to initiate pore formation for individual vesicle at different C_{nk2} , as the average response of many GUV was obtained in our study. However, we can unambiguously determine the behavior of the rate constant (k) for different C_{nk2} . Decaying part in Fig. 3.5 (j) was fitted to exponential decay in order to estimate k . For 0.45 μM of NK-2, k was found to be 0.007 sec^{-1} . For $C_{nk2} = 0.9$ and 1.3 μM , k were obtained as 0.01 and 0.03 Sec^{-1} respectively. Therefore, I_{ptp} (Fig. 3.5) decreases much faster at higher C_{nk2} than that of lower C_{nk2} . We did not seem to observe any significant change in size of GUV with time. GUV does not show any significant change in I_{ptp} with time in the absence of NK-2 (as shown by a diamond symbol in Fig. 3.5 j). GUVs, made from DOPC do not show significant decrease in I_{ptp} in the presence of NK-2, indicating NK-2 does not form pores on these membranes. This behavior is supported by the fact that NK-2 has very weak binding affinity to PC, which is consistent with the results obtained from zeta potential.

It is clear from our observation (Fig 3.5) that NK-2 modifies the permeability of the membranes, which is in agreement with previous studies of similar system (40,43,44). Leakage of internal fluid, leading to decrease in I_{ptp} suggests the formation of transmembrane pores in DOPC-DOPG GUV (Fig.3.5 a-i and j). No significant change in I_{ptp} as shown in Fig.4 (k) for DOPC, suggests that NK-2 has no significant influence on PC vesicles, in contrast with other AMP, such as melittin (44) and Maculatin (40).



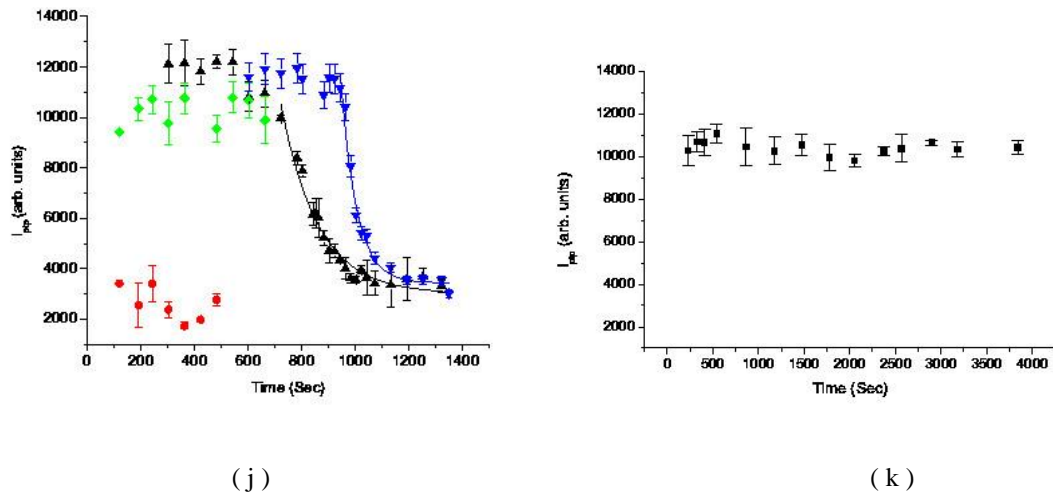


Figure 3.5: (a-i) Microscopy images of GUV (diameter = 48 μm), made from DOPC-DOPG (4:1) mixture, exposed to 0.45 μM NK-2. Numbers, below the images, indicate time sequence in second at which images are captured. This is a direct visualization of membrane leakage induced by NK-2 due to pore formation without perturbing membrane with any fluorescence dye. (j) Kinetic of pore formation obtained at $C_{nk2} = 0.45 \mu\text{M}$ (Δ) and $C_{nk2} = 1.3 \mu\text{M}$ (∇). Diameters of GUV in these two C_{nk2} are 24 μm and 48 μm , respectively. For comparison kinetics of DOPC GUV (diameter 22 μm), exposed to NK-2 at $C_{nk2} = 0.45 \mu\text{M}$, is shown in (k). Rate constant k , obtained from the fit to exponential decay function (Indicated by solid lines) were 0.007 and 0.03 Sec^{-1} for $C_{nk2} = 0.45$ and 1.3 μM , respectively. I_{ptp} , indicated by circles (\bullet) are obtained from GUV, having no density contrast between interior and exterior of it. I_{ptp} indicated by diamond (\diamond) show GUV without exposed to NK-2, but having contrast between interior and exterior of it. Error bars are standard deviations of three independent measurements of I_{ptp} in a single GUV.

The time scale involved to initiate the pore formation process for various C_{nk2} was difficult to conclude in the present study, as I_{ptp} was found to decrease at different time for various GUV at a given C_{nk2} . The difference in amount of PG in each GUV could result such behavior, as NK-2 mainly interacts with PG. A slight variation of C_{nk2} in different parts of the sample, pore size, size of GUV are also key factors in determining the time scale involved in the process of pore formation. Dependence of k with the C_{nk2} was derived at three different C_{nk2} . Larger τ at higher C_{nk2} (Fig. 4 (j)) can be a result of larger pore size or larger number of pores than that of lower

C_{nk2} . Structure and charge of AMP might have an important role in determining the time scale involved in the process of pore formation.

Recent experiments on non-labelled antimicrobial peptide PGLa suggest the translocation of peptide without pore formation (45). However, previous literatures also suggest that PGLa forms transmembranes pores (46,47). Further, a computer simulation at all-atomistic level reported that individual peptide spontaneously translocates across the membrane without forming pores (48). Such translocation begins with tilting of individual peptide and finally deep insertion in the membrane core occurs due to interaction three peptide in mutual contact. This process facilitates the opening of transient water channel through which peptide enters into the lumen of GUV. In the present study we could rule out this possibility as the contrast loss of GUV remains stable. Further, aggregation of vesicles due to membrane –membrane interaction in the presence of peptide, as evidenced from DLS study supports the fact that the leakage induced by NK-2 is indeed a collective phenomenon. Therefore, it is unlikely that NK-2 will translocate without pore formation. In order to validate and complement our conclusion on pore formation, we have also looked at GUV in the presence pore forming peptide magainin 2. In preliminary experiment we have found similar exchange of fluid between interior and exterior of GUV (Fig.3.5). As it is well established that magainin 2 forms transmembrane pores (44). As we have observed similar contrast loss, as in the case NK-2, we expect that contrast loss is due to pore formation and not due to any other process, reported in some simulation study (48).

It is clearly evidenced from the zeta potential results that the stronger electrostatic interaction along with some entropic contribution to the binding of NK-2 to the membrane lead to formation of transmembrane pores. It is important to mention that the zeta potential measurements are blind to provide the information on the translocation of NK-2 from outer leaflet to the inner leaflet of the bilayer, leading to change in binding isotherm. Further, vesicles, as impermeable charged sphere, assumed in the zeta potential analysis was also not able to capture the translocation feature of the NK-2. However, we proposed a mechanism of action that NK-2 may translocate through trans-membrane pores as evidenced from the change in the binding isotherm obtained from isothermal titration calorimetry. Previous study has shown that transfer of NK-2 into the membrane results in an increase in area per molecule and hence increases membrane tension (41,44). Although simulation study did not predict the tension induced pores, the micropipette experiments on another AMP, such as, melittin showed increase in membrane tension upon

melittin adsorption on the membrane (41). We believe that NK-2 also increases the membrane tension, as the structure is very similar to the melittin.

3.4 DISCUSSION

A systematic investigation of the interaction of an important antimicrobial peptide NK-2 with model membranes shows strong binding affinity toward the negatively charged lipid, DOPG, as revealed from ITC and ζ potential. The adsorption of NK-2 on the membranes, as indicated by an increase in ζ potential (Figure 3.2), is primarily driven by electrostatic interaction between negatively charged membranes and positively charged NK-2. This is indeed an essential requirement for an AMP to exhibit antimicrobial activity. However, the interaction is very weak in the case of neutral DOPC and DOPC–DOPE membranes. The positive ζ potential (+10 mV) of DOPC LUV at very low NK-2/L (1:250) suggests that NK-2 adsorbs even in PC membranes, which has not been reported in any of the earlier studies. The ζ potential was measured previously for DPPC in the gel phase, suggesting no significant interaction with DPPC (22). However, a more biologically relevant study would be to measure the ζ potential in the fluid phase. Xray scattering and Fourier transform infrared spectroscopy showed that NK-2 has no influence even on 1-palmitoyl-2-oleoyl-sn-glycero-3-phosphocholine vesicles that are in the fluid phase. They have not measured the ζ potential of PC vesicles in the fluid phase. Therefore, we cannot compare our results on DOPC with those obtained in ref (22). However, the behavior of the ζ potential of DOPG and DOPE–DOPG LUV were found to be consistent with those reported in the previous studies for DPPG and DPPE (22) and for LPS (11). Binding of NK-2 to the negatively charged membranes results in charge neutralization.

Therefore, the charge neutralization depends on the amount of charge lipids present on the outer membranes. This explains why very low NK-2/L (1:250) is required to neutralize the membrane charge for zwitterionic phospholipids. The charge neutralization at much higher NK-2/L (1:5) for DOPG suggests binding affinity to PG is much stronger than that to PC. If the binding of NK-2 to charged lipids is only due to electrostatic interaction, one would expect the charge overcompensation at the same ζ potential. The fact that we have obtained charge overcompensation at different ζ potential for different lipids (see Figure 3.2) implies entropic contribution in these

systems. This is consistent with the ITC results in these mixtures. For DOPG, ITC shows saturation, indicating all of the NK-2 binds to the lipids at NK-2/L of $\sim 1:3$, which is very similar to the NK-2/L (3:10) for charge overcompensation, as found from ζ potential. Similarly, ITC isotherm for DOPE–DOPG mixtures shows saturation at NK-2/L (1:20), which is again consistent with the results of ζ potential.

It is important to mention that change in the size distribution of the vesicles does not influence the ζ potential significantly. The ζ potential is estimated from the Smoluchowski approximation, where the Henry function $f(\kappa a)$ takes its maximum value as 1.5. In other words, ζ potential is determined from the electrostatic double layer formation, which does not depend on the size of the particle. Therefore, whatever change we observe in the ζ potential is not due to change in size but due to binding of peptide in the membrane.

The DLS technique can, in principle, show the evidence of membrane–membrane interaction mediated by NK-2 or the leakage of LUV induced by NK-2. Size distributions of LUV made from various compositions of phospholipids in the absence and presence of NK-2 clearly indicate stronger affinity of NK-2 toward negatively charged membranes. It is interesting to observe the turbid solution of LUV for those NK-2 concentrations in which the ITC shows saturation before completing all injections. This would mean that when there is no NK-2 available in the solution, LUV, introduced from successive injections can adhere due to electrostatic interaction between negatively charged injected LUV with positively charged LUV already present in the solution. Adhesion can eventually lead to the aggregation of LUV. This result clearly implies the antimicrobial activity of NK-2 toward negatively charged lipids and is consistent with the ζ potential result. Although size distributions do not alter significantly for pure DOPC, the mixture of DOPE and DOPC at 4:1 shows a slight increase in the average size (Figure 3.1a). Further, the presence of PE with PC enhances the heat signals in the ITC experiment. This indicates that PE plays a significant role in the interaction. Therefore, the PE–PG system is indeed an appropriate model system to look at the antimicrobial activity. Interestingly, this composition happens to be the major constituent of many bacterial membranes.

The binding of a positively charged AMP with negatively charged membrane usually leads to exothermic heat signal (49). The overall endothermic response observed in all isotherms is thus intriguing. The overall endothermic response, found in all lipid mixtures, can be explained in terms

of entropy gain in liberating water molecules from the hydration shell of LUV due to adsorption of NK-2 at the interface. Entropic contribution can also arise due to conformational change of NK-2 (random coil to α helix) in the presence of lipids and also reorientation of NK-2 prior to the formation of pores. Such transitions were found for this peptide in a previous study by Olak et al (8). As the initial L/NK-2 ratio is small, we would expect pores in almost all LUVs. This is due to the fact that a threshold NK-2/L is required for the formation of pores and this condition is already achieved at the beginning of the isotherm (13,38). Our microscopy result on giant unilamellar vesicles also shows the leakage of internal fluid, supporting the pore formation on the membrane induced by NK-2. Although the appearance of the exothermic heat signal at PG/NK-2 \sim 5:1 in both DOPE–DOPG and DOPG mixtures is very intriguing, the origin of these exothermic peaks is difficult to confirm at present. However, we believe that when there is no NK-2 available for binding, NK-2 can translocate through the pores and interact with the bare LUV present in the solution due to further injections. This process might lead to closing of pores, resulting in an exothermic heat signal. This hypothesis is based on the assumption that if the pore formation is endothermic, pore closure must be exothermic in nature. It is true that the resultant heat due to pore closure and binding of NK-2 together can cancel out. However, at this stage, the unbound peptide-to-lipid molar ratio is too small to produce considerable heat that can give rise to an endothermic response. Such an exothermic response in between two endothermic regions has not been observed in any of the earlier studies.

Surprisingly, a second set of endothermic regions were obtained in the case of DOPG (Figure 3.4), even though there are no NK-2s available for further binding with LUV. This can be explained qualitatively, as follows. It was known by a previous study that desorption kinetics of NK-2 are much slower than adsorption due to trapping of α helix at the membrane interface (8). Therefore, it is expected that no free NK-2 is available to give rise to a second region of isotherm. Further injections of LUV can lead to attraction toward positively charged LUV already present in the solution. When the membranes of negatively charged LUV come closer to the NK-2, water molecules in the hydration shell start to liberate giving rise to the entropic gain of two membranes of LUV. Such membrane–membrane interaction was also evidenced by the DLS measurement, as the average size of LUV was found to increase.

NK-2 has a strong binding affinity to the lipid bilayer interface, relative to its water solubility, as evidenced from the ζ potential. This leads to an excessive interfacial area due to NK-2 binding, which increases the membrane tension. Such an increase in the membrane tension results in the formation of transmembrane pores (38). It has been shown in the earlier study by Lee et al (38) that the asymmetry of interfacial tension due to one-sided binding could lead to translocation of peptide (melittin) via transient pores. The binding of peptide to both outer and inner monolayers forms a stable pore at a critical peptide-to-lipid ratio. Therefore, it is desirable to use total (current) lipid concentration in the ITC cell to estimate the binding constant. It was also reported earlier that some peptides are not able to translocate across the membrane and only the outer monolayer of the membrane (60% of total lipid) is available for binding (50). One of the striking features obtained in the present study, compared to those of other pore-forming peptides, such as melittin, is that the NK-2 interacts only with negatively charged membranes. On the contrary, melittin can interact significantly with the electrically neutral PC membrane (13).

It is evident from Table 3 that entropic contribution ($T\Delta S$) is much larger than that of enthalpy (ΔH). This is not surprising, as hydrophobic interaction between the hydrophobic part of NK-2 and hydrophobic core of the membranes is entropic in origin. This is also necessary for the transmembrane pore formation, observed in this system. The intrinsic binding constant K_{int} ($= 2.5 \times 10^8 \text{ M}^{-1}$) of NK-2 found in DOPG (see Table 2) LUV is 2 orders of magnitude higher than that obtained from earlier studies of different AMP (49). It is important to note that K_{int} changes significantly with the effective charge z_p of the NK-2. We have optimized the value of z_p at 5 in the model so that a linear relationship of C_M versus X_b with a small intercept was maintained. This value can also be realized from the ratio L/NK-2 for which the charge compensation as well as the saturation of the heat signals occurs. Previous ITC measurements on the NK-2-LPS system have shown similar endothermic and exothermic response to the binding heat depending on the structure of LPS (11). However, these results were not analyzed. As evidenced from Table 2, the slight increase in the K_{int} with increasing lipid/NK-2 is the consequence of membrane–membrane interaction induced by NK-2. This result is also supported by DLS experiment, where we have observed an increase in the size distribution.

The mechanism of action of NK-2 on negatively charged membranes has been inferred from ITC result, as illustrated in Figure 3.5. Initially, positively charged NK-2 in the coiled configuration

(8), when binds to an outer monolayer of the membranes, increases the membrane tension and induces transient pores to translocate NK-2 into the inner monolayer (38).

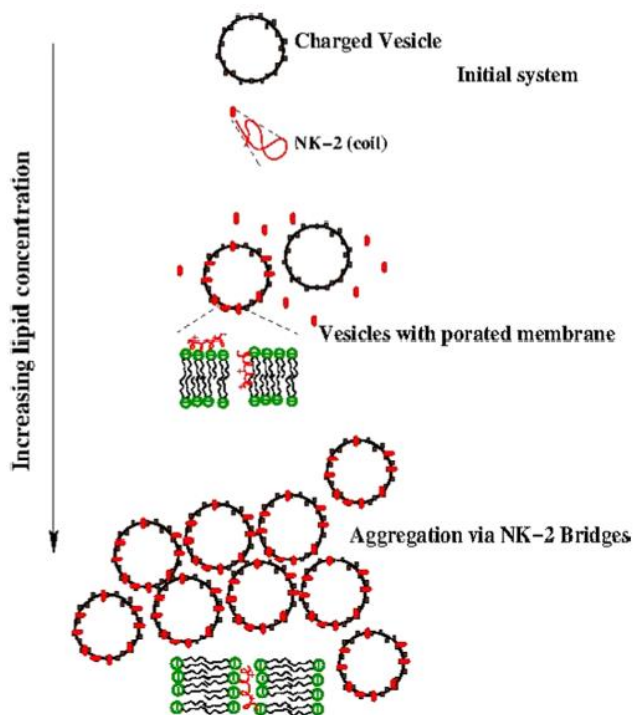


Figure 3.6 Interaction mechanism of NK-2 and vesicles.

The increase in membrane tension was also evidenced from the membrane thinning effect of melittin and other AMPs (13,38). Such tension-induced (stretch-activated) pore formation has also been reported for an AMP Magainin 2 (51). Although there have been no earlier reports on NK-2, we expect that NK-2 also induces membrane tension, as in the case of melittin or Magainin 2. As the concentration of lipid is increased (i.e., the number of LUV), the NK-2 may come out through the pores and negatively charged LUV move closer to the positively charged vesicles due to electrostatic attraction. This process eventually leads to aggregation of vesicles via NK-2 bridges. The process of aggregation has been clearly envisaged from the size distribution. The increase in the value of K_{int} , as mentioned in Results section, might be the consequence of the aggregation of vesicles at a higher lipid to NK-2 ratio.

3.5 CONCLUSIONS

We have systematically studied the interaction of NK-2 with phospholipid membranes to obtain insights into the antimicrobial activity. The binding affinity of NK-2 to the negatively charged membranes, PG, as well as the neutral phospholipids PC and PE was determined using ITC and ζ potential. We compare binding affinity of NK-2 to PG, PE, and PC as $PG \gg PE > PC$. Weaker affinity toward neutral phospholipids suggest that interactions of NK-2 with lipids are mainly governed by negatively charged lipids, which are major constituents of the bacterial membranes. The very weak affinity of NK-2 toward the PC membrane (which is the major constituent of eukaryotic cell membranes) propels the development of peptide antibiotics. The evidence of pores on these membranes seen in the present study implies antimicrobial activity of NK-2. The significant increase in the size of negatively charged LUV, found in DLS measurement, confirms membrane–membrane interactions induced by NK-2 in these systems, which eventually leads to vesicle aggregates in the solution. Finally, we have proposed the mechanism of action of NK-2 based on our experimental results. More detailed studies are required to understand the mechanism of the kinetic process involved during pore formation. As already established, the NK-2 can be used as therapeutics to kill malaria parasite *Plasmodium falciparum*. It also shows activity against *Escherichia coli* and preferentially kills cancer cells. Further, low toxicity toward human cells is a great advantage for the development of antibiotics. Therefore, the present study will definitely reinforce the therapeutics applications. Nevertheless, our study provides important insights into the NK-2-lipids interaction.

References

1. M Zasloff. Antimicrobial peptides of multicellular organisms. *Nature* 2002, 415, 389–395.
2. N Stempel, J Strehmel, J Overhage. Potential application of antimicrobial peptides in the treatment of bacterial biofilm infections. *Curr. Pharm. Des.* 2015, 21, 67–84.
3. T Jacobs, H Bruhn, I Gaworski, B Fleischer, M Leippe. NK-Lysin and its shortened analog NK-2 exhibit potential activities against *Trypanosoma cruzi*. *Antimicrob. Agents Chemother.* 2003, 47, 607–613.
4. C Ciobanasu, A Rzeszutek, U Kubitscheck, R Willumeit. NKCS, a Mutant of the NK-2 Peptide, Causes Severe Distortions and Perforations in Bacterial, But Not Human Model Lipid Membranes. *Molecules* 2015, 20, 6941–6958.
5. L J Zhang, R L Gallo. Antimicrobial peptides. *Curr. Biol.* 2016, 26, R14–R19.
6. K A Brogden. Antimicrobial peptides: Pore formers or metabolic inhibitors in bacteria? *Nat. Rev. Microbiol.* 2005, 3, 238–250.
7. B Bechinger. The structure dynamics and orientation of antimicrobial peptides in membranes by multidimensional solid-state NMR spectroscopy. *Biochim. Biophys. Acta, Biomembr.* 1999, 1462, 157–183.
8. C Olak, A Muentner, J Andrä, G Brezesinski. Interfacial properties and structural analysis of the antimicrobial peptide NK-2. *J. Pept. Sci.* 2008, 14, 510–517.
9. J Bankovic, J Andra, N Todorovic, A Podolski-Renic, Z Milosevica, D Miljkovic, J Krause, S Ruzdijic, N Tanic, M Pesic. The elimination of P-glycoprotein over-expressing cancer cells by antimicrobial cationic peptide NK-2: The unique way of multi-drug resistance modulation. *Exp. Cell Res.* 2013, 319, 1013–1027.
10. J Andra, M Leippe. Candidacidal activity of shortened synthetic analogs of amoebapores and NK-lysin. *Med. Microbiol. Immunol.* 1999, 188, 117–124.
11. J Andra, M J H Koch, R Bartels, K Brandenburg. Biophysical characterization of Endotoxin inactivation of NK-2, an antimicrobial peptide derived from mammalian NK-Lysin. *Antimicrob. Agents Chemother.* 2004, 48, 1593–1599.
12. M Zhang, M F Li., L Sun. NKLP27: A Teleost NK-Lysin Peptide that Modulates Immune Response, Induces Degradation of Bacterial DNA, and Inhibits Bacterial and Viral Infection. *PLoS One* 2014, 9, No. e106543.

13. M T Lee, W C Hung, F Y Chen, H W Huang. Mechanism and kinetics of pore formation in membranes by water-soluble amphipathic peptides. *Proc. Natl. Acad. Sci. U.S.A.* 2008, 105,5087–5092.
14. E E Ambroggio, F Separovic, J H Bowie, G D Fidelio, L A Bagatolli. Direct visualization of membrane leakage induced by the antibiotic peptides: Maculatin, Citropin, and Aurein. *Biophys. J.* 2005, 89, 1874–1881.
15. H Zhao, J P Mattila, J M Holopainen, P K J Kinnunen. Comparison of the membrane association of two antimicrobial peptides, Magainin 2 and Indolicidin. *Biophys. J.* 2001, 81, 2979–2991.
16. Y Tamba, M Yamazaki. Magainin 2-induced pore formation in the lipid membranes depends on its concentration in the membrane interface. *J. Phys. Chem. B* 2009, 113, 4846–4852.
17. M T Lee, F Y Chen, H W Huang. Energetics of pore formation induced by membrane active peptides. *Biochemistry* 2004, 43, 3590–3599.
18. K He, S J Ludtke, D L Worcester, H W Huang. Neutron Scattering in the plane of membranes: structure of alamethicin pores. *Biophys. J.* 1996, 70, 2659–2666.
19. T Wieprecht, O Apostolov, M Beyermann, J Seelig. Membrane binding and pore formation of the antibacterial peptide PGLa: Thermodynamic and Mechanistic aspects. *Biochemistry* 2000, 39, 442–452.
20. K Lohner, E J Prenne. Differential scanning calorimetry and X-ray diffraction studies of the specificity of the interaction of antimicrobial peptide with membrane-mimetic system. *Biochim. Biophys. Acta, Biomembr.* 1999, 1462, 141–156.
21. H Schröder-Borm, R Bakalova, J Andrä. The NK-lysin derived peptide NK-2 preferentially kills cancer cells with increased surface levels of negatively charged phosphatidylserine. *FEBS Lett.* 2005, 579, 6128–6124.
22. R Willumeit, M Kumpugdee, S S Funari, K Lohner, B P Navas, K Brandenburg, S Linser, J Andrä. Structural rearrangement of model membranes by the peptide antibiotic NK-2. *Biochim. Biophys. Acta, Biomembr.* 2005, 1669, 125–134.
23. H Vogel, F Jähnig. The structure of melittin in membranes. *Biophys. J.* 1986, 50, 573–582.

24. B Bechinger, M Zasloff, S J Opella. Structure and orientation of the antibiotic peptide magainin in membranes by solid-state nuclear magnetic resonance spectroscopy. *Protein Sci.* 1993, 2, 2077–2084.
25. H M Chen, K W Leung, N Thakur, A Tan, R W Jack. Distinguishing between different pathways of bilayer disruption by the related antimicrobial peptides cecropin B, B1 and B3. *Eur. J. Biochem.* 2003, 270, 911–920.
26. H W Huang, F Y Chen, M T Lee. Molecular Mechanism of peptide induced pores in Membranes. *Phys. Rev. Lett.* 2004, 92, No. 198304.
27. M Miteva, M Andersson, A Karshikoff, G Otting. Molecular electroporation: a unifying concept for the description of membrane pore formation by antibacterial peptides, exemplified with NK-lysin. *FEBS Lett.* 1999, 462, 155–158.
28. R Dimova, S Aranda, N Bezlyepkina, V Nikolov, K A Riske, R Lipowsky. A practical guide to giant vesicles. Probing the membrane nanoregime via optical microscopy. *J. Phys.: Condens. Matter* 2006, 18, S1151–S1176.
29. D Murray, A Arbuzova, G Hangyás-Mihályné, A Gambhir, N Ben-Tal, B Honig. Electrostatic Properties of Membranes Containing Acidic Lipids and Adsorbed Basic Peptides: Theory and Experiment. *Biophys. J* 1999, 77, 3176–3188.
30. S Stefan. Surface charging by large multivalent molecules Extending the standard Gouy-Chapman treatment. *Biophys. J* 1991, 60, 341-351.
31. B Klasczyk, V Knecht. Specific Binding of Chloride Ions to Lipid Vesicles and Implications at Molecular Scale. *Biophys. J* 2013, 4, 818-824.
32. R D Hills Jr, N McGlinchey. Model Parameters for Simulation of Physiological Lipids. *J. Comp. Chem.* 2016, 37, 1112–1118.
33. C Olak, A Muenther, J Andra, G Brezesinski. Interfacial properties and structural analysis of the antimicrobial peptide NK-2. *J. Pep Sci.* 2008, 14, 510-517.
34. R M Willumeit, M Kumpugdee, S S Funari, K Lohner, B P Navas, K Brandenburg, S Linser, J Andrä. Structural rearrangement of model membranes by the peptide antibiotic NK-2. *Biochim. Biophys. Acta.* 2005, 1669, 125-134
35. C I E von Deuster, V Knecht. Competing interactions for antimicrobial selectivity based on charge complementarity. *Biochim. Biophys. Acta* 2011, 1808, 2867-2876.

36. H W Huang, F YU Chen, M T Lee. Molecular Mechanism of peptide-induced pores in Membranes. 2004, *Phys. Rev. Lett.* 2004, 92, 198304-198307.
37. Y Chen, M T Guarnieri, A I Vasil, M L Vasil, C T Mant, R S Hodges. Role of Peptide Hydrophobicity in the Mechanism of Action of α -Helical Antimicrobial Peptides. *Antimicrob. Agents Chemother.* 2007, 51, 1398-1406.
38. M T Lee, T L Sun, W C Hung, H W Huang. Process of inducing pores in membranes by melittin. *Proc. Natl. Acad. Sci. U.S.A.* 2013, 110, 14243–14248.
39. J M Boggs. Lipid intermolecular hydrogen bonding: influence on structural organization and membrane function. *Biochim. Biophys. Acta, Rev. Biomembr.* 1987, 906, 353–404.
40. E E Ambroggio, F Separovic, J H Bowie, G D Fidelio, L A Bagatolli. Direct visualization of membrane leakage induced by the antibiotic peptides: Maculatin, Citropin, and Aurein. *Biophys. J* 2005, 89, 1674-1881.
41. M T Lee, W C Hung, F YU Chen, H W Huang. Mechanism and kinetics of pore formation in membranes by water-soluble amphipathic peptides. 2008, *Proc. Natl. Acad. Sci. USA* 2008, 105, 5087-5092.
42. J Steinkühler, J Agudo-Canalejo, R Lipowsky, R Dimova. Modulating Vesicle Adhesion by Electric Fields. *Biophys. J* 2016, 111, 1454-1464.
43. Y Tamba, M Yamazaki. Magainin 2 induced pore formation in the lipid membranes depends on its concentration in the membrane interface. *J. Phys. Chem. B* 2009, 113, 4846-4852.
44. M T Lee, F YU Chen, H W Huang. Energetics of pore formation induced by membrane active peptides. *Biochemistry* 2004, 43, 3590-3599.
45. M H Ali, M LataShuma, H Dohra, M Yamazaki. Translocation of the nonlabeled antimicrobial peptide PGLa across lipid bilayers and its entry into vesicle lumens without pore formation. *Biochim. Biophys. Acta* 2021, 1863, 183680.
46. T Wieprecht, O Apostolov, M Beyermann, J Seelig. Membrane Binding and Pore Formation of the Antibacterial Peptide PGLa: Thermodynamic and Mechanistic Aspects. *Biochemistry* 2000, 39, 442–452.
47. F Parvez, J M Alam, H Dohra, M Yamazaki. Elementary processes of antimicrobial peptide PGLa-induced pore formation in lipid bilayers. *Biochim. Biophys. Acta* 2018, 1860(11), 2262-2271.

48. J P Ulmschneider. Charged Antimicrobial Peptides Can Translocate across Membranes without Forming Channel-like pores. *Biophys. J* 2021, 113, 73-81.
49. T M Domingues, B Mattei, J Seelig, K R Perez, A Miranda, K A Riske. Interaction of the Antimicrobial Peptide Gomesin with Model Membrane: A calorimetric Study. *Langmuir* 2013, 29, 8609–8618.
50. M Meier, J Seelig. Length dependence of the coil \rightleftharpoons β -sheet transition in a membrane environment. *J. Am. Chem. Soc.* 2008, 130, 1017–1024.
51. M A S Karal, J M Alam, T Takahashi, V Levadny, M Yamazaki. Stretch-Activated Pore of the Antimicrobial Peptide, Magainin 2. *Langmuir* 2015, 31, 3391–3401.

Chapter 4

Interaction of antimicrobial peptide, magainin 2 with phospholipid membrane: effect of cholesterol

4.1 Introduction

Magainin 2, a peptide derived from the skin of *Xenopus laevis*, has emerged as a promising candidate for new antibiotics. In contrast to classical antibiotics, antimicrobial peptides target bacterial membranes and disintegrate the membrane by forming the transmembrane pores. However, complete understanding of the precise mechanisms of cellular apoptosis and molecular basis of membrane selectivity is still in dispute. We have studied the interaction of magainin 2 with various phospholipid membranes, using a variety of experimental techniques, such as, isothermal titration calorimetry (ITC), ζ potential, and dynamic light scattering. As bacteria mimicking membranes, we have chosen large unilamellar vesicles (LUV) and giant unilamellar vesicles (GUV) composed of negatively charged phospholipid, dioleoyl phosphatidyl glycerol (DOPG) and neutral phospholipid, dioleoyl phosphatidylcholine (DOPC). Our experimental results show the stronger binding affinity of magainin 2 to negatively charged membranes than to neutral membranes. In the present study, we have shown that magainin 2 forms trans-membrane pores on negatively charged phospholipid membranes using phase contrast microscopy. Leakage of internal fluid of giant unilamellar vesicles (GUV), leading to decrease in intensity in the halo region of phase contrast micrographs, suggests the formation of transmembrane pores. No such reduction of intensity in the halo region of DOPC was observed, indicating, neutral vesicles does not exhibit pores.

we summarize earlier studies on the interaction of magainin 2 to the phospholipid membranes in section 4.2. All experimental results have been described in section 4.3. Finally, we summarized the overall conclusion of this chapter in section 4.4.

4.2 Earlier studies

Antimicrobial peptides (AMPs) are the unique and diverse group of molecules which are part of innate immune response found in all animal and human body (1). They are the host defense peptides and works against invading pathogens, such as viruses, fungi, bacteria etc. (2,3). AMPs are known to disrupt the bacterial membranes directly without interacting with any specific receptor (4). AMPs commonly possess amphipathic structures and cationic in nature which strongly bind to the bacterial membranes. This results in a formation of trans-membrane pores which eventually rupture the essential cellular contents by disintegrating lipid organization (5). There are several proposed mechanisms that AMP uses to destroy the cellular membrane (cell lysis) (6). The essential and common feature of these mechanisms is the formation of trans-membrane pores (7). Therefore, foremost study for an AMP would to be to investigate the ability to form the transmembrane pores in order to gain insights into its antimicrobial activity. This motivates us to look at the pore forming activity of a promising peptide magainin 2.

Bacterial membranes are usually negatively charged. Therefore, interaction of positively charged AMP with the bacterial membranes initiates with the electrostatic attraction. Besides charge, orientation of the peptide, the hydrophobicity index plays an important role in determining the antimicrobial activity (8,9). Selectivity of the anionic membranes encourages us to use anionic lipid DOPG to prepare bacteria mimicking membranes (10). The implications of AMP as a replacement of conventional antibiotics demands that, AMP should be inert to the phosphatidylcholine (PC) which is the major constituent of the eukaryotic cellular membrane. Ideally, one should use PE-PG mixture to mimic the composition of bacterial membrane. But unfortunately, such mixture does not form GUV. Therefore, as model system, we have taken PC/PG mixture.

Magainins are a group of antibacterial peptides which is secreted from the skin of the African clawed frog *Xenopus laevis*. (11). The peptides consist of 21-23 amino acid residues and have a

net positive charge (+3 to +5). They act selectively against tumor cells and uses as anti-cancer therapies. They permeabilize biological membrane and display antimicrobial activity (12,13). Magainin 2 composed of all-D-amino acid and all-L-amino acid have same antimicrobial activity (14). These peptides are highly soluble in aqueous solution. When magainin 2 interacts with the lipid membrane at the membrane surface, it forms an α -helix transitions from random coil (15-17). Interaction between peptide and lipid membrane depends on their charge. Cationic magainins have a high affinity for negatively charged bacterial membranes. As outer leaflet of plasma membrane does not contain negatively charged lipid, it will not interact with these peptides. The interaction of magainin 2 with lipid membranes has been investigated using a suspension of liposomes (18-20). As model membranes, we have used large unilamellar vesicles (LUV) to study the interaction of magainin 2 with different phospholipids using isothermal titration calorimetry (ITC), zeta potential and dynamic light scattering (DLS). Major constituents of Bacterial membranes are phosphatidylethanolamine (PE) and phosphatidylglycerol (PG) (\sim 4:1). Therefore, in our present study we have chosen model systems, composed of DOPG and mixtures of DOPG with DOPE and DOPC. These lipids also show fluid phase at room temperature (25°C). In particular, the electrostatic behavior as well as size distribution of the membranes in the presence of magainin 2 was systematically characterized using zeta potential and DLS, respectively.

4.3 Experimental results and discussions:

4.3.1. Size distributions of LUV:

Size distribution of LUV, made from different phospholipid and lipid mixture, has been measured before and after the interaction of magainin 2 using dynamic light scattering (DLS). DLS technique can, in principle, provide the evidence of membrane-membrane interaction induced by magainin 2. The extrusion of MLV gives the average diameter of the vesicle \sim 100 nm. LUVs were found to be very stable, as no significant change in the size distribution was seen in DLS measurement even after couple of month later. Fig. 4.1 shows the size distribution of LUV exposed to magainin 2. As the magainin 2/lipid (molar ratio) is increased, the size of LUV increases gradually and eventually sample exhibits high value of average size as well as large polydispersity. This result suggests the formation of large aggregates due to membrane-membrane interaction. The process of aggregation is also evident from the high degree of fluctuations near the tail of the auto

correlation curve. The error bars in the Fig. 4.1 represent the width of the distribution which is a measure of Polydispersity of LUV. The width of the size distribution indicating polydispersity, also increases with the increase of magainin 2 concentration. Size distributions do not alter significantly for pure DOPC, the mixture of DOPE and DOPG at 4:1 shows a slight increase in the average size ~ 95 nm. However, average size of the negatively charged vesicle DOPG increases to ~ 400 nm with the increasing concentration of magainin 2. The increase in size distributions of LUV due to binding of magainin 2 is a consequence of stronger affinity of magainin 2 towards negatively charged membranes.

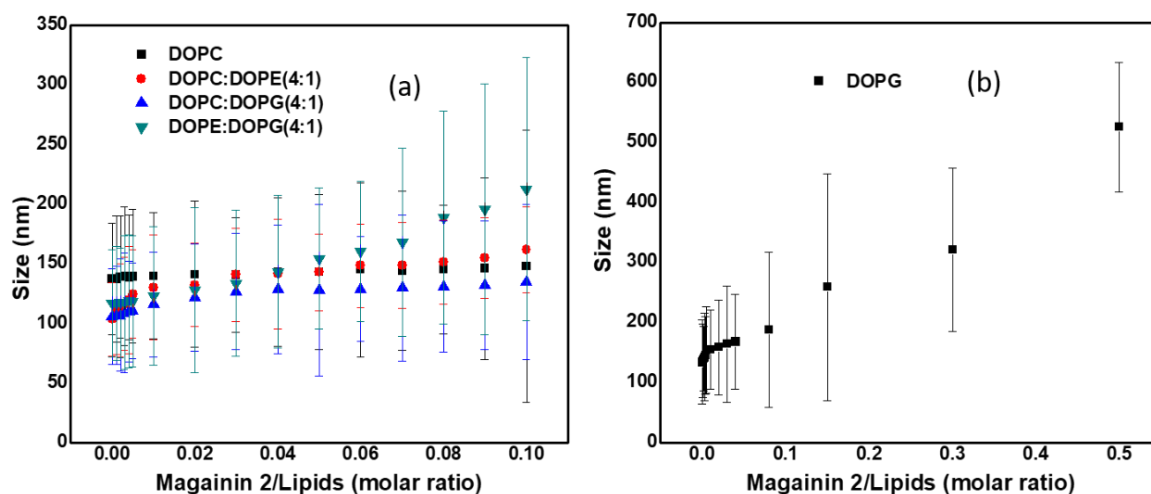


Figure 4.1: Size distribution of LUV made from various lipid compositions in the presence of magainin 2. Error bar is the standard deviation (SD) and was obtained from the width of the distribution.

4.3.2. Zeta potential of LUV:

The ζ was obtained from LUV dispersion prepared from different phospholipid and lipid mixture before and after introducing peptide. Zeta potential (ζ) of LUV in presence of antimicrobial peptide magainin 2 is illustrated in Fig. 4.2. As shown in Fig. 4.2, ζ increases with increasing magainin 2 to lipid molar ratio (M2/L) and charge compensation occurs at different M2/L for different lipid

mixtures. Although phospholipids, such as DOPC and mixture of DOPC-DOPE are neutral, they exhibit low negative value. Small negative zeta potential gets neutralized at $M2/L \sim (3:100)$. In comparison, charge neutralization happens for DOPC: DOPG (4:1) at much higher $M2/L \sim (6:100)$ and (7:100) for DOPE: DOPG (4:1). For others vesicle DOPG, charge neutralization occurs at $M2/L \sim (28:100)$. These differences are due to the fact that charge compensation occurs with the amount of charge present in the membrane, i.e., with respect to charge lipids. The ζ was found to exhibit its saturation value, indicating overcharge compensation, at different $M2/L$ for different phospholipid vesicles. The overcharge compensation at different zeta values suggests the significant contribution of entropy besides electrostatic interaction as discussed in our previous paper (21). The results of zeta potential along with DLS clearly reveal that interaction of magainin 2 with membranes is primarily driven by electrostatic interaction. The charge neutralization at much higher $M2/L$ for DOPG suggests binding affinity to PG is much stronger than that to PC. Therefore, magainin 2 has a stronger affinity towards the negatively charged lipids.

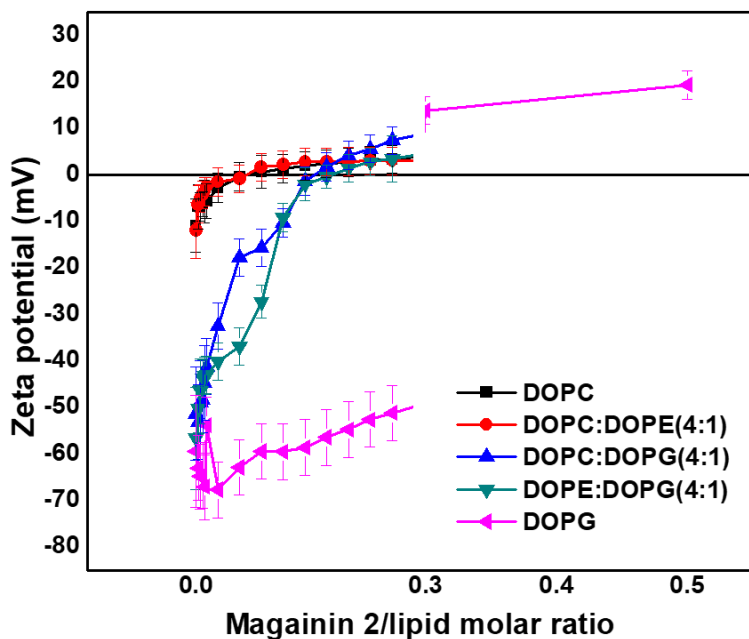


Figure 4.2: Zeta potential of phospholipid LUV at various magainin 2 to Lipids molar ratio. Error bars indicate width of the distribution profile of zeta potential.

4.3.3. Binding study of magainin 2 with model membrane: Isothermal Titration Calorimetry.

As model membranes, we have used negatively charged phospholipid DOPG and two zwitterionic phospholipids DOPC and DOPE to prepare LUV. DOPE and DOPG are abundant phospholipids found in bacterial cell surface, whereas, DOPC is mostly found in the eukaryotic plasma membrane. Therefore, DOPE and DOPG resemble the composition of bacterial membranes and DOPC has been used for comparison. These phospholipids in aqueous solvent also exhibit fluid phase above -18° C. Therefore, vesicles can easily be prepared at room temperature (25° C). cationic magainin 2 exhibits a strong affinity towards negatively charged membrane than neutral membrane which is confirmed by our previous zeta and DLS result. We have used high sensitive titration calorimetry to investigate the binding of magainin 2 to phospholipid membranes which is accompanied by a considerable release of heat. Various concentrations of magainin 2 ranging from 10-200 μ M were titrated with LUV. The binding isotherm was determined by injecting lipid vesicles into peptide solution. Titration of LUV into magainin 2 produces exothermic heat when the heat of dilution has been subtracted. In the beginning of titration, there are plenty of magainin 2 for binding with lipids. However, as the titration progresses, less and less magainin 2 are available for binding, indicating by the gradual decrease in the heat signal. The titration curve attains its saturation value when all the magainin 2 are exhausted and no peptide is remaining for binding to lipids. Besides binding of magainin 2, contributions of initial heat also arise due to conformational change, i.e., transformation of random coil to α –helix, change of orientation of peptide when associates with the membrane. The exothermic heat could also arise from the liberation of water molecules from the hydration layer at the membrane-water interface, when magainin 2 binds to the membrane. Normalized heat per injection, obtained from integrating each peak as a function of molar ratio is shown in Fig.4.3. One site binding model fits this isotherm very nicely and we have obtained thermodynamic parameters of the interaction. Binding constant were derived from lipid into peptide titrations using the one site binding model which is given below in table 1. The value of binding constant varies from $\sim 10^5$ to 10^3 M^{-1} depending on the membrane surface charge. Free energies and entropies were calculated using the equations $\Delta G = -RT \ln 55.5 K$ and $\Delta G = \Delta H - T\Delta S$.

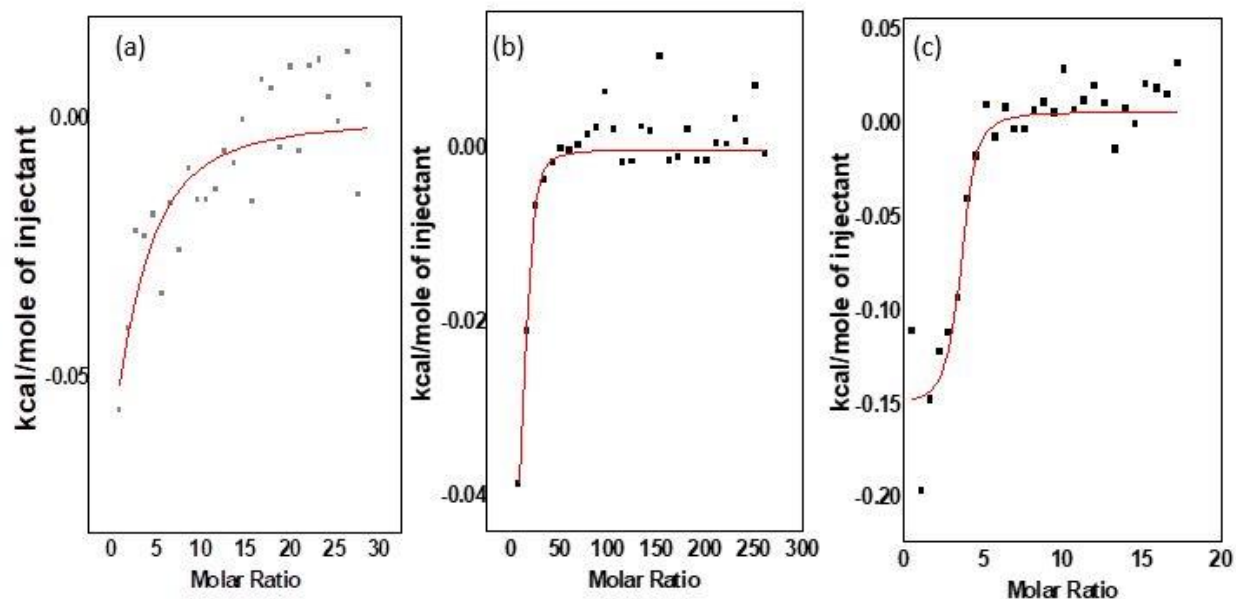


Figure 4.3: Isotherm obtained from the integrated heat per injection when 50 μM magainin 2 were titrated with 4 mM LUV made from (a) DOPC, (b) DOPC: DOPG (4:1) and (c) DOPE: DOPG (4:1). Heat of dilution, obtained from injecting 4 mM LUV into buffer, was subtracted from the actual measurement. Here we assume, lipids from both monolayers interact with the magainin 2. The solid line is obtained from the fit using one site model given by the microcal origin.

Table 1. Thermodynamical Parameters of Binding Kinetics of magainin 2

Thermodynamic parameters obtained from ITC experiment:				
System	K (M^{-1})	$(\Delta G^\circ \text{ kcal mol}^{-1})$	$(\Delta H^\circ \text{ cal mol}^{-1})$	$(T\Delta S^\circ \text{ kcal mol}^{-1})$
DOPE+DOPG	3.24×10^5	-7.56	-157.5	-7.4
DOPC+DOPG	7.69×10^4	-6.71	-46.38	-6.66
DOPC	7.19×10^3	-5.29	-195.7	-5.1

4.3.4. Observation of trans-membrane pores: Phase contrast Microscopy

Phase contrast microscopy on GUV has been performed in order to visualize directly the antimicrobial activity of Magainin 2. As shown in Figure 4.4, a straight line was drawn across the GUV to obtain an intensity profile. The peak-to-peak intensity (I_{ptp}) across the halo region was calculated. Average I_{ptp} was obtained from several line profiles across the GUV. The time in seconds versus I_{ptp} was plotted to observe any significant change in the intensity profile of the GUV. GUV, made from DOPC and mixtures of DOPC with DOPG were observed with four different peptide concentrations (0.98,1.11,2.17,4.16 μM). If Magainin-2 forms pores on the membranes, we would expect leakage of internal fluid through the pores. Therefore, halo regions are expected to disappear with time and GUV should look similar to that without diluting in glucose. Experiments on GUV, exposed to Magainin-2, show direct evidence of formation of trans-membrane pores. Change in the difference of the grey value (I_{ptp}) of the halo region with time for DOPC-DOPG (4:1) GUV, as shown in Fig. 4.6, indicates leakage of internal fluid, leading to the loss of contrast. I_{ptp} decreases until GUV completely loses its contrast in the halo region. We have compared I_{ptp} between GUV, exposed to magainin 2 and GUV without magainin 2, but interior and exterior regions contain same glucose solution. This behavior is attributed to the fact that pores are large enough to permeate the sucrose and glucose molecules and fluids between interior and exterior of the GUV are exchanged, leading to loss of contrast in the halo region. Pores are stable, as GUV remains stable with time. Different GUV seems to take different time to initiate pore formation. We cannot precisely determine time taken to initiate pore formation for individual GUV at different peptide concentrations, as average response of many GUV were obtained in our study. However, we can unambiguously determine the behavior of rate constant for different peptide concentrations. We want to calculate decay constant from the following equation

$$y = y_0 + A \exp\left(-\frac{t}{\tau}\right)$$

We also investigate the effect of size of GUV as well as concentration of magainin 2 on the kinetics of pore formation in the membrane. GUV, made from DOPC do not show significant decrease in I_{ptp} in the presence of magainin 2, indicating magainin 2 does not form pores on these membranes. This behavior is supported by the fact that magainin 2 has very weak binding affinity to PC membranes.

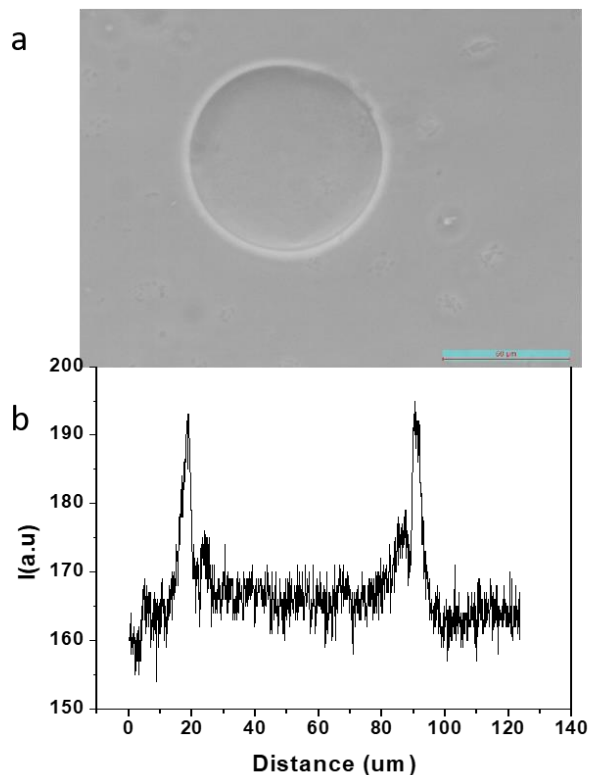


FIGURE 4.4: (a) Phase contrast microscopy of a giant vesicle showing the phase contrast image of pure DOPC vesicle in 0.1 M glucose solution. (b) shows the intensity profiles across the equator. In this graph, the y axis measures gray levels and the x axis corresponds to distance (μm) in the above images; the higher intensity curve measures the gray levels in the high phase contrast condition and the lower intensity curve (intentionally displaced up to the zero average) measures the gray levels after completely losing the contrast.

As we have studied four different sized GUV ($17,25,38,47 \mu\text{m}$) made from DOPC for a fixed magainin 2 concentration ($4.16 \mu\text{M}$), we have seen no peak to peak intensity different with wide range time.

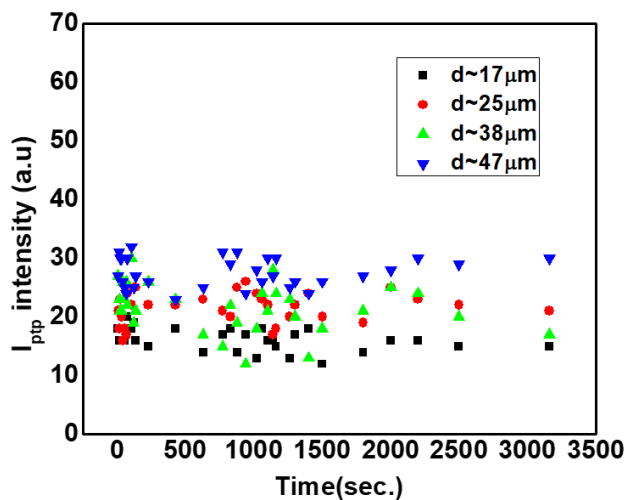


Figure 4.5: Peak to peak intensity profile of GUV made from DOPC with time.

We systematically study effect of magainin 2 on different size ($17.5,27,35.27,38 \mu\text{m}$) of GUV made of DOPC: DOPG (4:1). After adding magainin 2 on the GUV solution kept on the microscopic slide, we looked at a particular size of the vesicles and monitored leakage of internal fluid. In a different experiment, peptide solution of same concentration was added to the solution and started observing different size of the vesicles. In this way, we could pick up different size of the GUV and observed their pore forming activity. We add same amount of peptide ($\sim 4.16 \mu\text{M}$) on different size vesicle.

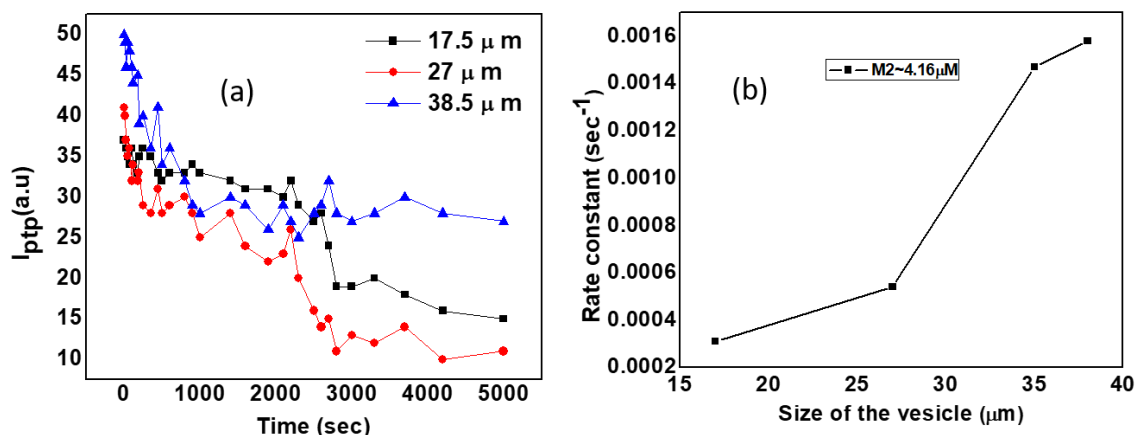


Figure 4.6: (a) shows the peak to peak intensity with time of different sized GUV (17.5,27,38.5 μm) when 4.16 μM magainin 2 added. (b) rate constant vs size of the GUV.

We see from fig. 4.6 (a), as the size of the vesicle bigger, peak to peak intensity falls faster than small sized vesicle. The reason behind this is the amount of peptide bind to bigger vesicle is more than small vesicle. So rate of pore forming obviously faster than small sized vesicle. From fig. 4.6 (b), we see that the decay time for 38.5 μm vesicle is 630 sec. and as the size of the GUV goes smaller the decay time also increases.

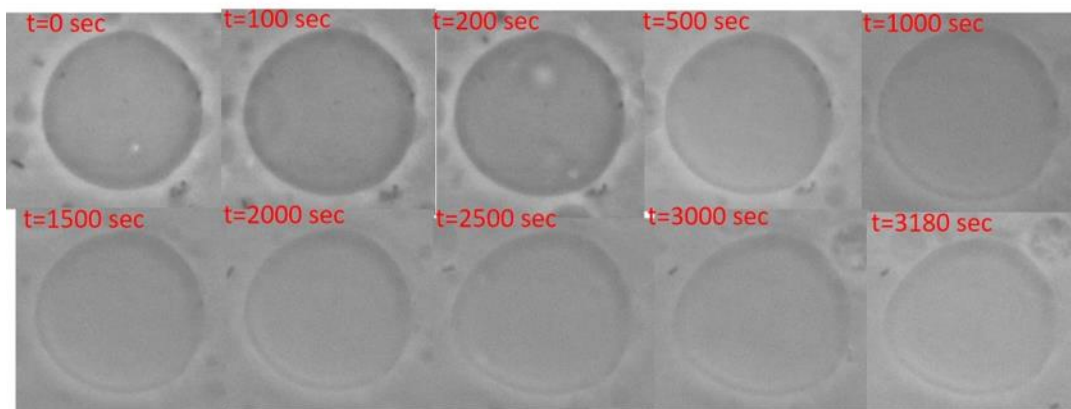


Figure 4.7: Phase contrast images of GUVs composed of DOPC–DOPG (4:1), exposed to 4.16 μM Magainin 2. Starting time of capturing images is not the time of initiation of pore formation. The diameter of the vesicle is $\sim 35 \mu\text{m}$

We observed GUV with four different peptide concentrations (0.98, 1.11, 2.17, 4.16 μM). From the decay fitting curve we have calculated decay constant for different concentration.

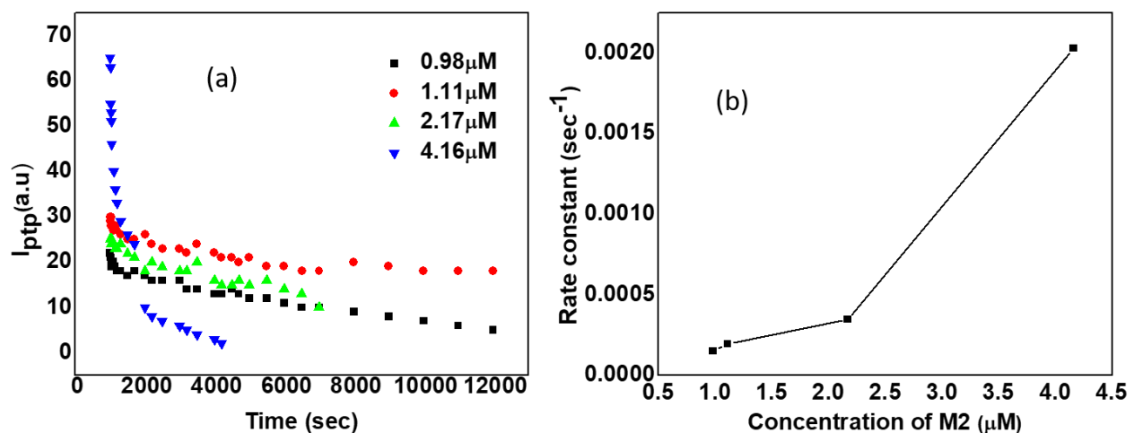


Fig. 4.8: (a) shows profile of contrast decay of GUV made from DOPC: DOPG (4:1) with increasing concentration of magainin 2. Each point corresponds to the average of at least three vesicles and the uncertainty is represented by the error bar. (b) shows decay constant vs concentration of magainin 2.

Therefore, I_{ptp} decreases much faster at higher peptide concentration than that of lower peptide concentration. Larger decay constant at higher magainin 2 concentration can be a results of larger pore size or larger number of pores than that of lower magainin 2 concentration. We did not seem to observe any significant change in size of GUV with time. GUV does not show any significant change in I_{ptp} with time in the absence of magainin 2. The time scale involved for the initiation of pore formation process for various magainin 2 concentration was difficult to conclude in the present study, as I_{ptp} was found to decrease at different time for various GUV at a given magainin 2 concentration. Slight variation of magainin 2 concentration in different parts of the sample, pore size, size of GUV are also key factors in determining the time scale involved in the process of pore formation.

4.3.5. Effect of cholesterol on the pore formation

cholesterol is an essential and ubiquitous component of plasma membranes. As discussed earlier in chapter 1, cholesterol is found in membranes but concentration of cholesterol is different in different membranes. One of the basic difference between plasma membrane and bacterial membrane is the complete absence of cholesterol in bacterial membrane and a large amount present in plasma membrane. Although, Matsuzaki et al. in their experiment have shown that cholesterol protects human erythrocytes plasma membrane from attack by magainin 2 (22). our previous studies on model membranes have demonstrated that that incorporation of cholesterol in model membrane tends to inhibit pore formation in the membrane by antimicrobial peptide (23).

Cholesterol is known to increase membrane stiffness which may prohibit antimicrobial activity by AMPs. Increase cholesterol content in membrane lead to liquid ordered (L_o) phase (cholesterol-rich) which has higher rigidity than that of the cholesterol-poor liquid-disordered (L_d) phase.

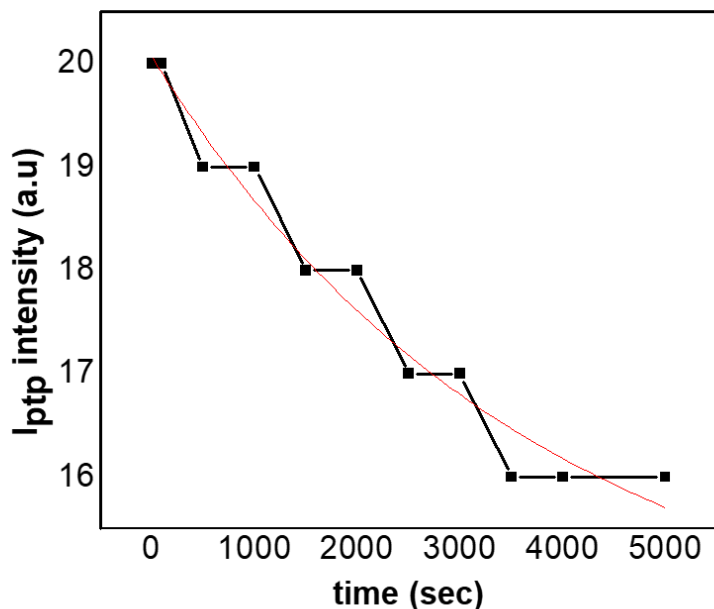


Figure 4.9: The peak to peak intensity across the halo region of GUV (Size $\sim 27 \mu\text{m}$) as a function of time. GUV is made from DOPC: DOPG (4:1) mixture at 10 mole% cholesterol. $4.16 \mu\text{M}$ magainin 2 added to the diluted GUV solution. Rate constant was found to be 0.00027 sec^{-1} .

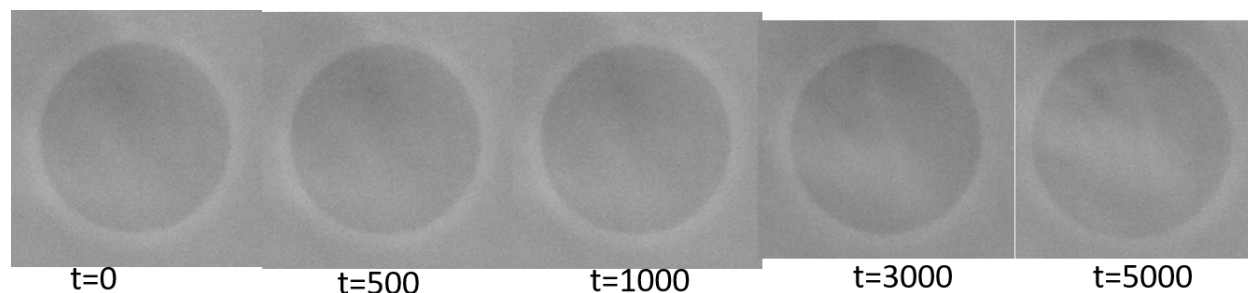


Fig. 4.10: Phase contrast images of GUVs composed of DOPC–DOPG (4:1) and 10 mole% cholesterol, exposed to $4.16 \mu\text{M}$ Magainin 2.

GUV containing 20 mole% cholesterol does not show any significant leakage in microscopy experiments. This result indicated that there was no significant leakage or exchange of fluid in the presence of 20 mole% cholesterol, suggesting that incorporation of cholesterol tends to inhibit magainin 2 induced pore formation.

4.3.6. Fluorescence spectroscopy and anisotropy measurement:

Nile red is widely used environment sensitive probe to monitor the membrane organization and dynamics. It emits fluorescence in the presence of lipid membrane. However, its fluorescence is significantly quenched in the aqueous or polar environment (24). Its fluorescence properties are known to alter by the polarity of its immediate environment due to a large change in its dipole moment upon excitation. This property of nile red is utilized to monitor hydrophobic surfaces in proteins and hydrocarbon core in lipid membranes. Therefore, the nile red is used on living cells as a fluorescence stain for the detection of intracellular lipid fluorescence emission intensity of nile red labeled large unilamellar vesicles composed of various lipids. We have measured the absorption spectrum of nile red and optimum excitation wavelength was found to be at 550 nm. Therefore, excitation wavelength has been kept fixed at 550 nm and emission spectra of nile red were monitored for different lipids with increasing magainin 2 concentrations.

The emission spectra in fig. 4.11 for different lipid show decrease in fluorescence intensity with increasing magainin 2 concentration. This decrease in fluorescence intensity might be the consequences of the increase in water penetration in the bilayers.

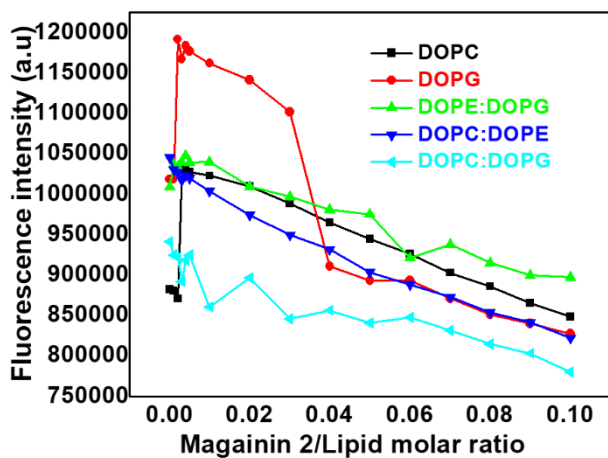


Figure 4.11: The decrease in fluorescence intensity of the LUV composed of different phospholipid mixture for varying concentration magainin 2. LUV are dispersed in a HEPES buffer of concentration 1 mM and pH adjusted to 7.4

The fluidity of membrane is very important in the context of drug delivery. It can influence liposomal bio functions such as drug encapsulation and drug release etc. The inverse of anisotropy is proportional to the membrane fluidity of the liposome, are calculated from the Nile red fluorescence anisotropy measurement. Steady state fluorescence anisotropy has been used to monitor the rotational diffusion rate of Nile red embedded in the membrane and it measures the extent of depolarization, i.e., the ability of the probe to reorient during the emission, it must be sensitive to the packing of lipid acyl chains. We observed that the anisotropy value increases for bacterial membrane and remains constant for neutral membrane with the increasing concentration of peptide magainin 2. This higher membrane fluidity suggests quick drug leakage or releasing (25).

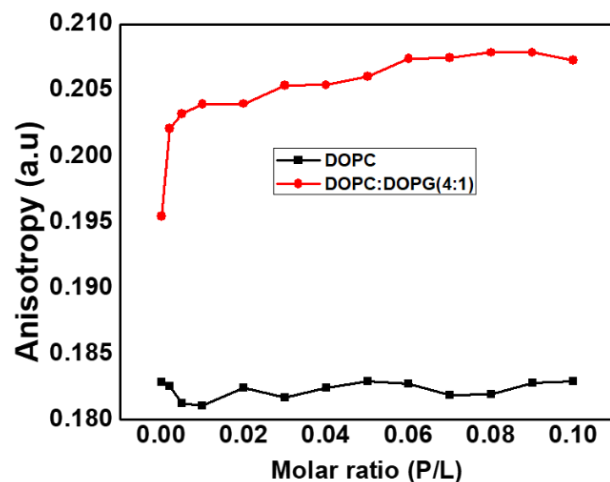


Figure 4.12: Effect of magainin 2 on the steady state anisotropy of Nile red in DOPC and DOPC:DOPG (4:1) liposome. The changes in anisotropy as a function of molar ratio only seen in bacterial membrane i.e. DOPC: DOPG (4:1).

4.3.7. Membrane permeabilization experiments:

We studied experimentally the ability of magainin 2 to form pores by measuring the fluorescence intensity of calcein-loaded LUV with time. Due to the high dye concentration (~70 mM), the fluorescence of calcein molecule within the vesicles is highly self-quenched. The addition of a magainin 2 solution to the dye-containing LUVs made from DOPC: DOPG (4:1) at 25°C induces dye release. Figure 4.13 shows the enhancement of fluorescence intensity over time indicating the release of entrapped dye from the vesicles. Such an increase in intensity was attributed to the formation of transmembrane pores. It is important to mention that fluorescence intensity did not increase in the absence of magainin 2.

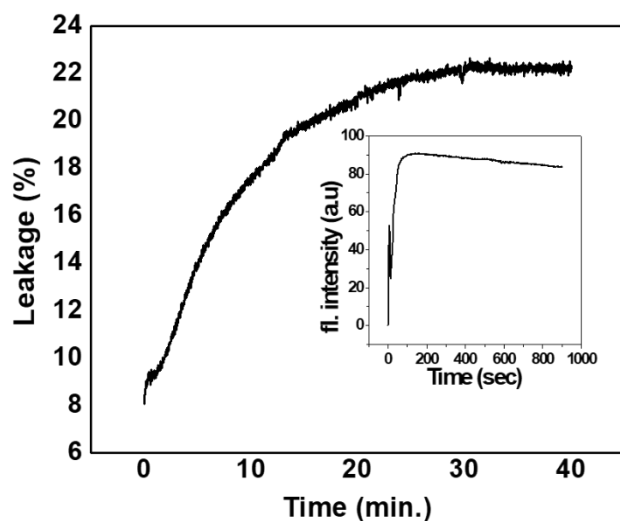


Figure 4.13: Time course of magainin 2 induced leakage of calcein from a suspension of DOPC:DOPG (4:1) LUV after the addition of 4 μM concentration of magainin 2.

4.4 Conclusion:

A systematic investigation on the interaction of antimicrobial peptide magainin 2 with phospholipid membranes reveals that magainin 2 is able to induce pores in the anionic phospholipid membrane. Phase contrast microscopy of giant unilamellar vesicles have been employed to show the leakage of internal fluid and exchange of fluids, suggesting the formation of transmembrane pores. We also explored the pore-forming activity of magainin 2 on the membrane containing cholesterol. We determine the value of rate constant for different sized vesicles and also for different concentration of peptide. Incorporation of cholesterol into the membrane increases rigidity and also decreases the pore forming ability of magainin 2. Above a particular concentration of cholesterol (~ 20 mole%), we have not observe any leakage of internal fluid of giant unilamellar vesicle. Besides pore forming activity, we have also studied the interaction of magainin 2 with various phospholipid membranes, using a variety of experimental techniques. The size distribution of negatively charged LUV in the presence of magainin 2 was found to increase drastically, indicating the presence of large aggregates. ζ potential results show

the stronger binding affinity of magainin 2 to negatively charged membranes than to neutral membranes. We have derived thermodynamical parameter from isothermal titration calorimetry (ITC) experiment using one site binding model. We have shown the ability of magainin 2 to form pores by measuring the fluorescence intensity of calcein-loaded LUV with time.

References

- (1) M Zasloff. Antimicrobial peptides of multicellular organisms. *Nature*, 2002, 415, 389-395.
- (2) J Wiesner, A Vilcinskas. Antimicrobial peptides: the ancient arm of the human immune system. *Virulence*, 2010, 1(5), 440-64.
- (3) M Hirano, C Saito, H Yokoo, C Goto, R Kawano, T Misawa, Y Demizu. Development of Antimicrobial Stapled Peptides Based on Magainin 2 Sequence., *Molecules*, 2021, 26, 444.
- (4) K A Brogden. Antimicrobial peptides: Pore formers or metabolic inhibitors in bacteria. *Nature* 2005, 3, 238-250.
- (5) J Cho, I Hwang, H Choi, J H Hwang, J S Hwang, D J Lee. The novel biological action of antimicrobial peptides via apoptosis induction. *J. Microbiol. Biotechnol.* 2012, 22, 1457-1466.
- (6) H M Chen, K W Leung, N Thakur, A Tan, R W Jack. Distinguishing between different pathways of bilayer disruption by the related antimicrobial peptides cecropin B, B1 and B3. *Eur. J. Biochem*, 2003, 270, 911-920.
- (7) K He, S J Ludtke, D L Worcester, H W Huang. Neutron Scattering in the plane of membranes: structure of alamethicin pores. *Biophys. J.* 1996, 2659-2666.
- (8) B Bechinger. The structure dynamics and orientation of antimicrobial peptides in membranes by multidimensional solid-state NMR spectroscopy. *Biochim. Biophys. Acta*, 1999, 1462, 157-183.
- (9) H Schroder-Borm, R Bakalova, J Andra. The NK-lysin derived peptide NK-2 preferentially kills cancer cells with increased surface levels of negatively charged phosphatidylserine. *FEBS Lett.* 2005, 579, 6128-6124.
- (10) E. G. Kholina, E. G. Kovalenko, I. B. Bozdaganyan, M. E. Strakhovskaya, M. G. Orekhov, P. S. Cationic Antiseptics Facilitate Pore Formation in Model Bacterial Membranes. *J. Phys. Chem. B* 2020, 124, 8593-8600.
- (11) M. Zasloff, Magainins, a class of antimicrobial peptides from *Xenopus* skin: Isolation, characterization of two active forms, and partial cDNA sequence of a precursor, *Proc. Natl. Acad. Sci.*, 1987, 5449-53.

- (12) H V Westerhoff, D Juretic, R W Hendler, M Zasloff, "Magainins and the disruption of membrane-linked free-energy transduction.," *Proc. Natl. Acad. Sci.* 1989, 86, 6597-601.
- (13) H V Westerhoff, R W Hendler, M Zasloff, D Juretic, "Interactions between a new class of eukaryotic antimicrobial agents and isolated rat liver mitochondria.," *Biochim. Biophys. Acta*, 1989, 975, 361-9.
- (14) D. Wade, A. Boman, B. Wahlin, C. M. Drain, A. Andreu, H. G. Boman and R. B. Merrifield, "All-D amino acid-containing channel forming antibiotic peptides," *Proc. Natl. Acad. Sci*, vol. 87, p. 4761–4765, 1990.
- (15) J Seelig, Thermodynamics of lipid–peptide interactions, *Biochim. Biophys. Acta*, 2004, 1666, 40-50.
- (16) B Bechinger, D W Juhl, E Glattard, C Aisenbrey, Revealing the Mechanisms of Synergistic Action of Two Magainin Antimicrobial Peptides, *Front. Med. Technol.* 2020, 2:615494.
- (17) L. M. Yin, M. A. Edwards, J. Li, C. M. Yip, C. M. Deber, Roles of hydrophobicity and charge distribution of cationic antimicrobial peptides in peptide-membrane interactions. *J. Biol. Chem.* 2012, 287, 7738–7745.
- (18) K. Matsuzaki, K. Murase, N. Fujii and K. Miyajima, Translocation of a channel-forming antimicrobial peptide, magainin 2, across lipid bilayers by forming a pore, *Biochemistry*, 1995, 34, 6521-6526.
- (19) K. Matsuzaki, K. Sugishita, N. Ishibe, M. Ueha, S. Nakata, K. Miyajima and R. M. Epand, Relationship of Membrane Curvature to the Formation of Pores by Magainin 2, *Biochemistry*, 1998, 37, 11856-11863.
- (20) J. M. Boggs, J. Euijung, I. V. Polozov, R. F. Epand, G. M. Anantharamaiah, J. Blazyk and R. M. Epand, Effect of magainin, class L, and class A amphipathic peptide on fatty acid spin labels in lipid bilayers, *Biochim. Biophys. Acta*, 2001, 1511, 28-41.
- (21) S Karmakar, P Maity, A Halder. Charge-Driven Interaction of Antimicrobial Peptide NK-2 with Phospholipid membranes. *ACS Omega* 2017, 2, 8859-8867.

- (22) K Matsuzaki. Why and how are peptide-lipid interactions utilized for self-defense? Magainins and tachyplesins as archetypes. *Biochim. Biophys. Acta* 1999, 1462, 1–10.
- (23) A Halder, A Sannigrahi, N De, K Chattopadhyay, S Karmakar. Kinetoplastid Membrane Protein-11 Induces Pores in Anionic Phospholipid Membranes: Effect of Cholesterol. *Langmuir* 2020, 36, 3522-5330.
- (24) A Halder, B Saha, P Maity, G S Kumar, D K Sinha, S Karmakar. Lipid chain saturation and the cholesterol in the phospholipid membrane affect the spectroscopic properties of lipophilic dye Nile red. *Spectrochim. Acta, Part A* 2018, 191, 104–110.
- (25) D Liu, J Zhang, S Xu, H Liu. Membrane property and biofunction of phospholiposome incorporated with anomeric galactolipids. *SpringerPlus* (2016) 5:655.

Chapter 5

Formation of transmembrane pores in anionic phospholipid membranes induced by kinetoplastid membrane protein-11 (KMP-11): Effect of Cholesterol

5.1 Introduction:

Kinetoplastid membrane protein-11 (KMP-11), expressed in all stages of leishmanial life circle, is considered a potential candidate for leishmaniasis vaccine. KMP-11 is found on the membrane surface of the parasite. Although the biological function of KMP-11 is unknown, we hypothesize from its sequence analysis that it may interact with the macrophage membrane, and may influence the entry process of the parasite into the host cell. To validate this hypothesis, we have investigated the interaction of KMP-11 with the unilamellar anionic phospholipid vesicles and explored its pore forming activity. Two types of model membranes have been used. The large unilamellar vesicles (LUVs) were prepared to investigate the interaction or binding affinity of KMP-11 with the membranes, whereas, giant unilamellar vesicles (GUVs) were used to visualize the pore formation.

Before we discuss our experimental results, we summarize earlier studies on the interaction of KMP-11 to the membranes in section 5.2. All experimental results have been described in section 5.3. Finally, we summarized the overall conclusion of this chapter in section 5.4.

5.2 Earlier studies:

Visceral Leishmaniasis (VL) which is the most severe form of leishmaniasis, is caused by the species *Leishmania Donovanii* (1). It is generally believed that specific pathogenic surface molecules can behave as chemical opsonins to facilitate the entry of pathogen into host cells by promoting host-pathogen interactions (2). In this connection, it is well known that many major pathogenic systems employ their pore-forming proteins (PFPs) as virulence factors. PFPs are common among bacteria, and about 25 to 30% of cytotoxic bacterial proteins are PFPs, making them the single largest category of virulence factors (3-4). Because of their nearly universal presence in bacterial pathogens, PFPs are a unique and important target for novel, broadly applicable antimicrobial prophylactics and therapeutics. PFPs function to perforate membranes of host cells, predominantly the plasma membrane but also intracellular organelle membranes (5). Several PFPs are reported to mediate the pathogen's internalization process through their membrane pore formation activity (6). Evavold et al reported one example, in which a pore forming protein gasdermin D regulates IL1 release from hyperactive macrophages (7). Pore forming proteins are presumably responsible not only for the pathogenic entry process but also for the significant immune suppression process (8).

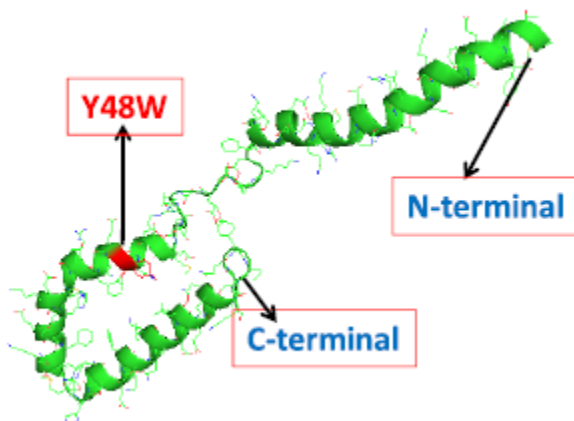


Figure 5.1: Model structure of KMP-11 as obtained from I-TASSER software. The model structure suggests the alpha helical character of the protein. The red region indicates the point of tryptophan mutation (Y48W).

Kinetoplastid membrane protein-11 (KMP-11) is a small immunogenic protein expressed in large copy number on the surface of *Leishmania Donovanii*. Although crystal structure is not available, modelling studies suggest a helical structure (Fig. 5.1), which has been supported by far UV CD measurements. KMP-11 shows strong immunogenic property and is believed to be a potential vaccine candidate (9). The function of KMP-11 and its roles in the process of infection are poorly understood. However, it is known that KMP-11 has high expression on parasite surface (9). We have recently observed that KMP-11 binds strongly to synthetic membrane (3). In addition, using a sequence analysis of KMP-11, we find comparable antimicrobial index with the pore forming peptide magainin-II (Fig. 5b). All these observations led us to hypothesize that KMP-11 may have a PFP like role of forming pore at the host membrane, which may or may not be relevant to the process of parasite internalization. Furthermore, we observed significant sequence homology of KMP-11 with apolipoprotein A, which prompted us to speculate further that the cholesterol may influence significantly to its pore forming activity. This is because, apolipoprotein A is known for its cholesterol transport properties (10). In recent years, the concept of a “cholesterol connection” in infectious diseases has emerged where pathogens have evolved virulence factor that reprograms eukaryotic cellular physiology. In particular, cholesterol plays a significant role in controlling the parasite entry into macrophage cells (11). It has already been reported that cholesterol depletion from the macrophage reduces the ability of leishmania to enter the host macrophages (12). There exists extensive literature on cholesterol connection with the pore forming activity and antimicrobial activity of proteins (13). The liposomal cholesterol delivery has been employed as a treatment for intracellular parasite killing through the successful enhancement of the innate immunity (14). Moreover, cholesterol regulates the activity of pathogenic PFPs in terms of pore forming nature and subsequent immune evasion (14).

In the present study, we have systematically investigated the interaction between KMP-11 and anionic membranes composed of DOPC-DOPG (4:1). Since a wide variety of lipid components is present in the native cell membrane, it is often useful to study model membrane of specific composition in order to obtain insights into the individual features and activities of the membrane. Although unsaturated lipids, such as DOPC are abundant in the macrophage membrane (4), negatively charged lipids contribute to the subcellular targeting of proteins with cationic domains via electrostatic interaction (15). This motivates us to choose DOPG as anionic component of the membrane. Two types of model membranes have been used. The large unilamellar vesicles

(LUVs) were prepared to investigate the interaction or binding affinity of KMP-11 with the membranes, whereas, giant unilamellar vesicles (GUVs) were used to visualize the pore formation. Fluorescence release of calcein loaded LUVs and phase contrast microscopy of GUVs have been successfully employed to obtain the evidence of pores in the membranes induced by KMP-11. We have also explored the effect of cholesterol on the pore forming ability of KMP-11. Microscopy images have been analyzed to obtain dependence of protein concentration, vesicle size on the kinetics of pore formation in the membrane. The binding affinity of KMP-11 with the phospholipid membranes was studied using zeta potential and fluorescence assay. The membrane-membrane interaction induced by KMP-11 is envisaged using dynamic light scattering. Our results showed for the first time that KMP-11 induces pores in model membrane and cholesterol incorporation significantly reduces the pore forming activity. Collectively, our study suggests an interplay between the binding, pore formation activity of KMP-11 with the architecture and composition of model membranes which further implicates the molecular mechanistic understanding of leishmaniasis.

5.3 Experimental results and discussion

5.3.1 Interaction of KMP-11 with Phospholipid LUV.

The membrane-specific dye DiI C-18 is widely used to monitor the large scale inhomogeneity on the surface of a living cell, including rafts and protein organization in artificial membranes (20,21). We used here a previously reported fluorescence assay using DiI C-18 to investigate the interaction of KMP-11 with DOPC–DOPG LUV (3). In the presence of membrane, DiI C-18 showed strong fluorescence at $\lambda_{em} = 675$ nm ($\lambda_{ex} = 600$ nm), while in aqueous buffer or a buffer containing KMP-11, its fluorescence was very low or absent (Figure 5.2a). Figure 5.2b shows that the fluorescence of DiI C-18 (in the presence of LUV) decreased with increasing KMP-11 concentrations. This happened because of protein-lipid association. The average lifetime of the dye (in the presence of the membrane) decreases as we add the protein, indicating a significant contribution of dynamic quenching as reported in our previous study (3). The change in relaxation behavior in the excited state of DiI C-18 could be due to an alteration of hydration dynamics at the membrane solvent interface as well as due to the change in translational diffusion of fluorophore.

In addition to these processes, we cannot eliminate the possibility of expulsion of DiI C-18 due to adsorption of KMP-11 which could also result in the decrease in fluorescence. We fitted the fluorescence decrease with protein concentration using a standard Hill equation and determined the values of binding constant (K) and cooperative index (n). The K value of KMP-11 was found to be $(2.46 \pm 0.15) \times 10^5 \text{ M}^{-1}$, which was consistent with the results obtained in our earlier study with LUV containing pure DOPC (3).

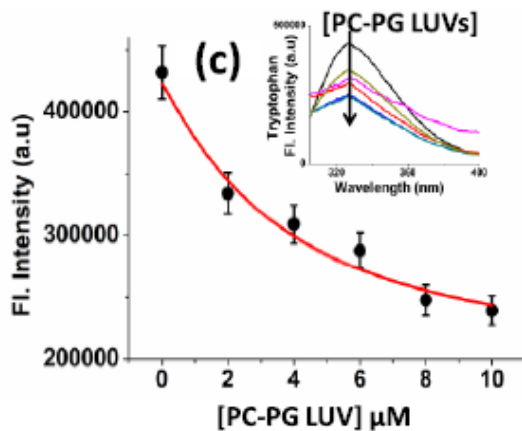
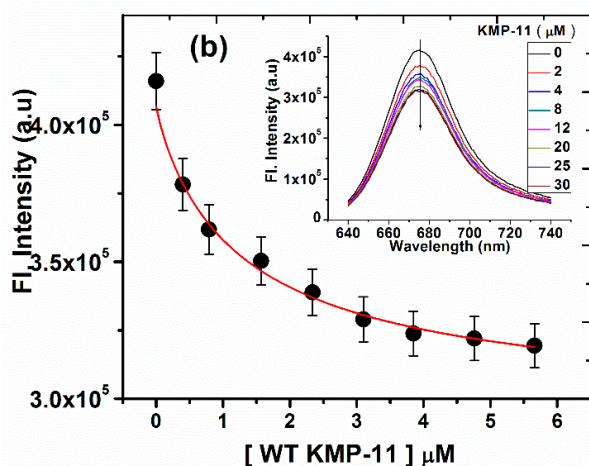
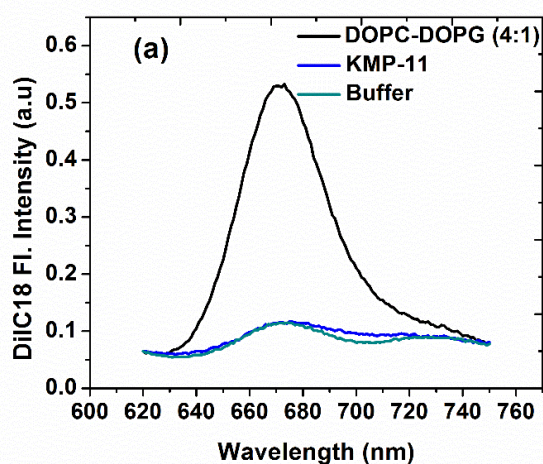


Figure 5.2: (a) Fluorescence emission spectra of DiI C-18, showing significant intensity in the presence of LUV, while fluorescence is very low or absent when the dye is present in aqueous buffer or buffer containing KMP-11 only. (b) shows the decrease in fluorescence intensities of DiI C-18 (present in solution of LUV) with increasing concentration of KMP-11. The solid red line is the fit using the Hill equation. Inset shows the fluorescence spectrum for increasing concentrations of KMP-11 indicated by an arrow. (c) Change in tryptophan emission with increasing concentration of DOPC: DOPG (4:1) LUVs. In this experiment, a single tryptophan mutant (Y48W) was used. The inset in (c) shows the fluorescence emission spectra with increasing LUV concentrations.

Unlike the binding of KMP-11 with DOPC, we found non-cooperative binding of KMP-11 with PC-PG, as cooperative index (n) was found to be ~ 1 .

We complemented the above DiI C-18 binding experiments using steady state fluorescence measurements. For this, we used a single tryptophan mutant of KMP-11 (Y48W), as wild type KMP-11 does not contain any tryptophan residue in its sequence. This single tryptophan mutant (Y48W) showed similar secondary conformation as that of wild type KMP-11 and the tryptophan residue was found to be fully buried inside the hydrophobic core region (22-23). Y48W showed maximum intrinsic fluorescence intensity at wavelength 327 nm. The addition of DOPC-DOPG LUVs significantly decreased the fluorescence intensity of tryptophan (Fig. 5.2c).

The fluorescence assay of Trp residue shows similar binding affinity as that obtained from DiI C18. The binding constant obtained from Trp assay ($K = 2.64 \times 10^5 \text{ M}^{-1}$) is in agreement with that obtained from DiI C18 assay ($2.46 \times 10^5 \text{ M}^{-1}$), confirming protein binding with the membrane.

To obtain further insights into the protein-lipid interactions, we used zeta potential and hydrodynamic radius measurements. Zeta potential is a good approximation to the surface potential at moderate electrolyte concentration. As both protein and the membrane were charged, the binding between the protein and lipid was expected to change the value of zeta potential. In addition, the binding might also increase hydrodynamic radius. However, mild aggregation due to lipid protein interaction could not be ruled out. Figs 5.3(a) and 5.3(b) showed the variation of zeta potential and hydrodynamic radius with different protein to lipid (P/L) ratio. It was interesting to

note that the change of these two parameters (zeta potential and hydrodynamic radius) did not seem to match very well, although they were expected to represent the same event (KMP-11-LUVs interaction). While the change in hydrodynamic radius was somewhat slow occurring in one step, zeta potential variation had two steps. The first step was a rapid increase (occurring within $P/L \sim 0.02$), which was followed by a slow decrease. While any mechanistic understanding of the early rapid increase in zeta potential is not available, we speculate that this is probably a rapid reorganization of the protein-lipid binding interface or the water environment. In order to understand the behavior of zeta potential and to obtain insights into the binding phenomenon and protein activity, it is now important to investigate the charge distribution of the amino acid residues of the entire protein.

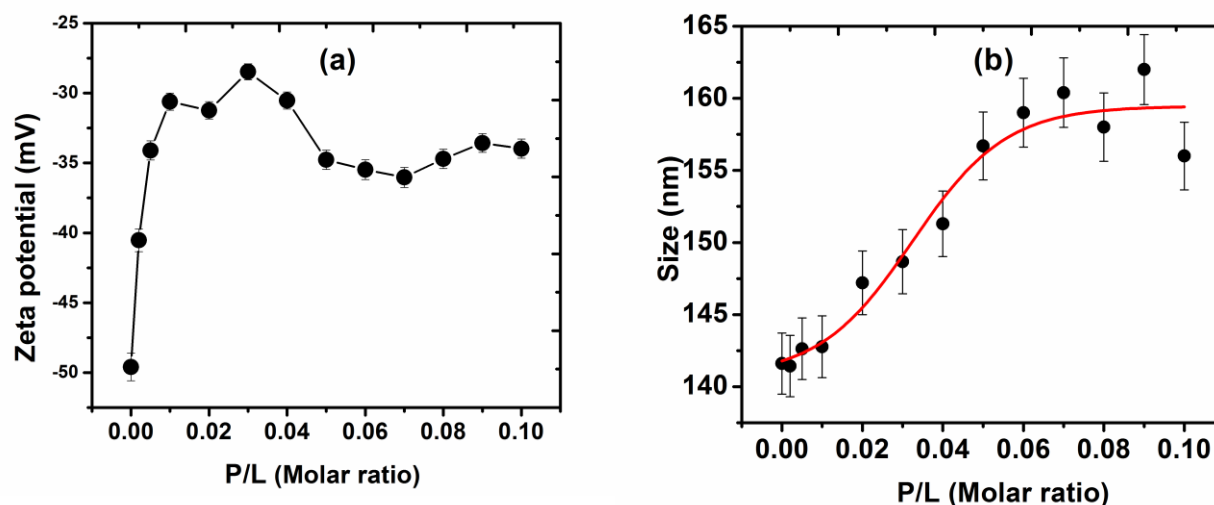


Figure 5.3: (a) Variation of zeta potential of LUV made from PC:PG (4:1) mixture with increasing protein to lipid (P/L) ratio. (b) Average hydrodynamic radius the LUV with increasing P/L obtained from the DLS measurement.

5.3.2 Charge distribution of the protein KMP-11

KMP-11 possesses a negative charge (-1.7) at physiological pH as determined by the protein calculator v3.4 server (<http://protpcalc.sourceforge.net/>). The association of negatively charged protein with anionic membranes was thus intriguing. We speculate that a local positively charged region might be able to initiate the binding process, which would be later facilitated by other factors, like non-polar interactions. We used EMBOSS software to determine the local cationic regions in the sequence. As shown in Fig. 5.4 (a), two stretch of positively charged sequence could be identified: one between residues 10 and 30 and the other between residues 40 and 70. Subsequently, we resorted to theoretical approach to spot active regions of KMP-11 and look for antimicrobial sequence stretch or domain. We found out that KMP-11 contains prominent antimicrobial propensity at the region 60-80 of its sequence (Fig. 5.4 (b)), and this sequence stretch (with microbacterial property) was close to one of the two positively charged regions. Since pore formation is the prerequisite of the antibacterial property of a peptide stretch, we hypothesize that an efficient binding through these local positive regions may trigger pore formation property of the protein.

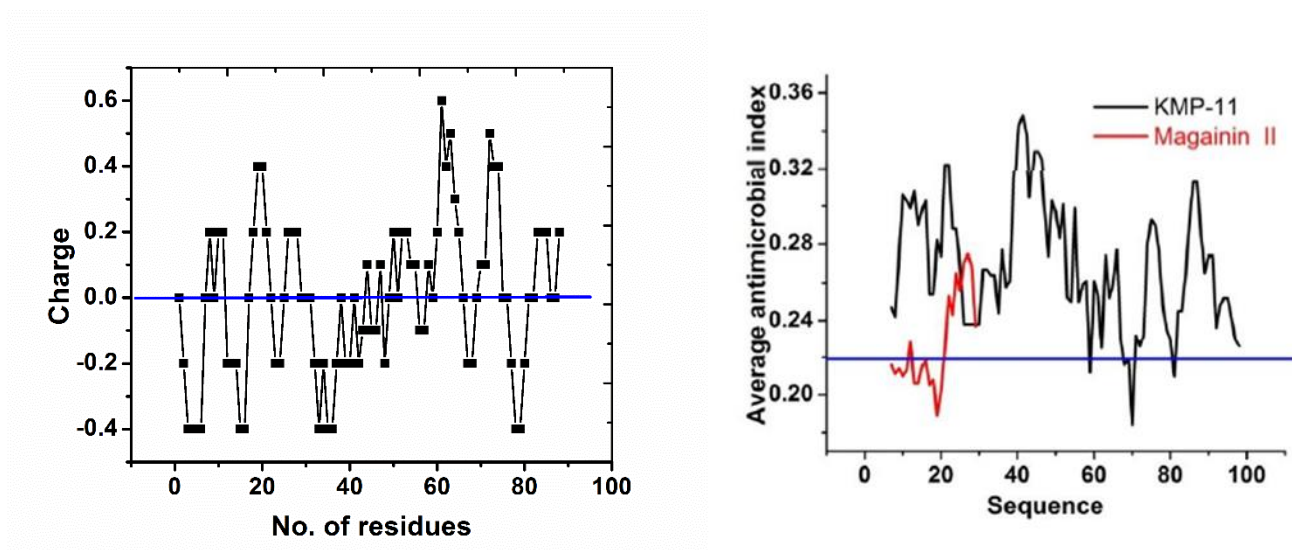


Figure 5.4: (a) Charge distribution of the amino acid residues of KMP-11 throughout the entire sequence of protein calculated using EMBOSS software. (b) Average antimicrobial index against

the sequence stretch of WT KMP-11 and magainin-II. The blue line suggests the threshold value of average antimicrobial index.

5.3.3 Formation of trans-membrane pores induced by KMP-11

5.3.3.1 KMP-11 induced leakage in phospholipid membrane

We then studied experimentally the ability of KMP-11 to form pores by measuring the fluorescence intensity of calcein loaded LUV with time. Fig. 5.5 showed the enhancement of fluorescence intensity over time at three different concentrations of KMP-11, indicating the release of entrapped dye from the vesicles. Such an increase in intensity was attributed to the formation of trans-membrane pores (24). It is important to mention that fluorescence intensity did not increase in the absence of KMP-11 (Fig. 5.5).

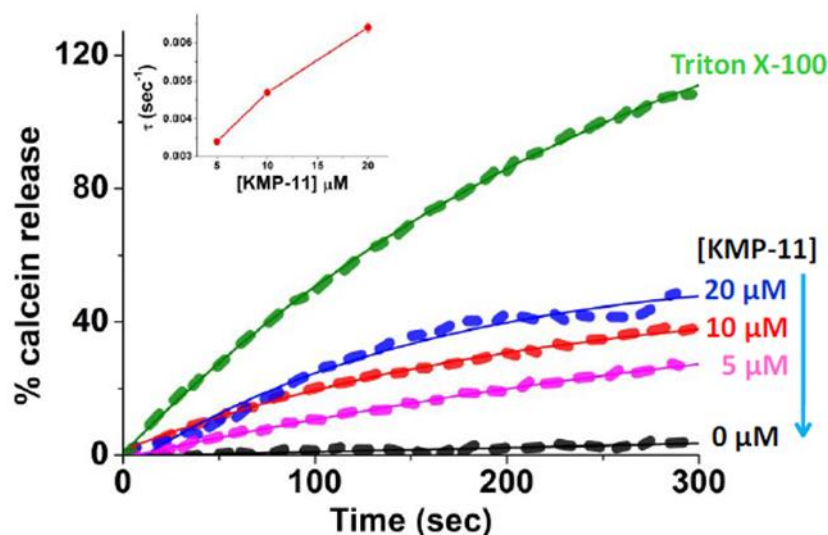


Figure 5.5: Calcein release assay showing the leakage of entrapped calcein from the LUV composed of PC:PG (4:1). This experiment has been performed using three different concentrations of KMP-11. Rate constant of calcein for three different protein concentrations is shown in inset of the figure. Typical lipid concentration was taken 20 μM.

This result clearly indicated that KMP-11 induced pores in the membrane, through which calceins were released. The pore size must be larger than the size of the calcein molecules enabling to translocate from the interior of the vesicle through pores. We found that the kinetics of pore formation was dependent on protein concentration (Fig. 5.5, inset). The rate of calcein release was determined by fitting the data using an exponential rate equation, the variation of which with protein concentration is shown in the inset of the Fig. 5.5. The growth rate was found to be $\sim 6.4 \times 10^{-3} \text{ sec}^{-1}$ when calcein loaded vesicles were exposed to $20 \mu\text{M}$ and decreased with reducing protein concentration. Unlike the antimicrobial peptide melittin, showing the pore formation in DOPC membrane (25), we found that KMP-11 exhibited higher rate of calcein release in DOPC LUV containing DOPG (Fig. 5.6). This result suggested a significant role of anionic lipids (DOPG) in pore formation. This is indeed the requirement of many antimicrobial peptides where they only target negatively charged membrane and remain inert to the neutral phospholipids (26-27). It may be noted that a previous report by T. Yeung et al indeed has shown that the negative surface charge of the inner leaflet of the plasma membrane determines the targeting of proteins with cationic domain (15). Therefore, negatively charged surface of macrophage may be required for targeting the immunogenic protein KMP-11 which eventually forms pores to facilitate the internalization of leishmania parasite.

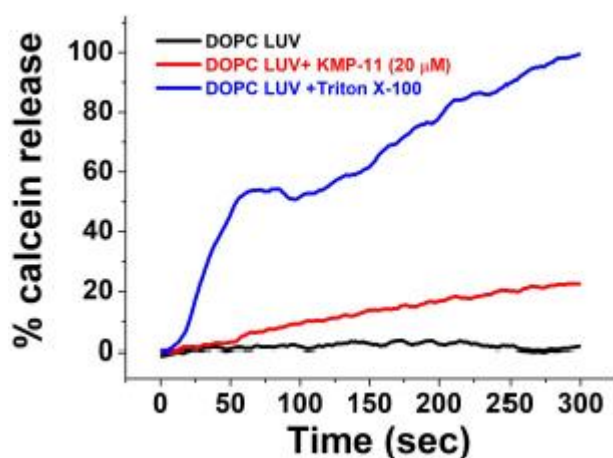


Figure 5.6: Dye leakage spectra of calcein entrapped LUVs composed of DOPC lipid in presence of KMP-11 (concentration was $20 \mu\text{M}$) and in presence of triton X-100.

5.3.3.2 KMP-11 induced pore formation as evidenced from the phase contrast micrographs of GUV

As KMP-11 showed the evidence of strong binding with the membrane, especially with anionic vesicles and has an antimicrobial sequence, it would be interesting to monitor directly the formation of pores using optical microscopy. Such an experiment would further validate pore formation hypothesis and complement the results obtained from calcein release experiments. For this purpose, we explored phase contrast microscopy of GUVs exposed to protein solution. In this method, any change in the morphology of GUV can be directly visualized without introducing the fluorescence probe. Therefore, the issue of alteration of membrane properties or the protein-membrane interaction due to the presence of fluorophores can be avoided. We could observe GUV with a good contrast in the halo region, as vesicles are prepared in a sucrose solution and diluted with glucose solution. GUV, made from DOPC and mixtures of DOPC with DOPG, were observed with three different protein concentrations (5, 10 and 20 μM). GUVs were prepared in 100 mM sucrose solution and diluted with 100 mM glucose solution. Identical concentrations of glucose and sucrose solutions were used to eliminate any resultant osmotic stress. Fig. 5.7 showed time sequence of phase contrast images of GUV exposed to 20 μM KMP-11 solutions. GUV images for 5 and 10 μM concentrations of KMP-11 were shown in Fig. 9. Halo region in the GUV image was formed due to the difference in contrast between the interior and exterior of GUV. Once the pores were formed on the membranes, we would expect leakage of internal fluid through the pores. As a result, halo regions were expected to disappear with time and GUV should look similar to that without diluting in glucose. Change in the difference of the gray value (I_{ptp}) of the halo region with time for DOPC-DOPG (4:1) GUV, indicated exchange of fluid between interior and exterior of the GUV, leading to the loss of contrast.

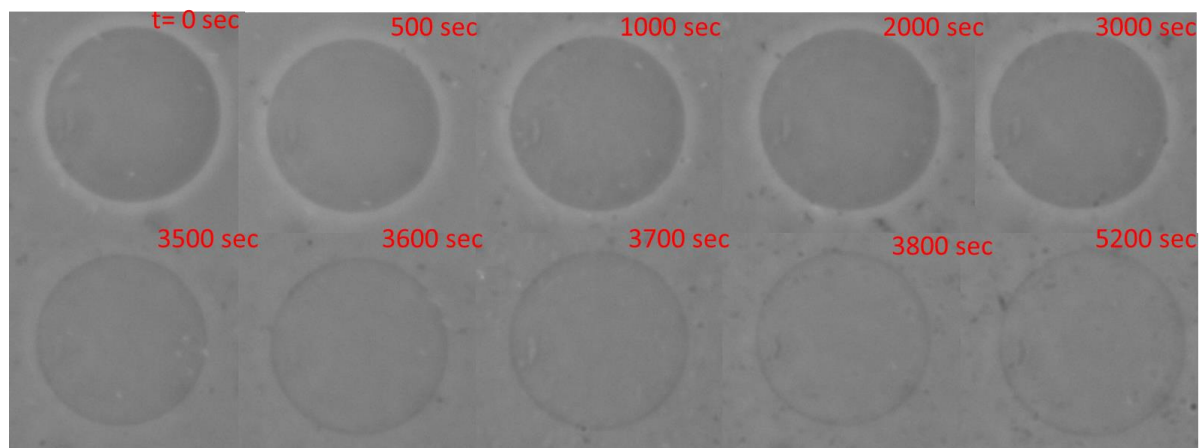


Figure 5.7: The phase contrast images of GUVs composed of DOPC-DOPG (4:1), which are exposed to 20 μM KMP-11. Protein to lipid ratio (P/L) \sim 0.02. Diameter of the vesicle \sim 34 μm .

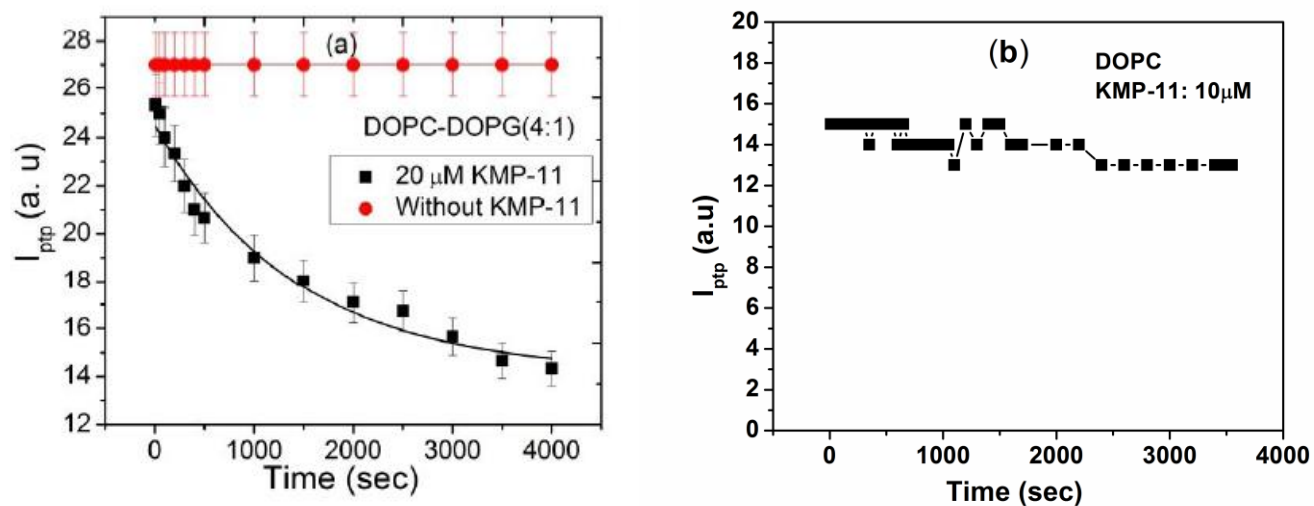


Figure 5.8: (a) The decay of (peak to peak intensity) with time for DOPC-DOPG and (b) DOPC GUVs. The solid line represents the fit, which was obtained from a single exponential decay. The decay rate constant (τ) was found to be $(0.7 \pm 0.06) \times 10^{-3} \text{ sec}^{-1}$. For comparison, red circles in (a) have been obtained from GUV without KMP-11.

Figure 5.8 (a) showed that I_{ptp} decreased until GUV in the presence of KMP-11 completely lost its contrast in the halo region. The analysis of phase contrast images to predict the pore formation has not been described in any of the earlier studies. It is important to mention that aqueous dispersion of GUVs in the absence of KMP-11 was found to be very stable and did not show any variation of I_{ptp} (Fig. 5.8, red circle). In addition, GUVs, prepared from only DOPC did not show any significant decrease of I_{ptp} when exposed to KMP-11 (Fig. 5.8 (b)). This result clearly indicated the importance of the negatively charged membrane in the pore formation which was found to be consistent with the results obtained from calcein release experiments.

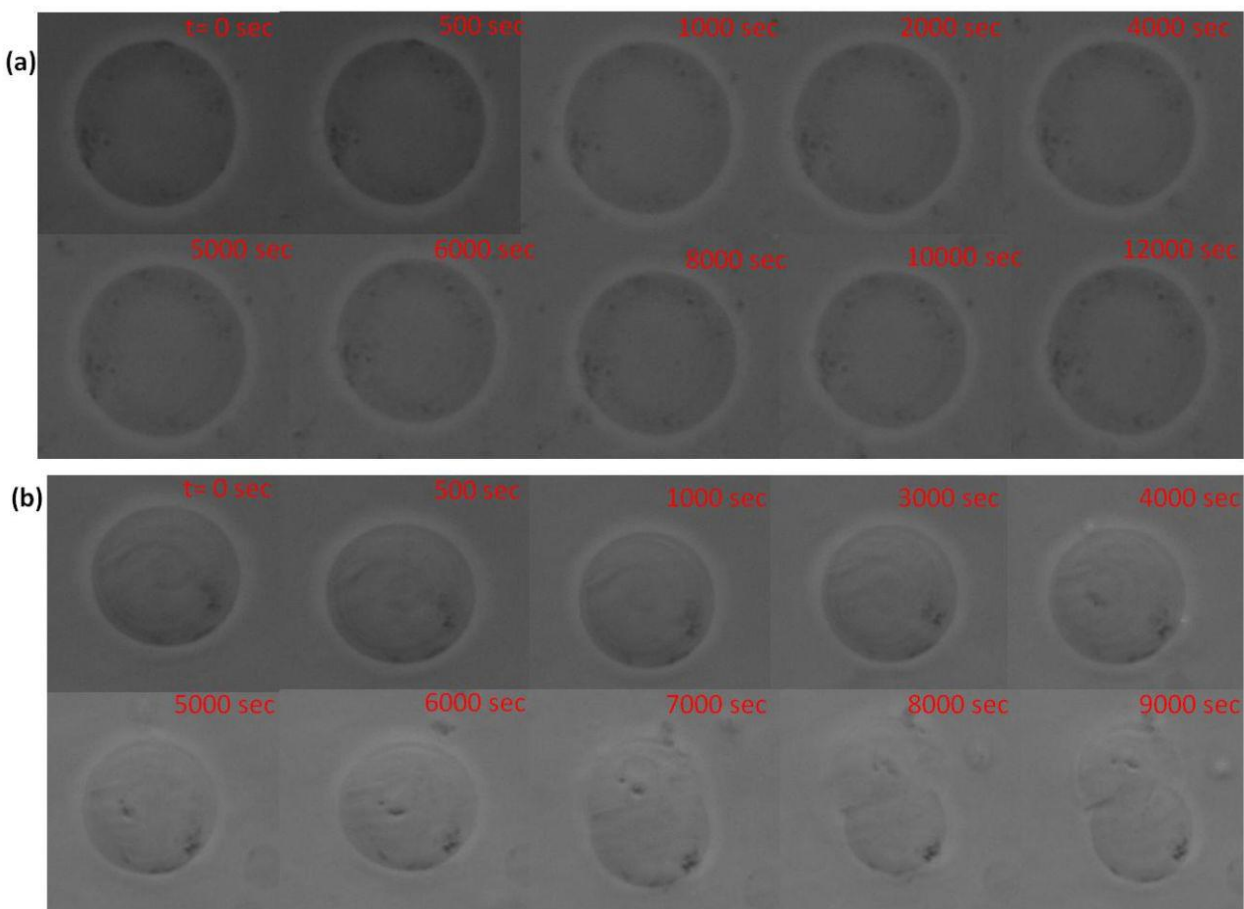
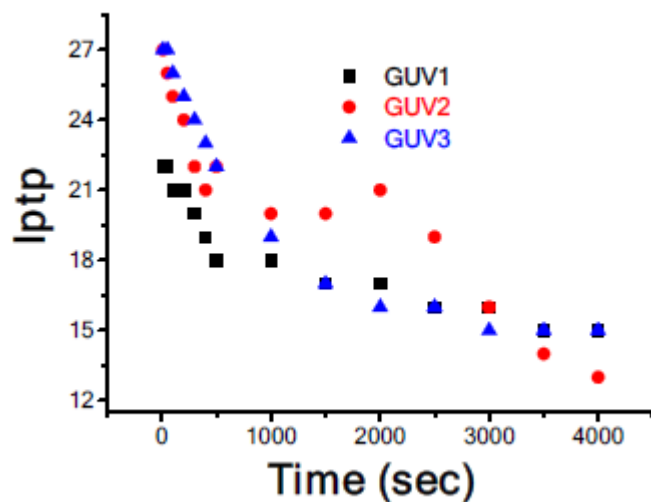
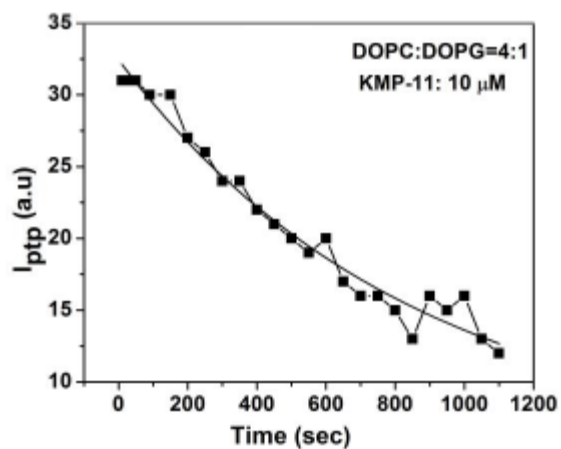


Figure 5.9: Phase contrast micrographs of GUV composed of DOPC-DOPG (4:1) exposed to (a) 5 μ M and (b) 10 μ M concentrations of KMP-11. The size of the vesicle \sim 34 μ m.

The prepared GUVs were found to show heterogeneity in terms of the time they take to start the pore formation process. As a result, we could not precisely determine the time point that initiates pore formation for a particular GUV. In addition, we have also experience some heterogeneity due to GUV size variations. As a result, the presented data represented the average response of several (at least three) GUVs (Fig. 5.10 a). Nevertheless, we could unambiguously determine the behavior of the rate constants for different protein concentrations. GUV exposed to 5 μM KMP-11 took longer time to form pores and complete disappearance of halo region was obtained at much higher time scale compared to one exposed to 10-20 μM KMP-11 (Fig. 5.10 b). The change in I_{ptp} with time was fit to a single exponential decay function to obtain the time constant (τ) (Fig. 5.8 a). The rate constants for two different concentrations 10 μM and 20 μM were found to be $1.2 \times 10^{-3} \text{ sec}^{-1}$ (Fig. 5.10 b) and $0.7 \times 10^{-3} \text{ sec}^{-1}$ (Fig. 5.8 a), respectively. For 5 μM of KMP-11 we have not observed significant decrease in I_{ptp} with time. The growth rate ($6.4 \times 10^{-3} \text{ sec}^{-1}$) of calcein release experiment was inconsistent with decay rate obtained from the analysis of phase contrast images. This differences of the rate constants obtained from two different experimental techniques could arise due to difference in vesicles size, as well as intrinsic concentration of KMP-11 at the vicinity of the membrane.



(a)



(b)

Figure 5.10: (a) Change in I_{ptp} values of three different GUVs when these were treated with 20 μM concentration of KMP-11. (b) The decay of I_{ptp} (peak to peak intensity) with time for GUV composed of DOPC-DOPG. Solid line represents the fit curve obtained from single exponential decay and decay rate constant (τ) was found to be 0.0012 sec^{-1} .

5.3.3.3 Effect of cholesterol on the pore formation

Previous studies have already shown that the presence of cholesterol strongly affects the process of internalization of parasite into host macrophages (11,14). Therefore, it would be interesting to know the role of cholesterol on the pore forming activity of protein.

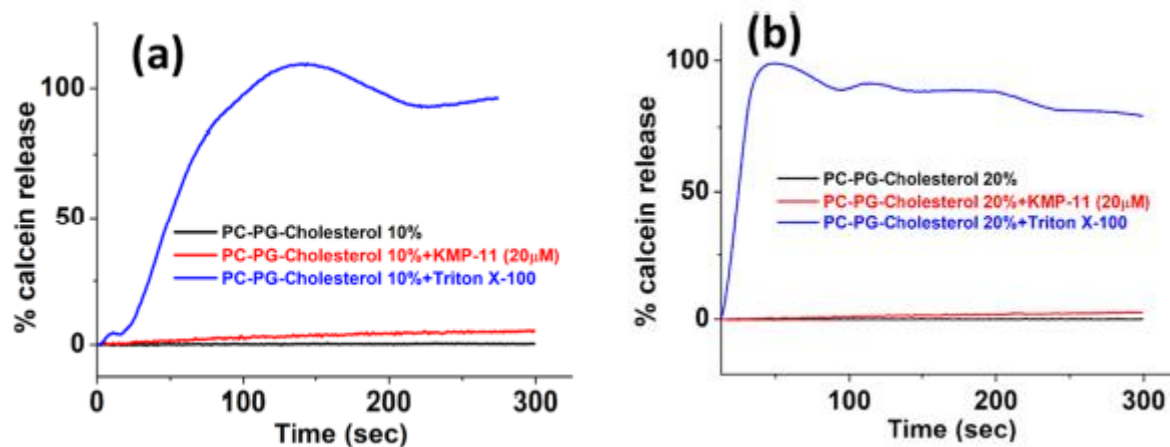


Figure 5.11: Calcein release assay showing the leakage of entrapped calcein from the LUV composed of PC:PG (4:1) at (a) 10 mole% and (b) 20 mole % of cholesterol. These experiments have been performed at 20 μM concentration of KMP-11 and typical lipid concentration was kept 20 μM .

Fig. 5.11(a) and 5.11(b) showed the percentage of calcein release from the LUV containing different mole% of cholesterol when exposed to 20 μM KMP-11. The percentage of calcein

release, which was measured by the increase in fluorescence intensity, decreased significantly with increasing cholesterol concentration. Further, as a control experiment, we found no calcein release in the absence of KMP-11 (Fig. 5.11a, 5.11b) and 100% leakage was found when LUVs were treated with triton X-100 and this 100% leakage was used to calculate the percentage of dye leakage from the LUVs at different cholesterol percentages. To complement this leakage assay, we also performed the GUV assay to find out the pore forming activity of KMP-11 in presence of different molar content of membrane cholesterol. Phase contrast microscopy experiment on GUV, containing 10 and 20 mole% of cholesterol, did not seem to show any significant decay of the I_{ptp} across the halo region (Fig. 5.11c). This result indicated that there was no significant leakage or exchange of fluid in the presence of cholesterol, suggesting that incorporation of cholesterol tends to inhibit KMP-11 induced pore formation.

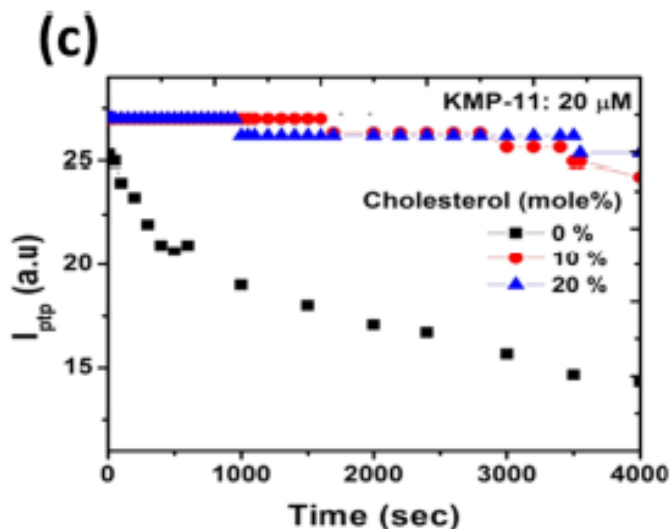


Figure 5.11: (c) Peak-to-peak intensity across the halo regions at two different cholesterol concentrations, indicated in the figure legend. GUV containing cholesterol does not show any significant leakage in microscopy experiments. For comparison, we have again shown the decay curve for 0 mole % cholesterol.

The driving force of pore formation is the membrane tension (σ) whereas line tension, around the pore determines the stability of the pores. Therefore, energetics of pore of radius r would be given by $E_{pore} = 2\pi r\gamma - \pi r^2\sigma$. The intrinsic scale of membrane tension is determined by the

spontaneous curvature and bending modulus of the membranes, whereas mechanical tension is governed by its stretching modulus (28). We can argue that the role of KMP-11 would be to create stress which is equivalent to membrane tension required for the formation of pore. In addition, these elastic parameters would change for a membrane containing cholesterol. However, it is known from previous literatures that the effect of cholesterol on the membrane tension is not universal; rather it depends on the specific architecture of the lipid building the membrane (29-30). Various experimental techniques, such as fluctuations spectroscopy, micropipette aspiration, electrodeformation etc. are insensitive to give change in stiffness of membrane made from DOPC-cholesterol mixture (31). However, it is well known that increase in cholesterol content leads to liquid ordered (L_o) phase (cholesterol rich), which has higher rigidity than cholesterol poor liquid disordered (L_d) phase (32). In order to validate this, we investigated the fluorescence emission of an environment sensitive probe Laurdan. At room temperature, DOPC: DOPG (4:1) LUVs remains in L_d phase which is confirmed by the emission maximum at 490 nm (Fig. 5.12). It is clearly evident from Fig. 5.12 that emission spectra get blue shifted with increasing cholesterol concentrations. Further, GP of Laurdan increases with increasing cholesterol content in the vesicles.

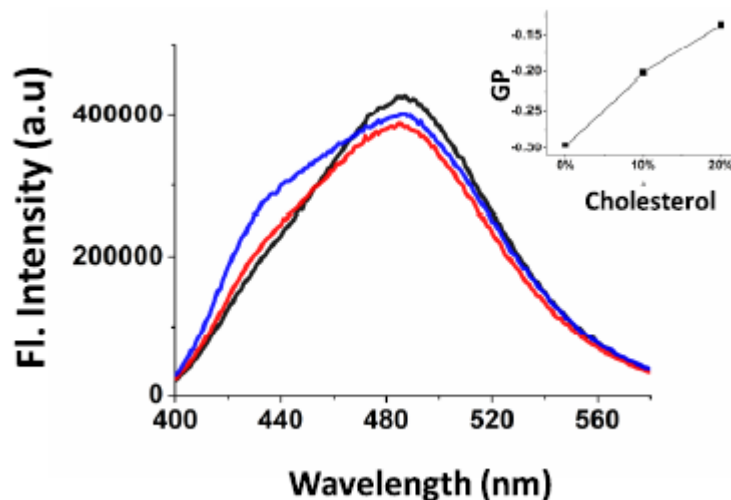


Figure 5.12: Laurdan emission spectra of DOPC: DOPG (4:1) LUVs containing 0 mole% (black), 10 mole% (blue) and 20 mole% (red) cholesterol. Inset shows the generalized polarization (GP) values of Laurdan obtained from 0, 10 and 20 mole% of cholesterol.

These results indicate that membrane rigidity increases with cholesterol. Further, it has been found in our previous study that the association constant of wild type KMP-11 decreases with increasing cholesterol concentration (3). Such a change in the elastic property of membrane and decrease in the binding affinity of KMP-11 in presence of membrane cholesterol may not facilitate the pore formation induced by KMP-11.

5.3.3.4 A conjecture on the mechanism of parasite entry and implications in leishmaniasis

The present study describes the pore forming activity of the protein KMP-11 in model membranes in view of the understanding the host-pathogen relationship in the context of leishmaniasis. While it is only an *in vitro* study and the actual disease scenario is expected to be complex, a simplified understanding of the parasite entry process (Fig. 5.13) could be hypothesized based on our present results. As reported in our previous study that an abundant immunogenic membrane protein, KMP-11, expressed on surface of parasite, play vital role in modulating membrane properties when binds to macrophage membrane (3). Therefore, this protein helps in the internalization of parasite for productive infection. In the present study we indeed found an efficient binding of the KMP-11 onto membrane, which facilitates pore formation. We believe that this process may eventually help the parasite to enter into the host macrophage (Fig. 5.14). A similar mechanisms found in case of antimicrobial peptide (33). It is established that parasites can translocate via transmembrane pores for their survival. It has been reported that cholesterol in the host macrophage plays vital role in leishmania infection (34). Therefore, interaction of KMP-11 with the model membranes is expected to alter in the presence of cholesterol. We indeed found that cholesterol affects the pore forming ability of KMP-11 as found in both calcein release and optical microscopy experiments. Further study is required in order to understand the cholesterol connection in the leishmaniasis.

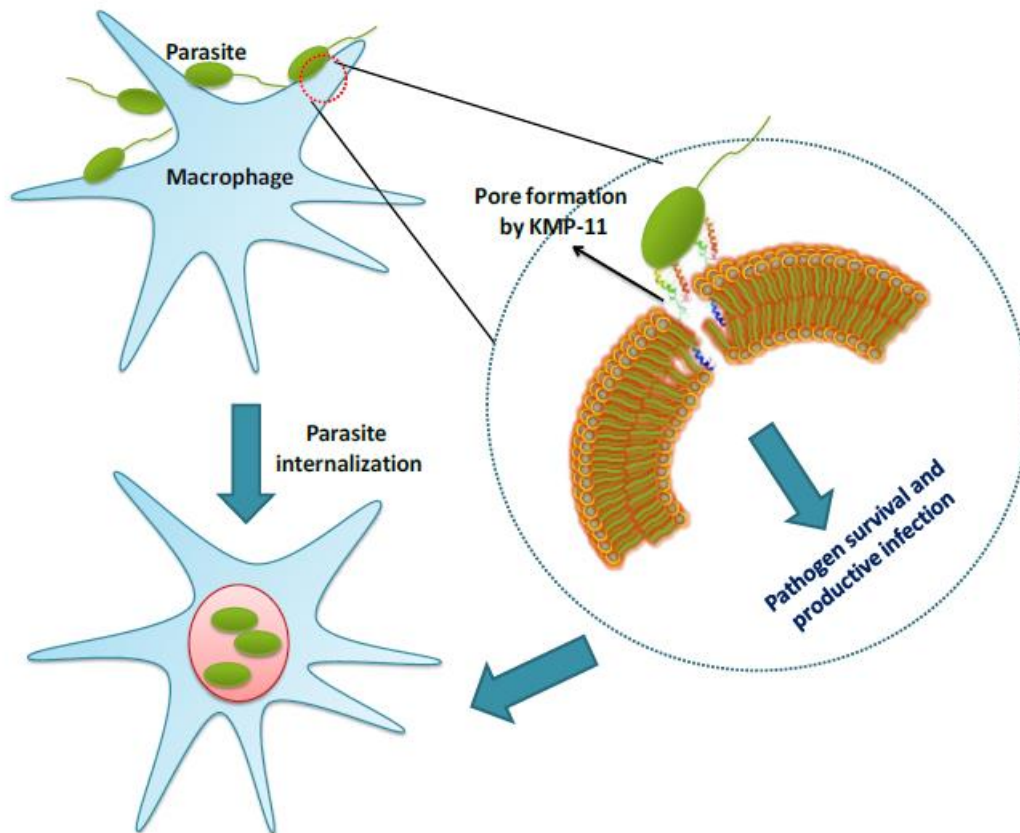


Figure 5.13: Schematic diagram of infection mechanism via trans-membrane pore formation induced by KMP-11.

5.4 Conclusion

A systematic investigation on the interaction of KMP-11 with anionic phospholipid membranes reveals, for the first time, that KMP-11 is able to induce pores in the anionic phospholipid membrane. Both calcein release fluorescence assay of large unilamellar vesicles and phase contrast microscopy of giant unilamellar vesicles have been employed to show the leakage of internal fluid and exchange of fluids suggesting the formation of trans-membrane pores. The rate of increase in the fluorescence intensity due to calcein release is consistent with the rate of decay in intensity across the halo region of phase contrast micrographs of GUV. We also explored pore forming activity of KMP-11 on the membrane containing cholesterol, no significant growth of intensity in

calcein release experiment on LUV containing 10-20 mole% of cholesterol, suggests that cholesterol inhibits pore formation in membranes. Further studies on interaction of KMP-11 with the negatively charged membranes using fluorescence spectroscopy and zeta potential revealed that the KMP-11 has a strong affinity to the membrane. The nature of decay of fluorescence intensity of DiIC-18 and decrease in the negative value of zeta potential suggest the non-cooperative binding of proteins. Binding constant obtained from fluorescence (DiIC-18) decay is in agreement with that obtained earlier in case of DOPC membrane. Based on our results, we hypothesize that the strong interaction of KMP-11 and its pore forming activity towards anionic membrane may have implications in the process of internalization of leishmania parasite into macrophages for parasite survival and replication.

References

- (1) J D Chulay, A D Bryceson. Quantitation of amastigotes of *Leishmania donovani* in smears of splenic aspirates from patients with visceral leishmaniasis. *Am. J. Trop. Med. Hyg.* **1983**, 32 (3), 475-479.
- (2) J D Lambris, D Ricklin, B V Geisbrecht. Complement evasion by human pathogens. *Nat. Rev. Microbiol.* 2008, 6 (2), 132.
- (3) A Sannigrahi, P Maity, S Karmakar, K Chattopadhyay. Interaction of KMP-11 with phospholipid membranes and its implications in leishmaniasis: effects of single tryptophan mutations and cholesterol. *J. Phys. Chem. B* 2017, 121 (8), 1824-1834.
- (4) A A Spector, M A Yorek, Membrane lipid composition and cellular function. *J. Lipid Res.* 1985, 26 (9), 1015-1035.
- (5) A Sannigrahi, I Nandi, S Chall, J J Jawed, A Halder, S Majumdar, S Karmakar, K Chattopadhyay. Conformational switch driven membrane pore formation by *Mycobacterium* secretory protein MPT63 induces macrophage cell death. *ACS Chem. Biol.* 2019, 14 (7), 1601-1610.
- (6) R Panchal, M Smart, D Bowser, D Williams, S Petrou. Pore-forming proteins and their application in biotechnology. *Curr. Pharm. biotechnol.* 2002, 3 (2), 99-115.
- (7) C L Evavold, J Ruan, Y Tan, S Xia, H Wu, J C Kagan. The pore-forming protein gasdermin D regulates interleukin-1 secretion from living macrophages. *Immunity* 2018, 48 (1), 35-44. e6.
- (8) F C Los, T M Randis, R V Aroian, A J Ratner. Role of pore-forming toxins in bacterial infectious diseases. *Microbiol. Mol. Biol. Rev.* 2013, 77 (2), 173-207.
- (9) S C F de Mendonça, L Cysne-Finkelstein, D C D S Matos. Kinetoplastid membrane protein-11 as a vaccine candidate and a virulence factor in *Leishmania*. *Front. Immunol.* 2015, 6, 524.
- (10) R W Mahley, E Apolipoprotein. cholesterol transport protein with expanding role in cell biology. *Science* 1988, 240 (4852), 622-630.

- (11) T J Pucadyil, P Tewary, R Madhubala, A Chattopadhyay. Cholesterol is required for *Leishmania donovani* infection: implications in leishmaniasis. *Mol. Biochem. Parasit.* 2004, 133 (2),145-152.
- (12) G A Kumar, S Roy, M Jafurulla, C Mandal, A Chattopadhyay. Statin-induced chronic cholesterol depletion inhibits *Leishmania donovani* infection: relevance of optimum host membrane cholesterol. *BBA-Biomembranes* 2016, 1858 (9), 2088-2096.
- (13) H Barman, M Walch, S Latinovic-Golic, C Dumrese, M Dolder, P Groscurth, U Ziegler. Cholesterol in negatively charged lipid bilayers modulates the effect of the antimicrobial protein granulysin. *J. Membr. Biol.* 2006, 212 (1), 29-39.
- (14) J Ghosh, R Guha, S Das, S Roy. Liposomal cholesterol delivery activates the macrophage innate immune arm to facilitate intracellular *Leishmania donovani* killing. *Infect. Immun.* 2014, 82 (2),607-617.
- (15) T Yeung, G E Gilbert, J Shi, J Silvius, A Kapus, S Grinstein. Membrane phosphatidylserine regulates surface charge and protein localization. *Science* 2008, 319 (5860), 210-213.
- (16) P Maity, B Saha, G S Kumar, S Karmakar. Binding of monovalent alkali metal ions with negatively charged phospholipid membranes. *BBA-Biomembranes* 2016, 1858 (4), 706-714.
- (17) J C M Stewart. Colorimetric determination of phospholipids with ammonium ferrothiocyanate. *Anal. Biochem.* 1980, 104 (1), 10-14.
- (18) T Benachir, M Monette, J Grenier, M Lafleur. Melittin-induced leakage from phosphatidylcholine vesicles is modulated by cholesterol: a property used for membrane targeting. *Euro.Biophys. J.* 1997, 25 (3), 201-210.
- (19) T Pott, H Bouvrais, P Méléard. Giant unilamellar vesicle formation under physiologically relevant conditions. *Chem. Phys. Lipids* 2008, 154 (2), 115-119.
- (20) A S Klymchenko, R Kreder. Fluorescent probes for lipid rafts: from model membranes to living cells. *Chem. Biol.* 2014, 21 (1), 97-113.
- (21) N Kahya. Protein–protein and protein–lipid interactions in domain-assembly: lessons from giant unilamellar vesicles. *BBA-Biomembranes* 2010, 1798 (7), 1392-1398.

- (22) S Sharma, S Sarkar, S S Paul, S Roy, K Chattopadhyay. A small molecule chemical chaperone optimizes its unfolded state contraction and denaturant like properties. *Sci. Rep.* 2013, 3, 3525.
- (23) A Sannigrahi, D Mullick, D Sanyal, S Sen, U Maulik, K Chattopadhyay. Effect of Ergosterol on the Binding of KMP-11 with Phospholipid Membranes: Implications in Leishmaniasis. *ACS Omega* 2019, 4 (3), 5155-5164.
- (24) O S Belokoneva, H Satake, E L Mal'tseva, N P Pal'mina, E Villegas, T Nakajima, G Corzo. Pore formation of phospholipid membranes by the action of two hemolytic arachnid peptides of different size. *BBA-Biomembranes* 2004, 1664 (2), 182-188.
- (25) G Van Den Bogaart, J V Guzmán, J T Mika, B Poolman. On the mechanism of pore formation by melittin. *J. Biol. Chem.* 2008, 283 (49), 33854-33857.
- (26) S Karmakar, P Maity, A Halder. Charge-Driven Interaction of Antimicrobial Peptide NK-2 with Phospholipid Membranes. *ACS omega* 2017, 2 (12), 8859-8867.
- (27) O S Ostroumova, S S Efimova, V V Malev. Modifiers of membrane dipole potentials as tools for investigating ion channel formation and functioning. In *Int. Rev. Cell Mol. Biol.* 2015, 315, 245-297.
- (28) R Lipowsky. Coupling of bending and stretching deformations in vesicle membranes. *Adv.colloid Interface Sci.* 2014, 208, 14-24.
- (29) B Hissa, B Pontes, P M S Roma, A P Alves, C D Rocha, T M Valverde, P H N Aguiar, F P Almeida, A J Guimarães, C Guatimosim. Membrane cholesterol removal changes mechanical properties of cells and induces secretion of a specific pool of lysosomes. *PloS one* 2013, 8 (12), e82988.
- (30) R Dimova. Recent developments in the field of bending rigidity measurements on membranes. *Adv. Colloid Interface Sci.* 2014, 208, 225-234.
- (31) R S Gracià, N Bezlyepkina, R L Knorr, R Lipowsky, R Dimova. Effect of cholesterol on the rigidity of saturated and unsaturated membranes: fluctuation and electrodeformation analysis of giant vesicles. *Soft Matter* 2010, 6 (7), 1472-1482.
- (32) W C Tsai, G W Feigenson. Lowering line tension with high cholesterol content induces a transition from macroscopic to nanoscopic phase domains in model biomembranes. *BBA-Biomembranes* 2019, 1861 (2), 478-485.

- (33) H K Kang, C Kim, C H Seo, Y Park. The therapeutic applications of antimicrobial peptides (AMPs): a patent review. *J. microbiol.* 2017, 55 (1), 1-12.
- (34) G Semini, D Paape, A Paterou, J Schroeder, M Barrios-Llerena, T Aebischer. Changes to cholesterol trafficking in macrophages by *Leishmania* parasites infection. *Microbiologyopen* 2017, 6 (4), e00469.

Chapter 6

Use of spectroscopic properties of lipophilic dye, Nile red to understand the physico-chemical properties of lipid bilayer: Effect of chain saturation and cholesterol.

6.1 Introduction

As discussed in earlier chapters, antimicrobial peptide interacts only bacterial cell membrane over mammalian membrane through electrostatic interaction. Therefore, it is important to study how physico-chemical properties of lipid bilayer get altered due to interaction of AMP. As Nile red is one of the widely used environment sensitive lipophilic dye, its spectroscopic properties can be used to probe the change in the properties of lipid bilayer. The emission spectra of Nile red are also expected to depend on lipid types, i.e. the composition of the membrane. Therefore, prior to introduction of peptide into the bilayer, it is necessary to understand spectroscopic behavior of Nile red with varying composition of membranes. In this chapter, we primarily concentrate on the spectroscopic properties of Nile red in the presence of membrane with different lipid composition and also with cholesterol. Further extension or outlook of the present study would be to introduce AMP to investigate the interaction with membrane using the spectroscopic properties of Nile red. In this chapter, we describe the effect of composition and the phase state of phospholipid membranes on the emission spectrum, anisotropy and lifetime of a lipophilic fluorescence probe Nile red. Fluorescence spectrum of Nile red in membranes containing cholesterol has also been investigated in order to get insights into the influence of cholesterol on the phospholipid membranes. The earlier studies are summarized in section 6.2. All experimental results have been discussed in section 6.3. We conclude this chapter in section 6.4.

6.2 Earlier studies

Large unilamellar vesicles (LUV) made from phospholipids serve as an excellent model system of biological membranes. Besides the model system of biological membranes, LUV are potential for diverse bio-technological applications (1). Cholesterol is a ubiquitous component of plasma membranes. Structure and functions of membranes are greatly influenced by lipid composition, chain saturation and the membrane-cholesterol (2). Cholesterol provides rigidity and integrity to the plasma membrane and prevents it from becoming overly fluid; It also helps to maintain its fluidity (3). The cholesterol-rich domains, called rafts are believed to exist in the membrane (4). These rafts resemble with the cholesterol-rich liquid ordered (l_o) phase and cholesterol-poor liquid disordered (l_d) phase arising due to phase separation in the model membranes composed of ternary mixtures of cholesterol with a saturated lipid, such as DPPC and an unsaturated lipid, such as DOPC (5). Fluorescence probes are widely used tools to characterize l_o and l_d phases in the cellular as well as artificial membranes. The coexistence of l_o and l_d phases can easily be envisaged using a fluorescence probe selectively stain for l_o phase (6). Some environment sensitive probes whose emission property depends on local polarity, hydration or fluidity of the membranes, have also been used to characterize the l_o and l_d phases (7,8). Nile red (9-diethylamino-5H-benzo(α) phenoxazine-5-one), is one such environment sensitive probe and is widely used to monitor the membrane organization and dynamics (9). It emits fluorescence in the presence of lipid membrane (10). However, its fluorescence is significantly quenched in the aqueous or polar environment. Its fluorescence properties are known to alter by the polarity of its immediate environment due to a large change in its dipole moment upon excitation (11). This property of nile red is utilized to monitor hydrophobic surfaces in proteins and hydrocarbon core in lipid membranes. Therefore, the nile red is used on living cells as a fluorescence stain for the detection of intracellular lipid droplets if the proper spectral condition is chosen (12,13). Lipid phase state and chain ordering, fluidity as well as in plane lateral diffusion etc. has significant implications in many biological functions. For example, lipid domains play a vital role in the process of development of the embryo of zebra fish (14). A basic and relevant question we would like to address that, can we use spectroscopic properties of nile red to identify the type of lipids and their phase state in the membrane? Further, in a cholesterol containing bilayer, is it possible

to calibrate or estimate the amount of cholesterol and to monitor the organization and heterogeneity induced by cholesterol in bio- membranes?

Therefore, the aim of the present article is to use the fluorescence properties of Nile red to identify the lipid type, phase state or the composition. As the temperature is one of the crucial parameters to determine the membrane environment, the temperature dependency of the emission properties of Nile red in the presence of phospholipid membranes has also been investigated. Further, we would like to monitor the organization, fluctuations and heterogeneity of membranes containing cholesterol. In the present study, we have systematically investigated fluorescence properties of Nile red in the presence of various lipids in the gel and fluid phases. Effect of cholesterol on the spectral properties of Nile red in these phases has been studied in details. Here, we report the effect of saturation of hydrocarbon chains on the emission spectra of Nile red. We have also shown that Nile red can be used to calibrate the amount of cholesterol in the membranes in l_o phase. Rotational correlation and hence rotational diffusion of Nile red in the cholesterol containing lipid membranes were also estimated from the present study. Change in rotational diffusion due to motional restriction of lipids in the presence of cholesterol has also been envisaged from red edge excitation shift (REES). Our study suggests that spectroscopic properties of Nile red can be utilized to monitor the functions, composition and structure of biological membrane at physiological condition.

6.3 Experimental results and discussions:

6.3.1 Effect of different phospholipids on the emission spectra of Nile red:

Nile red is an environment-sensitive probe, which shows fluorescence in the presence of lipid bilayer. Nile red is known to exhibit efficient fluorescence emission in hydrophobic environment and increases its efficiency with increasing hydrophobicity or decreasing the solvent polarity, resulting in a progressive blue shifted emission maximum (9). However, Nile red shows a very low quantum yield in a polar aqueous environment (Fig. 6.1). In our study, we have used large unilamellar vesicles made from different phospholipids and observed the emission spectra of Nile red to understand the effect of lipid composition on the emission spectra. The Nile red emission in the presence of different phospholipid vesicles is summarized in table-1. The λ_{em} (632 ± 2 nm)

of Nile red fluid phase is found to be independent of unsaturated lipid types used in our experiment, when excited at 550 nm. Our result on DOPC is in agreement with the previous study by Kucherak et al. (9). However, much lower value of λ_{em} (~ 618 nm) was reported by Mukherjee et al. (17). Although, Mukherjee et al., in their experiment, has incorporated the probe Nile red by co-drying with the lipids, the symmetric distribution of Nile red in both leaflet of the bilayer, due to negligible differences in curvature, cannot be the consequence of different λ_{em} . Nevertheless, we have obtained same λ_{em} irrespective of whether Nile was incorporated before or after the preparation of LUV. Moreover, the manner of probe insertion in the case is a moot point as the flip-flop rate of Nile red is very fast (9). We have also found that the λ_{em} is independent of solvent pH and consistently obtained the similar value of λ_{em} for all unsaturated lipids. We trust our results on DOPC, as we have consistently obtained the same results (within the experimental error) from several independent experiments.

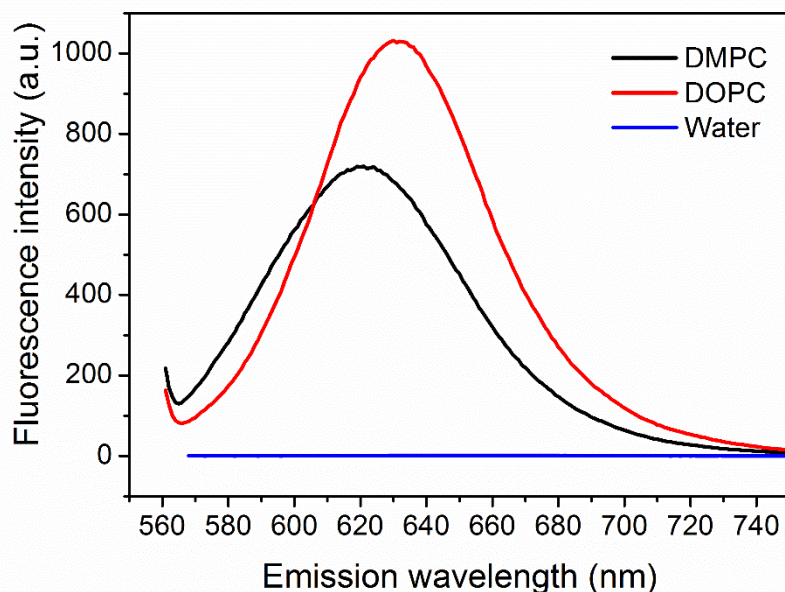


Figure 6.1: Emission spectrum of Nile red in DOPC and DMPC LUV at 25⁰ C. For comparison, the emission spectrum of pure aqueous medium is also shown. The intensity of the emission spectrum of water is negligible compared to that in the presence of LUV.

In order to explore the effect of charge and head group on the λ_{em} , we have prepared LUV from charged phospholipids. The λ_{em} does not seem to alter in the presence of negatively charged lipids (DOPG) and positively charged vesicles made from DOTAP and DOPC-DDAB mixture (4:1). Therefore, it is conceivable that the charge and head group of the membrane has no role in the emission of Nile red. To check the influence of chain length on the λ_{em} , fluorescence experiments with DPPC, DMPC and DLPC have been performed. Interestingly, the λ_{em} in the presence of saturated lipids, such as DPPC, DMPC at temperatures above their chain melting transition (T_m) was found to be very similar (within the error bar) when we have raised the temperature by 20⁰ C from the T_m for all above lipids. This is to avoid the temperature dependency of the λ_{em} in the fluid phase. As both the saturated phospholipids with different chain length show similar emission, the length of the hydrocarbon chain does not have any influence on the emission spectra of Nile red. This is contrary to the fact that Nile red selectively interacts with the hydrophobic sites of the bilayer. However, as found in the previous study (17), the Nile red is located at the interface between hydrocarbon chains and the head group. The interaction length is about 10-15 Å from the interface assuming the monolayer thickness ~26-30 Å. Therefore, it is expected that chain length should not influence the emission properties of Nile red. The fact that the saturated lipids DPPC, DMPC and DLPC in the fluid phase show very different emission than that of DOPC, the emission spectra indeed depend on the chain saturation of the membrane even though all above lipids are in the fluid phase. As we can access the gel phase of saturated lipids only, the emission spectrum in the gel phase has been monitored and λ_{em} was found to be 617 ± 2 nm. Since, λ_{em} does not depend significantly on head group and chain length, it is possible to compare the λ_{em} of Nile red in the fluid and gel phases of two different phospholipid membranes having same head group and similar chain length. Above emission properties of Nile red in the presence of vesicles, composed of various phospholipids, have not been emphasized in earlier studies.

In summary, the emission spectrum of Nile red in the fluid phase of DOPC differs by 9 ± 2 nm from the fluid phase of DPPC. However, in the fluid phase of two different phospholipids (DPPC and DMPC) with saturated chains, the λ_{em} are very close. Interestingly, λ_{em} in the gel phase of DPPC differs by 15 nm and 6 nm from the fluid phase of DOPC and DMPC (or DPPC), respectively. These differences might be the consequence of all *trans* conformation of hydrocarbon

chains in DPPC and the presence of kink (*cis* configuration) in DOPC. The hydrophobic dye, Nile red is expected to penetrate more in the flexible hydrocarbon chains of DOPC bilayer than the comparatively rigid chains of DPPC. It is important to mention that it is difficult to identify two different saturated phospholipids (DPPC and DMPC) as their emission spectra are very close to each other. Although, we can identify the lipids in terms of chain saturation by looking at the individual Nile red spectra, the chemical details of the lipids have to be determined from some other experimental techniques. The obvious question that arises: can we identify two different phospholipids from the spectrum of Nile red in the presence of DOPC-DPPC mixture? In order to check this possibility, we have measured the emission spectra of an equimolar mixture of DOPC and DPPC at two different temperatures (see table 1). It is known from the previous studies that DOPC-DPPC mixture exhibits gel-fluid coexistence below the T_m of DPPC (18; 19). Therefore, it is expected to have two characteristic emission wavelengths arising from the coexistence of gel and fluid phases at 25^o C. However, we could not distinguish two phases from the spectral decompositions using two Gaussian fit. This could be due to a large difference in intensities of two coexisting phases. A large difference in intensities would result in smearing out the spectrum obtained from individual phases. To reduce such difference in intensities, we have also prepared LUV from different molar ratios of the mixture to change the relative amount of gel and fluid phases. We have still not been able to distinguish two phases from the spectra. We suggest that a good quality optical filter with a very narrow band may be able to decompose two spectral lines arising from gel and fluid phases. Further fluorescence microscopy experiments need to be performed in order to check this possibility.

Table:1 Summary of maximum emission wavelength (λ_{em}) of Nile red at temperature 25^o C in the presence of LUV composed of various lipids and lipid mixtures. Numbers in bracket in the first column represent the molar ratio of the two lipid mixture. Number in the second column represents the length and saturation of the hydrocarbon chains. All unsaturated lipids listed here have one double bond at 9th position (Δ^9 -*Cis*). DDAB is a double-chain (16 Carbon in each chain) cationic surfactant. For all experiments pH of the LUV dispersion was kept fixed at 7.

Lipids	Hydrocarbon chains, charge	Phase state	$\lambda_{em\pm 2}$ (nm)
DOPC	18:1	Fluid	632
DOPG	18:1, -ve charge	Fluid	634
DOTAP	18:1, +ve charge	Fluid	632
DPPC	16:0	Gel/Fluid	617/623
DMPC	14:0	Fluid	624
DLPC	12:0	Fluid	624
DOPC:DPPC(4:1)	-	Gel-Fluid	628
DOPC:DOPE(4:1)	-	Fluid	632
DOPC:DDAB(3:1)	+ve charge	Fluid	631
DOPC:cholesterol(4:1)	-	Liquid disordered	628
DPPC:cholesterol(4:1)	-	Liquid ordered	594
DMPC:cholesterol(4:1)	-	Liquid ordered	607

A higher fluorescence intensity has been observed below the T_m (gel phase) of DPPC as compared to above T_m . This is in contrast with the fact that the more rigid gel phase must prevent Nile red to penetrate into the membrane core, resulting in the decrease in local concentration, whereas, the loosely packed fluid phase must have larger vacancy for Nile red (9). The increase in fluorescence intensity at gel phase is thus intriguing. The transition from the fluid phase to gel phase increases the number of defects in bilayer which might favor the incorporation of Nile red. Much above T_m (60°C), thermal quenching is important due to the opening up of completely non-radiative relaxation pathways and hence it is expected to decrease the fluorescence intensity although bilayer is too flexible to incorporate Nile red. In order to confirm thermal quenching, emission spectra were taken with increasing temperature (Fig. 6.2) for different lipids. All of them show the decrease in fluorescence intensity with increasing temperature in the fluid phase only. This is supported by the fact that fluorescence quenching does not occur below T_m of DPPC and DMPC. It is known that bilayer becomes more flexible, as evidenced from the decrease in bending modulus and area compressibility modulus with increasing temperature (20). Therefore, the decrease in fluorescence intensity might be the consequence of the increase in water penetration in the fluid phase, as compared to gel phase with increasing temperature. This is also further

supported by the fact that the bilayer thickness decreases and the thickness of water layer increases in membrane stacks with increasing temperature (21). It is also important to note that the λ_{em} of DPPC decreases initially in the gel phase and again increases to a similar value when temperature is further increased from 30⁰ C as shown in the inset of Fig. 6.2. The hydration dynamics in the vicinity of the Nile red could influence the excited state leading to the change in its emission wavelength. The temperature dependence of the Nile red emission has not been reported in any of the earlier studies.

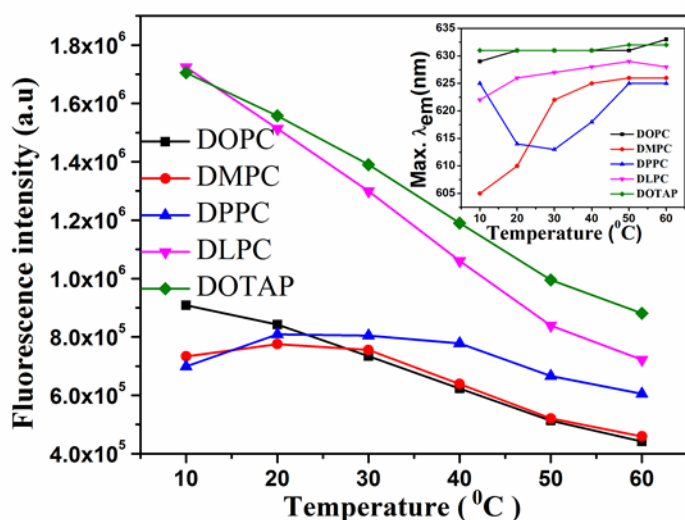


Figure 6.2: Temperature variation of fluorescence emission intensity of Nile red for different lipids, as indicated in the figure legend. Maximum emission wavelength seems to be blue shifted in the gel phase of DPPC and red shifted in the fluid phase of DPPC, DMPC. However, the λ_{em} for unsaturated lipids DOPC, DOTAP does not seem to alter with increasing temperature.

6.3.2 Effect of cholesterol on the emission spectra of Nile Red in the presence different phospholipids.

Fluorescence emission of Nile red has been used to investigate the effect of cholesterol on the membranes. Previous literatures have shown that ternary mixture composed of DPPC (or DMPC), DOPC and cholesterol exhibits two phases, namely liquid ordered (l_o) and liquid disordered (l_d)

at temperature below T_m of saturated lipid (22). The l_o phase is rich in cholesterol and saturated lipid (DPPC/DMPC) and l_d phase contains unsaturated lipid (DOPC) and little amount of cholesterol. Therefore, we have studied the binary mixtures of cholesterol with DPPC, DMPC and DOPC in order to gain some insights into the l_o and l_d phases, respectively. The location of cholesterol is believed to be in the interfacial regions of head group and acyl chains of the membranes (23). Our previous study on the small angle x-ray diffraction have shown a small peak in the electron density profile at a distance of 10 Å from the center of the bilayer, indicating the presence of cholesterol at the interfacial regions (24). Further, it is known that Nile red shows fluorescence when it penetrates into the membrane core region. Therefore, it is conceivable that fluorescence properties of Nile red are expected to alter in the presence of cholesterol and hence Nile red can be a useful probe to study the effect of cholesterol on the membranes. Fig. 3 shows the effect of cholesterol on the λ_{em} of Nile red in the presence of saturated lipid DPPC and DMPC and unsaturated lipids DOPC. It is clearly evident that the λ_{em} decreases (blue shifted) very rapidly from 618 nm to 595 nm with increasing cholesterol concentration up to 10 mole% in the l_o phase of DPPC-cholesterol membranes. Above 10 mole% of cholesterol, there is no significant decrease in the λ_{em} . However, λ_{em} decreases progressively (blue shifted) with increasing cholesterol concentration for DMPC cholesterol membranes. On the other hand, Nile red emission maximum does not show significant decrease in the l_d phase, containing DOPC. The decrease in the λ_{em} at lower cholesterol concentration (< 10 mole%) for DPPC is the consequence of the two phase coexistence of gel and l_o at cholesterol concentration below 10 mole% (24). Further, this feature of DPPC can be attributed to the fact that, gel phase of DPPC shows tilt of $\sim 30^\circ$ with respect to bilayer normal. This tilt ensures the deeper insertion of the small Nile red molecule, resulting the significantly blue shifted spectrum. Rough estimate from area differences of lipid and cholesterol gives about 10-20 mole% of cholesterol that can be incorporated into the bilayer to remove the tilt (25). Once the tilt is removed, as in the case of l_o phase Nile red the λ_{em} shows nearly the same value, indicating that the Nile red interacts nonspecifically in the l_o phase due to shallow penetration of Nile red into the bilayer.

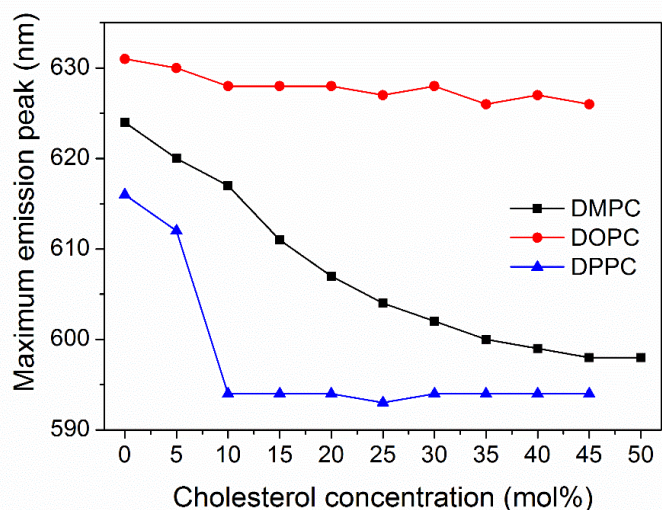


Figure 6.3: Variation of maximum emission peak of Nile red obtained from different phospholipids at 25^o C for different cholesterol concentration. Solid lines are intended as guide to the points and not obtained from fit.

It has been known that incorporation of cholesterol reduces the hydrophobicity in the membrane leading to an increase in water penetration (26). The increase in water content in the bilayers was also confirmed in terms of increase in d-spacing as seen the small angle x-ray scattering experiment (24). Therefore, the reduction of fluorescence intensity with increasing cholesterol concentration could be due to an increase in environmental polarity and increase water penetration in the membrane interfacial region (17). It is interesting to note that Fig. 3 can be used as a calibration curve of cholesterol content in the l_o phase containing saturated lipids by observing fluorescence emission of Nile red. The amount of blue shift in case of DMPC can be an estimation of cholesterol concentration in the l_o phase. However, no such prediction is possible for l_d phase as cholesterol has very little influence on the emission spectrum of Nile red for DOPC membrane. However, this result does not rule out the possibility that l_d phase contains very little amount cholesterol.

6.3.3 Red edge excitation shift (REES) of Nile red in DOPC vesicles containing cholesterol

A shift in the λ_{em} fluorescence emission toward higher wavelength caused by a shift in the excitation wavelength (λ_{ex}) toward the red edge of absorption band is termed as REES. The slow rate of solvent relaxation relative to fluorophore lifetime due to reorientation of dipoles around the excited state of fluorophore is known to be responsible for REES. The solvent relaxation in the immediate vicinity of the fluorophore indeed depends on the motional restriction of lipid molecules induced by the cholesterol in the lipid bilayer. Therefore, the REES effect has a direct consequence of change of rotational diffusion of fluorophore in the presence of lipid-cholesterol membranes. Therefore, it is conceivable that Nile red, located in the confined water within the bilayer as well as a hydration layer at the vicinity of the membrane, is expected to show REES. We now focus on REES to monitor effect of cholesterol in the membranes.

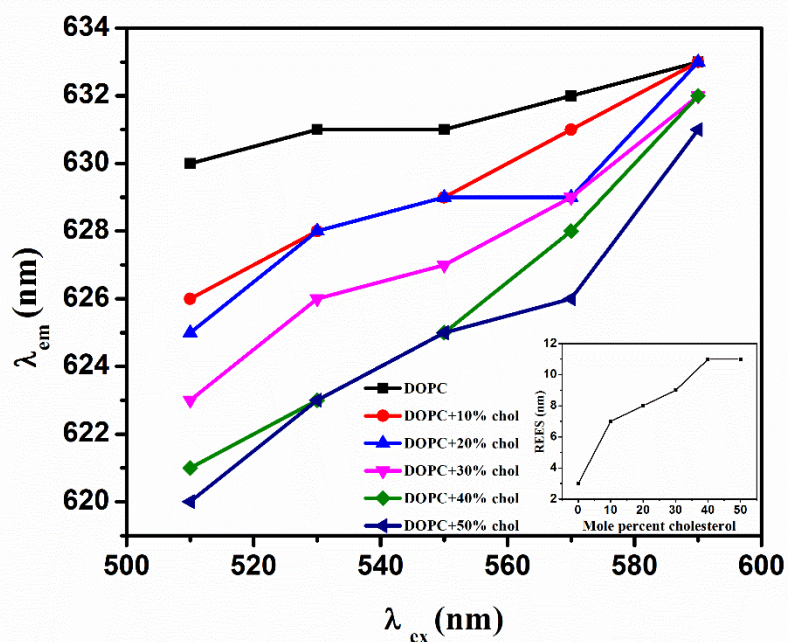


Figure 6.4: Variation of maximum emission wavelength ($\lambda_{em} \pm 2$ nm) at different excitation wavelength (λ_{ex}) of Nile red in the presence of DOPC-cholesterol membranes. Cholesterol concentrations (mole%) are indicated in the figure legend. The Red edge emission shift (REES)

has been shown in the inset of the figure. Solid lines are intended as guide to the points and not obtained from the fit.

The shift in the λ_{em} of Nile red in DOPC vesicles with increasing λ_{ex} (510 nm to 590 nm) for different cholesterol concentration is shown in Fig. 6.4. As the λ_{ex} is changed from 510 to 590 nm, the λ_{em} of Nile red displays the shift toward higher wavelengths. In the absence of the cholesterol there is no significant shift in the λ_{em} . However, ~ 11 nm shift was observed for all cholesterol concentration studied. In case of saturated lipid, DMPC, λ_{em} changes from 618 nm to 625 nm upon variation of λ_{ex} from 510 nm to 590 nm (data not shown). The significant REES dependence of Nile red in the presence of cholesterol indicates that rotational diffusion of Nile red is restricted within the bilayers as cholesterol induces the straightening of the chains near the interface. This result is further supported by the fact that the rotational diffusion decreases with increasing cholesterol concentration (see later). As discussed before, the λ_{em} obtained from our study and from Kucherak et al. (9) at the excitation of 550 nm was in stark disagreement with λ_{em} value reported by Mukherjee et al. (17). Therefore, the data in Fig. 4 is expected to be different from the REES data presented in ref. 17. This is the reason that we have again looked at these data, although REES has already been reported in case of DOPC-cholesterol membranes (17). Observation of REES in DOPC vesicles implies that the Nile red is in a motionally restricted environment and is strongly interacting with the solvent. The change in dipole moment during the excited state reaction, as shown in previous study (11) enforces the solvent dipoles surrounding the Nile red to reorganize around the excited state and to reach to the equilibrium prior to the emission. Therefore, fluorescence emission alters due to change in polarity of the surrounding environment.

6.3.4 Rotational dynamics of lipid bilayers as revealed from steady state fluorescence anisotropy.

Steady state fluorescence anisotropy has been extensively used to monitor the rotational diffusion rate of Nile red embedded in the membrane. As fluorescence anisotropy measures the extent of depolarization, i.e., the ability of the probe to reorient during the emission, it must be sensitive to the packing of lipid acyl chains. The rigid environment surrounding the fluorophore probe

increases the anisotropy. Thus, the probable location of cholesterol in the membrane can also be suggested by monitoring the anisotropy. Therefore, the effect of cholesterol on the lateral as well rotational diffusion of lipids in the membranes can be envisaged from the anisotropy measurement. The increase in anisotropy, in the presence of DMPC and DPPC bilayers containing cholesterol, suggests that cholesterol restricts the rotational motion of the Nile red by providing the rigidity to the membrane (Fig. 6.5). Interestingly, cholesterol does not change the anisotropy for DOPC membrane. This is consistent with the fact that the bending rigidity ($\kappa \sim 11 \times 10^{-20}$ J) of DOPC membranes containing various amounts of cholesterol did not change significantly (27). However, it is believed that the cholesterol orders the acyl chain of the saturated lipids above the chain melting transition leading to an increase in κ . The anisotropy (r) value is the lowest in the liquid disordered phase and highest in the liquid ordered phase at higher cholesterol concentration. This is due to the relatively loose packing of the lipid acyl chains in the liquid disordered phase. This is further supported by the fact that the affinity of cholesterol to the phospholipid bilayers was known to decrease significantly with increasing the degree of unsaturation of the acyl chains (28). These results are consistent with those obtained from the Fig. 3.

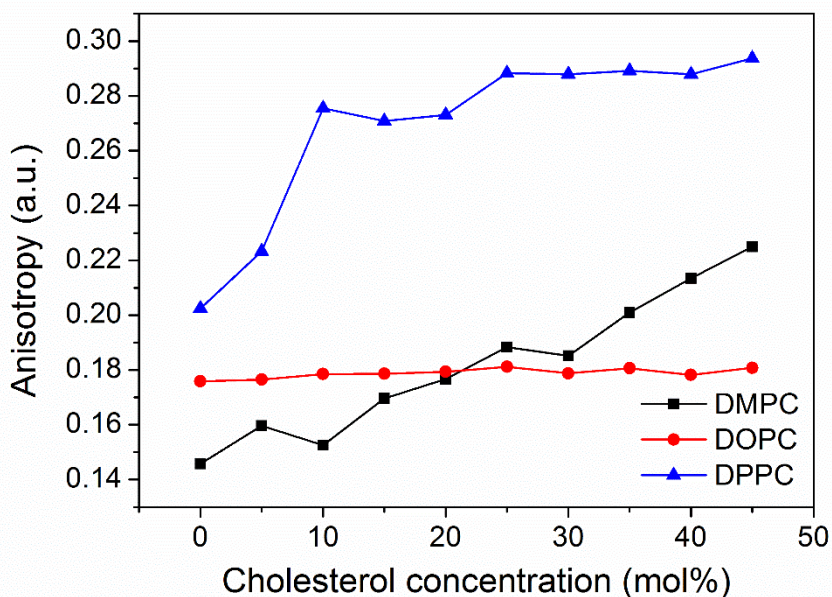


Figure 6.5: The steady state fluorescence anisotropy of Nile red in the presence of DMPC, DOPC and DPPC vesicles for different concentration of cholesterol at 25⁰ C. Solid lines are intended as guide to the points and not obtained from the fit.

6.3.5 Lifetime of Nile red in phospholipid vesicles: effect of cholesterol

Fluorescence lifetime serves as a reliable indicator of the local environment in which a fluorophore is localized. Fig. 6 shows the fluorescence lifetime of Nile red in the presence of three different lipids containing cholesterol. It is clearly evident that lifetime does not increase significantly for DOPC, whereas it increases markedly for DMPC and DPPC. This is consistent with the results obtained from emission spectrum and anisotropy measurement.

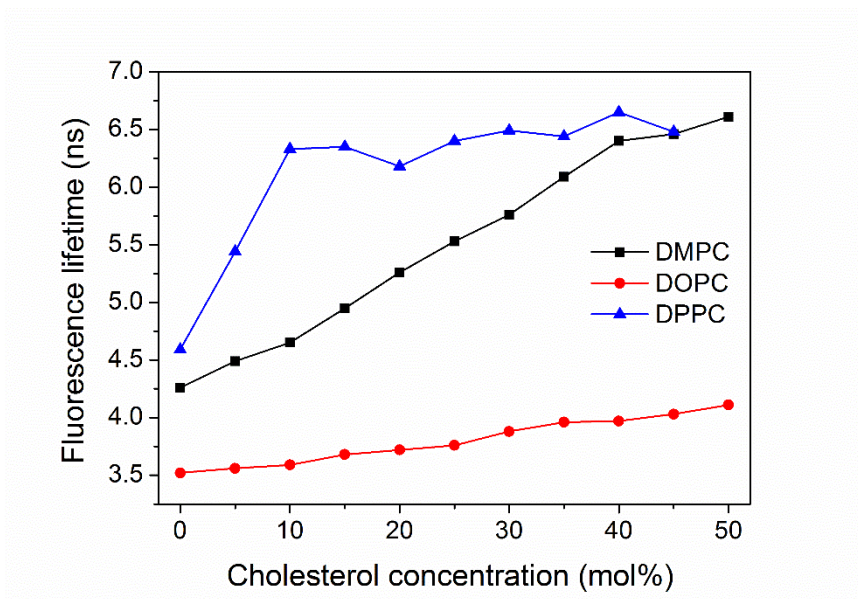


Figure 6.6: Steady state fluorescence lifetime of Nile red in the presence of three different phospholipids for different cholesterol concentration (mole %) at 25⁰ C

The mean fluorescence lifetime of Nile red in DMPC vesicles increases from ~4.26 ns to 6.61 ns with increasing membrane cholesterol content up to 50 mole%. For DOPC, lifetime increases from 3.52 ns to 4.11 ns. Cholesterol is known to decrease the water penetration significantly and increases the dipole potential of the membrane (29). Further, cholesterol in the membrane restricts

the rotation of the fluorophore in the rigid environment. Such rigidification of the feeble parts of the molecules as well as increase in polarity of the membrane would marginalize the role of the non-radiative pathway, resulting in an increase of fluorescence lifetime (30). The increase in membrane viscosity when cholesterol is incorporated into the membrane could also increase the lifetime of the Nile red. The rotational rate D_R of Nile red estimated from equation (2) in the presence of LUV with different concentration of cholesterol is shown in Fig. 6.7.

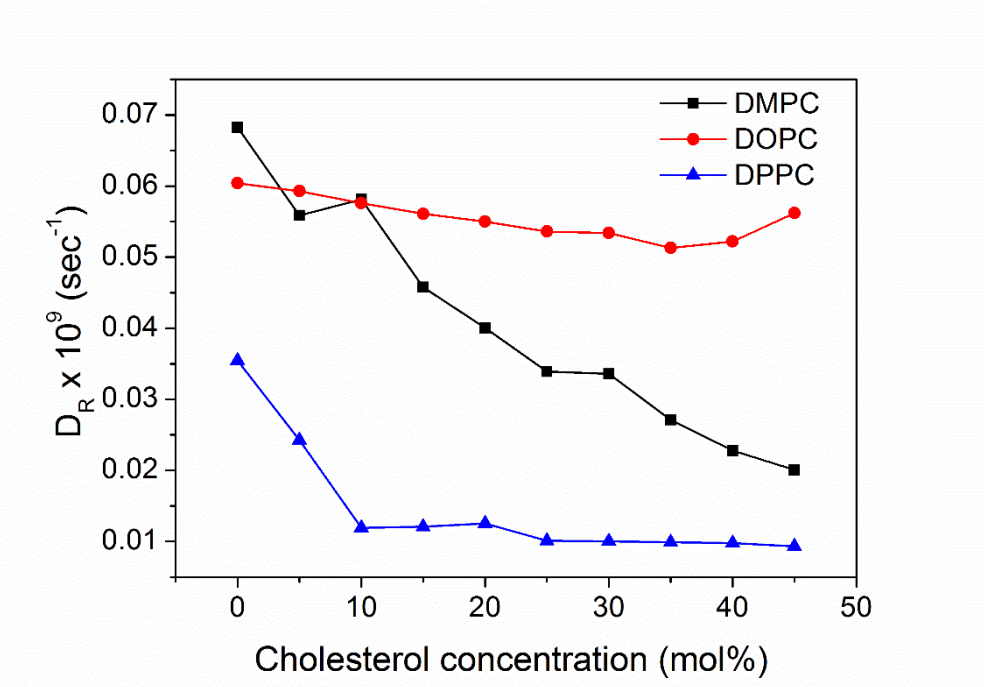


Figure 6.7: Rotational rate of Nile red in the presence of three different lipid vesicles ($T = 25^{\circ} \text{C}$), indicated in the figure legend for different cholesterol concentration (mole %).

There is no previous literature to verify the values of D_R with our estimated value. In order to check the effect of rotational diffusion on the anisotropy value, we assume a constant rotational rate (same as without cholesterol) to estimate the anisotropy (r) from the measured value of fluorescence lifetime with varying cholesterol concentration. Such an estimation gives a much lower value of r and it does not alter significantly with cholesterol concentration. This analysis clearly indicates that increase in anisotropy in the case of saturated lipids is due to motional restriction of lipids induced by cholesterol and lifetime has no significant influence on the rotational correlation time.

6.4 Conclusion:

In this work, we have monitored the organization, dynamics and solvent relaxation characteristics by measuring emission wavelength, anisotropy and lifetime of Nile red in various phospholipid membranes. The spectroscopic properties of Nile red change significantly in the presence of phospholipids with saturated acyl chains and not with the lipid phase state. The effect of cholesterol can be envisaged only with the saturated lipid and not with the unsaturated lipids which is consistent with the fact that the elastic properties of the membrane does not alter significantly with increasing cholesterol concentration. Interestingly, in the gel phase of DPPC, the fluorescence properties of Nile red change rapidly with cholesterol concentration up to 10 mole%. Beyond that spectroscopic properties of Nile red do not change significantly. Therefore, the membrane in the gel phase can accommodate cholesterol up to 10 mole% and converted into the pure liquid ordered phase. This is also a consequence of the fact that at lower concentrations of cholesterol, there exists two phase coexistence of gel and l_o . Therefore, above ~ 10 mole%, the gel phase completely converted into the single l_o phase. It is important to note that ~ 10 -15 mole% of cholesterol can remove the tilt of the hydrocarbon chain of the lipids in the gel phase. Therefore, once the tilt is removed, the Nile red cannot penetrate into the membranes and it remains in the solution. Hence Nile red does not seem to show any significant change in its spectroscopic properties. On the other hand, the emission wavelength decreases and anisotropy as well as lifetime of Nile red in the fluid phase of DMPC membrane increases monotonically with increasing cholesterol concentration. These results clearly indicate that cholesterol can alter the acyl chain environment in the fluid phase and membrane can accommodate the cholesterol till the miscibility limit. Above spectroscopic properties remain unaltered in case of unsaturated lipid DOPC. The effect of temperature on the emission spectrum of Nile red in the presence of both saturated and unsaturated lipids has been discussed. The lifetime measurement along with the steady state anisotropy result provides us to estimate the rotational rate of Nile red. The acyl chain environment in turn affects the rotational diffusion of Nile red which is known to reside at the interface. Although one of the primary objectives was to identify the lipid type from the spectral properties of Nile red, it is not straightforward to identify the lipid type from the spectral analysis of Nile red alone. However, correlations between the membrane compositions and fluorescence spectral features can be utilized in a wide range of biophysical fields as well the cell biology. For example, effect of cholesterol on the emission spectra can possibly be used in bioanalytical applications.

Reference

- (1) A. Akbarzadeh, R. Rezaei-Sadabady, S. Davaran, Sang. W. Joo, N. Zarghami, Y.Hanifehpour, M. Samiei, M. Kouhi, K. Nejati-Koshki, Liposome: classification, preparation, and applications, *Nanoscale Res Lett.*, 2013, 8, 102-110.
- (2) L. Finegold (Ed.), *Cholesterol in Membrane models* (ed.) (CRS Press, 1992).
- (3) J. Pan, S. Tristram-Nagle, J.F. Nagle, Effect of cholesterol on structural and mechanical properties of membranes, *Phys. Rev. E*, 2009, 80, 21931-21942.
- (4) K. Simons, M. J. Gerl, Revitalizing membrane rafts: new tools and insights, *Nat. Rev. Mol.Cell. Biol.*, 2010, 11, 688-699.
- (5) N. Bezlyepkina, R.S. Gracià, P. Shchelokovskyy, R. Lipowsky, R. Dimova, Phase Diagram and Tie-Line Determination for the Ternary Mixture DOPC/eSM/Cholesterol, *Biophys. J.*, 2013, 104, 1456-1464.
- (6) T. Baumgart, S. T. Hess, W. W. Webb, Imaging coexisting fluid domains in biomembrane models coupling curvature and line tension, *Nature*, 2003, 425, 821-824.
- (7) H-J Kaiser, D. Lingwood, I. Levental, J. L. Sampaio, L. Kalvodova, L. Rajendran, and K.Simons, Order of lipid phases in model and plasma membranes, *proc. Natl. Acad. Sci. USA*, 2009, 106, 16645-16650.
- (8) A. Arora, H. Raghuraman, A. Chattopadhyay, Influence of cholesterol and ergosterol on membrane dynamics: a fluorescence approach, *Biochem. Biophys. Res. Commun.*, 2004, 318, 920-926.
- (9) O. A. Kucherak, S. Oncul, Z. Darwich, D. A. Yushchenko, Y. Arntz, P. Didier, Y. Mély, A. S.Klymchenko, Switchable Nile Red-Based Probe for Cholesterol and Lipid Order at the Outer Leaflet of Biomembranes, *J. Am. Chem. Soc.*, 2010, 132, 4907-4916.
- (10) P. Maity, B. Saha. G. S. Kumar, S. Karmakar, Effect of counterions on the binding affinity of Na⁺ ions with phospholipid membranes, *RSC Adv.*, 2016, 6, 83916-83925.
- (11) N. Ghoneim, Photophysics of Nile Red in solution steady state spectroscopy, *Spectrochim.Acta*, 2000, 56, 1003-1010.

- (12) P. Greenspan, E. P. Mayer, S. D. Fowler, Nile red: a selective fluorescent stain for intracellular lipid droplets, *J. cell biol*, 1985, 100, 965-973.
- (13) I.R. Sitepu, L. Ignatia, A. K. Franz, D. M. Wong, S.A. Faulina, M. Tsui, A. Kanti, K. Boundy-Millsa, An improved high-throughput Nile red fluorescence assay for estimating intracellular lipids in a variety of yeast species, *J. Microbiol. Methods*, 2012, 91, 321-328.
- (14) A. Dutta, D. K. Sinha, Turnover of the actomyosin complex in zebrafish embryos directs geometric remodelling and the recruitment of lipid droplets, *Sci. Rep.*, 2015, 5, 13915.
- (15) M. J. Hope, M. B. Bally, G. Webb, P. R. Cullis, Production of large unilamellar vesicles by a rapid extrusion procedure: characterization of size distribution, trapped volume and ability to maintain a membrane potential, *Biophys. Biochim. Acta.*, 1985, 812, 55-65.
- (16) J. R. Lakowicz, *Principles of Fluorescence Spectroscopy*, (Plenum Press, New York, 1983).
- (17) S. Mukherjee, H. Raghuraman and A. Chattopadhyay, Membrane localization and dynamics of Nile red: Effect of cholesterol, *Biochim. Biophys. Acta*, 2007, 1768, 59-66.
- (18) S. L. Veatch, S. L. Keller, Separation of Liquid Phases in Giant Vesicles of Ternary Mixtures of Phospholipids and Cholesterol, *Biophys. J.*, 2003, 85, 3074-3084.
- (19) S. Karmakar, B. R. Sarangi and V. A. Raghunathan, Phase behaviour of lipid-cholesterol membranes, *Solid State Comm.*, 2006, 139, 630-634.
- (20) J. Pan, S. Tristram-Nagle, N. Kucerka, J. F. Nagle. Temperature Dependence of Structure, Bending Rigidity, and Bilayer Interactions of Dioleoylphosphatidylcholine Bilayers, *Biophys. J.* 2008, 94, 117-124.
- (21) N. Kučerka, M-P Nieh, J. Katsarasa, Fluid phase lipid areas and bilayer thicknesses of commonly used phosphatidylcholines as a function of temperature, *Biochim. Biophys. Acta*, 2011, 1808, 2761-2771.
- (22) J. V. Bleecker, P. A. Cox, S. L. Keller, Comparing Lo/Ld Membrane Thickness Mismatch and Miscibility Transition Temperatures using Fluorescence and Atomic Force Microscopy, *Biophys. J.*, 2016, 110, 2305-2308.

- (23) D. Marquardt, N. Kučerka, S. R. Wassalle, T. A. Harrounf, J. Katsaras, Cholesterol's location in lipid bilayers, *Chem. Phys. Lipids*, 2016, 199, 17-25.
- (24) S. Karmakar and V. A. Raghunathan, Structure of phospholipid-cholesterol membranes: An x-ray diffraction study, *Phys. Rev. E*, 2005, 71, 61924-61934.
- (25) S. Karmakar and V. A. Raghunathan, Cholesterol induced modulated phase in phospholipid membranes, *Phys. Rev. Lett*, 2003, 91, 98102-98106.
- (26) W. K. Subczynski, A. Wisniewska, J. J. Yin, J.S. Hyde, A. Kusumi, Hydrophobic barriers of lipid bilayer membranes formed by reduction of water penetration by alkyl chain unsaturation and cholesterol, *Biochemistry*, 1994, 33, 7670-7681.
- (27) R. S. Gracia, N. Bezlyepkina, R.L. Knorr, R. Lipowsky and R. Dimova, Effect of cholesterol on the rigidity of saturated and unsaturated membranes, *Soft Matter*, 2010, 6, 1472-1482.
- (28) T. P. W. McMullen, R. N. A. H. Lewis and R. N. McElhaney, Cholesterol-phospholipid interactions, the liquid ordered phase and lipid rafts in model and biological membranes, *Curr.Opin. Colloid Interface Sc.*, 2004, 8, 459-468.
- (29) T. Starke-Peterkovic, N. Turner, M. F. Vitha, M. P. Waller, D. E. Hibbs, Cholesterol Effect on the Dipole Potential of Lipid Membranes, *Biophys. J*, 2006, 90, 4060-4070.
- (30) M. Y. Berezin, S. Achilefu, Fluorescence Lifetime Measurements and Biological Imaging, *Chem Rev.*, 2010, 110, 2641-2684.

List of publications

(included in the thesis)

1. Sanat Karmakar, Pabitra Maity and **Animesh Halder**, *Charge-Driven Interaction of Antimicrobial Peptide NK-2 with Phospholipid Membranes*, ACS Omega 2017, 2, 8859–8867. (Impact factor 3.512)
2. **Animesh Halder**, Baishakhi Saha, Pabitra Maity, Gopinatha Suresh Kumar, Deepak Kumar Sinha, Sanat Karmakar, *Lipid chain saturation and the cholesterol in the membrane affect the spectroscopic properties of lipophilic dye Nile Red*, Spectrochimica Acta Part A: Molecular and Biomolecular Spectroscopy, 2018, 191, 104-110. (Impact factor: 4.098)
3. **Animesh Halder**, Achinta Sannigrahi, Nayan De, Krishnananda Chattopadhyay, and Sanat Karmakar, *Kinetoplastid Membrane Protein-11 Induces Pores in Anionic Phospholipid Membranes: Effect of Cholesterol*, Langmuir, 2020, 36, 3522–3530. (Impact factor: 3.882)
4. **Animesh Halder** and Sanat Karmakar, *An evidence of pores in phospholipid membrane induced by an antimicrobial peptide NK-2*, Biophysical Chemistry, 2022, 282, 106759. (Impact factor: 2.19)
5. **Animesh Halder** and Sanat Karmakar, *Cholesterol influences the antimicrobial activity of Magainin 2 in phospholipid membrane*, (Manuscript under preparation).

Other publications

1. Achinta Sannigrahi, Indrani Nandi, Sayantani Chall, Junaid Jibrán Jawed, **Animesh Halder**, Subrata Majumdar, Sanat Karmakar, and Krishnananda Chattopadhyay, *Conformational Switch Driven Membrane Pore Formation by Mycobacterium Secretory Protein MPT63 Induces Macrophage Cell Death*, ACS Chem. Biol. 2019, 14, 1601–1610. (Impact factor 4.374)
2. Sanat Karmakar, Pabitra Maity, **Animesh Halder**, *Antimicrobial Peptide NK-2 as an Emerging Therapeutic Agent: A Study with Phospholipid Membranes*, Materials Today: Proceedings 18 (2019) 879–886. (Impact factor: 1.24)
3. Ujjal Kumar Sur, Balaprasad Ankamwar, Sanat Karmakar, **Animesh Halder**, Pulak Das, *Green synthesis of Silver nanoparticles using the plant extract of Shikakai and Reetha*, Materials Today: Proceedings 5 (2018) 2321–2329. (Impact factor: 1.24)
4. Ujjal Kumar Sur, Abhijit Saha, Aparna Datta, **Animesh Halder** and Sanat Karmakar, *Green synthesis of highly stable zinc sulphide nanostructures using high-energy gamma radiation*, Bull. Mater. Sci. © Indian Academy of Sciences DOI 10.1007/s12034-017-1408-y. (Impact factor: 1.783)
5. Achinta Sannigrahi, Sourav Chowdhury, Bidisha Das, Amrita Banerjee, **Animesh Halder**, Amaresh Kumar, Mohammed Saleem, Athi N Naganathan , Sanat Karmakar, Krishnananda Chattopadhyay, *The metal cofactor zinc and interacting membranes modulate SOD1 conformation-aggregation landscape in an in vitro ALS model*, eLife 2021;10:e61453. (Impact factor: 8.14)

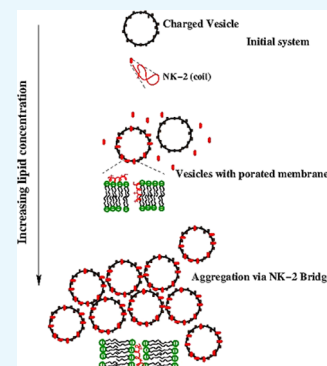
**Reprint of papers
included in the thesis**

Charge-Driven Interaction of Antimicrobial Peptide NK-2 with Phospholipid Membranes

Sanat Karmakar,*¹ Pabitra Maity, and Animesh Halder

Department of Physics, Soft Matter and Biophysics Laboratory, Jadavpur University, 188, Raja S.C. Mullick Road, Kolkata 700032, India

ABSTRACT: NK-2, derived from a cationic core region of NK-lysin, displays antimicrobial activity toward negatively charged bacterial membranes. We have studied the interaction of NK-2 with various phospholipid membranes, using a variety of experimental techniques, such as, isothermal titration calorimetry (ITC), ζ potential, and dynamic light scattering. As bacteria mimicking membranes, we have chosen large unilamellar vesicles (LUVs) composed of negatively charged phospholipid and neutral phospholipids. ITC and ζ potential results show the stronger binding affinity of NK-2 to negatively charged membranes than to neutral membranes. Saturation of the isotherm, obtained from ITC, at a given lipid to NK-2 ratio, was found to be consistent with the charge compensation, determined from ζ potential. A surface partition model with electrostatic contribution was used to estimate the intrinsic binding constant and other thermodynamical parameters of binding kinetics of NK-2. The size distribution of negatively charged LUV in the presence of NK-2 was found to increase drastically, indicating the presence of large aggregates. Such a large aggregate has not been observed in neutral membranes, which supports the ITC and ζ potential results.



1. INTRODUCTION

Antimicrobial peptides (AMPs) are an innate immune response in animal and human body against invading pathogens, such as viruses, fungi, bacteria, etc.^{1,2} They target the bacterial membrane, especially negatively charged surface, and create defects, such as pores, leading to disruption of the membrane.³ An important property of AMP is the specificity of bacterial targets and excludes the killing of most eukaryotic cells.⁴ The resistance to conventional antibiotics and the natural cell lytic activity of many AMP and their unique mode of action have led to a new possibility in the development of AMP as human therapeutics.⁵ Therefore, studies on the interaction of AMP with lipid membranes have drawn a lot of attention due to their potential biomedical applications.^{1,6–8} Diverse applications of AMP include as anti-infective agents, anticancer agents, drug delivery and nonviral gene transfer.^{1,9} A major problem that has impeded the development of drug design is the toxicity. NK-2, an AMP, which is nontoxic and nonhemolytic to the human skin cells, can be a potential candidate for designing antibiotics.¹⁰

NK-2 is a water soluble linear amphipathic helical peptide.⁸ It is the highest density region of NK-lysin having cationic charge of +10 at physiological pH. The high positive charges within the NK-2 promote strong binding to the negatively charged membranes.¹¹ The antimicrobial activity of NK-2 toward parasitic membranes involves the interaction with lipids in the membranes. A teleost NK-lysin peptide, NKLP27, is known to induce degradation of bacterial DNA and inhibits bacterial and viral infection.¹² There have been a large number of studies of many AMP, using a variety of experimental techniques, such as optical microscopy,^{13–16} oriented circular dichroism,¹⁷ X-ray and neutron scattering,¹⁸ isothermal titration calorimetry

(ITC),¹⁹ and differential scanning calorimetry.²⁰ However, very little is known in the case of NK-2. NK-2 impels significant changes in cellular morphology of human cancer cells and eventually cells lose their cellular integrity until destruction.²¹ NK-2 intercalates and binds to the negatively charged membranes, such as 1,2-dipalmitoyl-sn-glycero-3-phosphoglycerol (DPPG) and 1,2-dioleoyl-sn-glycero-3-phospho-L-serine (DOPS), but does not interact with the phosphatidylcholine (PC) or sphingomyelin, as revealed by the fluorescence resonance energy transfer²¹ and ζ potential.²² Conformational changes as well as the orientation of AMP play a vital role in the formation of transmembrane pores.^{7,21} Previous study of NK-2, dissolved in different aqueous solutions, has shown mainly α -helical conformation in the presence of negatively charged amphiphiles.⁸ Similar α -helical confirmation in the membrane environment has also been found in other AMP, such as melittin²³ and Magainin 2.²⁴ However, NK-2 adopts an unoriented random coil structure in the buffer, including water and in the presence of cationic and neutral amphiphiles below their critical micellar concentration. The conformational transition from random coil to helix arises mainly due to electrostatic interaction of positively charged residues of the peptide with the negatively charged head group of amphiphiles.⁸ However, penetration of peptides into the hydrophobic core is a result of hydrophobic interaction between the hydrophobic chain of the amphiphiles and hydrophobic residues of the peptide.

Received: August 22, 2017

Accepted: November 28, 2017

Published: December 12, 2017

Lipopolysaccharide (LPS), the major constituent of the outer membrane of gram negative bacteria, shows strong binding affinity to NK-2, as determined by various experimental techniques, such as small angle X-ray diffraction, ζ potential, and isothermal titration calorimetry.¹⁰ It is believed that the main pathway to disrupt the integrity of the cellular membrane is the formation of transmembrane pores. Different AMPs seem to follow different pathways to create transmembrane pores.²⁵ Therefore, in spite of a large number of attempts, the mechanism of transmembrane pore formation is still under dispute.^{6,26} For example, molecular electroporation was proposed as the mechanism of membrane pore formation, induced by NK-lysin.²⁷

Biological membranes are complex, regulated by various membrane components. Therefore, it is often useful to study model membranes to understand more complex lipid–peptide interactions and hence to get some insight into the mechanism of cellular damage induced by AMP. Giant unilamellar vesicles (GUVs), made from lipid molecules, serve as an excellent model system to study many biological activities.²⁸ For example, a kinetic process involving interaction of melittin and other AMP with PC vesicles have previously been demonstrated using the micropipette aspiration technique¹³ and leakage assay using fluorescence spectroscopy.^{14,16} It was found from previous studies of various AMP that the activity of pore formation initiates above a threshold lipid to the peptide ratio (~ 70 for melittin).^{13,17} This threshold seems to be different for different peptides.

There have not been systematic studies on the interaction of NK-2 with phospholipid membranes. Therefore, there are several open questions which have not been addressed in the literature. Does NK-2 make pores on the membranes, as in the case of other AMPs? If NK-2 makes pores, what is the mechanism that NK-2 uses to form transmembrane pores? How does the size of pores depend on lipid composition and concentration of NK-2? Although there was a previous study on the interaction of NK-2 with LPS,¹¹ the binding affinity of NK-2 with negatively charged phospholipid is still not well understood. It is also important to know how the binding affinity of NK-2 with phospholipids depends on the head group charge and size of the head group. It would also be interesting to observe any morphological change induced by NK-2 in the model membrane.

The major constituents of bacterial membranes are phosphatidylethanolamine (PE) and phosphatidyl-glycerol (PG) ($\sim 4:1$).²⁰ Therefore, in our present study, we have chosen model systems, composed of dioleoyl phosphatidyl-glycerol (DOPG) and mixtures of DOPG with dioleoyl phosphatidylethanolamine (DOPE) and dioleoyl phosphatidylcholine (DOPC). These lipids also show fluid phase at room temperature (25 °C). As model membranes, we have used large unilamellar vesicles (LUVs) to study the interaction of NK-2 with different phospholipids using isothermal titration calorimetry (ITC), ζ potential, and dynamic light scattering (DLS). In particular, the electrostatic behavior as well as the size distribution of the membranes in the presence of NK-2 was systematically characterized using ζ potential and DLS, respectively. Thermodynamics of the interaction of this system have been thoroughly investigated using ITC study. We have determined, for the first time, the binding affinity of NK-2 with negatively charged phospholipid membranes.

2. RESULTS

2.1. ζ Potential. The summary of results on ζ potential is illustrated in Figure 1. The ζ potential was measured in LUV

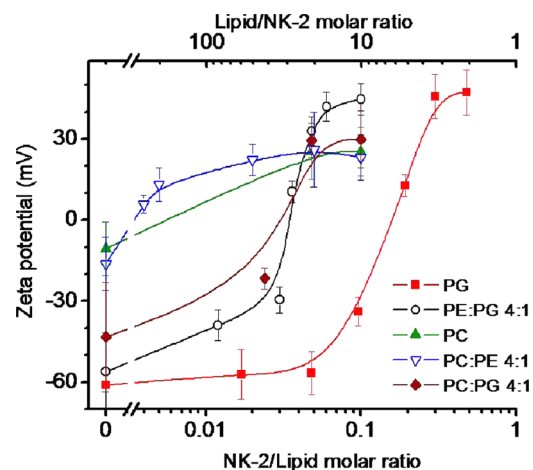


Figure 1. ζ Potential of phospholipid LUV at various NK-2 to lipid molar ratios. Solid lines are intended only as guides to the points. Error bars indicate the width of the distribution profile of ζ potential.

dispersion, made from DOPC, DOPG, DOPE–DOPG (4:1) mixture, and mixtures of DOPC with DOPE and DOPG, before and after introducing peptides (i.e., before and after ITC measurements). As shown in Figure 1, ζ potential increases with increasing NK-2 to lipid molar ratio (NK-2/L) and charge compensation occurs at different NK-2/L for different lipid mixtures. Although phospholipids, such as DOPC and a mixture of DOPC–DOPE, are neutral, they exhibit a low negative value. A small negative ζ potential gets neutralized at NK-2/L, $\sim 1:250$. In comparison, charge neutralization happens for DOPG at much higher NK-2/L (1:5). For DOPE–DOPG (4:1) mixtures, charge compensation occurs at intermediate NK-2/L (1:25). These differences are due to the fact that charge compensation occurs with respect to charge lipids. Interestingly, the ζ potential shows its saturation value, indicating overcharge compensation at different NK-2/L for various lipid mixtures (Figure 1). The ζ potential of DOPG shows a saturation at a much higher NK-2/L (3:10) than that of DOPC and DOPC–DOPE (1:250), whereas the ζ potential for DOPE–DOPG and DOPC–DOPG mixtures shows this at intermediate NK-2/L (1:20). The above result clearly indicates that NK-2 has a stronger affinity toward the negatively charged lipids.

2.2. Size Distributions of LUV. LUVs composed of pure DOPC and DOPG were found to be very stable, as no significant change in the size distribution was seen in DLS measurement even a couple of months later. The size distribution was measured for all lipid mixtures before (absence of NK-2) and after (presence of NK-2) ITC. The average diameter of LUV at different NK-2/lipid ratios is presented in Figure 2. The error bars in Figure 2 represent the width of the distribution, which is a measure of polydispersity of LUV. This error is relevant for understanding the effect of NK-2 on the membranes. However, errors, obtained from different measurements, are small and are not shown in the plot. Neutral LUVs, made from DOPC and a mixture of DOPC and DOPE, do not exhibit any significant change in their size distribution in the presence of NK-2 (Figure 2a). However, the average size of the

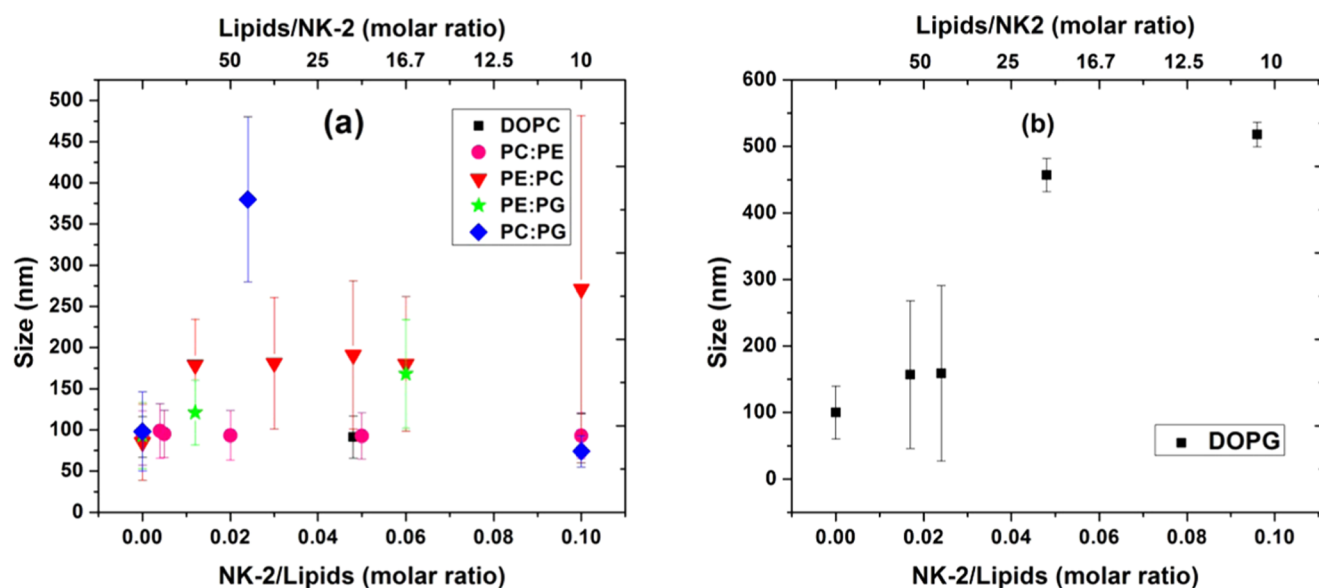


Figure 2. Size distribution of LUV made from various lipid compositions in the presence of NK-2. (a) LUV are composed of DOPC and other phospholipid mixtures, as indicated by the figure legend. (b) LUV composed of DOPG. Error bar is the standard deviation and was obtained from the width of the distribution.

negatively charged LUV increases with increasing C_{nk2} . Interestingly, LUVs made from pure DOPG show a dramatic increase in their average size in the presence of NK-2 (Figure 2b). The width of the size distribution (error bar in Figure 2), indicating polydispersity, also increases with the increase of C_{nk2} . In all samples containing DOPG, transparent LUV dispersion becomes turbid after ITC measurement. Therefore, as the NK-2/lipid ratio is increased, the sample exhibits a high value of size as well as high polydispersity and eventually shows large aggregates. After a couple of hours, the sample appears very turbid and hence the sample was not suitable for DLS measurement. This behavior clearly indicates that sample contains large aggregates induced by NK-2.

2.3. Binding Affinity of NK-2 with Model Membranes Measured from ITC. NK-2 of various concentrations, C_{nk2} (100, 50, 40, 30, 25, and 10 μM) was titrated with 4 mM of LUV made from the DOPE–DOPG (4:1) mixture. For first few injections, heat flow remains constant, then starts decreasing as less and less NK-2 is available for binding. Typical raw data of ITC measurement at $C_{nk2} = 50 \mu\text{M}$ are shown in Figure 3. The lipid to NK-2 (L/NK-2) ratio at which saturation of the heat flow occurs is $\sim 20:1$, taking into account all lipids (i.e., both monolayers of the LUV) interacting with the NK-2. The overall binding reaction was endothermic for all C_{nk2} . Interestingly, when the endothermic signal attains its saturation at $\sim L/NK-2 = 20$, further successive one to three injections show an exothermic signal and then successive injections contribute almost negligible heat (data not shown). This behavior is displayed in the raw ITC thermogram when lower C_{nk2} , typically $<40 \mu\text{M}$, was used. For these concentrations, saturation occurs before completing all injections of LUV. At the beginning of the titration, there are plenty of peptides to bind with lipids. Therefore, we have analyzed the data taking into account only the initial part of the endothermic heat signals or the data where all injections of LUV have been finished before the exothermic peaks appear, i.e., for $C_{nk2} > 40 \mu\text{M}$. Although some of the isotherms can be fitted to one site binding model given by microcal origin, it gives us the apparent binding constant (K_{app}), which is

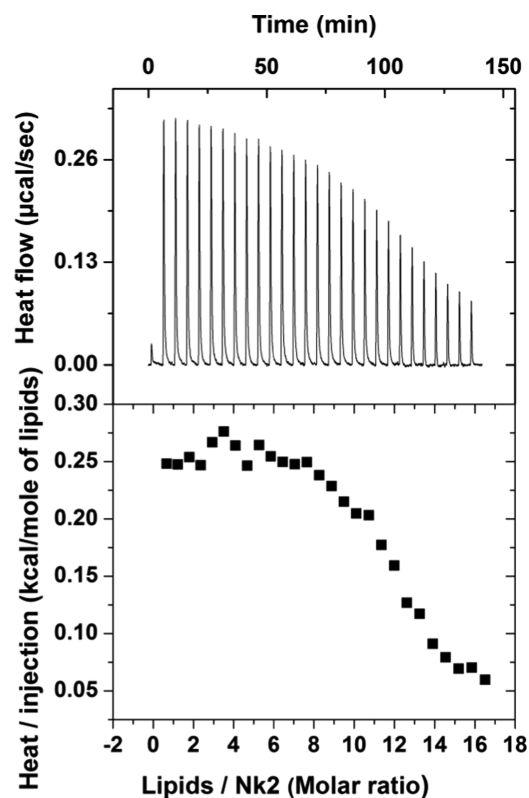


Figure 3. Titration calorimetry of 50 μM NK-2 with 4 mM DOPE–DOPG (4:1) LUV (top); normalized heat of injection/mole of lipids, obtained from the integration of the individual peak (bottom). Heat of dilution, obtained from injecting 4 mM LUV into buffer, was subtracted from the actual measurement. Here we assume, lipids from both monolayers interact with the NK-2.

expected to vary with concentrations of unbound or free NK-2 concentration. However, the order of magnitude of the K_{app} has been found to be consistent with the value obtained from the surface partition model. As the interaction of NK-2 with the

Table 1. Parameters Obtained from Each Data Point in an ITC Experiment Using the Surface Partition Model Including Electrostatic Contribution^a

lipid + peptide	lipid/NK-2	C_f (mM)	$C_M \times 10^{-6}$ (mM)	X_b	K_{int} (M^{-1})
DOPG (5 mM) + NK-2 (0.1 mM)	0.34	0.08	3.29	0.420	1.28×10^8
	0.62	0.07	2.86	0.414	1.45×10^8
	0.90	0.06	2.41	0.422	1.75×10^8
	1.19	0.05	1.97	0.422	2.14×10^8
	1.47	0.04	1.58	0.415	2.64×10^8
	1.76	0.03	1.20	0.407	3.41×10^8
	2.05	0.02	1.33	0.395	2.98×10^8
	2.34	0.01	1.07	0.381	3.56×10^8
	2.63	0.01	0.96	0.365	3.80×10^8
	DOPE–DOPG (4:1—4 mM) + NK-2 (0.05 mM)	1.79	0.047	16.2	0.121
2.36		0.045	15.4	0.112	7.30×10^6
2.93		0.042	14.6	0.110	7.56×10^6
3.51		0.040	13.8	0.108	7.85×10^6
4.09		0.038	13.0	0.109	8.41×10^6
4.67		0.035	12.1	0.110	9.11×10^6
5.26		0.032	11.3	0.110	9.79×10^6
5.85		0.030	10.5	0.109	10.4×10^6

^a X_b : binding fraction; C_f : free peptide concentration; C_M : intrinsic peptide concentration, K_{int} : intrinsic binding constant. The lipid concentration used in the analysis is the total lipid concentration considering NK-2 interaction with both monolayers of the membrane.²⁹

Table 2. Thermodynamical Parameters of Binding Kinetics of NK-2.^{a,b}

lipids	ΔH (kcal/mol)	K_{int} (M^{-1})	ΔG (kcal/mol)	$T\Delta S$ (kcal/mol)
DOPG	0.8 ± 0.2	$2.5 \times 10^8 \pm 3.5 \times 10^7$	-13.8 ± 0.2	14.6 ± 0.4
DOPE–DOPG (4:1)	2.9 ± 0.8	$7.3 \times 10^6 \pm 4.5 \times 10^5$	-11.7 ± 0.6	14.6 ± 0.8

^aBinding enthalpy (ΔH), intrinsic binding constant K_{int} , entropy (ΔS), obtained numerically using surface partition model taking into account the electrostatic contribution.³⁰ ^bHere, the K_{int} is the mean value calculated from Table 1. Here, we have assumed NK-2 interacts with both leaflets of the membrane.²⁹ The heat of dilution has been subtracted from all data. ζ Potential in the absence of NK-2 is also shown. The effective charge, z_p , of the NK-2 when binding to the membrane has been taken as 5. Note that ΔH for DOPG was estimated from the first endothermic part (Figure 4) of the ITC thermogram.

negatively charged membranes is primarily driven by the surface charge of the membranes, it is desirable to fit the data taking into account the electrostatic contributions. Therefore, the more relevant parameter would be the intrinsic binding constant (K_{int}), where the surface concentration of peptide (C_M) is more relevant than the bulk or free peptide concentration (C_f).

The model parameters, such as the extent of peptide binding (X_b), C_f , C_M , K_{int} , etc, obtained numerically from experimental data, have been summarized in Table 1 (see Materials and Methods for details). In the case of DOPE–DOPG mixture, it is interesting to observe that C_M versus X_b behaves linearly for lower lipid/NK-2, corresponding to 9–10 injections. However, the tendency to increase the value of K_{int} is evident from Table 1. Above 10 injections, the K_{int} increases with increasing the number of injections. Therefore, we have presented only the linear part of the data to estimate the K_{int} . The possible reason for increasing the value of K_{int} at higher lipid/NK-2 has been discussed later. The estimated values of molar binding enthalpy, ΔH , K_{int} , and binding entropy ΔS , obtained from the surface partition model with electrostatic contribution, have been summarized in Table 2.

Titration isotherm of DOPG is shown in Figure 4. Surprisingly, it shows few exothermic signals at L/NK-2 (4:1) between two regions of endothermic response. In this case, exothermic peaks begin at much lower L/NK-2 (~ 5). It is important to note that such an exothermic signal also occurs at a similar PG/NK-2 ratio for DOPE–DOPG (4:1) mixture. To understand the detailed behavior of two regions of the

isotherm, 100 μM NK-2 was titrated with five different DOPG concentrations (10, 5, 2.5, 1.6, and 1 mM). The second region of the isotherm was accessed when two different C_{nk2} (50, 35) were titrated with 10 mM DOPG LUV. At present, we are not able to fit the entire isotherm with the model available in the literature. However, we have determined the average thermodynamic parameters obtained from the first region using a partition model, taking into account the electrostatic contribution. The parameters obtained from the model have been presented in Table 1. In the model, we have reduced the effective charge of the NK-2 starting from the maximum charge +10 and found the linear relationship between X_b and C_M at $z_p = 5$. This can also be realized as L/NK-2 ~ 5 to neutralize the membrane.

The large binding constants in the case of DOPG and DOPE–DOPG mixture, as shown in Table 1, suggest that NK-2 strongly binds to negatively charged membranes. Therefore, it is interesting to check the affinity of NK-2 with neutral lipids, such as DOPC and DOPE. Unfortunately, LUVs from DOPE alone are not formed using the extrusion method used here. This is because PE bilayers are more rigid than PCs in the fluid phase due to hydrogen bonding between the head groups.³⁰ Therefore, bending of PE bilayers costs more energy, which in turn prevents the formation of unilamellar vesicles. Therefore, a mixture of DOPE–DOPC (4:1) was used to investigate the influence of PE in the binding isotherm. A 100 μM NK-2 was titrated with 10 mM DOPE–DOPC (4:1). For comparison, 10 mM of DOPE/DOPC (1:4) mixture was injected in to three different C_{nk2} (10, 100, and 200 μM). Similar experiments were

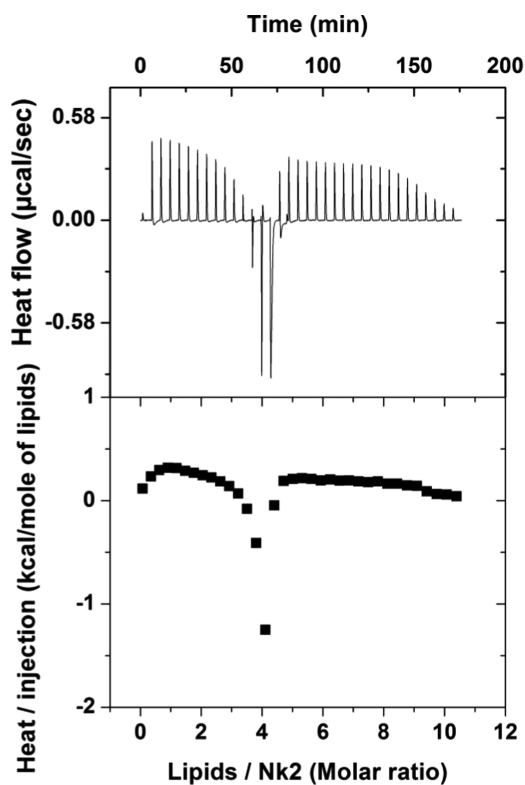


Figure 4. Raw titration calorimetry data of DOPG, where NK-2 of 100 μM is titrated with 5 mM of DOPG LUV (top); the corresponding normalized heat per injection obtained from the integration of the individual peak (bottom). Here, we have assumed NK-2 interacts with all lipids.

done for DOPC. For DOPE–DOPC (4:1), the heat signal is stronger than that of DOPE–DOPC (1:4) but weaker than that of the DOPE–DOPG mixture. In all above mixtures, the binding reaction is endothermic, whereas the simple dilution experiment shows an exothermic response. The interaction of NK-2 with DOPC and DOPC–DOPE LUV is too weak to obtain a binding constant and other thermodynamic parameters. Considering all ITC results, we can easily conclude that the interaction of NK-2 with PE is stronger than with PC but weaker than with PG ($\text{PG} \gg \text{PE} > \text{PC}$).

3. DISCUSSION

A systematic investigation of the interaction of an important antimicrobial peptide NK-2 with model membranes shows strong binding affinity toward the negatively charged lipid, DOPG, as revealed from ITC and ζ potential. The adsorption of NK-2 on the membranes, as indicated by an increase in ζ potential (Figure 1), is primarily driven by electrostatic interaction between negatively charged membranes and positively charged NK-2. This is indeed an essential requirement for an AMP to exhibit antimicrobial activity. However, the interaction is very weak in the case of neutral DOPC and DOPC–DOPE membranes. The positive ζ potential (+10 mV) of DOPC LUV at very low NK-2/L (1:250) suggests that NK-2 adsorbs even in PC membranes, which has not been reported in any of the earlier studies. The ζ potential was measured previously for DPPC in the gel phase, suggesting no significant interaction with DPPC.²² However, a more biologically relevant study would be to measure the ζ potential in the fluid phase. X-ray scattering and Fourier transform infrared spectroscopy

showed that NK-2 has no influence even on 1-palmitoyl-2-oleoyl-*sn*-glycero-3-phosphocholine vesicles that are in the fluid phase. They have not measured the ζ potential of PC vesicles in the fluid phase. Therefore, we cannot compare our results on DOPC with those obtained in ref 22. However, the behavior of the ζ potential of DOPG and DOPE–DOPG LUV were found to be consistent with those reported in the previous studies for DPPG and DPPE²² and for LPS.¹¹ Binding of NK-2 to the negatively charged membranes results in charge neutralization. Therefore, the charge neutralization depends on the amount of charge lipids present on the outer membranes. This explains why very low NK-2/L (1:250) is required to neutralize the membrane charge for zwitterionic phospholipids. The charge neutralization at much higher NK-2/L (1:5) for DOPG suggests binding affinity to PG is much stronger than that to PC. If the binding of NK-2 to charged lipids is only due to electrostatic interaction, one would expect the charge overcompensation at the same ζ potential. The fact that we have obtained charge overcompensation at different ζ potential for different lipids (see Figure 1) implies entropic contribution in these systems. This is consistent with the ITC results in these mixtures. For DOPG, ITC shows saturation, indicating all of the NK-2 binds to the lipids at NK-2/L of $\sim 1:3$, which is very similar to the NK-2/L (3:10) for charge overcompensation, as found from ζ potential. Similarly, ITC isotherm for DOPE–DOPG mixtures shows saturation at NK-2/L (1:20), which is again consistent with the results of ζ potential.

It is important to mention that change in the size distribution of the vesicles does not influence the ζ potential significantly. The ζ potential is estimated from the Smoluchowski approximation, where the Henry function $f(\kappa a)$ takes its maximum value as 1.5. In other words, ζ potential is determined from the electrostatic double layer formation, which does not depend on the size of the particle. Therefore, whatever change we observe in the ζ potential is not due to change in size but due to binding of peptide in the membrane.

The DLS technique can, in principle, show the evidence of membrane–membrane interaction mediated by NK-2 or the leakage of LUV induced by NK-2. Size distributions of LUV made from various compositions of phospholipids in the absence and presence of NK-2 clearly indicate stronger affinity of NK-2 toward negatively charged membranes. It is interesting to observe the turbid solution of LUV for those NK-2 concentrations in which the ITC shows saturation before completing all injections. This would mean that when there are no NK-2 available in the solution, LUV, introduced from successive injections can adhere due to electrostatic interaction between negatively charged injected LUV with positively charged LUV already present in the solution. Adhesion can eventually lead to the aggregation of LUV. This result clearly implies the antimicrobial activity of NK-2 toward negatively charged lipids and is consistent with the ζ potential result. Although size distributions do not alter significantly for pure DOPC, the mixture of DOPE and DOPC at 4:1 shows a slight increase in the average size (Figure 2a). Further, the presence of PE with PC enhances the heat signals in the ITC experiment. This indicates that PE plays a significant role in the interaction. Therefore, the PE–PG system is indeed an appropriate model system to look at the antimicrobial activity. Interestingly, this composition happens to be the major constituent of many bacterial membranes.

The binding of a positively charged AMP with negatively charged membrane usually leads to exothermic heat signal.³¹

The overall endothermic response observed in all isotherms is thus intriguing. The overall endothermic response, found in all lipid mixtures, can be explained in terms of entropy gain in liberating water molecules from the hydration shell of LUV due to adsorption of NK-2 at the interface. Entropic contribution can also arise due to conformational change of NK-2 (random coil to α helix) in the presence of lipids and also reorientation of NK-2 prior to the formation of pores. Such transitions were found for this peptide in a previous study by Olak et al.⁸ As the initial L/NK-2 ratio is small, we would expect pores in almost all LUVs. This is due to the fact that a threshold NK-2/L is required for the formation of pores and this condition is already achieved at the beginning of the isotherm.^{13,29} Our preliminary result on giant unilamellar vesicles also shows the leakage of internal fluid, supporting the pore formation on the membrane induced by NK-2 (data not shown). Although the appearance of the exothermic heat signal at PG/NK-2 \sim 5:1 in both DOPE–DOPG and DOPG mixtures is very intriguing, the origin of these exothermic peaks is difficult to confirm at present. However, we believe that when there are no NK-2 available for binding, NK-2 can translocate through the pores and interact with the bare LUV present in the solution due to further injections. This process might lead to closing of pores, resulting in an exothermic heat signal. This hypothesis is based on the assumption that if the pore formation is endothermic, pore closure must be exothermic in nature. It is true that the resultant heat due to pore closure and binding of NK-2 together can cancel out. However, at this stage, the unbound peptide-to-lipid molar ratio is too small to produce considerable heat that can give rise to an endothermic response. Such an exothermic response in between two endothermic regions has not been observed in any of the earlier studies.

Surprisingly, a second set of endothermic regions were obtained in the case of DOPG (Figure 4), even though there are no NK-2s available for further binding with LUV. This can be explained qualitatively, as follows. It was known by a previous study that desorption kinetics of NK-2 are much slower than adsorption due to trapping of α helix at the membrane interface.⁸ Therefore, it is expected that no free NK-2 are available to give rise to a second region of isotherm. Further injections of LUV can lead to attraction toward positively charged LUV already present in the solution. When the membranes of negatively charged LUV come closer to the NK-2, water molecules in the hydration shell start to liberate giving rise to the entropic gain of two membranes of LUV. Such membrane–membrane interaction was also evidenced by the DLS measurement, as the average size of LUV was found to increase.

NK-2 has a strong binding affinity to the lipid bilayer interface, relative to its water solubility, as evidenced from the ζ potential. This leads to an excessive interfacial area due to NK-2 binding, which increases the membrane tension. Such an increase in the membrane tension results in the formation of transmembrane pores.²⁹ It has been shown in the earlier study by Lee et al.²⁹ that the asymmetry of interfacial tension due to one-sided binding could lead to translocation of peptide (melittin) via transient pores. The binding of peptide to both outer and inner monolayers forms a stable pore at a critical peptide-to-lipid ratio. Therefore, it is desirable to use total (current) lipid concentration in the ITC cell to estimate the binding constant. It was also reported earlier that some peptides are not able to translocate across the membrane and only the outer monolayer of the membrane (60% of total lipid)

is available for binding.³² One of the striking features obtained in the present study, compared to those of other pore-forming peptides, such as melittin, is that the NK-2 interacts only with negatively charged membranes. On the contrary, melittin can interact significantly with the electrically neutral PC membrane.¹³

It is evident from Table 2 that entropic contribution ($T\Delta S$) is much larger than that of enthalpy (ΔH). This is not surprising, as hydrophobic interaction between the hydrophobic part of NK-2 and hydrophobic core of the membranes is entropic in origin. This is also necessary for the transmembrane pore formation, observed in this system. The intrinsic binding constant K_{int} ($= 2.5 \times 10^8 \text{ M}^{-1}$) of NK-2 found in DOPG (see Table 2) LUV is 2 orders of magnitude higher than that obtained from earlier studies of different AMP.^{19,31} It is important to note that K_{int} changes significantly with the effective charge z_p of the NK-2. We have optimized the value of z_p at 5 in the model so that a linear relationship of C_M versus X_b with a small intercept was maintained. This value can also be realized from the ratio L/NK-2 for which the charge compensation as well as the saturation of the heat signals occurs. Previous ITC measurements on the NK-2-LPS system have shown similar endothermic and exothermic response to the binding heat depending on the structure of LPS.¹¹ However, these results were not analyzed. As evidenced from Table 1, the slight increase in the K_{int} with increasing lipid/NK-2 is the consequence of membrane–membrane interaction induced by NK-2. This result is also supported by DLS experiment, where we have observed an increase in the size distribution.

The mechanism of action of NK-2 on negatively charged membranes has been inferred from ITC result, as illustrated in Figure 5. Initially, positively charged NK-2 in the coiled configuration,⁸ when binds to an outer monolayer of the

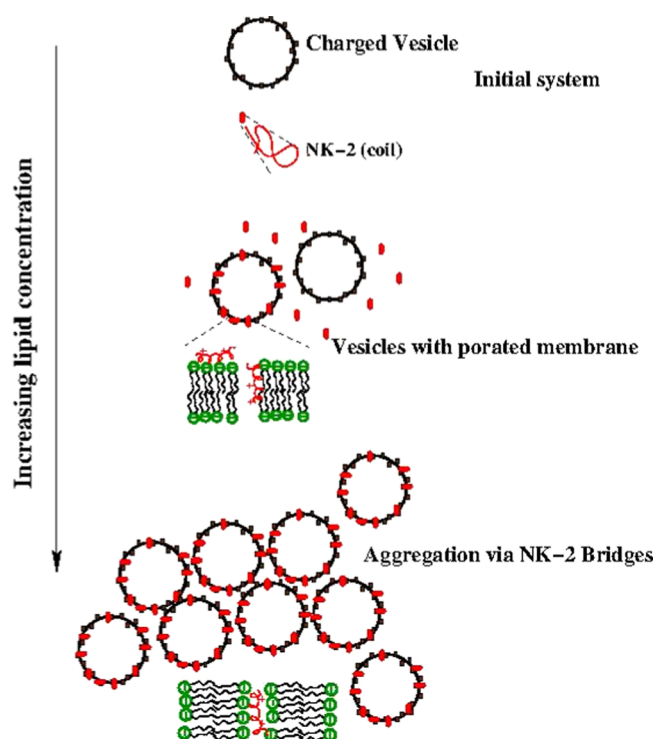


Figure 5. Interaction mechanism of NK-2 and vesicles.

membranes, increases the membrane tension and induces transient pores to translocate NK-2 into the inner monolayer.²⁹ The increase in membrane tension was also evidenced from the membrane thinning effect of melittin and other AMPs (13, 25, and 29). Such tension-induced (stretch-activated) pore formation has also been reported for an AMP Magainin 2.³³ Although there have been no earlier reports on NK-2, we expect that NK-2 also induces membrane tension, as in the case of melittin or Magainin 2. As the concentration of lipid is increased (i.e., the number of LUV), the NK-2 may come out through the pores and negatively charged LUV move closer to the positively charged vesicles due to electrostatic attraction. This process eventually leads to aggregation of vesicles via NK-2 bridges. The process of aggregation has been clearly envisaged from the size distribution. The increase in the value of K_{inv} as mentioned in Results section, might be the consequence of the aggregation of vesicles at a higher lipid to NK-2 ratio.

4. CONCLUSIONS

We have systematically studied the interaction of NK-2 with phospholipid membranes to obtain insights into the antimicrobial activity. The binding affinity of NK-2 to the negatively charged membranes, PG, as well as the neutral phospholipids PC and PE was determined using ITC and ζ potential. We compare binding affinity of NK-2 to PG, PE, and PC as PG \gg PE > PC. Weaker affinity toward neutral phospholipids suggests that interactions of NK-2 with lipids are mainly governed by negatively charged lipids, which are major constituents of the bacterial membranes. The very weak affinity of NK-2 toward the PC membrane (which is the major constituent of eukaryotic cell membranes) propels the development of peptide antibiotics. The evidence of pores on these membranes seen in the present study implies antimicrobial activity of NK-2. The significant increase in the size of negatively charged LUV, found in DLS measurement, confirms membrane–membrane interactions induced by NK-2 in these systems, which eventually leads to vesicle aggregates in the solution. Finally, we have proposed the mechanism of action of NK-2 based on our experimental results. More detailed studies are required to understand the mechanism of the kinetic process involved during pore formation. As already established, the NK-2 can be used as therapeutics to kill malaria parasite *Plasmodium falciparum*. It also shows activity against *Escherichia coli* and preferentially kills cancer cells. Further, low toxicity toward human cells is a great advantage for the development of antibiotics. Therefore, the present study will definitely reinforce the therapeutics applications. Nevertheless, our study provides important insights into the NK-2-lipids interaction.

5. MATERIALS AND METHODS

5.1. Materials. Dioleoyl phosphatidylcholine (DOPC), dioleoyl phosphatidylethanolamine (DOPE), and dioleoyl phosphatidyl-glycerol (DOPG) were purchased from Avanti Polar Lipids and peptide NK-2 (KILRGVCKKIMRTFLRRISK-DILTGKK-NH₂) was purchased from WITA GmbH, Berlin, Germany. They were used without further purification.

5.2. Preparation of LUV. An appropriate amount of lipid solution in chloroform (concentration of stock solution is 10 mg/mL) was transferred to a 10 mL glass vial. The organic solvent was removed by gently passing nitrogen gas. The

sample was then placed for a couple of hours in a desiccator connected to a vacuum pump to remove the traces of the solvent. Two and a half milliliters of 1 mM *N*-(2-hydroxyethyl)-piperazine-*N'*-ethanesulfonic acid (HEPES) (pH 7.4 adjusted with 1 M KOH) was added to the dried lipid film so that final desired concentration was obtained. The lipid film with the buffer was kept overnight at 4 °C to ensure the better hydration of phospholipid heads. Vortexing of the hydrated lipid film for about 30 min produces multilamellar vesicles (MLVs). Sometimes long vortexing is required to make uniform lipid mixtures. LUVs were prepared by the extrusion method using LiposoFast-Pneumatic from AVESTIN (Canada). MLV suspensions are extruded successively through polycarbonate membranes having pore diameters of 400, 200, and 100 nm. This results in the formation of a well-defined size of LUV. This method produces vesicles of diameter \sim 100 nm, as measured by dynamic light scattering.

5.3. Measurement of ζ Potential and Size Distributions Using DLS. ζ Potential and vesicle sizes were measured with a Zetasizer Nano ZS from Malvern Instruments. Same LUV, as used for ITC, was used for these measurements. The instrument uses 2 mW He–Ne laser of wavelength 633 nm to illuminate the sample. ζ Potential is obtained from the electrophoretic mobility by laser Doppler velocimetry using the Helmholtz–Smoluchowski equation.³⁴

$$\zeta = \frac{3\mu\eta}{2\epsilon f(\kappa a)} \quad (1)$$

where η and ϵ are the coefficient of viscosity and the permittivity of the aqueous medium, respectively. The Henry function, $f(\kappa a)$ depends on the inverse Debye length (κ) and the radius (a) of the vesicle.

In DLS, back scattered light at an angle of 173° is detected and sent to a digital signal processing correlator. The rate of decay of intensity–intensity autocorrelation function was measured, which was used to calculate the size of the LUV using the Stokes–Einstein relation $a = \frac{kT}{6\pi\eta D}$, D being the diffusion constant and kT the thermal energy. The average ζ potential and size were obtained from 3 to 4 successive measurements. Each measurement includes 100–200 runs. The same cuvette is used for both ζ potential and DLS measurements. All experiments were performed at 25 °C.

5.4. Isothermal Titration Calorimetry (ITC). The binding affinity of NK-2 to the lipids was measured using a VP-ITC microcalorimeter produced by MicroCal Inc. (Northampton, MA). In all experiments, the injection syringe was filled with degassed LUV suspension. The sample cell (1.442 mL) contains various concentrations of NK-2 dissolved in 1 mM HEPES buffer (pH 7.4). The reference cell is filled with HEPES buffer only. All solutions were degassed prior to filling the syringe and ITC cells to eliminate air bubbles. A series of 28 injections, each of 8 μ L, was introduced into the sample cell at 300 s intervals. All experiments were performed at 25 °C. Interaction of NK-2 with lipids produces a characteristic heat signal. The amount of heat of binding in every injection was obtained by integrating individual calorimetry traces. In a control experiment, LUV was injected into only buffer to measure the heat of dilution. The heat of dilution (\sim –0.1 μ cal/injection) was found to be small as compared to the actual measurement. Other heat of dilution (\sim –0.07 μ cal/injection), appearing from the dilution of NK-2, was even smaller, as compared to dilution of the former case. However, we have

obtained heat per injection by subtracting heat of dilution, obtained from injecting LUV into buffer, from the actual measurement. ITC data have been analyzed without altering the lipid concentration. This would ensure that the peptides interact with both monolayers of the membrane. All dilution measurements show exothermic signal. The binding constant (K) and binding enthalpy (ΔH) and Gibbs free energy ($\Delta G = -RT \ln K$) and entropic contributions ($T\Delta S = \Delta H - \Delta G$) of the binding kinetics can be obtained from the model, as described by Domingues et al.³¹ A summary of the model is described below.

5.5. Surface Partition Model with Electrostatic Contributions. In a typical ITC experiment, when LUVs are injected into the peptide solution, the total concentration of the peptide is the sum of the concentration of bound peptides and the free peptides. The apparent binding constant K_{app} is defined as $X_{\text{b}} = K_{\text{app}}C_{\text{f}}$ where X_{b} is the extent of peptide binding per mole of lipid and C_{f} is the free peptide concentration of the solution. When the charged peptide adsorbs, the membrane becomes changed. Hence, further adsorption of peptide onto the membrane is restricted by the electrostatic repulsion. Therefore, K_{app} is no longer a constant but rather changes with C_{f} . Therefore, the most relevant binding parameter would be the intrinsic binding constant K_{int} ($X_{\text{b}} = K_{\text{int}}C_{\text{M}}$), which is assumed to be directly proportional to the surface concentration of the peptide in the membrane. The model essentially calculates X_{b} and C_{M} for each injection of the ITC experiment. As the C_{M} of the peptide is governed by the electrostatic contribution, it is determined by the Boltzmann distribution.

$$C_{\text{M}} = C_{\text{f}} e^{-z_{\text{p}}F\psi_0/RT} \quad (2)$$

where z_{p} is the effective peptide charge. The maximum charge of NK-2 is +10. F is the Faraday constant (= charge of 1 mol of electron = electronic charge \times Avogadro's number = 96 485 C/mol). ψ_0 is the surface potential. R is the universal gas constant and T is the absolute temperature. As the ψ_0 is related to surface charge density, σ , of the peptide, it can be estimated from the well-known Gouy–Chapman theory. As the ζ potential can be a good approximation to the surface potential, we have taken ψ_0 same as the ζ potential. Now we need to know the ζ potential for each peptide-to-lipid molar ratio obtained after every injection. However, we have measured the ζ potential for few peptide-to-lipid ratios. To obtain the ζ potential for all peptide-to-lipid ratios required for the calculation of C_{M} , we have fitted the ζ potential data to a Hill equation originally used to describe cooperative binding of ligand to macromolecules.³⁵ Hence, we have obtained ζ potentials for all required concentrations from interpolation or extrapolation of the fitted curve. Now, for each data point, the concentration of the free peptide and ψ_0 have been determined. Once C_{f} and ψ_0 are known, C_{M} can be calculated. We now discuss briefly how X_{b} and C_{f} have been estimated from an ITC experiment.

In an ITC experiment (lipids into peptide injection), the X_{b} and the enthalpy change ΔH per mole of peptides can be measured directly. The ΔH has been estimated from the sum over all heat per injection divided by the number of moles of peptide in the calorimeter cell.

$$\Delta H = \frac{\sum_i \delta h_i}{C_{\text{p}}^0 V_{\text{cell}}} \quad (3)$$

where δh_i is the heat per injection in the ITC experiment. C_{p}^0 is the initial molar concentration of peptide in the ITC cell, and V_{cell} is the volume of the ITC cell. Now, the extent of peptide binding, X_{b} , per mole of lipid after completion of i th is given by

$$X_{\text{b}}^i = \frac{\sum_k^i \delta h_k}{\Delta H i V_{\text{inj}} C_{\text{L}}} \quad (4)$$

where V_{inj} is the volume of each injection with lipid of concentration C_{L} . Now, the fraction of bound peptide after i th injection is given by

$$X_{\text{p}}^i = \frac{\sum_k^i \delta h_k}{\Delta H V_{\text{cell}} C_{\text{p}}^0}$$

where the free peptide concentration C_{f} can be obtained from

$$C_{\text{f}} = C_{\text{p}}^0 (1 - X_{\text{p}}^i) \quad (5)$$

Now, the K_{app} can be obtained from the X_{b} and C_{f} . Therefore, C_{M} and K_{int} can be estimated for each pair of X_{b} and C_{f} obtained from experimental data, as discussed above.

AUTHOR INFORMATION

Corresponding Author

*E-mail: sanat@phys.jdvu.ac.in.

ORCID

Sanat Karmakar: 0000-0002-2421-9475

Notes

The authors declare no competing financial interest.

ACKNOWLEDGMENTS

This work was funded by the Department of Biotechnology (DBT), Govt. of India (BT/PR8475/BRB/10/1248/2013). P.M. and A.H. are grateful to UGC for providing research fellowship. We thank Drs. Rumiana Dimova and Volker Knecht, Max Planck Institute of Colloids and Interfaces, Potsdam, Germany for their keen interest in this study and for academic discussions.

REFERENCES

- Zaslhoff, M. Antimicrobial peptides of multicellular organisms. *Nature* **2002**, *415*, 389–395.
- Stempel, N.; Strehmel, J.; Overhage, J. Potential application of antimicrobial peptides in the treatment of bacterial biofilm infections. *Curr. Pharm. Des.* **2015**, *21*, 67–84.
- Jacobs, T.; Bruhn, H.; Gaworski, I.; Fleischer, B.; Leippe, M. NK-Lysin and its shortened analog NK-2 exhibit potential activities against *Trypanosoma cruzi*. *Antimicrob. Agents Chemother.* **2003**, *47*, 607–613.
- Ciobanaru, C.; Rzeszutek, A.; Kubitscheck, U.; Willumeit, R. NKCS, a Mutant of the NK-2 Peptide, Causes Severe Distortions and Perforations in Bacterial, But Not Human Model Lipid Membranes. *Molecules* **2015**, *20*, 6941–6958.
- Zhang, L.-j.; Gallo, R. L. Antimicrobial peptides. *Curr. Biol.* **2016**, *26*, R14–R19.
- Brogden, K. A. Antimicrobial peptides: Pore formers or metabolic inhibitors in bacteria? *Nat. Rev. Microbiol.* **2005**, *3*, 238–250.
- Bechinger, B. The structure dynamics and orientation of antimicrobial peptides in membranes by multidimensional solid-state NMR spectroscopy. *Biochim. Biophys. Acta, Biomembr.* **1999**, *1462*, 157–183.
- Olak, C.; Muentner, A.; Andrä, J.; Brezesinski, G. Interfacial properties and structural analysis of the antimicrobial peptide NK-2. *J. Pept. Sci.* **2008**, *14*, 510–517.

- (9) Banković, J.; Andrić, J.; Todorović, N.; Podolski-Renić, A.; Milošević, Z.; Miljković, D.; Krause, J.; Ruždijić, S.; Tanić, N.; Pešić, M. The elimination of P-glycoprotein over-expressing cancer cells by antimicrobial cationic peptide NK-2: The unique way of multi-drug resistance modulation. *Exp. Cell Res.* **2013**, *319*, 1013–1027.
- (10) Andrić, J.; Leippe, M. Candidacidal activity of shortened synthetic analogs of amoebapores and NK-lysin. *Med. Microbiol. Immunol.* **1999**, *188*, 117–124.
- (11) Andrić, J.; Koch, M. J. H.; Bartels, R.; Brandenburg, K. Biophysical characterization of Endotoxin inactivation of NK-2, an antimicrobial peptide derived from mammalian NK-Lysin. *Antimicrob. Agents Chemother.* **2004**, *48*, 1593–1599.
- (12) Zhang, M.; Li, M.-f.; Sun, L. NKLP27: A Teleost NK-Lysin Peptide that Modulates Immune Response, Induces Degradation of Bacterial DNA, and Inhibits Bacterial and Viral Infection. *PLoS One* **2014**, *9*, No. e106543.
- (13) Lee, M.-T.; Hung, W.-C.; Chen, F.-Y.; Huang, H. W. Mechanism and kinetics of pore formation in membranes by water-soluble amphipathic peptides. *Proc. Natl. Acad. Sci. U.S.A.* **2008**, *105*, 5087–5092.
- (14) Ambroggio, E. E.; Separovic, F.; Bowie, J. H.; Fidelio, G. D.; Bagatolli, L. A. Direct visualization of membrane leakage induced by the antibiotic peptides: Maculatin, Citropin, and Aurein. *Biophys. J.* **2005**, *89*, 1874–1881.
- (15) Zhao, H.; Mattila, J.-P.; Holopainen, J. M.; Kinnunen, P. K. J. Comparison of the membrane association of two antimicrobial peptides, Magainin 2 and Indolicidin. *Biophys. J.* **2001**, *81*, 2979–2991.
- (16) Tamba, Y.; Yamazaki, M. Magainin 2-induced pore formation in the lipid membranes depends on its concentration in the membrane interface. *J. Phys. Chem. B* **2009**, *113*, 4846–4852.
- (17) Lee, M.-T.; Chen, F.-Y.; Huang, H. W. Energetics of pore formation induced by membrane active peptides. *Biochemistry* **2004**, *43*, 3590–3599.
- (18) He, K.; Ludtke, S. J.; Worcester, D. L.; Huang, H. W. Neutron Scattering in the plane of membranes: structure of alamethicin pores. *Biophys. J.* **1996**, *70*, 2659–2666.
- (19) Wieprecht, T.; Apostolov, O.; Beyermann, M.; Seelig, J. Membrane binding and pore formation of the antibacterial peptide PGLa: Thermodynamic and Mechanistic aspects. *Biochemistry* **2000**, *39*, 442–452.
- (20) Lohner, K.; Prenne, E. J. Differential scanning calorimetry and X-ray diffraction studies of the specificity of the interaction of antimicrobial peptide with membrane-mimetic system. *Biochim. Biophys. Acta, Biomembr.* **1999**, *1462*, 141–156.
- (21) Schröder-Borm, H.; Bakalova, R.; Andrić, J. The NK-lysin derived peptide NK-2 preferentially kills cancer cells with increased surface levels of negatively charged phosphatidylserine. *FEBS Lett.* **2005**, *579*, 6128–6124.
- (22) Willumeit, R.; Kumpugdee, M.; Funari, S. S.; Lohner, K.; Navas, B. P.; Brandenburg, K.; Linser, S.; Andrić, J. Structural rearrangement of model membranes by the peptide antibiotic NK-2. *Biochim. Biophys. Acta, Biomembr.* **2005**, *1669*, 125–134.
- (23) Vogel, H.; Jähnig, F. The structure of melittin in membranes. *Biophys. J.* **1986**, *50*, 573–582.
- (24) Bechinger, B.; Zasloff, M.; Opella, S. J. Structure and orientation of the antibiotic peptide magainin in membranes by solid-state nuclear magnetic resonance spectroscopy. *Protein Sci.* **1993**, *2*, 2077–2084.
- (25) Chen, H. M.; Leung, K. W.; Thakur, N. N.; Tan, A.; Jack, R. W. Distinguishing between different pathways of bilayer disruption by the related antimicrobial peptides cecropin B, B1 and B3. *Eur. J. Biochem.* **2003**, *270*, 911–920.
- (26) Huang, H. W.; Chen, F.-Y.; Lee, M.-T. Molecular Mechanism of peptide induced pores in Membranes. *Phys. Rev. Lett.* **2004**, *92*, No. 198304.
- (27) Miteva, M.; Andersson, M.; Karshikoff, A.; Otting, G. Molecular electroporation: a unifying concept for the description of membrane pore formation by antibacterial peptides, exemplified with NK-lysin. *FEBS Lett.* **1999**, *462*, 155–158.
- (28) Dimova, R.; Aranda, S.; Bezlyepkina, N.; Nikolov, V.; Riske, K. A.; Lipowsky, R. A practical guide to giant vesicles. Probing the membrane nanoregime via optical microscopy. *J. Phys.: Condens. Matter* **2006**, *18*, S1151–S1176.
- (29) Lee, M.-T.; Sun, T.-L.; Hung, W.-C.; Huang, H. W. Process of inducing pores in membranes by melittin. *Proc. Natl. Acad. Sci. U.S.A.* **2013**, *110*, 14243–14248.
- (30) Boggs, J. M. Lipid intermolecular hydrogen bonding: influence on structural organization and membrane function. *Biochim. Biophys. Acta, Rev. Biomembr.* **1987**, *906*, 353–404.
- (31) Domingues, T. M.; Mattei, B.; Seelig, J.; Perez, K. R.; Miranda, A.; Riske, K. A. Interaction of the Antimicrobial Peptide Gomesin with Model Membrane: A calorimetric Study. *Langmuir* **2013**, *29*, 8609–8618.
- (32) Meier, M.; Seelig, J. Length dependence of the coil \rightleftharpoons β -sheet transition in a membrane environment. *J. Am. Chem. Soc.* **2008**, *130*, 1017–1024.
- (33) Karal, M. A. S.; Alam, J. M.; Takahashi, T.; Levadny, V.; Yamazaki, M. Stretch-Activated Pore of the Antimicrobial Peptide, Magainin 2. *Langmuir* **2015**, *31*, 3391–3401.
- (34) Hunter, R. J. *Zeta Potential in Colloid Science: Principles and Applications*; Ottewill, R. H., Rowell, R. L., Eds.; Academic Press: New York, 1981; pp 59–124.
- (35) Sannigrahi, A.; Maity, P.; Karmakar, S.; Chattopadhyay, K. Interaction of KMP-11 with Phospholipid Membranes and Its Implications in Leishmaniasis: Effects of Single Tryptophan, Mutation and Cholesterol. *J. Phys. Chem. B* **2017**, *121*, 1824–1834.



Lipid chain saturation and the cholesterol in the phospholipid membrane affect the spectroscopic properties of lipophilic dye Nile red

Animesh Halder ^a, Baishakhi Saha ^b, Pabitra Maity ^a, Gopinatha Suresh Kumar ^b, Deepak Kumar Sinha ^c, Sanat Karmakar ^{a,*}

^a Department of Physics, Jadavpur University, Raja S. C. Mullick Road, Kolkata 700032, India

^b Biophysical Chemistry Laboratory, Organic and Medicinal Chemistry Division, CSIR-Indian, Institute of Chemical Biology, 4, Raja S. C. Mullick Road, Kolkata 700 032, India

^c Department of Biological Chemistry, Indian Association for Cultivation of Sciences, Raja.S. C. Mullick Road, Kolkata – 700 032, India

ARTICLE INFO

Article history:

Received 15 May 2017

Received in revised form 18 August 2017

Accepted 1 October 2017

Available online 5 October 2017

Keywords:

Phospholipid membranes

Nile red

Fluorescence spectroscopy

Lipid-cholesterol membranes

Vesicles

ABSTRACT

We have studied the effect of composition and the phase state of phospholipid membranes on the emission spectrum, anisotropy and lifetime of a lipophilic fluorescence probe Nile red. Fluorescence spectrum of Nile red in membranes containing cholesterol has also been investigated in order to get insights into the influence of cholesterol on the phospholipid membranes. Maximum emission wavelength (λ_{em}) of Nile red in the fluid phase of saturated and unsaturated phospholipids was found to differ by ~10 nm. The λ_{em} was also found to be independent of chain length and charge of the membrane. However, the λ_{em} is strongly dependent on the temperature in the gel phase. The λ_{em} and rotational diffusion rate decrease, whereas the anisotropy and lifetime increase markedly with increasing cholesterol concentration for saturated phospholipids, such as, dimyristoyl phosphatidylcholine (DMPC) in the liquid ordered phase. However, these spectroscopic properties do not alter significantly in case of unsaturated phospholipids, such as, dioleoyl phosphatidylcholine (DOPC) in liquid disordered phase. Interestingly, red edge excitation shift (REES) in the presence of lipid-cholesterol membranes is the direct consequence of change in rotational diffusion due to motional restriction of lipids in the presence of cholesterol. This study provides correlations between the membrane compositions and fluorescence spectral features which can be utilized in a wide range of biophysical fields as well the cell biology.

© 2017 Elsevier B.V. All rights reserved.

1. Introduction

Lipid bilayer is the building block of all biological membranes in which cholesterol, proteins and other bio-active molecules are embedded. Biological membranes are complex and regulated by various proteins and cholesterol. Therefore, it is often useful to study the artificial lipid bilayer as bio-mimetic system in order to gain insights into the structure and functions of the membranes. Large unilamellar vesicles (LUV) made from phospholipids serve as an excellent model system of biological membranes. Besides the model system of biological membranes, LUV are potential for diverse bio-technological applications [1]. Cholesterol is a ubiquitous component of plasma membranes. Structure and functions of membranes are greatly influenced by lipid composition, chain saturation and the membrane-cholesterol [2]. Cholesterol provides rigidity and integrity to the plasma membrane and prevents it from becoming overly fluid; It also helps to maintain its fluidity [3]. The cholesterol-rich domains, called rafts are believed to exist in the membrane [4]. These rafts resemble with the cholesterol-rich liquid

ordered (l_o) phase and cholesterol-poor liquid disordered (l_d) phase arising due to phase separation in the model membranes composed of ternary mixtures of cholesterol with a saturated lipid, such as DPPC and an unsaturated lipid, such as DOPC [5].

Fluorescence probes are widely used tools to characterize l_o and l_d phases in the cellular as well as artificial membranes. The coexistence of l_o and l_d phases can easily be envisaged using a fluorescence probe selectively stain for l_o phase [6]. Some environment sensitive probes whose emission property depends on local polarity, hydration or fluidity of the membranes, have also been used to characterize the l_o and l_d phases [7,8]. Nile red (9-diethylamino-5H-benzo(α) phenoxazine-5-one), is one such environment sensitive probe and is widely used to monitor the membrane organization and dynamics [9]. It emits fluorescence in the presence of lipid membrane [10]. However, its fluorescence is significantly quenched in the aqueous or polar environment. Its fluorescence properties are known to alter by the polarity of its immediate environment due to a large change in its dipole moment upon excitation [11]. This property of Nile red is utilized to monitor hydrophobic surfaces in proteins and hydrocarbon core in lipid membranes. Therefore, the Nile red is used on living cells as a fluorescence stain for the detection of intracellular lipid droplets if the proper spectral condition is

* Corresponding author.

E-mail address: sanat@phys.jdvu.ac.in (S. Karmakar).

chosen [12,13]. Lipid phase state and chain ordering, fluidity as well as in plane lateral diffusion etc. has a significant implications in many biological functions. For example, lipid domains play a vital role in the process of development of the embryo of zebra fish [14]. A basic and relevant question we would like to address that, can we use spectroscopic properties of Nile red to identify the type of lipids and their phase state in the membrane? Further, in a cholesterol containing bilayer, is it possible to calibrate or estimate the amount of cholesterol and to monitor the organization and heterogeneity induced by cholesterol in bio-membranes?

Therefore, the aim of the present article is to use the fluorescence properties of Nile red to identify the lipid type, phase state or the composition. As the temperature is one of the crucial parameters to determine the membrane environment, the temperature dependency of the emission properties of Nile red in the presence of phospholipid membranes has also been investigated. Further, we would like to monitor the organization, fluctuations and heterogeneity membranes containing cholesterol. In the present study, we have systematically investigated fluorescence properties of Nile red in the presence of various lipids in the gel and fluid phases. Effect of cholesterol on the spectral properties of Nile red in these phases has been studied in details. Here, we report the effect of saturation of hydrocarbon chains on the emission spectra of Nile red. We have also shown that Nile red can be used to calibrate the amount of cholesterol in the membranes in l_o phase. Rotational correlation and hence rotational diffusion of Nile red in the cholesterol containing lipid membranes were also estimated from the present study. Change in rotational diffusion due to motional restriction of lipids in the presence of cholesterol has also been envisaged from red edge excitation shift (REES). Our study suggests that spectroscopic properties of Nile red can be utilized to monitor the functions, composition and structure of biological membrane at physiological condition.

2. Materials and Methods

2.1. Materials

Phospholipids, such as, 1,2-dioleoyl-*sn*-glycero-3-phosphocholine (DOPC), 1,2-dioleoyl-*sn*-glycero-3-phospho-(1'-*rac*-glycerol) (sodium salt) (DOPG), 1,2-dioleoyl-*sn*-glycero-3-phosphoethanolamine (DOPE), 1,2-dipalmitoyl-*sn*-glycero-3-phosphocholine (DPPC), 1,2-dimyristoyl-*sn*-glycero-3-phosphocholine (DMPC), 1,2-dilauroyl-*sn*-glycero-3-phosphocholine (DLPC) were purchased from Avanti Polar lipids. 1,2-dioleoyl-3-trimethylammonium-propane, chloride salt (DOTAP), Didodecyltrimethylammonium bromide (DDAB), cholesterol, Nile red was obtained from Sigma Chemical Co., St Louis, MO, USA.

2.2. Preparation of LUV and SUV

Large unilamellar vesicles (LUV) were prepared using an extrusion technique (LiposoFast from AVESTIN (Canada) as described by Hope et al. [15]. Various phospholipids and phospholipid-cholesterol mixtures have been used for vesicle preparation. An appropriate amount of lipid or lipid-cholesterol mixture in chloroform was transferred to a 5 ml glass vial. Chloroform solvent was removed by gently passing dry nitrogen gas. The traces of the solvent were then removed by keeping the sample in a vacuum desiccator for a couple of hours. Milli Q water was added to the dried lipid film so that the final desired concentration (1 mM) was obtained. Vortexing of hydrated lipid film for about 30 min produces multilamellar vesicles (MLV). MLV suspensions were extruded through polycarbonate membranes of pore diameters 100 nm. This results in a formation of fairly monodispersed LUV (average diameter ~100 nm). Size distribution and the polydispersity index were measured using dynamic light scattering (See the supplementary information). LUV solution was degassed prior to all measurements to eliminate the artefacts caused by the air bubble formation. For lipid, such as, DPPC whose chain melting transition temperature (T_m) is 42 °C, SUV were

prepared by ultrasonating MLV at temperature (50 °C) much above the T_m . For SUV preparation, all above steps up to formation of MLV remains same. 0.1 wt% of Nile red in aqueous solution was introduced into the LUV or SUV solution and kept it for half an hour for equilibration. The final concentration of Nile red in the LUV solution is ~2.5 μ M. We have also incorporated Nile red by co-drying it with the lipids in a chloroform solvent. In this case we kept Nile red to lipid ratio as 1:350.

2.3. Fluorescence Spectroscopy

2.3.1. Steady State Fluorescence Measurement

We have measured the steady state fluorescence emission intensity of Nile red labeled large unilamellar vesicles composed of various lipids and lipid-cholesterol mixtures. Fluorescence measurements were carried out using a PTI Quantamaster 400 spectrofluorimeter (Horiba-PTI, Canada). We have measured the absorption spectrum of Nile red and optimum excitation wavelength was found to be at 550 nm. Therefore, excitation wavelength has been kept fixed at 550 nm and emission spectra of Nile red were monitored for different lipids and at different cholesterol concentration. We have also observed emission for different excitation in order to check any red edge excitation shift. We have kept the emission and excitation band pass filters at 5 nm for all measurements. Emission spectra were recorded only in the fluid phase for unsaturated lipids, such as DOPC, DOPG and DOTAP, and in the both fluid and gel phases for saturated lipids, such as DMPC and DPPC. Spectra were also observed at different cholesterol concentration at temperatures below and above the chain melting transition for saturated lipids. The effect of temperature on the emission spectrum has also been investigated. Emission spectrum of Nile red in the presence of short chain phospholipid, DLPC and mixture of cholesterol with DOPC, DPPC and DMPC has also been observed.

2.3.2. Fluorescence Anisotropy

Fluorescence anisotropy is widely used to characterize the extent of linear polarization of fluorescence emission. Fluorescence anisotropy was obtained using the PTI Quantamaster 400 spectrofluorimeter (Horiba-PTI, Canada). Nile Red was excited at 550 nm with a vertically polarised light. The intensity of emission was then measured at 630 nm through a polariser/analyser at crossed (I_{vh}) and parallel (I_{vv}) positions of the analyser with respect to polarised excitation. Steady state polarization anisotropy (r) is defined as

$$r = \frac{I_{vv} - GI_{vh}}{I_{vv} + 2GI_{vh}} \quad (1)$$

where, G is an instrument and a wavelength dependent correction factor to compensate for the polarization bias of the detection system and for the ratio $\frac{I_{vh}}{I_{hh}}$. The I_{vv} , I_{vh} , I_{hv} and I_{hh} represents the excitation and emission fluorescence signal with the polarizer positions set at (0°, 0°), (0°, 90°), (90°, 0°) and (90°, 90°) respectively.

2.3.3. Fluorescence Lifetime

Fluorescence lifetime measurement was carried out using time-correlated single photon counting set up from Horiba Jobin-Yvon. The luminescence decay data were collected on a Hamamatsu MCP Photomultiplier (R3809) and were analyzed using IBH DAS6 software. Rotational rate constant was estimated from the knowledge of fluorescence anisotropy and lifetime measurement using well known Perrin equation

$$\frac{r_0}{r} = 1 + \frac{\tau}{\theta} = 1 + 6D_R\tau \quad (2)$$

where, r_0 is the intrinsic or fundamental anisotropy present between absorption and emission transition moments. Assuming absorption and emission transition moments are parallel, r_0 can have value equal

to 0.4 [16]. θ and D_R are the rotational correlation time and rotational rate of fluorophore, respectively.

3. Results and Discussions

3.1. Effect of Different Phospholipids on the Emission Spectra of Nile Red

Nile red is an environment-sensitive probe, which shows fluorescence in the presence of lipid bilayer. The Nile red is known to exhibit efficient fluorescence emission in hydrophobic environment and increases its efficiency with increasing hydrophobicity or decreasing the solvent polarity, resulting in a progressive blue shifted emission maximum [9]. However, Nile red shows a very low quantum yield in a polar aqueous environment (Fig. 1). In our study, we have used large unilamellar vesicles made from different phospholipids and observed the emission spectra of Nile red to understand the effect of lipid composition on the emission spectra. The Nile red emission in the presence of different phospholipid vesicles is summarized in Table 1. The λ_{em} (632 \pm 2 nm) of Nile red fluid phase is found to be independent of unsaturated lipid types used in our experiment, when excited at 550 nm. Our result on DOPC is in agreement with the previous study by Kucherak et al. [9]. However, much lower value of λ_{em} (~618 nm) was reported by Mukherjee et al. [17]. Although, Mukherjee et al., in their experiment, has incorporated the probe Nile red by co-drying with the lipids, the symmetric distribution of Nile red in both leaflet of the bilayer, due to negligible differences in curvature, cannot be the consequence of different λ_{em} . Nevertheless, we have obtained same λ_{em} irrespective of whether Nile was incorporated before or after the preparation of LUV. Moreover, the manner of probe insertion in the case is a moot point as the flip-flop rate of Nile red is very fast [9]. We have also found that the λ_{em} is independent of solvent pH (see supporting information) and consistently obtained the similar value of λ_{em} for all unsaturated lipids. We trust our results on DOPC, as we have consistently obtained the same results (within the experimental error) from several independent experiments.

In order to explore the effect of charge and head group on the λ_{em} , we have prepared LUV from charged phospholipids. The λ_{em} does not seem to alter in the presence of negatively charged lipids (DOPG) and positively charged vesicles made from DOTAP and DOPC-DDAB mixture (4:1). Therefore, it is conceivable that the charge and head group of the membrane has no role in the emission of Nile red. To check the influence of chain length on the λ_{em} , fluorescence experiments with DPPC, DMPC and DLPC have been performed. Interestingly, the λ_{em} in the presence of saturated lipids, such as DPPC, DMPC at temperatures above their chain melting transition (T_m) was found to be very similar (within the error

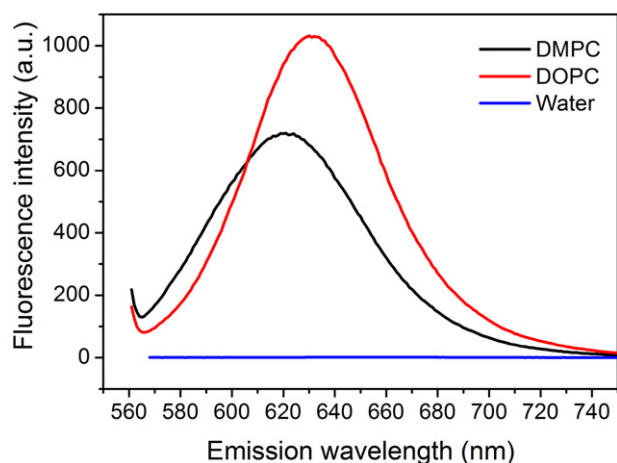


Fig. 1. Emission spectrum of Nile red in DOPC and DMPC LUV at 25 °C. For comparison, the emission spectrum of pure aqueous medium is also shown. The intensity of the emission spectrum of water is negligible compared to that in the presence of LUV.

Table 1

Summary of maximum emission wavelength (λ_{em}) of Nile red at temperature 25 °C in the presence of LUV composed of various lipids and lipid mixtures. Numbers in bracket in the first column represent the molar ratio of the two lipid mixture. Number in the second column represents the length and saturation of the hydrocarbon chains. All unsaturated lipids listed here have one double bond at 9th position ($\Delta 9$ -Cis). DDAB is a double-chain (16 Carbon in each chain) cationic surfactant. For all experiments pH of the LUV dispersion was kept.

Lipids	Hydrocarbon chains, charge	Phase state	$\lambda_{em} \pm 2$ (nm)
DOPC	18:1	Fluid	632
DOPG	18:1, - ve charge	Fluid	634
DOTAP	18:1, + ve charge	Fluid	632
DPPC	16:0,	Gel (Fluid)	617 (623)
DMPC	14:0	Fluid	624
DLPC	12:0	Fluid	624
DOPC:DPPC (4:1)	-	Gel-fluid	628
DOPC:DOPE (4:1)	-	Fluid	632
DOPC:DDAB (3:1)	+ ve charged	Fluid	631
DOPC:Cholesterol (4:1)	-	Liquid disordered	628
DPPC:Cholesterol (4:1)	-	Liquid ordered	594
DMPC:Cholesterol (4:1)	-	Liquid ordered	607

bar) when we have raised the temperature by 20 °C from the T_m for all above lipids. This is to avoid the temperature dependency of the λ_{em} in the fluid phase. As both the saturated phospholipids with different chain length show similar emission, the length of the hydrocarbon chain does not have any influence on the emission spectra of Nile red. This is contrary to the fact that Nile selectively interacts with the hydrophobic sites of the bilayer. However, as found in the previous study [17], the Nile red is located at the interface between hydrocarbon chains and the head group. The interaction length is about 10–15 Å from the interface assuming the monolayer thickness ~26–30 Å. Therefore, it is expected that chain length should not influence the emission properties of Nile red. The fact that the saturated lipids DPPC, DMPC and DLPC in the fluid phase show very different emission than that of DOPC, the emission spectra indeed depend on the chain saturation of the membrane even though all above lipids are in the fluid phase. As we can access the gel phase of saturated lipids only, the emission spectrum in the gel phase has been monitored and λ_{em} was found to be 617 \pm 2 nm. Since, λ_{em} does not depend significantly on head group and chain length, it is possible to compare the λ_{em} of Nile red in the fluid and gel phases of two different phospholipid membranes having same head group and similar chain length. Above emission properties of Nile red in the presence of vesicles, composed of various phospholipids, have not been emphasized in earlier studies.

In summary, the emission spectrum of Nile red in the fluid phase of DOPC differs by 9 \pm 2 nm from the fluid phase of DPPC. However, in the fluid phase of two different phospholipids (DPPC and DMPC) with saturated chains, the λ_{em} are very close. Interestingly, λ_{em} in the gel phase of DPPC differs by 15 nm and 6 nm from the fluid phase of DOPC and DMPC (or DPPC), respectively. These differences might be the consequence of all *trans* conformation of hydrocarbon chains in DPPC and the presence of kink (*cis* configuration) in DOPC. The hydrophobic dye, Nile red is expected to penetrate more in the flexible hydrocarbon chains of DOPC bilayer than the comparatively rigid chains of DPPC. It is important to mention that it is difficult to identify two different saturated phospholipids (DPPC and DMPC) as their emission spectra are very close to each other. Although, we can identify the lipids in terms of chain saturation by looking at the individual Nile red spectra, the chemical details of the lipids have to be determined from some other experimental techniques. The obvious question that arises: can we identify two different phospholipids from the spectrum of Nile red in the presence of DOPC-DPPC mixture? In order to check this possibility, we have measured the emission spectra of an equimolar mixture of DOPC and DPPC at two different temperatures (see Table 1). It is known from the previous studies that DOPC-DPPC mixture exhibits gel-fluid coexistence below the T_m of DPPC [18,19]. Therefore, it is expected to

have two characteristic emission wavelengths arising from the coexistence of gel and fluid phases at 25 °C. However, we could not distinguish two phases from the spectral decompositions using two Gaussian fit. This could be due to a large difference in intensities of two coexisting phases. A large difference in intensities would result the smearing out the spectrum obtained from individual phases. To reduce such difference in intensities, we have also prepared LUV from different molar ratios of the mixture to change the relative amount of gel and fluid phases. We have still not been able to distinguish two phases from the spectra. We suggest that a good quality optical filter with a very narrow band may be able to decompose two spectral lines arising from gel and fluid phases. Further fluorescence microscopy experiments need to perform in order to check this possibility.

A higher fluorescence intensity has been observed below the T_m (gel phase) of DPPC as compared to above T_m (See supporting information). This is in contrast with the fact that the more rigid gel phase must prevent Nile red to penetrate into the membrane core, resulting the decrease in local concentration, whereas, the loosely packed fluid phase must have larger vacancy for Nile red [9]. The increase in fluorescence intensity at gel phase is thus intriguing. The transition from the fluid phase to gel phase increases the number of defects in bilayer which might favor the incorporation of Nile red. Much above T_m (60 °C), the thermal quenching is important due to opening up of completely non-radiative relaxation pathways and hence it is expected to decrease the fluorescence intensity although bilayer is too flexible to incorporate the Nile red. In order to confirm the thermal quenching, the emission spectra were taken with increasing temperature (Fig. 2) for different lipids. All of them show the decrease in fluorescence intensity with increasing temperature in the fluid phase only. This is supported by the fact that the fluorescence quenching does not occur below T_m of DPPC and DMPC. It is known that bilayer becomes more flexible, as evidenced from the decrease in bending modulus and area compressibility modulus with increasing temperature [20]. Therefore, the decrease in fluorescence intensity might be the consequence of the increase in water penetration in the fluid phase, as compare to gel phase with increasing temperature. This is also further supported by the fact that the bilayer thickness decreases and the thickness of water layer increases in membrane stacks with increasing temperature [21]. It is also important to note that the λ_{em} of DPPC decreases initially in the gel phase and again increases to a similar value when temperature is further increased from 30 °C as shown in the inset of Fig. 2. The hydration dynamics in the vicinity of the Nile red could influence the excited state leading to the

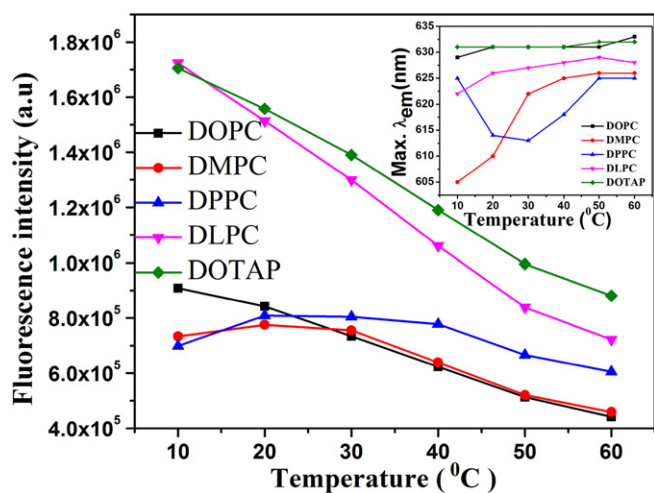


Fig. 2. Temperature variation of fluorescence emission intensity of Nile red for different lipids, as indicated in the figure legend. Maximum emission wavelength seems to be blue shifted in the gel phase of DPPC and red shifted in the fluid phase of DPPC, DMPC. However, the λ_{em} for unsaturated lipids DOPC, DOTAP does not seem to alter with increasing temperature.

change in its emission wavelength. The temperature dependence of the Nile red emission has not been reported in any of the earlier studies.

3.2. Effect of Cholesterol on the Emission Spectra of Nile Red in the Presence of Different Phospholipids

Fluorescence emission of Nile red has been used to investigate the effect of cholesterol on the membranes. Previous literatures have shown that ternary mixture composed of DPPC (or DMPC), DOPC and cholesterol exhibits two phases, namely liquid ordered (l_o) and liquid disordered (l_d) at temperature below T_m of saturated lipid [22]. The l_o phase is rich in cholesterol and saturated lipid (DPPC/DMPC) and l_d phase contains unsaturated lipid (DOPC) and little amount of cholesterol. Therefore, we have studied the binary mixtures of cholesterol with DPPC, DMPC and DOPC in order to gain some insights into the l_o and l_d phases, respectively. The location of cholesterol is believed to be in the interfacial regions of head group and acyl chains of the membranes [23]. Our previous study on the small angle x-ray diffraction has shown a small peak in the electron density profile at a distance of 10 Å from the center of the bilayer, indicating the presence of cholesterol at the interfacial regions [24]. Further, it is known that Nile red shows fluorescence when it penetrates into the membrane core region. Therefore, it is conceivable that fluorescence properties of Nile red are expected to alter in the presence of cholesterol and hence Nile red can be an useful probe to study the effect of cholesterol on the membranes. Fig. 3 shows the effect of cholesterol on the λ_{em} of Nile red in the presence of saturated lipid DPPC and DMPC and unsaturated lipids DOPC. It is clearly evident that the λ_{em} decreases (blue shifted) very rapidly from 618 nm to 595 nm with increasing cholesterol concentration up to 10 mol% in the l_o phase of DPPC-cholesterol membranes. Above 10 mol% of cholesterol, there is no significant decrease in the λ_{em} . However, λ_{em} decreases progressively (blue shifted) with increasing cholesterol concentration for DMPC-cholesterol membranes. On the other hand, Nile red emission maximum does not show significant decrease in the l_d phase, containing DOPC. The decrease in the λ_{em} at lower cholesterol concentration (< 10 mol%) for DPPC is the consequence of the two phase coexistence of gel and l_o at cholesterol concentration below 10 mol% [24]. Further, this feature of DPPC can be attributed to the fact that, gel phase of DPPC shows tilt of ~ 30° with respect to bilayer normal. This tilt ensures the deeper insertion of the small Nile red molecule, resulting the significantly blue shifted spectrum. Rough estimate from area differences of lipid and cholesterol gives about 10–20 mol% of cholesterol that can be incorporated into the bilayer to remove the tilt [25]. Once the tilt is removed, as in the case of l_o phase Nile red the

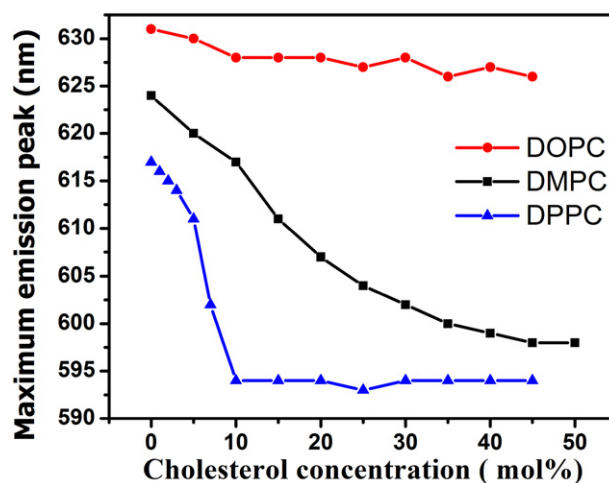


Fig. 3. Variation of maximum emission peak of Nile red obtained from different phospholipids at 25 °C for different cholesterol concentration. Solid lines are intended as guide to the points and not obtained from fit.

λ_{em} shows nearly the same value, indicating that the Nile red interacts nonspecifically in the l_o phase due to shallow penetration of Nile red into the bilayer.

It has been known that incorporation of cholesterol reduces the hydrophobicity in the membrane leading to an increase in water penetration [26]. The increase in water content in the bilayers was also confirmed in terms of increase in d-spacing as seen in the small angle x-ray scattering experiment [24]. Therefore, the reduction of fluorescence intensity with increasing cholesterol concentration could be due to an increase in environmental polarity and increase in water penetration in the membrane interfacial region [17]. It is interesting to note that Fig. 3 can be used as a calibration curve of cholesterol content in the l_o phase containing saturated lipids by observing fluorescence emission of Nile red. The amount of blue shift in case of DMPC can be an estimation of cholesterol concentration in the l_o phase. However, no such prediction is possible for l_d phase as cholesterol has very little influence on the emission spectrum of Nile red for DOPC membrane. However, this result does not rule out the possibility that l_d phase contains very little amount of cholesterol.

3.3. Red Edge Excitation Shift (REES) of Nile Red in DOPC Vesicles Containing Cholesterol

A shift in the λ_{em} fluorescence emission toward higher wavelength caused by a shift in the excitation wavelength (λ_{ex}) toward the red edge of absorption band is termed as REES. The slow rate of solvent relaxation relative to fluorophore lifetime due to reorientation of dipoles around the excited state of fluorophore is known to be responsible for REES. The solvent relaxation in the immediate vicinity of the fluorophore indeed depends on the motional restriction of lipid molecules induced by the cholesterol in the lipid bilayer. Therefore, the REES effect has a direct consequence of change of rotational diffusion of fluorophore in the presence of lipid-cholesterol membranes. Therefore, it is conceivable that Nile red, located in the confined water within the bilayer as well as a hydration layer at the vicinity of the membrane, is expected to show REES. We now focus on REES to monitor the effect of cholesterol in the membranes.

The shift in the λ_{em} of Nile red in DOPC vesicles with increasing λ_{ex} (510 nm to 590 nm) for different cholesterol concentrations is shown in Fig. 4. As the λ_{ex} is changed from 510 to 590 nm, the λ_{em} of Nile red displays the shift toward higher wavelengths. In the absence of cholesterol there is no significant shift in the λ_{em} . However, ~ 11 nm shift

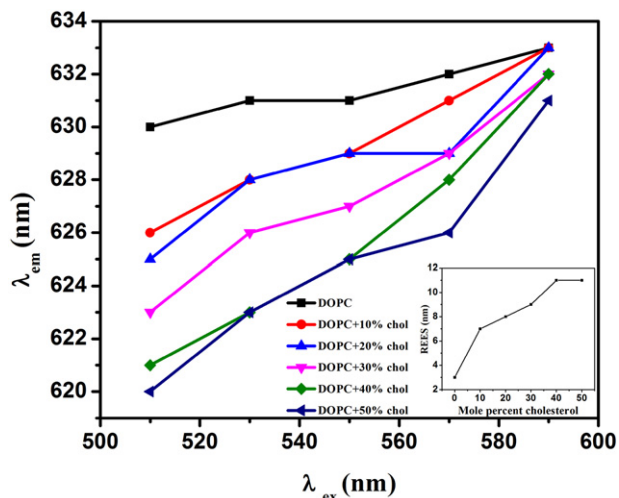


Fig. 4. Variation of maximum emission wavelength ($\lambda_{em} \pm 2$ nm) at different excitation wavelength (λ_{ex}) of Nile red in the presence of DOPC-cholesterol membranes. Cholesterol concentrations (mol%) are indicated in the figure legend. The red edge emission shift (REES) has been shown in the inset of the figure. Solid lines are intended as guide to the points and not obtained from the fit.

was observed for all cholesterol concentration studied. In case of saturated lipid, DMPC, λ_{em} changes from 618 nm to 625 nm upon variation of λ_{ex} from 510 nm to 590 nm (data not shown). The significant REES dependence of Nile red in the presence of cholesterol indicates that rotational diffusion of Nile red is restricted within the bilayers as cholesterol induces the straightening of the chains near the interface. This result is further supported by the fact that the rotational diffusion decreases with increasing cholesterol concentration (see later). As discussed before, the λ_{em} obtained from our study and from Kucherak et al. [9] at the excitation of 550 nm was in stark disagreement with λ_{em} value reported by Mukherjee et al. [17]. Therefore, the data in Fig. 4 is expected to be different from the REES data presented in ref. 17. This is the reason that we have again looked at these data, although REES has already been reported in case of DOPC-cholesterol membranes [17]. Observation of REES in DOPC vesicles implies that the Nile red is in a motionally restricted environment and is strongly interacting with the solvent. The change in dipole moment during the excited state reaction, as shown in previous study [11] enforces the solvent dipoles surrounding the Nile red to reorganize around the excited state and to reach to the equilibrium prior to the emission. Therefore, fluorescence emission alters due to change in polarity of the surrounding environment.

3.4. Rotational Dynamics of Lipid Bilayers as Revealed from Steady State Fluorescence Anisotropy

Steady state fluorescence anisotropy has been extensively used to monitor the rotational diffusion rate of Nile red embedded in the membrane. As fluorescence anisotropy measures the extent of depolarization, i.e., the ability of the probe to reorient during the emission, it must be sensitive to the packing of lipid acyl chains. The rigid environment surrounding the fluorophore probe increases the anisotropy. Thus, the probable location of cholesterol in the membrane can also be suggested by monitoring the anisotropy. Therefore, the effect of cholesterol on the lateral as well as rotational diffusion of lipids in the membranes can be envisaged from the anisotropy measurement. The increase in anisotropy, in the presence of DMPC and DPPC bilayers containing cholesterol, suggests that cholesterol restricts the rotational motion of the Nile red by providing the rigidity to the membrane (Fig. 5). Interestingly, cholesterol does not change the anisotropy for DOPC membrane. This is consistent with the fact that the bending rigidity ($\kappa \sim 11 \times 10^{-20}$ J) of DOPC membranes containing various amounts of cholesterol did not change significantly [27]. However, it is believed that the cholesterol orders the acyl chain of the saturated lipids above the chain melting transition leading to an increase in κ . The anisotropy (r) value is the lowest in the liquid disordered phase and highest in the liquid ordered phase at higher cholesterol concentration. This is

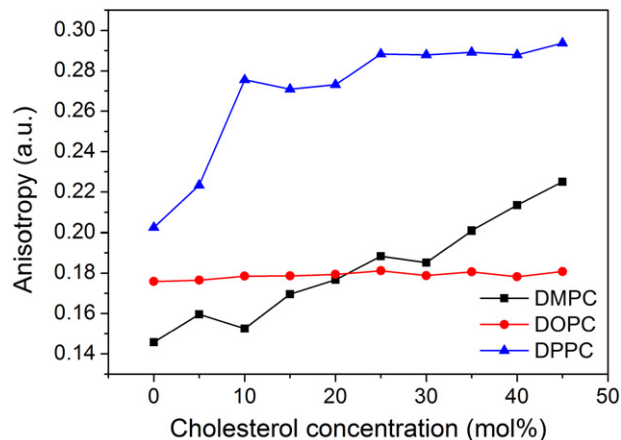


Fig. 5. The steady state fluorescence anisotropy of Nile red in the presence of DMPC, DOPC and DPPC vesicles for different concentrations of cholesterol at 25 °C. Solid lines are intended as guide to the points and not obtained from the fit.

due to the relatively loose packing of the lipid acyl chains in the liquid disordered phase. This is further supported by the fact that the affinity of cholesterol to the phospholipid bilayers was known to decrease significantly with increasing the degree of unsaturation of the acyl chains [28]. These results are consistent with those obtained from the Fig. 3.

3.5. Lifetime of Nile Red in Phospholipid Vesicles: Effect of Cholesterol

Fluorescence lifetime serves as a reliable indicator of the local environment in which a fluorophore is localized. Fig. 6 shows the fluorescence lifetime of Nile Red in the presence of three different lipids containing cholesterol. It is clearly evident that lifetime does not increase significantly for DOPC, whereas it increases markedly for DMPC and DPPC. This is consistent with the results obtained from emission spectrum and anisotropy measurement.

The mean fluorescence lifetime of Nile Red in DMPC vesicles increases from ~4.26 ns to 6.61 ns with increasing membrane cholesterol content up to 50 mol%. For DOPC, lifetime increases from 3.52 ns to 4.11 ns. Cholesterol is known to decrease the water penetration significantly and increases the dipole potential of the membrane [29]. Further, cholesterol in the membrane restricts the rotation of the fluorophore in the rigid environment. Such rigidification of the feeble parts of the molecules as well as increase in polarity of the membrane would marginalize the role of the non-radiative pathway, resulting in an increase of fluorescence lifetime [30]. The increase in membrane viscosity when cholesterol is incorporated into the membrane could also increase the lifetime of the Nile Red.

The rotational rate D_R of Nile Red estimated from Eq. (2) in the presence of LUV with different concentration of cholesterol is shown in Fig. 7. There is no previous literature to verify the values of D_R with our estimated value. In order to check the effect of rotational diffusion on the anisotropy value, we assume a constant rotational rate (same as without cholesterol) to estimate the anisotropy (r) from the measured value of fluorescence lifetime with varying cholesterol concentration. Such an estimation gives a much lower value of r and it does not alter significantly with cholesterol concentration (See supporting information). This analysis clearly indicates that increase in anisotropy in the case of saturated lipids is due to motional restriction of lipids induced by cholesterol and lifetime has no significant influence on the rotational correlation time.

4. Conclusion

In this work, we have monitored the organization, dynamics and solvent relaxation characteristics by measuring emission wavelength,

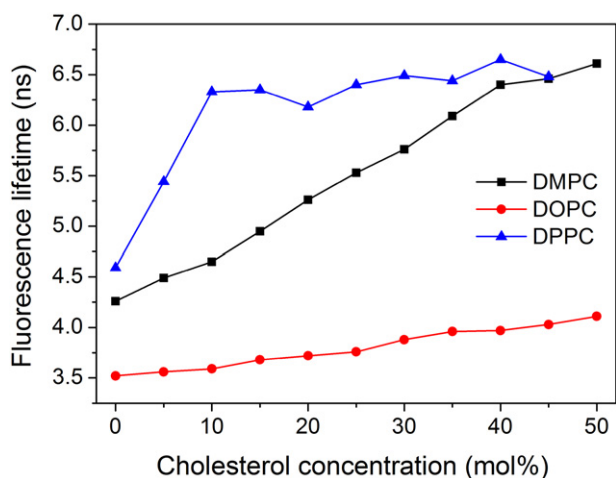


Fig. 6. Steady state fluorescence lifetime of Nile Red in the presence of three different phospholipids for different cholesterol concentration (mol %) at 25 °C.

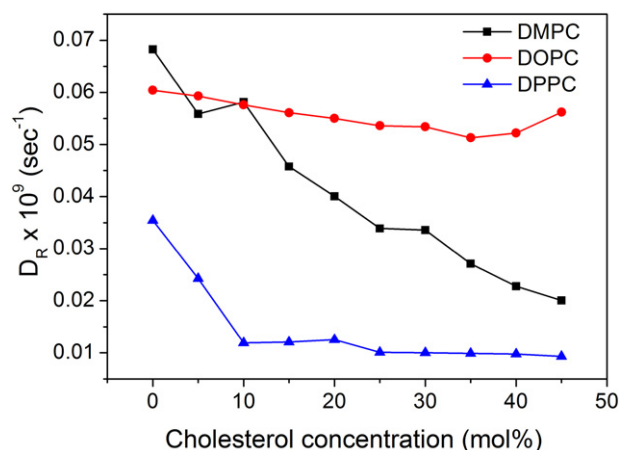


Fig. 7. Rotational rate of Nile Red in the presence of three different lipid vesicles ($T = 25$ °C), indicated in the figure legend for different cholesterol concentration (mol %).

anisotropy and lifetime of Nile Red in various phospholipid membranes. The spectroscopic properties of Nile Red change significantly in the presence of phospholipids with saturated acyl chains and not with the lipid phase state. The effect of cholesterol can be envisaged only with the saturated lipid and not with the unsaturated lipids which is consistent with the fact that the elastic properties of the membrane does not alter significantly with increasing cholesterol concentration. Interestingly, in the gel phase of DPPC, the fluorescence properties of Nile Red change rapidly with cholesterol concentration up to 10 mol%. Beyond that spectroscopic properties of Nile Red do not change significantly. Therefore, the membrane in the gel phase can accommodate cholesterol up to 10 mol% and converted into the pure liquid ordered phase. This is also a consequence of the fact that at lower concentrations of cholesterol, there exists two phase coexistence of gel and l_0 . Therefore, above ~ 10 mol%, the gel phase completely converted into the single l_0 phase. It is important to note that ~ 10–15 mol% of cholesterol can remove the tilt of the hydrocarbon chain of the lipids in the gel phase. Therefore, once the tilt is removed, the Nile Red cannot penetrate into the membranes and it remains in the solution. Hence Nile Red does not seem to show any significant change in its spectroscopic properties. On the other hand, the emission wavelength decreases and anisotropy as well as lifetime of Nile Red in the fluid phase of DMPC membrane increases monotonically with increasing cholesterol concentration. These results clearly indicate that cholesterol can alter the acyl chain environment in the fluid phase and membrane can accommodate the cholesterol till the miscibility limit. Above spectroscopic properties remain unaltered in case of unsaturated lipid DOPC. The effect of temperature on the emission spectrum of Nile Red in the presence of both saturated and unsaturated lipids has been discussed. The lifetime measurement along with the steady state anisotropy result provides us to estimate the rotational rate of Nile Red. The acyl chain environment in turn affects the rotational diffusion of Nile Red which is known to reside at the interface. Although one of the primary objectives was to identify the lipid type from the spectral properties of Nile Red, it is not straightforward to identify the lipid type from the spectral analysis of Nile Red alone. However, correlations between the membrane compositions and fluorescence spectral features can be utilized in a wide range of biophysical fields as well the cell biology. For example, effect of cholesterol on the emission spectra can possibly be used in bioanalytical applications.

Acknowledgements

This work was supported by the major research project funded by the Department of Biotechnology (BT/PR8475/BRB/10/1248/2013) and University Grand Commission (42-769/2013(SR)) Govt. of India. GSK acknowledges financial assistance from CSIR Network project

BIOCERAM (ESC0103). A. Halder thanks to UGC for providing Rajiv Gandhi National Fellowship. Authors also thank Dr. Prosenjit Sen, IACS, Kolkata for academic discussion.

Appendix A. Supplementary data

Supplementary data to this article can be found online at <https://doi.org/10.1016/j.saa.2017.10.002>.

References

- [1] A. Akbarzadeh, R. Rezaei-Sadabady, S. Davaran, Sang, W. Joo, N. Zarghami, Y. Hanifehpour, M. Samiei, M. Kouhi, K. Nejati-Koshki, Liposome: classification, preparation, and applications, *Nanoscale Res. Lett.* 8 (2013) 102–110.
- [2] L. Finegold (Ed.), *Cholesterol in Membrane Models*, CRS Press, 1992.
- [3] J. Pan, S. Tristram-Nagle, J.F. Nagle, Effect of cholesterol on structural and mechanical properties of membranes, *Phys. Rev. E* 80 (2009) 21931–21942.
- [4] K. Simons, M.J. Gerl, Revitalizing membrane rafts: new tools and insights, *Nat. Rev. Mol. Cell Biol.* 11 (2010) 688–699.
- [5] N. Bezlyepkina, R.S. Gracià, P. Shchelokovskyy, R. Lipowsky, R. Dimova, Phase diagram and tie-line determination for the ternary mixture DOPC/eSM/cholesterol, *Biophys. J.* 104 (2013) 1456–1464.
- [6] T. Baumgart, S.T. Hess, W.W. Webb, Imaging coexisting fluid domains in biomembrane models coupling curvature and line tension, *Nature* 425 (2003) 821–824.
- [7] D. H-J Kaiser, I. Lingwood, J.L. Levental, L. Sampaio, L. Kalvodova, Rajendran, K. Simons, Order of lipid phases in model and plasma membranes, *Proc. Natl. Acad. Sci. U. S. A.* 106 (2009) 16645–16650.
- [8] A. Arora, H. Raghuraman, A. Chattopadhyay, Influence of cholesterol and ergosterol on membrane dynamics: a fluorescence approach, *Biochem. Biophys. Res. Commun.* 318 (2004) 920–926.
- [9] O.A. Kucherak, S. Oncul, Z. Darwich, D.A. Yushchenko, Y. Arntz, P. Didier, Y. Mély, A.S. Klymchenko, Switchable Nile red-based probe for cholesterol and lipid order at the outer leaflet of biomembranes, *J. Am. Chem. Soc.* 132 (2010) 4907–4916.
- [10] P. Maity, B. Saha, G.S. Kumar, S. Karmakar, Effect of counterions on the binding affinity of Na⁺ ions with phospholipid membranes, *RSC Adv.* 6 (2016) 83916–83925.
- [11] N. Ghoneim, Photophysics of Nile red in solution steady state spectroscopy, *Spectrochim. Acta* 56 (2000) 1003–1010.
- [12] P. Greenspan, E.P. Mayer, S.D. Fowler, Nile red: a selective fluorescent stain for intracellular lipid droplets, *J. Cell Biol.* 100 (1985) 965–973.
- [13] I.R. Sitepu, L. Ignatia, A.K. Franz, D.M. Wong, S.A. Faulina, M. Tsui, A. Kanti, K. Boundy-Millsa, An improved high-throughput Nile red fluorescence assay for estimating intracellular lipids in a variety of yeast species, *J. Microbiol. Methods* 91 (2012) 321–328.
- [14] A. Dutta, D.K. Sinha, Turnover of the actomyosin complex in zebrafish embryos directs geometric remodelling and the recruitment of lipid droplets, *Sci Rep* 5 (2015), 13915.
- [15] M.J. Hope, M.B. Bally, G. Webb, P.R. Cullis, Production of large unilamellar vesicles by a rapid extrusion procedure: characterization of size distribution, trapped volume and ability to maintain a membrane potential, *Biochim. Biophys. Acta* 812 (1985) 55–65.
- [16] J.R. Lakowicz, *Principles of Fluorescence Spectroscopy*, Plenum Press, New York, 1983.
- [17] S. Mukherjee, H. Raghuraman, A. Chattopadhyay, Membrane localization and dynamics of Nile red: effect of cholesterol, *Biochim. Biophys. Acta* 1768 (2007) 59–66.
- [18] S.L. Veatch, S.L. Keller, Separation of liquid phases in giant vesicles of ternary mixtures of phospholipids and cholesterol, *Biophys. J.* 85 (2003) 3074–3084.
- [19] S. Karmakar, B.R. Sarangi, V.A. Raghunathan, Phase behaviour of lipid-cholesterol membranes, *Solid State Commun.* 139 (2006) 630–634.
- [20] J. Pan, S. Tristram-Nagle, N. Kucerka, J.F. Nagle, Temperature dependence of structure, bending rigidity, and bilayer interactions of dioleoylphosphatidylcholine bilayers, *Biophys. J.* 94 (2008) 117–124.
- [21] N. Kučerka, M.-P. Niehc, J. Katsarasa, Fluid phase lipid areas and bilayer thicknesses of commonly used phosphatidylcholines as a function of temperature, *Biochim. Biophys. Acta* 1808 (2011) 2761–2771.
- [22] J.V. Bleecker, P.A. Cox, S.L. Keller, Comparing Lo/Ld membrane thickness mismatch and miscibility transition temperatures using fluorescence and atomic force microscopy, *Biophys. J.* 110 (2016) 2305–2308.
- [23] D. Marquardt, N. Kučerka, S.R. Wassalle, T.A. Harrounf, J. Katsaras, Cholesterol's location in lipid bilayers, *Chem. Phys. Lipids* 199 (2016) 17–25.
- [24] S. Karmakar, V.A. Raghunathan, Structure of phospholipid-cholesterol membranes: an x-ray diffraction study, *Phys. Rev. E* 71 (2005) 61924–61934.
- [25] S. Karmakar, V.A. Raghunathan, Cholesterol induced modulated phase in phospholipid membranes, *Phys. Rev. Lett.* 91 (2003) 98102–98106.
- [26] W.K. Subczynski, A. Wisniewska, J.J. Yin, J.S. Hyde, A. Kusumi, Hydrophobic barriers of lipid bilayer membranes formed by reduction of water penetration by alkyl chain unsaturation and cholesterol, *Biochemistry* 33 (1994) 7670–7681.
- [27] R.S. Gracia, N. Bezlyepkina, R.L. Knorr, R. Lipowsky, R. Dimova, Effect of cholesterol on the rigidity of saturated and unsaturated membranes, *Soft Matter* 6 (2010) 1472–1482.
- [28] T.P.W. McMullen, R.N.A.H. Lewis, R.N. McElhaney, Cholesterol-phospholipid interactions, the liquid ordered phase and lipid rafts in model and biological membranes, *Curr. Opin. Colloid Interface Sci.* 8 (2004) 459–468.
- [29] T. Starke-Peterkovic, N. Turner, M.F. Vitha, M.P. Waller, D.E. Hibbs, Cholesterol effect on the dipole potential of lipid membranes, *Biophys. J.* 90 (2006) 4060–4070.
- [30] M.Y. Berezin, S. Achilefu, Fluorescence lifetime measurements and biological imaging, *Chem. Rev.* 110 (2010) 2641–2684.

Kinetoplastid Membrane Protein-11 Induces Pores in Anionic Phospholipid Membranes: Effect of Cholesterol

Animesh Halder,[§] Achinta Sannigrahi,[§] Nayan De,[§] Krishnananda Chattopadhyay,^{*} and Sanat Karmakar^{*}



Cite This: *Langmuir* 2020, 36, 3522–3530



Read Online

ACCESS |



Metrics & More

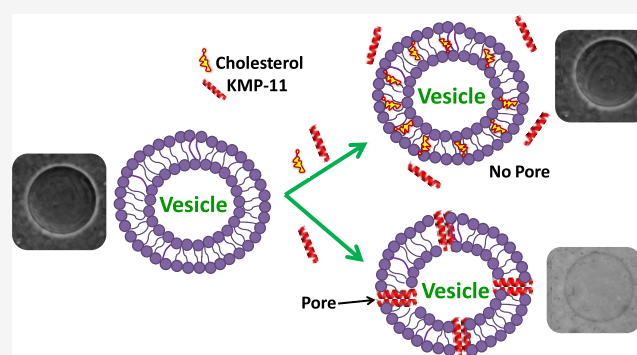


Article Recommendations



Supporting Information

ABSTRACT: Kinetoplastid membrane protein-11 (KMP-11), expressed in all stages of leishmanial life cycle, is considered a potential candidate for leishmaniasis vaccine. KMP-11 is found on the membrane surface of the parasite. Although the biological function of KMP-11 is unknown, we hypothesize from its sequence analysis that it may interact with the macrophage membrane and may influence the entry process of the parasite into the host cell. To validate this hypothesis, we have investigated the interaction of KMP-11 with unilamellar anionic phospholipid vesicles and explored its pore-forming activity. The decrease in negative ζ -potential of the vesicles and reduction in the fluorescence intensity of membrane-bound dye DiI C-18 suggest a strong association of KMP-11 with the membrane. The fluorescence leakage experiment as well as phase contrast microscopy shows direct evidence of KMP-11-induced pore formation in an anionic membrane. Incorporation of cholesterol into the membrane has been found to inhibit pore formation induced by KMP-11, suggesting an important role of cholesterol in leishmaniasis. Interestingly, vesicles containing only neutral phospholipid do not exhibit any tendency toward pore formation.



1. INTRODUCTION

Visceral Leishmaniasis (VL), which is the most severe form of leishmaniasis, is caused by the species *Leishmania donovani*.¹ It is generally believed that specific pathogenic surface molecules can behave as chemical opsonins to facilitate the entry of pathogen into host cells by promoting host–pathogen interactions.² In this connection, it is well known that many major pathogenic systems employ their pore-forming proteins (PFPs) as virulence factors. PFPs are common among bacteria, and about 25–30% of cytotoxic bacterial proteins are PFPs, making them the single largest category of virulence factors.^{3,4} Because of their nearly universal presence in bacterial pathogens, PFPs are a unique and important target for novel, broadly applicable antimicrobial prophylactics and therapeutics. PFPs function to perforate membranes of host cells, predominantly the plasma membrane but also intracellular organelle membranes.⁵ Several PFPs are reported to mediate the pathogen's internalization process through their membrane pore formation activity.⁶ Evavold et al. reported one example in which a pore-forming protein gasdermin D regulates IL1 release from hyperactive macrophages.⁷ Pore-forming proteins are presumably responsible not only for the pathogenic entry process but also for the significant immune suppression process.⁸

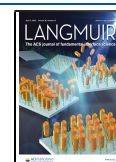
Kinetoplastid membrane protein-11 (KMP-11) is a small immunogenic protein expressed in large copy number on the surface of *L. donovani*. Although the crystal structure is not available, modeling studies suggest a helical structure (Figure 1), which has been supported by far-UV CD measurements. KMP-11 shows strong immunogenic property and is believed to be a potential vaccine candidate.⁹

The function of KMP-11 and its roles in the process of infection are poorly understood. However, it is known that KMP-11 has high expression on parasite surface.⁹ We have recently observed that KMP-11 binds strongly to a synthetic membrane.³ In addition, using a sequence analysis of KMP-11, we find comparable antimicrobial index with the pore-forming peptide magainin-II (Figure S1). All of these observations led us to hypothesize that KMP-11 may have a PFP-like role of forming pores at the host membrane, which may or may not be relevant to the process of parasite internalization. Furthermore, we observed significant sequence homology of KMP-11 with

Received: December 11, 2019

Revised: March 10, 2020

Published: March 12, 2020



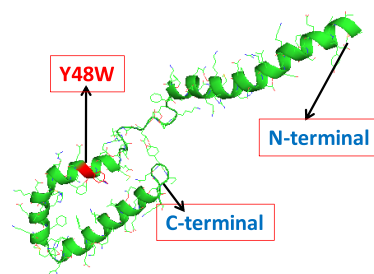


Figure 1. Model structure of KMP-11 as obtained from I-TASSER software. The model structure suggests the α -helical character of the protein. The red region indicates the point of tryptophan mutation (Y48W).

apolipoprotein A (Figure S2), which prompted us to speculate further that cholesterol may influence its pore-forming activity significantly. This is because apolipoprotein A is known for its cholesterol transport properties.¹⁰ In recent years, the concept of a “cholesterol connection” in infectious diseases has emerged where pathogens have evolved a virulence factor that reprograms eukaryotic cellular physiology. In particular, cholesterol plays a significant role in controlling the parasite entry into macrophage cells.¹¹ It has already been reported that cholesterol depletion from the macrophage reduces the ability of leishmania to enter the host macrophages.¹² There exists extensive literature on cholesterol connection with the pore-forming activity and antimicrobial activity of proteins.¹³ The liposomal cholesterol delivery has been employed as a treatment for intracellular parasite killing through the successful enhancement of innate immunity.¹⁴ Moreover, cholesterol regulates the activity of pathogenic PFPs in terms of pore-forming nature and subsequent immune evasion.¹⁴

In the present study, we have systematically investigated the interaction between KMP-11 and anionic membranes composed of 1,2-dioleoyl-*sn*-glycero-3-phosphocholine-1,2-dioleoyl-*sn*-glycero-3-phospho-(1'-*rac*-glycerol) (DOPC–DOPG) (4:1). Since a wide variety of lipid components are present in the native cell membrane, it is often useful to study a model membrane of specific composition to obtain insights into the individual features and activities of the membrane. Although unsaturated lipids, such as DOPC, are abundant in the macrophage membrane,⁴ negatively charged lipids contribute to the subcellular targeting of proteins with cationic domains via electrostatic interaction.¹⁵ This motivates us to choose DOPG as the anionic component of the membrane. Two types of model membranes have been used. The large unilamellar vesicles (LUVs) were prepared to investigate the interaction or binding affinity of KMP-11 with the membranes, whereas giant unilamellar vesicles (GUVs) were used to visualize the pore formation. Fluorescence release of calcein-loaded LUVs and phase contrast microscopy of GUVs have been successfully employed to obtain the evidence of pores in the membranes induced by KMP-11. We have also explored the effect of cholesterol on the pore-forming ability of KMP-11. Microscopy images have been analyzed to obtain dependence of protein concentration and vesicle size on the kinetics of pore formation in the membrane. The binding affinity of KMP-11 with the phospholipid membranes was studied using the ζ -potential and fluorescence assay. The membrane–membrane interaction induced by KMP-11 is envisaged using dynamic light scattering. Our results showed, for the first time, that KMP-11 induces pores in the model

membrane and cholesterol incorporation significantly reduces the pore-forming activity. Collectively, our study suggests an interplay of the binding and pore formation activity of KMP-11 with the architecture and composition of model membranes, which further implicates the molecular mechanistic understanding of leishmaniasis.

2. EXPERIMENTAL SECTION

2.1. Materials and Methods. 1,2-Dioleoyl-*sn*-glycero-3-phosphocholine (DOPC) and 1,2-dioleoyl-*sn*-glycero-3-phospho-(1'-*rac*-glycerol) (DOPG) were purchased from Avanti Polar Lipids Inc. (Alabaster, AL). The 1,1'-dioctadecyl-3,3,3',3'-tetramethylindocarbocyanine perchlorate (“DiI”; DiI_{C18}(3)) dye was purchased from Invitrogen (Eugene, Oregon). These were used without further purification. All other necessary chemicals including salts were obtained from Aldrich (St. Louis) and Merck (Mumbai, India).

2.2. Purification of KMP-11. Recombinant KMP-11 was expressed and purified in Ni-NTA affinity chromatography using a Qiagen-supplied protocol (Qiaexpressionistm; Qiagen, Germany) after slight modifications. The modifications included the use of 20 mM imidazole in both lysis and wash buffers during cell lysis. The purified protein fractions were checked using 15% sodium dodecyl sulfate-polyacrylamide gel electrophoresis (SDS-PAGE). The collected protein-containing fractions were pooled together and dialyzed using 20 mM sodium phosphate buffer of pH 7.4 to remove excess imidazole. The concentration of the protein was determined using the BCA Protein Assay Kit (Pierce, Thermo Scientific).

2.3. Preparation of Large Unilamellar Vesicles (LUVs). An appropriate amount of lipid in chloroform (concentration of stock solution is 25 mg mL⁻¹) was transferred to a 5 mL glass vial. Chloroform was removed by gently passing dry nitrogen gas. This procedure resulted in the formation of a thin lipid layer on the bottom inner wall of the vial. The vial was then kept in a vacuum desiccator for 2 h to eliminate traces of leftover solvent. The required volume of 20 mM sodium phosphate buffer at pH 7.4 was added to the dried lipid film to obtain the final desired lipid concentration of 10 mM. Vortexing of the hydrated lipid film for about 30 min produced the multilamellar vesicles (MLVs). Large unilamellar vesicles (LUVs) were obtained by extruding MLVs using LiposoFast (AVESTIN, Canada). MLV suspensions were extruded through polycarbonate membranes of pore diameter 100 nm. This procedure resulted in the formation of fairly monodisperse LUVs (average diameter ~100 nm) and LUVs. The size distribution was measured using dynamic light scattering (DLS).

2.4. DLS and ζ -Potential Measurements. The ζ -potential and vesicle size distribution were measured using a Zetasizer Nano ZS (Malvern Instruments, U.K.). The instrument uses a 2 mW He–Ne laser of wavelength 633 nm to illuminate the sample. A disposable zeta cuvette was used for both size and ζ -potential measurements. In DLS, back-scattered light at an angle of 173° was detected and fed to the digital signal processing correlator. The intensity–intensity autocorrelation function was measured, which was used to estimate the average size of the LUV using the Stokes–Einstein relation

$$a = \frac{kT}{6\pi\eta D}. D \text{ is the diffusion constant, and } kT \text{ is the thermal energy.}$$

The size distribution was obtained using three successive measurements. The ζ -potential was measured from the electrophoretic mobility by laser Doppler velocimetry using the Helmholtz–Smoluchowski equation.

$$\zeta = \frac{3\mu\eta}{2\epsilon f(\kappa a)} \quad (1)$$

where η and ϵ are the coefficient of viscosity and the permittivity of the aqueous medium, respectively. $f(\kappa a)$ is the Henry function, which depends on the inverse Debye length (κ) and the radius (a) of the vesicle. In Smoluchowski approximation, the maximum value of the function $f(\kappa a)$ is equal to 1.5 when particles are in aqueous media.¹⁶ However, when the particles are suspended in a nonaqueous medium, the value of $f(\kappa a)$ would be 1 (Huckel approximation). In this study,

we have used $f(\kappa a) = 1.5$ to calculate the ζ -potential from measured electrophoretic mobility. The average ζ -potential was obtained using three successive measurements. Each measurement included 10–100 runs.

2.5. Fluorescence Spectroscopy. We used a fluorescence-based assay for studying the binding of wild-type(WT) KMP-11 with the phospholipid membrane composed of a DOPC–DOPG (4:1) mixture. The LUV sample of 1 mM concentration was used as the stock. In each sample vial, 0.5 wt % membrane-specific DiI C-18 dye was added, and the samples were kept at 37 °C for overnight incubation. Subsequently, the appropriate amount of protein was added into the vials by maintaining the lipid/protein molar ratio between 1:0 and 50:1. The samples were then incubated at room temperature (25 °C) for 2 h. The steady-state fluorescence emission spectra were recorded using an excitation wavelength of 600 nm. The decrease in the peak intensity with increasing protein concentration for DOPC–DOPG LUV was fitted using a sigmoidal Hill equation

$$F = F_0 + \frac{(F_e - F_0)x^n}{(x^n + K^n)} \quad (2)$$

where F and F_0 refer to the fluorescence intensities of DiI C-18 in the presence and absence of the protein, respectively. F_e denotes the minimum intensity in the presence of a saturating concentration of protein, and K is the equilibrium dissociation constant of the lipid–protein complex. n is the Hill coefficient, which measures the cooperativity of binding, and x is the concentration of the protein. A PTI fluorimeter (Photon Technology International, Inc.) and a cuvette with a 1 cm path length were used for the fluorescence measurements.

2.6. Membrane Permeabilization Assay of Lipid Vesicles. Calcein-loaded LUVs, prepared in 20 mM sodium phosphate buffer, were separated from non-encapsulated free calcein by gel filtration on a Sephadex G-75 column (Sigma) using an elution buffer of 10 mM MOPS, 150 mM NaCl, and 5 mM EDTA (pH 7.4), and lipid concentrations were estimated by complexation with ammonium ferro-thiocyanate.¹⁷ Fluorescence was measured at room temperature (25 °C) in a PTI spectrofluorometer using 1 cm path length cuvettes. The excitation wavelength was 490 nm, and emission was set at 520 nm. Excitation and emission slits with a nominal bandpass of 3 and 5 nm were used, respectively. The high concentration (10 mM) of the entrapped calcein led to self-quenching of its fluorescence, resulting in low fluorescence intensity of the vesicles (I_B). The fluorescence intensity (I_F) was monitored upon addition of proteins into calcein-loaded vesicles. The enhancement of fluorescence due to release of calcein from the LUV is a measure of the extent of vesicle permeabilization. The experiments were normalized relative to the total fluorescence intensity (I_T) corresponding to the total release of calcein after complete disruption of all of the vesicles by addition of Triton X-100 (2% v/v). The percentage of calcein release in the presence of KMP-11 was calculated using the following equation¹⁸

$$\text{percentage of release} = \frac{(I_F - I_B)}{(I_T - I_B)} \times 100 \quad (3)$$

where I_F and I_B are the fluorescence intensities after and before protein addition. I_T denotes the fluorescence intensity after addition of Triton X-100. It is important to mention that the resultant osmotic stress of LUV might influence the membrane permeability. We used the same buffer concentration (i.e., same osmolarity) to prepare calcein-loaded vesicles and the solution outside the vesicles. As there is no concentration gradient in the interior and exterior of the vesicles, the osmotic stress is not expected to develop.

2.7. Preparation of GUV. GUVs were prepared in 0.1 M sucrose in 1 mM *N*-(2-hydroxyethyl)piperazine-*N'*-ethanesulfonic acid (HEPES) (pH 7.4) buffer using electroformation, as described by Pott et al.¹⁹ Briefly, 20 μ L of a 1 mM lipid solution in chloroform was spread onto the surfaces of two conductive indium tin oxide (ITO) glasses. The coated lipid solutions were then allowed to dry overnight in a closed chamber containing saturated solution of NaCl. This is to avoid complete drying of the droplets. The hydration of these droplets

facilitates the electroformation process. The electroformation chamber was prepared using a Teflon spacer of \sim 2 mm thickness. This electroswelling chamber was filled with 0.1 M sucrose solution, and an alternating voltage of 1.5 V and frequency of 15 Hz were applied for 2 h at room temperature (22–25 °C). The vesicle solution was then carefully transferred to an Eppendorf vial and kept at rest at 4 °C before use. The average diameter of the GUV obtained was 10–100 μ m. GUVs were diluted in 0.1 M glucose, prepared in 1 mM HEPES (pH 7.4), for observation. A typical observation experiment, using an inverted microscope, was made in an observation chamber by mixing 30 μ L of the GUV solution with 100 μ L of a 0.1 M glucose solution. The slight density difference between the inner and outer solutions drives the vesicles to settle at the bottom of the slide and provides better contrast while observing under phase contrast.

2.8. Phase Contrast Optical Microscopy. For the microscopy experiment, different concentrations of KMP-11 dissolved in the glucose solution prepared in 1 mM HEPES buffer (pH 7.4) were added to the vesicle solution. The final concentrations of KMP-11 in the observation chamber were chosen to be 5, 10, and 20 μ M. Phase contrast microscopy was performed using an inverted microscope (DMI8) from Leica (Wetzlar, Germany). The observation chamber consisted of a glass slide with rubber spacers. The chamber was then closed immediately for observation under a phase contrast microscope after placing the samples. Although we could not determine the exact KMP-11/lipid molar ratio, a rough estimate was obtained. For example, introducing 10 μ L of diluted GUV solution (\sim 0.1 mM) to the chamber containing 100 μ L of 1 μ M KMP-11 solution, we estimated that the final KMP-11/lipid (molar ratio) would become 0.1 (number of moles = molar concentration \times volume in liters). The response of individual GUV when exposed to the protein solution was continuously recorded with time using a CCD camera. Images were analyzed using an image analysis software, ImageJ, as shown in Figure 2. A straight line was drawn across the GUV to obtain an intensity

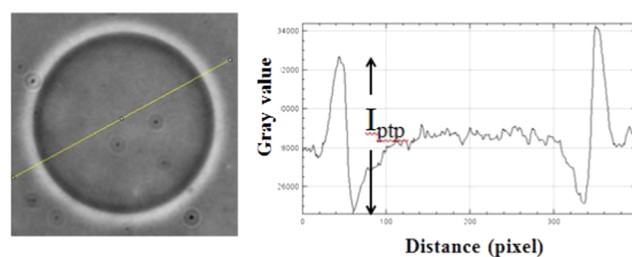


Figure 2. Estimation of the peak-to-peak intensity (gray value), I_{ptp} , across the halo region of the phase contrast micrograph of GUV.

profile. The peak-to-peak intensity (I_{ptp}) across the halo region was calculated. Average I_{ptp} was obtained from several line profiles across the GUV. The time in seconds versus I_{ptp} was plotted to observe any significant change in the intensity profile of the GUV.

2.9. Fluorescence Emission of Laurdan: Generalized Polarization (GP). Laurdan is a widely used environment-sensitive probe. Laurdan is introduced in the membrane to monitor the change in membrane rigidity with increasing cholesterol content. Laurdan excitation and emission spectra are extremely sensitive to the local environments, such as solvent polarity and the phase state of lipids. In the gel phase (more rigid membrane), it shows a blue emission (440 nm), but the spectrum gets red shifted (490 nm) when the membrane is in a fluid phase (flexible membrane). The amount of water penetrating into the membranes determines the extent of the red shift. This feature can be used to identify the transition from cholesterol-poor liquid-disordered (Ld) to cholesterol-rich liquid-ordered (Lo) phases. The phase state of the membrane can be obtained from the generalized polarization (GP) defined as

$$\text{GP} = (I_{440} - I_{490}) / (I_{440} + I_{490}) \quad (4)$$

where I_{440} (I_{490}) is the intensity of the blue (red shifted) emission.

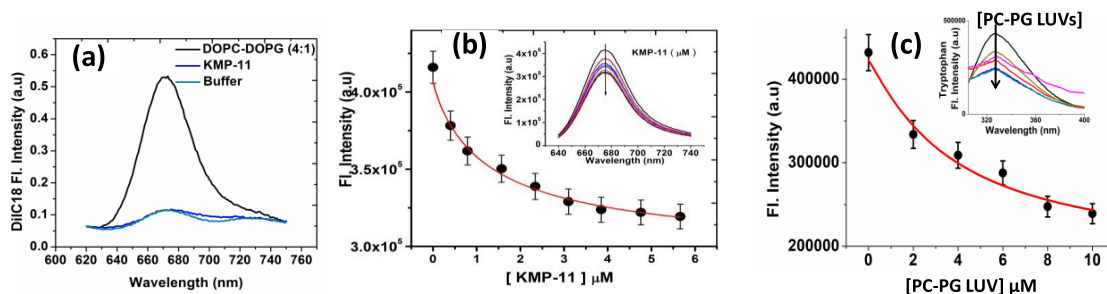


Figure 3. (a) Fluorescence emission spectra of DiI C-18, showing significant intensity in the presence of LUV, while fluorescence is very low or absent when the dye is present in aqueous buffer or buffer containing KMP-11 only. (b) Shows the decrease in fluorescence intensities of DiI C-18 (present in solution of LUV) with increasing concentration of KMP-11. The solid red line is the fit using the Hill equation. The inset shows the fluorescence spectrum for increasing concentrations of KMP-11 indicated by an arrow. (c) Change in tryptophan emission with increasing concentration of DOPC–DOPG (4:1) LUVs. In this experiment, a single tryptophan mutant (Y48W) was used. The inset in (c) shows the fluorescence emission spectra with increasing LUV concentrations.

3. RESULTS AND DISCUSSION

3.1. Interaction of KMP-11 with Phospholipid LUV.

The membrane-specific dye DiI C-18 is widely used to monitor the large-scale inhomogeneity on the surface of a living cell, including rafts and protein organization in artificial membranes.^{20,21} We used here a previously reported fluorescence assay using DiI C-18 to investigate the interaction of KMP-11 with DOPC–DOPG LUV.³ In the presence of membrane, DiI C-18 showed strong fluorescence at $\lambda_{em} = 675$ nm ($\lambda_{ex} = 600$ nm), while in aqueous buffer or a buffer containing KMP-11, its fluorescence was very low or absent (Figure 3a). Figure 3b shows that the fluorescence of DiI C-18 (in the presence of LUV) decreased with increasing KMP-11 concentrations. This happened because of the protein–lipid association. The average lifetime of the dye (in the presence of the membrane) decreases as we add the protein, indicating a significant contribution of dynamic quenching, as reported in our previous study.³ The change in relaxation behavior in the excited state of DiI C-18 could be due to an alteration of hydration dynamics at the membrane–solvent interface as well as due to the change in translational diffusion of fluorophore. In addition to these processes, we cannot eliminate the possibility of expulsion of DiI C-18 due to adsorption of KMP-11, which could also result in the decrease in fluorescence. We fitted the fluorescence decrease with protein concentration using a standard Hill equation (eq 2) and determined the values of binding constant (K) and cooperative index (n). The K value of KMP-11 was found to be $(2.46 \pm 0.15) \times 10^5$ M⁻¹, which was consistent with the results obtained in our earlier study with LUV containing pure DOPC.³ Unlike the binding of KMP-11 with DOPC, we found non-cooperative binding of KMP-11 with PC-PG, as the cooperative index (n) was found to be ~ 1 .

We complemented the above DiI C-18 binding experiments using steady-state fluorescence measurements. For this, we used a single tryptophan mutant of KMP-11 (Y48W), as wild-type KMP-11 does not contain any tryptophan residue in its sequence. This single tryptophan mutant (Y48W) showed similar secondary conformation to that of wild-type KMP-11, and the tryptophan residue was found to be fully buried inside the hydrophobic core region.^{22,23} Y48W showed maximum intrinsic fluorescence intensity at wavelength 327 nm. The addition of DOPC–DOPG LUVs significantly decreased the fluorescence intensity of tryptophan (Figure 3c). The fluorescence assay of the Trp residue shows similar binding

affinity to that obtained from DiI C-18. The binding constant obtained from the Trp assay ($K = 2.64 \times 10^5$ M⁻¹) is in agreement with that obtained from the DiI C-18 assay (2.46×10^5 M⁻¹), confirming protein binding with the membrane.

To obtain further insights into the protein–lipid interactions, we used ζ -potential and hydrodynamic radius measurements. The ζ -potential is a good approximation to the surface potential at moderate electrolyte concentration. As both protein and the membrane were charged, the binding between the protein and lipid was expected to change the value of ζ -potential. In addition, the binding might also increase the hydrodynamic radius. However, mild aggregation due to the lipid–protein interaction could not be ruled out. Figure 4a,b

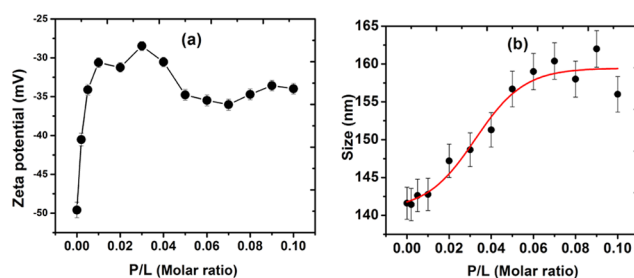


Figure 4. (a) Variation of ζ -potential of LUV made from a PC/PG (4:1) mixture with increasing protein-to-lipid (P/L) ratio. (b) Average hydrodynamic radius of the LUV with increasing P/L obtained from the DLS measurement.

shows the variation of ζ -potential and hydrodynamic radius with different protein-to-lipid (P/L) ratios. It was interesting to note that the change of these two parameters (ζ -potential and hydrodynamic radius) did not seem to match very well, although they were expected to represent the same event (KMP-11–LUV interaction). While the change in hydrodynamic radius was somewhat slow occurring in one step, ζ -potential variation had two steps. The first step was a rapid increase (occurring within P/L ~ 0.02), which was followed by a slow decrease. While any mechanistic understanding of the early rapid increase in ζ -potential is not available, we speculate that this is probably a rapid reorganization of the protein–lipid binding interface or the water environment. To understand the behavior of ζ -potential and to obtain insights into the binding phenomenon and protein activity, it is now important to investigate the charge distribution of the amino acid residues of the entire protein.

3.2. Charge Distribution of the Protein KMP-11. KMP-11 possesses a negative charge (-1.7) at physiological pH as determined by the protein calculator v3.4 server (<http://protecalc.sourceforge.net/>). The association of negatively charged protein with anionic membranes was thus intriguing. We speculate that a local positively charged region might be able to initiate the binding process, which would be later facilitated by other factors, like nonpolar interactions. We used EMBOSS software (Figure S3, Supporting Information) to determine the local cationic regions in the sequence. As shown in Figure S3, two stretches of the positively charged sequence could be identified: one between residues 10 and 30 and the other between residues 40 and 70. Subsequently, we resorted to the theoretical approach to spot active regions of KMP-11 and look for the antimicrobial sequence stretch or domain (see the Supporting Information for details). We found out that KMP-11 contains prominent antimicrobial propensity at the region 60–80 of its sequence (Figure S1), and this sequence stretch (with microbacterial property) was close to one of the two positively charged regions. Since pore formation is the prerequisite of the antibacterial property of a peptide stretch, we hypothesize that an efficient binding through these local positive regions may trigger the pore formation property of the protein.

3.3. Formation of Transmembrane Pores Induced by KMP-11. **3.3.1. KMP-11 Induced Leakage in Phospholipid Membrane.** We then studied experimentally the ability of KMP-11 to form pores by measuring the fluorescence intensity of calcein-loaded LUV with time. Figure 5 shows the

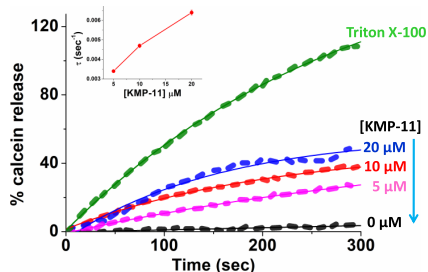


Figure 5. Calcein release assay showing the leakage of entrapped calcein from the LUV composed of PC/PG (4:1). This experiment has been performed using three different concentrations of KMP-11. The rate constant of calcein for three different protein concentrations is shown in the inset of the figure. The typical lipid concentration was taken as $20 \mu\text{M}$.

enhancement of fluorescence intensity over time at three different concentrations of KMP-11, indicating the release of entrapped dye from the vesicles. Such an increase in intensity was attributed to the formation of transmembrane pores.²⁴ It is important to mention that fluorescence intensity did not increase in the absence of KMP-11 (Figure 5).

This result clearly indicated that KMP-11 induced pores in the membrane, through which calceins were released. The pore size must be larger than the size of the calcein molecules enabling their translocation from the interior of the vesicle through pores. We found that the kinetics of pore formation was dependent on protein concentration (Figure 5, inset). The rate of calcein release was determined by fitting the data using an exponential rate equation, the variation of which with protein concentration is shown in the inset of Figure 5. The growth rate was found to be $\sim 6.4 \times 10^{-3} \text{ s}^{-1}$ when calcein-loaded vesicles were exposed to $20 \mu\text{M}$ and decreased with reducing protein concentration. Unlike the antimicrobial peptide melittin, showing the pore formation in the DOPC membrane,²⁵ we found that KMP-11 exhibited a higher rate of calcein release in DOPC LUV containing DOPG (Figure S4). This result suggested a significant role of anionic lipids (DOPG) in pore formation. This is indeed the requirement of many antimicrobial peptides where they only target negatively charged membranes and remain inert to the neutral phospholipids.^{26,27} It may be noted that a previous report by Yeung et al. indeed has shown that the negative surface charge of the inner leaflet of the plasma membrane determines the targeting of proteins with a cationic domain.¹⁵ Therefore, the negatively charged surface of macrophage may be required for targeting the immunogenic protein KMP-11, which eventually forms pores to facilitate the internalization of leishmania parasite.

3.3.2. KMP-11 Induced Pore Formation as Evidenced from the Phase Contrast Micrographs of GUV. As KMP-11 showed the evidence of strong binding with the membrane, especially with anionic vesicles, and has an antimicrobial sequence, it would be interesting to monitor directly the formation of pores using optical microscopy. Such an experiment would further validate the pore formation hypothesis and complement the results obtained from calcein release experiments. For this purpose, we explored phase contrast microscopy of GUVs exposed to protein solution. In this method, any change in the morphology of GUV can be directly visualized without introducing the fluorescence probe. Therefore, the issue of alteration of membrane properties or the protein–membrane

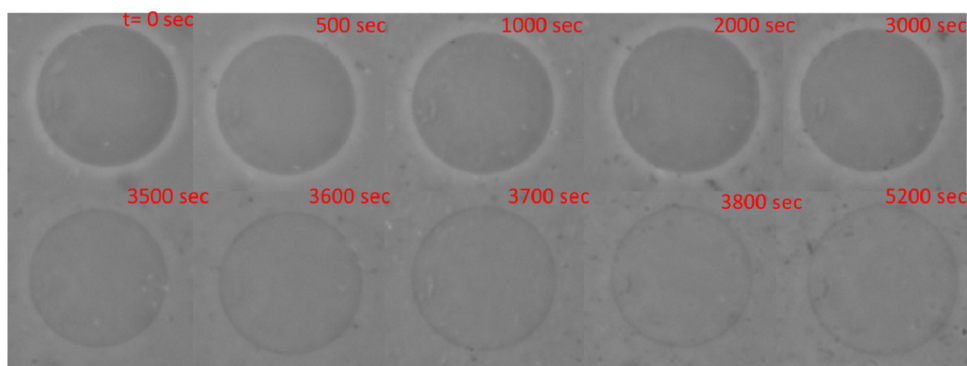


Figure 6. Phase contrast images of GUVs composed of DOPC–DOPG (4:1), which are exposed to $20 \mu\text{M}$ KMP-11. The protein-to-lipid (P/L) ratio ~ 0.02 . The diameter of the vesicle is $\sim 34 \mu\text{m}$.

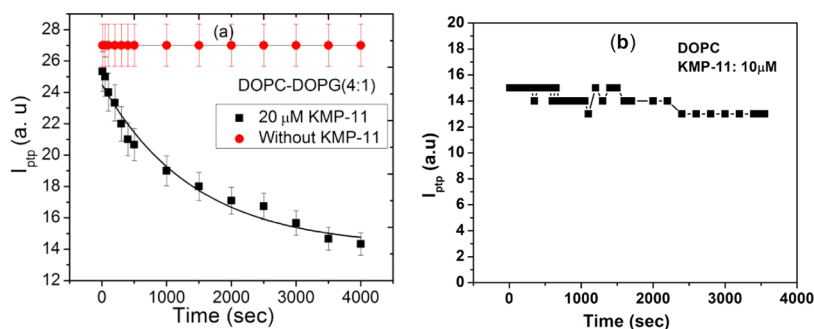


Figure 7. (a) Decay of I_{ptp} (peak-to-peak intensity) with time for DOPC–DOPG and (b) DOPC GUVs. The solid line represents the fit, which was obtained from a single exponential decay. The decay rate constant (τ) was found to be $(0.7 \pm 0.06) \times 10^{-3} \text{ s}^{-1}$. For comparison, red circles in (a) have been obtained from GUV without KMP-11.

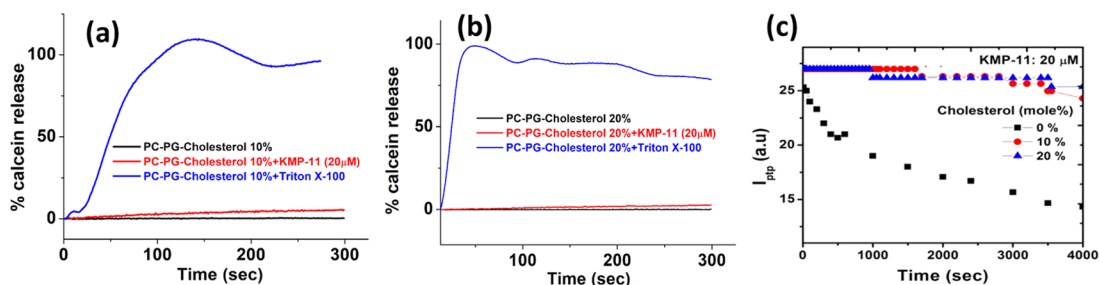


Figure 8. Calcein release assay showing the leakage of entrapped calcein from the LUV composed of PC/PG (4:1) at (a) 10 mol % and (b) 20 mol % cholesterol. These experiments have been performed at 20 μ M concentration of KMP-11, and the typical lipid concentration was kept as 20 μ M. (c) Peak-to-peak intensity across the halo regions at two different cholesterol concentrations, indicated in the figure legend. GUV containing cholesterol does not show any significant leakage in microscopy experiments. For comparison, we have again shown the decay curve for 0 mol % cholesterol.

interaction due to the presence of fluorophores can be avoided. We could observe GUV with a good contrast in the halo region, as vesicles are prepared in a sucrose solution and diluted with glucose solution. GUV, made from DOPC and mixtures of DOPC with DOPG, were observed with three different protein concentrations (5, 10, and 20 μ M). GUVs were prepared in a 100 mM sucrose solution and diluted with a 100 mM glucose solution. Identical concentrations of glucose and sucrose solutions were used to eliminate any resultant osmotic stress. Figure 6 shows the time sequence of phase contrast images of GUV exposed to 20 μ M KMP-11 solutions. GUV images for 5 and 10 μ M concentrations of KMP-11 are shown in Figure S5 (Supporting Information). The halo region in the GUV image was formed due to the difference in contrast between the interior and exterior of GUV. Once the pores were formed on the membranes, we would expect leakage of internal fluid through the pores. As a result, halo regions were expected to disappear with time and GUV should look similar to that without diluting in glucose. The change in the difference of the gray value (I_{ptp}) of the halo region with time for DOPC–DOPG (4:1) GUV indicated exchange of fluid between the interior and exterior of the GUV, leading to the loss of contrast.

Figure 7a shows that I_{ptp} decreased until GUV, in the presence of KMP-11, completely lost its contrast in the halo region. The analysis of phase contrast images to predict the pore formation has not been described in any of the earlier studies. It is important to mention that aqueous dispersion of GUVs in the absence of KMP-11 was found to be very stable and did not show any variation of I_{ptp} (Figure 7, red circle). In addition, GUVs prepared from only DOPC did not show any significant decrease of I_{ptp} when exposed to KMP-11 (Figure

7b). This result clearly indicated the importance of the negatively charged membrane in the pore formation, which was found to be consistent with the results obtained from calcein release experiments.

The prepared GUVs were found to show heterogeneity in terms of the time they take to start the pore formation process. As a result, we could not precisely determine the time point that initiates pore formation for a particular GUV. In addition, we have also experienced some heterogeneity due to GUV size variations. As a result, the presented data represented the average response of several (at least three) GUVs (Figure S6). Nevertheless, we could unambiguously determine the behavior of the rate constants for different protein concentrations. GUV exposed to 5 μ M KMP-11 took longer time to form pores, and complete disappearance of the halo region was obtained at a much higher time scale compared to one exposed to 10–20 μ M KMP-11 (Figure S7, Supporting Information). The change in I_{ptp} with time was fit to a single exponential decay function to obtain the time constant (τ) (Figure 7a). The rate constants for two different concentrations 10 and 20 μ M were found to be $1.2 \times 10^{-3} \text{ s}^{-1}$ (Figure S7) and $0.7 \times 10^{-3} \text{ s}^{-1}$ (Figure 7a), respectively. For 5 μ M KMP-11, we have not observed significant decrease in I_{ptp} with time. The growth rate ($6.4 \times 10^{-3} \text{ s}^{-1}$) of the calcein release experiment was consistent with the decay rate obtained from the analysis of phase contrast images. This differences of the rate constants obtained from two different experimental techniques could arise due to the difference in vesicle size, as well as the intrinsic concentration of KMP-11 in the vicinity of the membrane.

3.3.3. Effect of Cholesterol on the Pore Formation. Previous studies have already shown that the presence of cholesterol strongly affects the process of internalization of

parasite into host macrophages.^{11,14} Therefore, it would be interesting to know the role of cholesterol in the pore-forming activity of a protein. Figure 8a,b shows the percentage of calcein release from the LUV containing different mol % of cholesterol when exposed to 20 μ M KMP-11. The percentage of calcein release, which was measured by the increase in fluorescence intensity, decreased significantly with increasing cholesterol concentration. Further, as a control experiment, we found no calcein release in the absence of KMP-11 (Figure 8a,b) and 100% leakage was found when LUVs were treated with triton X-100, and this 100% leakage was used to calculate the percentage of dye leakage from the LUVs at different cholesterol percentages. To complement this leakage assay, we also performed the GUV assay to find out the pore-forming activity of KMP-11 in the presence of different molar contents of membrane cholesterol. The phase contrast microscopy experiment on GUV, containing 10 and 20 mol % cholesterol, did not seem to show any significant decay of the I_{ptp} across the halo region (Figure 8c). This result indicated that there was no significant leakage or exchange of fluid in the presence of cholesterol, suggesting that incorporation of cholesterol tends to inhibit KMP-11-induced pore formation.

The driving force of pore formation is the membrane tension (σ), whereas line tension (γ) around the pore determines the stability of the pores. Therefore, energetics of the pore of radius r would be given by $E_{\text{pore}} = 2\pi r\gamma - \pi r^2\sigma$. The intrinsic scale of membrane tension is determined by the spontaneous curvature and bending modulus of the membranes, whereas mechanical tension is governed by its stretching modulus.²⁸ We can argue that the role of KMP-11 would be to create stress, which is equivalent to membrane tension required for the formation of pore. In addition, these elastic parameters would change for a membrane containing cholesterol. However, it is known from the previous literature that the effect of cholesterol on the membrane tension is not universal; rather, it depends on the specific architecture of the lipid building the membrane.^{29,30} Various experimental techniques, such as fluctuation spectroscopy, micropipette aspiration, electrodeformation, etc., are insensitive to give change in the stiffness of a membrane made from a DOPC–cholesterol mixture.³¹ However, it is well known that increase in cholesterol content leads to a liquid-ordered (Lo) phase (cholesterol-rich), which has higher rigidity than that of the cholesterol-poor liquid-disordered (Ld) phase.³² To validate this, we investigated the fluorescence emission of an environment-sensitive probe Laurdan. At room temperature, DOPC–DOPG (4:1) LUVs remain in the Ld phase, which is confirmed by the emission maximum at 490 nm (Figure 9). It is clearly evident from Figure 9 that emission spectra get blue-shifted with increasing cholesterol concentrations. Further, GP of Laurdan increases with the increasing cholesterol content in the vesicles. These results indicate that membrane rigidity increases with cholesterol. Further, it has been found in our previous study that the association constant of wild-type KMP-11 decreases with increasing cholesterol concentration.³ Such a change in the elastic property of the membrane and decreases in the binding affinity of KMP-11 in the presence of membrane cholesterol may not facilitate the pore formation induced by KMP-11.

3.4. Conjecture on the Mechanism of Parasite Entry and Implications in Leishmaniasis. The present study describes the pore-forming activity of the protein KMP-11 in model membranes in view of the understanding of the host–

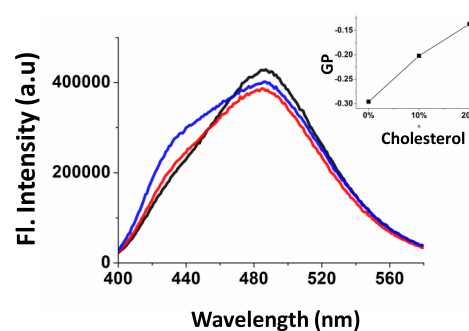


Figure 9. Laurdan emission spectra of DOPC–DOPG (4:1) LUVs containing 0 mol % (black), 10 mol % (blue), and 20 mol % (red) cholesterol. The inset shows the generalized polarization (GP) values of Laurdan obtained from 0, 10, and 20 mol % cholesterol.

pathogen relationship in the context of leishmaniasis. While it is only an *in vitro* study and the actual disease scenario is expected to be complex, a simplified understanding of the parasite entry process (Figure 10) could be hypothesized based on our present results. As reported in our previous study, an abundant immunogenic membrane protein, KMP-11, expressed on the surface of parasite plays a vital role in modulating membrane properties when binds to the macrophage membrane.³ Therefore, this protein helps in the internalization of parasite for productive infection. In the present study, we indeed found an efficient binding of KMP-11 onto the membrane, which facilitates pore formation. We believe that this process may eventually help the parasite to enter into the host macrophage (Figure 10). A similar mechanism was found in the case of an antimicrobial peptide.³³ It is established that parasites can translocate via transmembrane pores for their survival.

It has been reported that cholesterol in the host macrophage plays a vital role in leishmania infection.³⁴ Therefore, interaction of KMP-11 with the model membranes is expected to alter in the presence of cholesterol. We indeed found that cholesterol affects the pore-forming ability of KMP-11 as found in both calcein release and optical microscopy experiments. Further study is required to understand the cholesterol connection in leishmaniasis.

4. CONCLUSIONS

A systematic investigation on the interaction of KMP-11 with anionic phospholipid membranes reveals, for the first time, that KMP-11 is able to induce pores in the anionic phospholipid membrane. Both the calcein release fluorescence assay of large unilamellar vesicles and phase contrast microscopy of giant unilamellar vesicles have been employed to show the leakage of internal fluid and exchange of fluids, suggesting the formation of transmembrane pores. The rate of increase in the fluorescence intensity due to calcein release is consistent with the rate of decay in intensity across the halo region of phase contrast micrographs of GUV. We also explored the pore-forming activity of KMP-11 on the membrane containing cholesterol. No significant growth of intensity in the calcein release experiment on LUV containing 10–20 mol % cholesterol suggests that cholesterol inhibits pore formation in membranes. Further studies on the interaction of KMP-11 with the negatively charged membranes using fluorescence spectroscopy and ζ -potential revealed that KMP-11 has a strong affinity to the membrane. The nature of decay of the

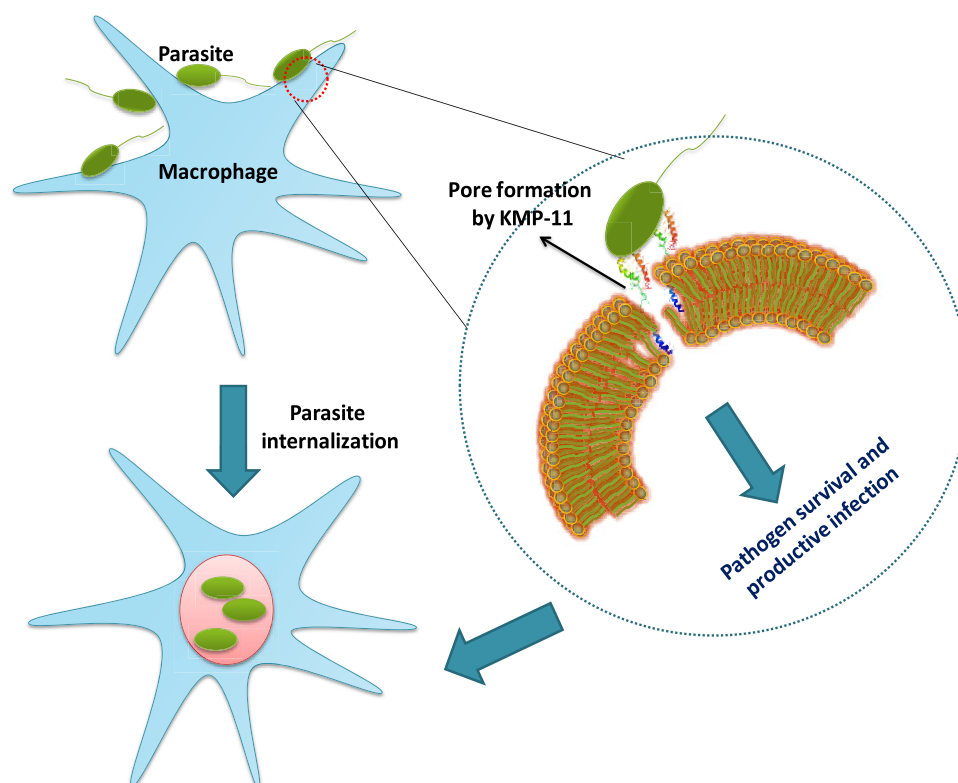


Figure 10. Schematic diagram of the infection mechanism via transmembrane pore formation induced by KMP-11.

fluorescence intensity of DiI C-18 and decrease in the negative value of ζ -potential suggest the non-cooperative binding of proteins. The binding constant obtained from fluorescence (DiI C-18) decay is in agreement with that obtained earlier in the case of the DOPC membrane. Based on our results, we hypothesize that the strong interaction of KMP-11 and its pore-forming activity toward an anionic membrane may have implications in the process of internalization of leishmania parasite into macrophages for parasite survival and replication.

■ ASSOCIATED CONTENT

SI Supporting Information

The Supporting Information is available free of charge at <https://pubs.acs.org/doi/10.1021/acs.langmuir.9b03816>.

Definition and plot of antimicrobial index; comparison of sequences of KMP-11 and APOA-1 protein; charge distribution of KMP-11; calcein release of LUV, GUV images containing KMP-11; intensity decay of the halo region of phase contrast images of GUV (PDF)

■ AUTHOR INFORMATION

Corresponding Authors

Krishnananda Chattopadhyay – Structural Biology & Bio-Informatics Division, CSIR—Indian Institute of Chemical Biology, Kolkata 700032, India; orcid.org/0000-0002-1449-8909; Email: krishn@iicb.res.in

Sanat Karmakar – Soft Matter and Biophysics Laboratory, Department of Physics, Jadavpur University, Kolkata 700032, India; orcid.org/0000-0002-2421-9475; Email: sanat.karmakar@jadavpuruniversity.in

Authors

Animesh Halder – Soft Matter and Biophysics Laboratory, Department of Physics, Jadavpur University, Kolkata 700032, India

Achinta Sannigrahi – Structural Biology & Bio-Informatics Division, CSIR—Indian Institute of Chemical Biology, Kolkata 700032, India

Nayan De – Structural Biology & Bio-Informatics Division, CSIR—Indian Institute of Chemical Biology, Kolkata 700032, India

Complete contact information is available at:

<https://pubs.acs.org/doi/10.1021/acs.langmuir.9b03816>

Author Contributions

[§]A.H., A.S., and N.D. contributed equally to this work.

Notes

The authors declare no competing financial interest.

■ ACKNOWLEDGMENTS

This work was funded by the Department of Biotechnology (DBT), Government of India (BT/PR8475/BRB/10/1248/2013). A.H. is grateful to UGC for providing research fellowship.

■ REFERENCES

- (1) Chulay, J. D.; Bryceson, A. D. Quantitation of amastigotes of *Leishmania donovani* in smears of splenic aspirates from patients with visceral leishmaniasis. *Am. J. Trop. Med. Hyg.* **1983**, *32*, 475–479.
- (2) Lambris, J. D.; Ricklin, D.; Geisbrecht, B. V. Complement evasion by human pathogens. *Nat. Rev. Microbiol.* **2008**, *6*, 132.
- (3) Sannigrahi, A.; Maity, P.; Karmakar, S.; Chattopadhyay, K. Interaction of KMP-11 with phospholipid membranes and its implications in leishmaniasis: effects of single tryptophan mutations and cholesterol. *J. Phys. Chem. B* **2017**, *121*, 1824–1834.

- (4) Spector, A. A.; Yorek, M. A. Membrane lipid composition and cellular function. *J. Lipid Res.* **1985**, *26*, 1015–1035.
- (5) Sannigrahi, A.; Nandi, I.; Chall, S.; Jawed, J. J.; Halder, A.; Majumdar, S.; Karmakar, S.; Chattopadhyay, K. Conformational switch driven membrane pore formation by Mycobacterium secretory protein MPT63 induces macrophage cell death. *ACS Chem. Biol.* **2019**, *14*, 1601–1610.
- (6) Panchal, R.; Smart, M.; Bowser, D.; Williams, D.; Petrou, S. Pore-forming proteins and their application in biotechnology. *Curr. Pharm. Biotechnol.* **2002**, *3*, 99–115.
- (7) Evavold, C. L.; Ruan, J.; Tan, Y.; Xia, S.; Wu, H.; Kagan, J. C. The pore-forming protein gasdermin D regulates interleukin-1 secretion from living macrophages. *Immunity* **2018**, *48*, 35.e6–44.e6.
- (8) Los, F. C.; Randis, T. M.; Aroian, R. V.; Ratner, A. J. Role of pore-forming toxins in bacterial infectious diseases. *Microbiol. Mol. Biol. Rev.* **2013**, *77*, 173–207.
- (9) de Mendonça, S. C. F.; Cysne-Finkelstein, L.; de Souza Matos, D. C. Kinetoplastid membrane protein-11 as a vaccine candidate and a virulence factor in *Leishmania*. *Front. Immunol.* **2015**, *6*, 524.
- (10) Mahley, R. W. Apolipoprotein E: cholesterol transport protein with expanding role in cell biology. *Science* **1988**, *240*, 622–630.
- (11) Pucadyil, T. J.; Tewary, P.; Madhubala, R.; Chattopadhyay, A. Cholesterol is required for *Leishmania donovani* infection: implications in leishmaniasis. *Mol. Biochem. Parasitol.* **2004**, *133*, 145–152.
- (12) Kumar, G. A.; Roy, S.; Jafurulla, M.; Mandal, C.; Chattopadhyay, A. Statin-induced chronic cholesterol depletion inhibits *Leishmania donovani* infection: relevance of optimum host membrane cholesterol. *Biochim. Biophys. Acta, Biomembr.* **2016**, *1858*, 2088–2096.
- (13) Barman, H.; Walch, M.; Latinovic-Golic, S.; Dumrese, C.; Dolder, M.; Groscurth, P.; Ziegler, U. Cholesterol in negatively charged lipid bilayers modulates the effect of the antimicrobial protein granulysin. *J. Membr. Biol.* **2006**, *212*, 29–39.
- (14) Ghosh, J.; Guha, R.; Das, S.; Roy, S. Liposomal cholesterol delivery activates the macrophage innate immune arm to facilitate intracellular *Leishmania donovani* killing. *Infect. Immun.* **2014**, *82*, 607–617.
- (15) Yeung, T.; Gilbert, G. E.; Shi, J.; Silvius, J.; Kapus, A.; Grinstein, S. Membrane phosphatidylserine regulates surface charge and protein localization. *Science* **2008**, *319*, 210–213.
- (16) Maity, P.; Saha, B.; Kumar, G. S.; Karmakar, S. Binding of monovalent alkali metal ions with negatively charged phospholipid membranes. *Biochim. Biophys. Acta, Biomembr.* **2016**, *1858*, 706–714.
- (17) Stewart, J. C. Colorimetric determination of phospholipids with ammonium ferrothiocyanate. *Anal. Biochem.* **1980**, *104*, 10–14.
- (18) Benachir, T.; Monette, M.; Grenier, J.; Lafleur, M. Melittin-induced leakage from phosphatidylcholine vesicles is modulated by cholesterol: a property used for membrane targeting. *Eur. Biophys. J.* **1997**, *25*, 201–210.
- (19) Pott, T.; Bouvrais, H.; Méléard, P. Giant unilamellar vesicle formation under physiologically relevant conditions. *Chem. Phys. Lipids* **2008**, *154*, 115–119.
- (20) Klymchenko, A. S.; Kreder, R. Fluorescent probes for lipid rafts: from model membranes to living cells. *Chem. Biol.* **2014**, *21*, 97–113.
- (21) Kahya, N. Protein–protein and protein–lipid interactions in domain-assembly: lessons from giant unilamellar vesicles. *Biochim. Biophys. Acta, Biomembr.* **2010**, *1798*, 1392–1398.
- (22) Sharma, S.; Sarkar, S.; Paul, S. S.; Roy, S.; Chattopadhyay, K. A small molecule chemical chaperone optimizes its unfolded state contraction and denaturant like properties. *Sci. Rep.* **2013**, *3*, No. 3525.
- (23) Sannigrahi, A.; Mullick, D.; Sanyal, D.; Sen, S.; Maulik, U.; Chattopadhyay, K. Effect of Ergosterol on the Binding of KMP-11 with Phospholipid Membranes: Implications in Leishmaniasis. *ACS Omega* **2019**, *4*, 5155–5164.
- (24) Belokoneva, O. S.; Satake, H.; Mal'tseva, E. L.; Pal'mina, N. P.; Villegas, E.; Nakajima, T.; Corzo, G. Pore formation of phospholipid membranes by the action of two hemolytic arachnid peptides of different size. *Biochim. Biophys. Acta, Biomembr.* **2004**, *1664*, 182–188.
- (25) Van Den Bogaart, G.; Guzmán, J. V.; Mika, J. T.; Poolman, B. On the mechanism of pore formation by melittin. *J. Biol. Chem.* **2008**, *283*, 33854–33857.
- (26) Karmakar, S.; Maity, P.; Halder, A. Charge-Driven Interaction of Antimicrobial Peptide NK-2 with Phospholipid Membranes. *ACS Omega* **2017**, *2*, 8859–8867.
- (27) Ostroumova, O. S.; Efimova, S. S.; Malev, V. V. Modifiers of membrane dipole potentials as tools for investigating ion channel formation and functioning. *Int. Rev. Cell Mol. Biol.* **2015**, *315*, 245–297.
- (28) Lipowsky, R. Coupling of bending and stretching deformations in vesicle membranes. *Adv. Colloid Interface Sci.* **2014**, *208*, 14–24.
- (29) Hissa, B.; Pontes, B.; Roma, P. M. S.; Alves, A. P.; Rocha, C. D.; Valverde, T. M.; Aguiar, P. H. N.; Almeida, F. P.; Guimarães, A. J.; Guatimosim, C.; et al. Membrane cholesterol removal changes mechanical properties of cells and induces secretion of a specific pool of lysosomes. *PLoS One* **2013**, *8*, No. e82988.
- (30) Dimova, R. Recent developments in the field of bending rigidity measurements on membranes. *Adv. Colloid Interface Sci.* **2014**, *208*, 225–234.
- (31) Gracià, R. S.; Bezlyepkina, N.; Knorr, R. L.; Lipowsky, R.; Dimova, R. Effect of cholesterol on the rigidity of saturated and unsaturated membranes: fluctuation and electrodeformation analysis of giant vesicles. *Soft Matter* **2010**, *6*, 1472–1482.
- (32) Tsai, W.-C.; Feigenson, G. W. Lowering line tension with high cholesterol content induces a transition from macroscopic to nanoscopic phase domains in model biomembranes. *Biochim. Biophys. Acta, Biomembr.* **2019**, *1861*, 478–485.
- (33) Kang, H.-K.; Kim, C.; Seo, C. H.; Park, Y. The therapeutic applications of antimicrobial peptides (AMPs): a patent review. *J. Microbiol.* **2017**, *55*, 1–12.
- (34) Semini, G.; Paape, D.; Paterou, A.; Schroeder, J.; Barrios-Llerena, M.; Aebischer, T. Changes to cholesterol trafficking in macrophages by *Leishmania* parasites infection. *MicrobiologyOpen* **2017**, *6*, No. e00469.



An evidence of pores in phospholipid membrane induced by an antimicrobial peptide NK-2

Animesh Halder, Sanat Karmakar*

Soft matter and Biophysics Laboratory, Department of Physics, Jadavpur University, 188, Raja S. C. Mullick Road, Kolkata 700032, India

ARTICLE INFO

Keywords:

Phospholipids
Biomembranes
Zeta potential
Antimicrobial peptide
NK-2

ABSTRACT

NK-2, a peptide derived from a cationic core region of NK-lysin, has emerged as a promising candidate for new antibiotics. In contrast to classical antibiotics, antimicrobial peptides target bacterial membranes and disintegrate the membrane by forming the transmembrane pores. However, complete understanding of the precise mechanisms of cellular apoptosis and molecular basis of membrane selectivity is still in dispute. In the present study, we have shown that NK-2 forms trans-membrane pores on negatively charged phospholipid membranes using phase contrast microscopy. As bacteria mimicking membranes, we have chosen large unilamellar vesicles (LUV) and giant unilamellar vesicles (GUV) composed of negatively charged phospholipid, dioleoyl phosphatidyl glycerol (DOPG) and neutral phospholipid, dioleoyl phosphatidylcholine (DOPC). Leakage of internal fluid of giant unilamellar vesicles (GUV), leading to decrease in intensity in the halo region of phase contrast micrographs, suggests the formation of transmembrane pores. No such reduction of intensity in the halo region of DOPC was observed, indicating, neutral vesicles does not exhibit pores. Rate constant reckoned from the decaying intensity in the halo region was found to be 0.007 s^{-1} . Further, significant interaction of NK-2 with anionic membranes has been envisaged from zeta potential and dynamic light scattering. Binding free energy and other interaction parameters have been delineated using theoretical ansatz. A proliferation of average size of anionic LUV on increasing NK-2 concentration indicates membrane-membrane interaction leading to peptide induced large aggregates of vesicles.

1. Introduction

Antimicrobial peptides (AMPs) are the unique and diverse group of molecules which are part of innate immune response found in all animal and human body [1]. They are the host defense peptides and work against invading pathogens, such as viruses, fungi, bacteria *etc.* [2,3]. AMPs are known to disrupt the bacterial membranes directly without interacting with any specific receptor [4]. AMPs commonly possess amphipathic structures and cationic in nature which strongly bind to the bacterial membranes. This results in a formation of trans-membrane pores which eventually rupture the essential cellular contents by disintegrating lipid organization [5]. There are several proposed mechanisms that AMP uses to destroy the cellular membrane (cell lysis) [6]. The essential and common feature of these mechanisms is the formation of trans-membrane pores [7]. Therefore, foremost study for an AMP would be to investigate the ability to form the transmembrane pores in order to gain insights into its antimicrobial activity. This motivates us to look at the pore forming activity of a promising peptide NK-2.

Bacterial membranes are usually negatively charged. Therefore, interaction of positively charged AMP with the bacterial membranes initiates with the electrostatic attraction. Besides charge, orientation of the peptide, the hydrophobicity index plays an important role in determining the antimicrobial activity [8,9]. Selectivity of the anionic membranes encourages us to use anionic lipid DOPG to prepare bacteria mimicking membranes [10]. The implications of AMP as a replacement of conventional antibiotics demands that, AMP should be inert to the phosphatidylcholine (PC) which is the major constituent of the eukaryotic cellular membrane. Earlier study indeed found that NK-2 does not interact significantly with PC membranes, but exhibit strong affinity with PG and PE membranes [9,11,12]. Ideally, one should use PE-PG mixture to mimic the composition of bacterial membrane. But unfortunately, such mixture does not form GUV. Therefore, as model system, we have taken PC/PG mixture.

NK-2 is the cationic (charge +10 at physiological pH) peptide with 27 residues derived from highest density positively charged core region of NK-lysin (residues K39–K65) [13]. The high positive charges within

* Corresponding author.

E-mail address: sanat.karmakar@jadavpuruniversity.in (S. Karmakar).

the NK-2 promote strong binding to the negatively charged membranes [11]. A variety of experimental and simulation studies have surmised the formation of transmembrane pores as the prerequisite of antimicrobial activity. For example, fluorescence leakage experiments of Magainin 2 [14], optical microscopy along with micropipette aspiration of giant unilamellar vesicles [15] in the presence of Melittin clearly show the evidence of pores. The formation of transmembrane pores is the consequence of increase in membrane tension induced by AMP leading to a membrane thinning effect [16]. Recently the stretch activated stable pores are reported in Magainin-2 [17]. The kinetic process involving the interaction of AMP with the membrane can directly be visualized in giant unilamellar vesicles (GUV). Previous studies have shown that the onset of activity of pore formation occurs above a threshold lipid to peptide ratio (~ 70 for melittin) [15,16]. This threshold seems to be different for different peptide.

Previous study of NK-2 by Olak et al. [18], have shown that NK-2 adopts unordered random coiled conformation when dissolved in different aqueous solutions. However, it adopts α helical conformation in the presence of negatively charged amphiphiles. The electrostatic interaction between positively charged residues of the peptide with the negatively charged head group of amphiphiles are responsible for the conformational transition from random coil to helix [18]. As already established that the NK-2 can be used as therapeutics to kill malaria parasite *Plasmodium falciparum* [19]. It also shows activity against *Escherichia coli* [20] and preferentially kills cancer cells [9]. Further, low toxicity towards human cells [21] is a great advantage for the development of antibiotics. Therefore, NK-2 derived from the natural killer cell NK-lysin is expected to have a potential for therapeutic applications for the replacement of conventional antibiotics.

Different AMP seems to follow different pathways to create transmembrane pores. Therefore, in spite of a large number of attempts, mechanism of trans-membrane pore formation is still poorly understood. Although, several mechanisms such as 'barrel-stave', 'carpet' or 'toroidal-pore' have been proposed in the literatures [4], detailed understanding the adverse effect of AMP on bacterial membranes needs to be elucidated. Molecular electroporation was proposed as the mechanism of membrane pore formation, induced by NK-lysin. [6]. Recent computer simulations have successfully employed in order to understand and gain insights into the underlying mechanics of antimicrobial activity [22,23]. A comparison between the free energy transfer of NK-2 from DOPC to DOPG (-56 KJ/mol) and from DOPC to DOPE (-10 KJ/mol) suggested the binding affinity of NK-2 in the order DOPC < DOPE < DOPG [22]. This finding was also verified by our recent experimental findings [11]. Such trend of binding affinity also indicates high selectivity of prokaryotic than Eukaryotic cells. Although the major contribution to the free energy of interaction is enthalpic, the significant entropic contribution arises due to release of counter ions as well as orientation of peptides as evidenced from the decrease in area per molecules and increase in the order parameter of hydrocarbon chains [23].

In our previous study, we have discussed interaction of NK-2 with lipid membranes of different composition in view of understanding the effect of composition on the antimicrobial activity [11]. Although it has been known from the previous studies that the NK-2 interact strongly with the negatively charged membrane and can be a potential candidate for the replacement of conventional antibiotics, there is no direct evidence of pore formation in this system. Therefore, the present study attempts to observe membrane permeabilization due to pores on the membrane induced by NK-2 using optical phase contrast microscopy. We have chosen model systems, composed of DOPG and mixtures of DOPG with DOPC. These lipids also show fluid phase at room temperature (25°C). We have used giant unilamellar vesicles to observe the evidence of transmembrane pores. As PC-PG mixture is used for GUV preparation for phase contrast microscopy experiments, it is always good to show the interaction of these mixture with NK-2 and some theoretical aspect to illustrate the free energy transfer. Therefore, we

have also investigated the interaction of NK-2 with negatively charged membranes in the form of large unilamellar vesicles using DLS, zeta potential. Binding free energy and effective peptide charge have been estimated using theoretical ansatz.

2. Materials and methods

2.1. Materials

Di-oleoyl Phosphatidylcholine (DOPC) and Di-oleoyl Phosphatidylglycerol (DOPG) were purchased from Avanti Polar Lipids and peptide NK-2 (KILRGVCKKIMRTFLRRISKDILTGKK-NH₂) from WITA GmbH, Berlin, Germany. They were used without further purification.

2.2. Preparation of unilamellar vesicles

2.2.1. Preparation of LUV

A required amount of phospholipid in chloroform (10 mg/mL) has been transferred to a 10 mL glass vial. The solvent was removed by gently passing nitrogen gas on the wall of the glass vial. The traces of the solvent was then removed by keeping the glass vial for couple of hours in a vacuum desiccator. This procedure leads to the formation of a thin dried lipid film on the wall of the vial. 2.5 mL of 1 mM HEPES (pH 7.4) was added to the dried lipid film and the final desired concentration was obtained. Multilamellar vesicles (MLV), prepared by vortexing of hydrated lipid film for about 30 min, were extruded successively through polycarbonate membranes having pore diameters of 400, 200 and 100 nm using LiposoFast-Pneumatic from AVESTIN (Canada). This results in a formation of LUV of diameter ~ 100 nm. The average size of the vesicles was measured by dynamic light scattering. Vesicles prepared in this method are fairly monodisperse, as indicated by the polydispersity index obtained from the width of the distribution. A range of concentration of NK-2 from 0 to 100 μM was used in experiments. Final concentration of NK-2 present in the membrane in terms of molar ratio of NK-2 to lipid is important and is discussed in the results and discussion section.

2.2.2. Preparation of GUV

GUV were formed in 100 mM Sucrose prepared in 1 mM HEPES (pH 7.4) buffer using electroformation, as described by Pott et al. [24]. In brief, 2 mM LUV suspension, prepared by extrusion method, was deposited on both the ITO glasses as few small droplets. These droplets were allowed to dry overnight in a closed chamber containing saturated solution of NaCl. This is to avoid complete drying of the droplets. The hydration of these droplets facilitates electroformation process. Electroformation chamber was made using Teflon spacer of thickness ~ 2 mm. Chamber was filled with 100 mM sucrose solution prepared in 1 mM Glucose using disposable syringe. An alternating voltage of 1–2 Volts (peak to peak amplitude) and 10 Hz frequency was applied to the chamber for a couple of hours. The average diameter of the GUV obtained was 20–100 μm . GUV were diluted in 100 mM Glucose, prepared in 1 mM HEPES (pH 7.4), for observation. GUV were also prepared from the lipid in a chloroform solution following the conventional electroformation method [25] for the preliminary experiments on Magainin 2. In this case, the chloroform solution of phospholipids instead of LUV was deposited onto the both conducting side of ITO electrodes. Solvent was allowed to evaporate and then kept the lipid deposited ITO glass in vacuum desiccator connected to a vacuum pump for couple of hour in order to remove the traces of the solvent. Now electroformation chamber was made using Teflon spacer and rest procedure is same as described above.

2.3. Experimental techniques

2.3.1. Measurement of zeta potential and size distributions using DLS

The zeta potential and average size of LUV have been determined

with a Zetasizer Nano ZS from Malvern Instruments, UK. The instrument uses 2 mW He—Ne Laser of wavelength 633 nm to illuminate the sample. In DLS experiment, back scattered light at an angle of 173° is detected. A digital signal processing correlator measures the intensity fluctuations of scattered light to obtain intensity autocorrelation function $G(\tau)$. The rate of decay of intensity auto-correlation function $G(\tau)$ was fitted to an exponential decay [$G(\tau) \sim \exp(-q^2 D\tau)$] to determine the diffusion constant D . Average hydrodynamic radius a of the LUV was estimated from the Stokes-Einstein relation $a = \frac{k_B T}{6\pi\eta D}$, k_B is the Boltzmann constant and T being the absolute temperature.

Zeta potential, ζ is measured from the electrophoretic mobility (μ) by laser Doppler velocimetry. The following Helmholtz-Smolushowski equation was used to determine ζ [26].

$$\zeta = \frac{3\mu\eta}{2\epsilon f(\kappa a)} \quad (1)$$

Where, η and ϵ are the coefficient of viscosity and the permittivity of the aqueous medium, respectively. In this study, the zeta potential is estimated from the Smoluchowski approximation, in which the Henry function $f(\kappa a)$ takes its maximum value 1.5. The mean zeta potential and size of LUV were obtained from three successive measurements. Each measurement includes 100 runs. Same cuvette is used for both zeta potential and DLS measurements. All experiments were performed at room temperature (25 °C).

We now present a theoretical description of the interaction in terms of binding free energy, binding constant and other binding parameters pertaining to the system. The minimal and maximal values of the zeta potentials were used to infer binding free energies for NK-2 using the following ansatz.

Theory: The overall binding free energy, ΔG_{app} denoted as apparent binding free energy for a given lipid composition, is given by

$$\Delta G_{app} = \Delta G_{el} + \Delta G_{int} \quad (2)$$

where, ΔG_{el} is the electrostatic and ΔG_{int} the intrinsic binding free energy. The intrinsic binding free energy presumably arises from the amphiphilic nature of the peptide and the lipids leading to binding affinity via the hydrophobic effect. The electrostatic binding free energy is given by

$$\Delta G_{el} = q_p \zeta \quad (3)$$

Where, ζ is the zeta potential and q_p be the effective peptide charge which is the charge of the bare peptide ($q_p = +10e$) minus the charge of the counterions released upon peptide binding. Therefore, we require to determine the effective peptide charge q_p . As ΔG_{el} and hence, ΔG_{app} , depend on ζ which varies with peptide concentration, c_p , both free energies also depend on c_p . As the liposomes are negatively charged and the peptide is cationic, the binding affinity will be highest in the limit of low peptide concentrations, that is, the values of ΔG_{el} and ΔG_{app} are lowest in the limit $c_p \rightarrow 0$. The value of ΔG_{app} in this limit denoted as $\Delta G_{app,0}$ obeys

$$\Delta G_{app,0} = q_p \zeta_0 + \Delta G_{int}. \quad (4)$$

This quantity is denoted as standard binding free energy. It is a measure for the affinity of NK-2 to membranes with a given lipid composition in the limit of low peptide concentrations where, intermolecular interactions between different NK-2 molecules can be neglected (dilute peptide concentrations).

The experiments show that for increasing peptide concentrations, the zeta potential increases and eventually becomes positive. If $\zeta > 0$ also the electrostatic binding free energy is positive. The maximal surface coverage by the cationic peptides, indicated by the plateau in the zeta potential at the maximal value ζ_{max} is reached when $\Delta G_{app} = 0$, hence $q_p \zeta_{max} + \Delta G_{int} = 0$, i.e.

$$\Delta G_{int} = -q_p \zeta_{max} \quad (5)$$

This implies $\Delta G_{int} < 0$ as we indeed find in the present study. The maximal surface charge, σ_{max} is inferred via the Grahame or Gouy equation,

$$\sigma_{max} = \sqrt{8\epsilon_w \epsilon_0 R T C_{ion}} \sinh\left(\frac{e\zeta_{max}}{2K_B T}\right) \quad (6)$$

where $\epsilon_w = 80$ denotes the relative dielectric permittivity (or dielectric constant) of water, ϵ_0 the relative dielectric permittivity of vacuum, $R (= 8.31 \text{ J. K}^{-1} \cdot \text{Mol}^{-1})$ is the universal gas constant, $K_B (= 1.38 \times 10^{-23} \text{ J/K})$ is the Boltzmann constant, and $T = 300 \text{ K}$ the absolute temperature. C_{ion} being the concentration of ions present in the electrolyte. Here we approximate the surface potential by zeta potential. This is a good approximation at low peptide concentration. It is assumed that's surface charges are smeared uniformly over the entire membrane surface and solvent is treated as continuous medium of fixed dielectric constant. Although use of Gouy Chapman theory underestimate the membrane association for high peptide concentration and overestimate due to adsorption of multivalent ions on the membrane, we could estimate the order of magnitude of maximal surface charge [27,28]. From σ_{max} the surface charge due to the membrane-bound peptides, σ_p is estimated from

$$\sigma_p = \sigma_{max} - \sigma_0 \quad (7)$$

Here, σ_0 is the surface charge at peptide-free conditions which is estimated from ζ_0 using Eq. (6), replacing σ_{max} by σ_0 and ζ_{max} by ζ_0 . From σ_0 , the surface charge from membrane-bound counterions, σ_l is estimated via

$$\sigma_l = \sigma_0 - \sigma_L \quad (8)$$

Here, σ_L denotes the surface charge from the lipids. For pure DOPG, σ_L is given by $\sigma_L = -\frac{e}{a_L}$ where a_L denotes the average area per lipid. The area per lipid for pure DOPC and DOPG was determined from the MD simulations [29], yielding $a_{L,PC} = 0.73 \text{ nm}^2$ for DOPC and $a_{L,PG} = 0.65 \text{ nm}^2$ for DOPG [30]. The average area per lipid for the 4:1 DOPC/DOPG mixture, $a_{L,mix}$ was determined from $a_{L,mix} = \frac{4a_{L,PC} + a_{L,PG}}{5}$. The surface charge from membrane-bound counterions is $\sigma_l = \alpha \frac{e}{a_l}$, where α denotes the fraction of lipids binding a counterion, i.e., $\alpha = \frac{\sigma_0 - \sigma_L}{\sigma_L}$. Hence, the charge of counterions released upon peptide binding, q_l , is estimated via

$$q_l = \alpha e n_L \quad (9)$$

Here, n_L is the number of lipids covered by a membrane-bound peptide as determined from.

$n_L = \frac{a_p}{a_L}$, where a_p denotes the area of the peptide. To estimate a_p , we consider that NK-2 when bound to a membrane is α -helical and that an α -helix has a thickness of $d = 0.54 \text{ nm}$ and a length of $l = 0.15 \text{ nm}$ times the number of residues, N , which is $N = 27$ here. Assuming that the helix is parallel to the membrane surface in agreement with the experimental observation by Olak et al. [18], the peptide thus covers a membrane area of $a_p = dlN = 2.2 \text{ nm}^2$. From q_l , the effective peptide charge is obtained via

$$q_p = q_p - q_l \quad (10)$$

2.3.2. Phase contrast optical microscopy

Phase contrast microscopy was performed with a DMi8 inverted microscope from Leica. Observation chamber consists of a glass slide with rubber spacers. Appropriate amount of NK-2 solution from the 50 μM stock solution in HEPES buffer was added to 200 μl of Glucose and uniformly mixed. Final NK-2 concentration was $\sim 1\text{--}2 \mu\text{M}$. 10–20 μl of GUV suspension was added to the chamber. The chamber was then closed immediately for observation under phase contrast microscope. In the present experiment, it is not possible to determine the exact NK-2 to lipid molar ratio. However, we can roughly estimate the NK-2/lipid. For example, if we introduce 10 μl of diluted GUV solution ($\sim 0.1 \text{ mM}$) to the chamber containing 100 μl of 1 μM NK-2 solution, the final NK-2/

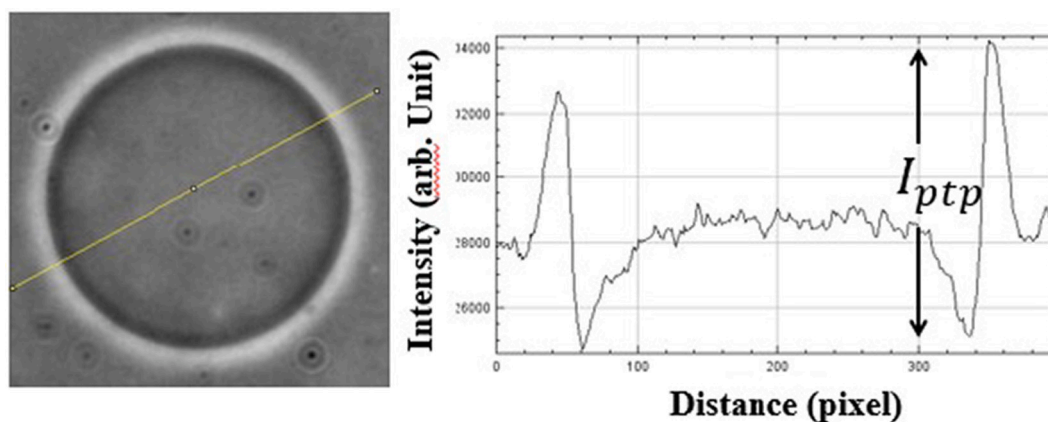


Fig. 1. Determination of the peak-to-peak intensity (gray value), I_{ptp} , across the halo region of the phase contrast micrograph of GUV. Average I_{ptp} was obtained by taking average of at least three such line profiles.

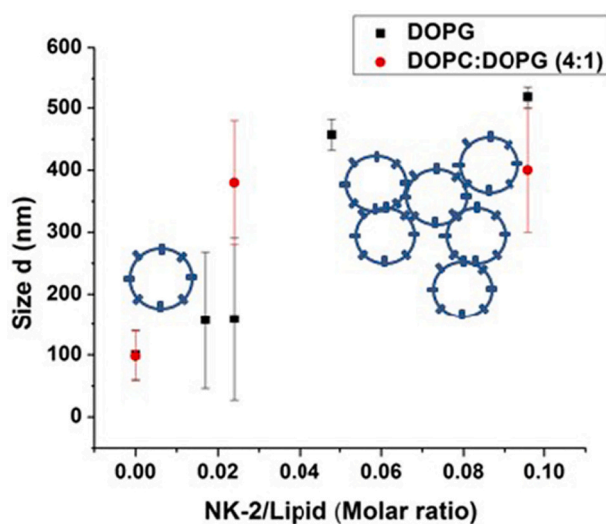


Fig. 2. Size distribution of LUV in the presence of NK-2. The increase in the size distribution is interpreted as the aggregation of vesicles induced by NK-2, as shown in schematic picture in the figure. The error bars in the Fig. 2 represent the width of the distribution which is a measure of polydispersity of LUV.

lipid (molar ratio) becomes 0.1 (Number of moles = molar concentration \times volume in litre). Response of individual GUV when exposed to the peptide solution was continuously recorded with time using a CCD camera.

Images were analyzed using image analysis software, ImageJ. A straight line was drawn across the GUV to obtain an intensity profile (Fig. 1). Peak to peak intensity (I_{ptp}) across the halo region is calculated. Average I_{ptp} is obtained from the several line profiles across the GUV, as described in our recent paper [31]. The time in second versus I_{ptp} was plotted in order to observe any significant change in the intensity profile of the GUV.

3. Results

We have used two types of model membranes, namely large unilamellar vesicles (LUV) and giant unilamellar vesicles (GUV) in order to obtain some insights into the specific interaction of the NK-2 with the membranes and pore formation activity, respectively. Direct evidence of pores induced by NK-2 has not been reported by any of the earlier literatures in this system. The formation of pores is the consequence of the strong affinity towards the anionic membranes [11,32]. Therefore, it is important to discuss how the electrostatic and thermodynamic

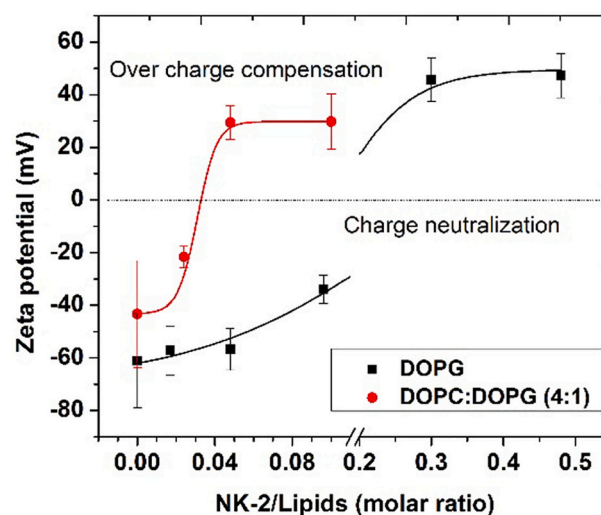


Fig. 3. Zeta potential of phospholipid LUV at various NK-2 to Lipid molar ratio. Charge neutralization occurs at lipid to NK-2 ratio for DOPG \sim 6 and for DOPC-DOPG \sim 30. Solid lines are intended only as guides to the points. Error bars indicate the width of the distribution profile of zeta potential.

properties of the membranes get modified upon adsorption of the NK-2. As NK-2 interacts with negatively charged membranes significantly [11], we have used negatively charged phospholipid DOPG and mixture of DOPC and DOPG at 4:1 for preparing both LUV and GUV. Before we present our phase contrast microscopy results to show the evidence of pores, it is important to delineate the interaction of NK-2 with membrane.

3.1. The membrane-membrane interaction induced by NK-2

Size distribution of LUV, made from DOPG and DOPC-DOPG mixture, has been measured before and after the interaction of NK-2 using dynamic light scattering (DLS). DLS technique can, in principle, provide the evidence of membrane-membrane interaction induced by NK-2. Fig. 2 shows the size distribution of LUV exposed to NK-2. The extrusion of MLV gives the average diameter of the vesicle \sim 100 nm. As the NK-2/lipid (molar ratio) is increased, the size of LUV increases gradually and eventually sample exhibits high value of average size as well as large polydispersity. This result suggests the formation of large aggregates due to membrane-membrane interaction (Fig. 2). The process of aggregation is also evident from the high degree of fluctuations near the tail of the auto correlation curve. Further, the appearance of

Table 1

Minimal and maximal zeta potentials observed experimentally, ζ_0 and ζ_{max} , and quantities hence inferred. σ_0 : the surface charge at peptide-free conditions; σ_{max} : the maximum surface charge density; q_p : the effective peptide charge; ΔG_{int} : the intrinsic binding free energy; $\Delta G_{app, 0}$: the total standard binding free energy.

Lipids	Zeta potential (mV)		Surface charge (C/m ²)		Effective peptide Charge q_p (e)	Binding free energies KJ/mol	
	ζ_0	ζ_{max}	σ_0	σ_{max}		ΔG_{int}	$\Delta G_{app, 0}$
DOPG	-61 ± 18	47 ± 8	-5.5 × 10 ⁻³	3.8 × 10 ⁻³	6.69	-36	-75
DOPC/DOPG (4:1)	-43 ± 20	30 ± 11	-3.5 × 10 ⁻³	2.3 × 10 ⁻³	7	-20	-59

turbid vesicle solution at a larger NK-2/lipid supports the evidence of aggregates induced by NK-2. The increase in size distributions of LUV due to binding of NK-2 is a consequence of stronger affinity of NK-2 towards negatively charged membranes. As found in our earlier study that NK-2 does not exhibit significant interaction with the PC membranes [11]. It is indeed desirable for an AMP not to interact with the PC membranes, as it is the major component of eukaryotic cells.

3.2. Binding affinity of NK-2 with negatively charged membrane as determined from zeta potential

The ζ was obtained from LUV dispersion prepared from DOPG and DOPC-DOPG (4:1) mixture before and after introducing peptide. As illustrated in Fig. 3, ζ increases with increasing NK-2 to lipid molar ratio (NK-2/L). This is an expected result, as found for any other cationic peptide interacting with negatively charged membrane [33]. The charge neutralization occurs at L/NK-2-6 and 30 for DOPG and DOPC-DOPG mixture, respectively. Therefore, charge neutralization ratio of DOPC to DOPG membrane is 4:1. As DOPC is present in the mixture at 4:1, it is expected that charge neutralization should also happen at the similar ratio as DOPC possesses no charge. In other word, this difference is due to the fact that charge neutralization occurs with the amount of charge present in the membrane, i.e., with respect to charge lipids. Interestingly, the value of ζ continues to increase even after charge neutralization, which is known as over charge compensation. Therefore, the ζ

was found to exhibit its saturation value, indicating overcharge compensation, at different NK-2/L for PG and mixture of PC-PG vesicles. The overcharge compensation at different zeta values suggests the significant contribution of entropy besides electrostatic interaction as discussed in our previous paper [11]. It is important to mention that hydrophobic interaction is entropic in origin arising mainly due to conformational and orientational change of peptide and release of water molecule upon adsorption of peptide. The effect of hydrophobic interaction was also revealed from the endothermic heat contribution to the isothermal titration calorimetry traces [11].

We have estimated binding free energies and other binding parameters from the minimal and maximal values of the zeta potential discussed in the theory (Section 2.3.1). The results of our analyses for the two different lipid compositions are listed in Table 1. The relative standard binding free energy for DOPG is $\Delta\Delta G_{DOPG} = -35 (\pm) 13$ kJ/mol.

It was suggested by previous studies of various AMP that antimicrobial activity is accompanied by the formation of trans-membrane pores in the phospholipid vesicles [15,17]. Experiments of LUV, discussed above, do not reveal pore formation activity directly. Therefore, it is desirable to look at GUV, exposed to NK-2 in-order to obtain complementary information of the system studied here. We have avoided in incorporating any fluorescence dye into the membrane, as the interaction of AMP with membranes might be affected by fluorescence dye.

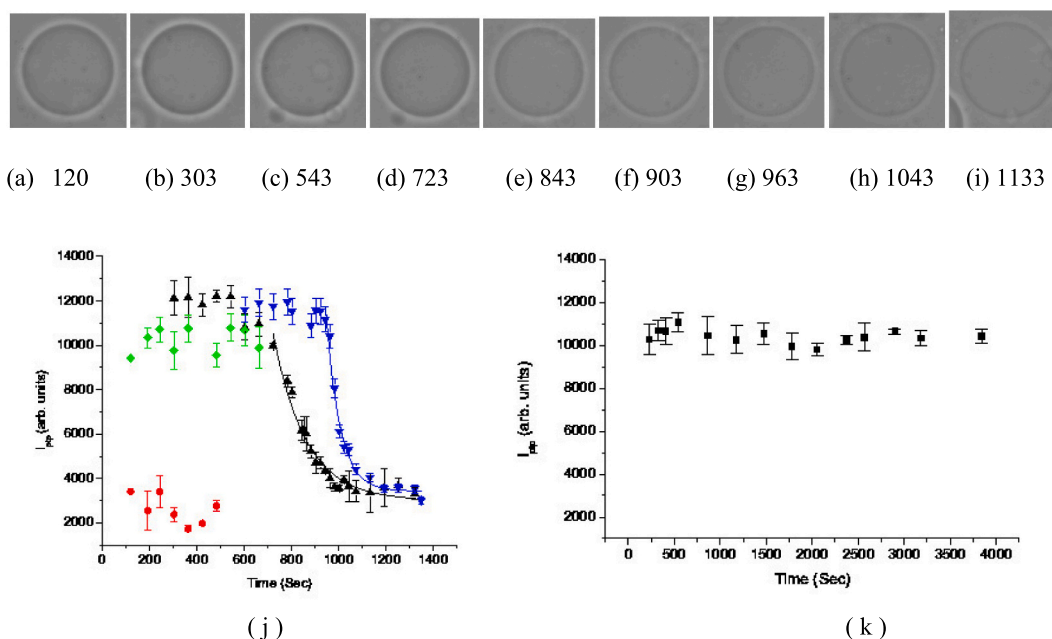


Fig. 4. (a–i) Microscopy images of GUV (diameter = 48 μm), made from DOPC-DOPG (4:1) mixture, exposed to 0.45 μM NK-2. Numbers, below the images, indicate time sequence in second at which images are captured. This is a direct visualization of membrane leakage induced by NK-2 due to pore formation without perturbing membrane with any fluorescence dye. (j) Kinetic of pore formation obtained at $C_{nk2} = 0.45 \mu\text{M}$ (Δ) and $C_{nk2} = 1.3 \mu\text{M}$ (∇). Diameters of GUV in these two C_{nk2} are 24 μm and 48 μm , respectively. For comparison kinetics of DOPC GUV (diameter 22 μm), exposed to NK-2 at $C_{nk2} = 0.45 \mu\text{M}$, is shown in (k). Rate constant k , obtained from the fit to exponential decay function (Indicated by solid lines) were 0.007 and 0.03 Sec^{-1} for $C_{nk2} = 0.45$ and 1.3 μM , respectively. I_{pp} , indicated by circles (\bullet) are obtained from GUV, having no density contrast between interior and exterior of it. I_{pp} indicated by diamond (\diamond) show GUV without exposed to NK-2, but having contrast between interior and exterior of it. Error bars are standard deviations of three independent measurements of I_{pp} in a single GUV.

3.3. Observation of trans-membrane pores (microscopy results)

Phase contrast microscopy on GUV has been performed in order to visualize directly the antimicrobial activity of NK-2 and also to obtain complementary information on the results obtained from DLS and zeta potential measurements. Previous studies of some other AMP have reported the evidence of transmembrane pores using fluorescence leakage [34] and micro-pipette aspiration [15]. We have avoided incorporating any fluorescence dye into the membrane, as the interaction of AMP with membranes might be affected by fluorescence dye. GUV, made from DOPC and mixtures of DOPC with DOPG at 4:1, were observed with three different C_{nk2} (1.3, 0.9, 0.45 μM). Pure DOPG did not seem to form GUV. The tendency to adhere the negatively charged lipid into the positive electrode might prevent the swelling of lipid film, which may not facilitate the formation of GUV [35]. Therefore, we have not used pure DOPG for GUV formation. The halo region of phase contrast images appears due to mismatch of refractive indices between interior (Glucose) and exterior (Sucrose) of the GUV. Therefore, there will be contrast in the intensity gray value across the halo region. If NK-2 forms pores in the membranes, we would expect leakage of internal fluid through the pores. Therefore, halo regions are expected to disappear (contrast loss) with time and GUV should look similar to that without diluting in glucose. Experiments on GUV, exposed to NK-2, show direct evidence of formation of trans-membrane pores. Fig. 1 shows the calculation of peak to peak intensity (I_{pp}) in the halo region of the phase contrast micrograph of GUV. Change in the difference of the gray value (I_{pp}) of the halo region with time for DOPC-DOPG (4:1) GUV, as shown in Fig. 4 (a–i), indicate leakage of internal fluid, leading to the loss of contrast. I_{pp} decreases until GUV completely loses its contrast in the halo region. We have compared I_{pp} between GUV, exposed to NK-2 and GUV without NK-2, but the interior and exterior regions contain the same glucose solution. (Fig. 4j). This behavior is attributed to the fact that pores are large enough to permeate the sucrose and glucose molecules and fluids between the interior and exterior of the GUV, leading to loss of contrast in the halo region. Pores are not found to be transient, as contrast loss across the halo region of GUV remain stable with time. If it would have been transient pores, one would not expect such contrast loss due to exchange of fluids as time scale of pore fluctuations is much faster than rate of exchange or diffusion of large size molecules, like glucose or sucrose. Since we have looked at an average response of many GUV, exposed to NK-2, it was not possible to determine the exact ratio of NK-2/L. However, rough estimation yields NK-2/L = 0.05 to 0.1 where, zeta potential already show saturation. Previous isothermal calorimetric study also exhibit saturation of heat signal at these NK-2/L [11]. Different GUV seems to take different time to initiate pore formation. Therefore, we cannot precisely determine the time point to initiate pore formation for individual vesicle at different C_{nk2} , as the average response of many GUV was obtained in our study. However, we can unambiguously determine the behavior of the rate constant (k) for different C_{nk2} . Decaying part in Fig. 4j (j) was fitted to exponential decay in order to estimate k . For 0.45 μM of NK-2, k was found to be 0.007 s^{-1} . For $C_{nk2} = 0.9$ and 1.3 μM , k were obtained as 0.01 and 0.03 Sec^{-1} respectively. Therefore, I_{pp} (Fig. 4) decreases much faster at higher C_{nk2} than that of lower C_{nk2} . We did not seem to observe any significant change in size of GUV with time. GUV does not show any significant change in I_{pp} with time in the absence of NK-2 (as shown by a diamond symbol in Fig. 4 j). GUVs, made from DOPC do not show significant decrease in I_{pp} in the presence of NK-2, indicating NK-2 does not form pores on these membranes. This behavior is supported by the fact that NK-2 has very weak binding affinity to PC, which is consistent with the results obtained from zeta potential [11].

It is clear from our observation (Fig. 4) that NK-2 modifies the permeability of the membranes, which is in agreement with previous studies of similar system [16,34,36]. Leakage of internal fluid, leading to decrease in I_{pp} suggests the formation of transmembrane pores in DOPC-DOPG GUV (Fig. 4 a–i and j). No significant change in I_{pp} as shown in

Fig. 4j (k) for DOPC, suggests that NK-2 has no significant influence on PC vesicles, in contrast with other AMP, such as melittin [16] and Maculatin [34].

4. Discussion

The results of zeta potential along with DLS clearly reveal that interaction of NK-2 with membranes is primarily driven by electrostatic interaction. Therefore, NK-2 has a stronger affinity towards the negatively charged lipids. This is indeed an essential requirement for an AMP to exhibit antimicrobial activity. It is interesting to mention that no significant effect was found in the gel phase of DPPC as reported by Willumeit et al. [12]. Further, NK-2 has no considerable influence even on fluid phase of POPC as revealed by x-ray scattering and Fourier transform infra-red spectroscopy. We indeed have found in our previous study that NK-2 has no significant effect on neutral lipid DOPC [11]. NK-2 with membrane is primarily governed by electrostatic attraction, it is expected that NK-2 would have very little effect of no influence on the neutral membrane. Therefore, it is inappropriate to compare earlier results on neutral membrane with our zeta potential of the anionic membranes. Our analysis of experimental results are in agreement with the simulation study by Knetch et al., where they showed the stronger affinity of negatively charged vesicles and also estimated the binding free energies of transfer of NK-2 on the membrane [22]. The decrease in maximal surface charge membrane and concomitant decrease the free energy in DOPC-DOPG membrane suggests that presence of PC interaction becomes much weaker. Further previous study already established that NK-2 does not exhibit significant interaction with the DOPC membranes. This study implicates that NK-2 primarily interacts with the negatively charged membranes which is indeed the pre-requisite for antimicrobial activity. Therefore, the difference in composition of the membrane helps NK-2 to discriminate the bacterial membrane from the eukaryotic cells.

Besides electrostatic contribution, hydrophobic interaction as well as the increase in membrane tension due to adsorption of NK-2 on the membrane play a significant role in antimicrobial activity. Although we have not explored effect of hydrophobicity and membrane tension in this study, we could as well hypothesize that the role of these parameters in the context of antimicrobial activity of NK-2 would also be similar as in the case of other alpha helical cationic peptides [17,37,38]. Further, we have reported earlier the significant entropic contribution of the NK-2 membrane interaction, suggesting the hydrophobic interaction between the hydrophobic part of NK-2 and hydrophobic core of the membranes [11].

Phase contrast microscopy experiments on GUV show evidence of transmembrane pores in anionic membranes. The time scale involved to initiate the pore formation process for various C_{nk2} was difficult to conclude in the present study, as I_{pp} was found to decrease at different time for various GUV at a given C_{nk2} . The difference in amount of PG in each GUV could result such behavior, as NK-2 mainly interacts with PG. A slight variation of C_{nk2} in different parts of the sample, pore size, size of GUV are also key factors in determining the time scale involved in the process of pore formation. Dependence of k with the C_{nk2} was derived at three different C_{nk2} . Larger k at higher C_{nk2} (Fig. 4 (j)) can be a result of larger pore size or larger number of pores than that of lower C_{nk2} . Structure and charge of AMP might have an important role in determining the time scale involved in the process of pore formation.

Recent experiments on non-labelled antimicrobial peptide PGLa suggest the translocation of peptide without pore formation [39]. However, previous literatures also suggest that PGLa forms transmembranes pores [40,41]. Further, a computer simulations at all-atomistic level reported that individual peptide spontaneously translocate across the membrane without forming pores [42]. Such translocation begins with tilting of individual peptide and finally deep insertion in the membrane core occurs due to interaction three peptide in mutual contact. This process facilitates the opening of transient water

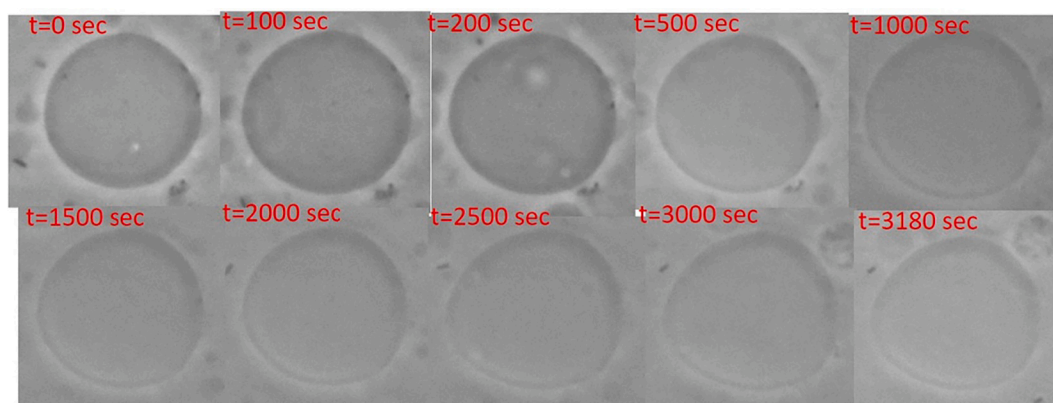


Fig. 5. Phase contrast images of GUVs composed of DOPC–DOPG (4:1), exposed to 4.16 μM Magainin. Starting time of capturing images is not the time of initiation of pore formation. The diameter of the vesicle is $\sim 35 \mu\text{m}$.

channel through which peptide enters into the lumen of GUV. In the present study we could rule out this possibility as the contrast loss of GUV remains stable. Further, aggregation of vesicles due to membrane–membrane interaction in the presence of peptide, as evidenced from DLS study supports the fact that the leakage induced by NK-2 is indeed a collective phenomenon. Therefore, it is unlikely that NK-2 will translocate without pore formation. In order to validate and complement our conclusion on pore formation, we have also looked at GUV in the presence pore forming peptide magainin 2. In preliminary experiment we have found similar exchange of fluid between interior and exterior of GUV (Fig. 5). As it is well established that magainin 2 forms trans-membrane pores [16,17]. As we have observed similar contrast loss, as in the case NK-2, we expect that contrast loss is due to pore formation and not due to any other process, reported in some simulation study [42].

It is clearly evidenced from the zeta potential results that the stronger electrostatic interaction along with some entropic contribution to the binding of NK-2 to the membrane. It is important to mention that the zeta potential measurements are blind to provide the information on the translocation of NK-2 from outer leaflet to the inner leaflet of the bilayer, leading to change in binding isotherm. Further, vesicles, as impermeable charged sphere, assumed in the zeta potential analysis was also not able to capture the translocation feature of the NK-2. However, we proposed a mechanism of action that NK-2 may translocate through trans-membrane pores as evidenced from the change in the binding isotherm obtained from isothermal titration calorimetry [11]. Previous study have shown that transfer of NK-2 into the membrane results in an increase in area per molecule and hence increases membrane tension [15,16]. Although simulation study did not predict the tension induced pores, the micropipette experiments on another AMP, such as, melittin showed increase in membrane tension upon melittin adsorption on the membrane [15]. We believe that NK-2 also increases the membrane tension, as the structure is very similar to the melittin.

5. Conclusion

We have explored pore formation activity of the anionic phospholipid membrane induced by an antimicrobial peptide NK-2. The charge driven interaction, as envisaged by zeta potential of the membrane, has been analyzed in details. The binding free energy, effective surface charge due to release of counter ion have been estimated from the minimal and maximal zeta potential. Phase contrast optical microscopy experiment on GUV reveals the formation of trans-membrane pores. Further, DLS study shows high value of hydrodynamic diameter, suggesting the aggregates of the LUV. The turbid solution appearing at higher NK-2 to lipid ratio confirms the disruption of the LUV. Therefore, DLS results along with the evidence of pores on these membranes in the

present study implies antimicrobial activity of NK-2. We compare pore formation in negatively charged membrane with neutral membrane. This study suggests that interactions of NK-2 with lipids are mainly governed by negatively charged lipids which are major constituents of the bacterial membranes. As neutral lipid, such as phosphatidylcholine (PC) is a major constituent of eukaryotic cell membranes, it is indeed an important and necessary prerequisite that NK-2 should not interact with PC significantly in order to reinforce the development of peptide antibiotics. It is important to mention that pore formation in the membrane are not always associated with the cell death. However, cell death by antimicrobial peptides are known and well establish fact that peptide induced pores before disintegrate of cellular content.

Declaration of Competing Interest

None.

Acknowledgements

This work was funded by Department of Biotechnology (DBT), Govt. of India (BT/PR8475/BRB/10/1248/2013). AH thank to UGC for providing research fellowship. We thank Dr. Rumiana Dimova and Dr. Volker Knecht, Max Planck Institute of Colloids and Interfaces, Potsdam, Germany for their keen interest in this study and for academic discussions.

References

- [1] M. Zasloff, Antimicrobial peptides of multicellular organisms. 2002, *Nature* 415 (2002) 389–395.
- [2] J. Wiesner, A. Vilcinskas, Antimicrobial peptides: the ancient arm of the human immune system, *Virulence* 1 (5) (2010) 440–464.
- [3] M. Hirano, C. Saito, H. Yokoo, C. Goto, R. Kawano, T. Misawa, Y. Demizu, Development of antimicrobial stapled peptides based on magainin 2 sequence., 2021, *Molecules* 26 (2021) 444.
- [4] K.A. Brogden, Antimicrobial peptides: pore formers or metabolic inhibitors in bacteria, *Nature* 3 (2005) 238–250.
- [5] J. Cho, I. Hwang, H. Choi, J.H. Hwang, J.S. Hwang, D.G. Lee, The novel biological action of antimicrobial peptides via apoptosis induction, *J. Microbiol. Biotechnol.* 22 (2012) 1457–1466.
- [6] H.M. Chen, K.W. Leung, N. Thakur, A. Tan, R.W. Jack, Distinguishing between different pathways of bilayer disruption by the related antimicrobial peptides cecropin B, B1 and B3, *Eur. J. Biochem.* 270 (2003) 911–920.
- [7] K. He, S.J. Ludtke, D.L. Worcester, H.W. Huang, Neutron scattering in the plane of membranes: structure of alamethicin pores, *Biophys. J.* (1996) 2659–2666.
- [8] B. Bechinger, The structure dynamics and orientation of antimicrobial peptides in membranes by multidimensional solid-state NMR spectroscopy, *Biochim. Biophys. Acta* 1462 (1999) 157–183.
- [9] H. Schröder-Born, R. Bakalova, J. Andr , The NK-lysin derived peptide NK-2 preferentially kills cancer cells with increased surface levels of negatively charged phosphatidylserine, *FEBS Lett.* 579 (2005), 6128–6124.

- [10] E.G. Kholina, I.B. Kovalenko, M.E. Bozdaganyan, M.G. Strakhovskaya, P. S. Orekhov, Cationic antiseptics facilitate pore formation in model bacterial membranes, *J. Phys. Chem. B* 124 (2020) 8593–8600.
- [11] S. Karmakar, P. Maity, A. Halder, Charge-driven interaction of antimicrobial peptide NK-2 with phospholipid membranes, *ACS Omega* 2 (2017) 8859–8867.
- [12] R. Willumeit, M. Kumpugdee, S.S. Funari, K. Lohner, B.P. Navas, K. Brandenburg, S. Linsler, J. Andr a, Structural rearrangement of model membranes by the peptide antibiotic NK-2, *Biochim. Biophys. Acta* 1669 (2005) 125–134.
- [13] T. Jacob, H. Bruhn, I. Gaworski, B. Fleischer, M. Leippe, NK-Lysin and its shortened analog NK-2 exhibit potential activities against *Trypanosoma cruzi* *Antimicrob. Agents. Chemother.* 47 (2003) 607–613.
- [14] S.M. Gregory, A. Pokorny, P.F.F. Almeida, Magainin 2 revisited: a test of the quantitative model for the all-or-none permeabilization of phospholipid Vesicles, *Biophys. J.* 96 (2009) 116–131.
- [15] M.-T. Lee, W.-C. Hung, F.-Yu. Chen, H.W. Huang, Mechanism and kinetics of pore formation in membranes by water-soluble amphipathic peptides. 2008, *Proc. Natl. Acad. Sci. U. S. A.* 105 (2008) 5087–5092.
- [16] M.-T. Lee, F.-Yu Chen, H.W. Huang, Energetics of pore formation induced by membrane active peptides, *Biochemistry* 43 (2004) 3590–3599.
- [17] M.A.S. Karal, J.M. Alam, T. Takahashi, V. Levadny, M. Yamazaki, Stretch-activated pore of the antimicrobial peptide, Magainin 2. *Langmuir* 31 (2015) 3391–3401.
- [18] C. Olak, A. Muentner, J. Andra, G. Brezesinski, Interfacial properties and structural analysis of the antimicrobial peptide NK-2, *J. Pept. Sci.* 14 (2008) 510–517.
- [19] M. Krugliak, R. Feder, V.Y. Zolotarev, L. Gaidukov, A. Dagan, H. Ginsburg, A. Mor, Antimalarial activities of dermaseptin S4 derivatives, *Antimicrob. Agents Chemother.* 44 (2000) 2442–2451.
- [20] M.U. Hammer, A. Brauser, C. Olak, G. Brezesinski, T. Goldmann, T. Gutschmann, J. Andr a, Lipopolysaccharide interaction is decisive for the activity of the antimicrobial peptide NK-2 against *Escherichia coli* and *Proteus mirabilis*. 2010, *Biochem. J.* 427 (3) (2010) 477–488.
- [21] J. Andra, M. Leippe, M., Candidacidal activity of shortened synthetic analogs of amoebapores and NK-lysin, *Med. Microbiol. Immunol.* 188 (1999) 117–124.
- [22] C.I.E. von Deuster, Knecht, V competing interactions for antimicrobial selectivity based on charge complementarity, *Biochim. Biophys. Acta* 1808 (2011) 2867–2876.
- [23] I.E. Carola, C.I.E. von Deuster, V. Knecht, Antimicrobial selectivity based on zwitterionic lipids and underlying balance of interaction, *Biochim. Biophys. Acta* 1818 (2012) 2192–2201.
- [24] T. Pott, H. Baurrais, P. M el eard, Giant unilamellar vesicles formation under physiologically relevant conditions, *Chem. Phys. Lipids* 154 (2008) 115–119.
- [25] R. Dimova, S. Aranda, N. Bezlyepkina, V. Nikolov, K.A. Riske, R. Lipowsky, A practical guide to giant vesicles. Probing the membrane nanoregime via optical microscopy, *J. Phys. Condens. Matter* 18 (2006) S1151–S1176.
- [26] R. Hunter, *Zeta Potential in Colloids Science*, Academic Press, New York, 1981.
- [27] D. Murray, A. Arbusova, G. Hangy as-Mih alyn e, A. Gambhir, N. Ben-Tal, B. Honig, Electrostatic properties of membranes containing acidic lipids and adsorbed basic peptides: theory and experiment, *Biophys. J.* 77 (1999) 3176–3188.
- [28] S. Stefan, Surface charging by large multivalent molecules extending the standard Gouy-chapman treatment, *Biophys. J.* 60 (1991) 341–351.
- [29] B. Klasczyk, V. Knecht, Specific binding of chloride ions to lipid vesicles and implications at molecular scale, *Biophys. J.* 4 (2013) 818–824.
- [30] R.D. Hills Jr., N. McGlinchey, Model parameters for simulation of physiological lipids, *J. Comput. Chem.* 37 (2016) 1112–1118.
- [31] A. Halder, A. Sannigrahi, N. De, K. Chattopadhyay, Kinetoplastid membrane protein-11 induces pores in anionic phospholipid membranes: effect of cholesterol, *Langmuir* 36 (2020) 3522–5330.
- [32] S. Karmakar, P. Maity, A. Halder, Antimicrobial peptide as an emerging therapeutic agent: a study with phospholipid membranes, *Mater. Today: Proc.* 18 (2019) 879–886.
- [33] L.R. Bogdanova, Y.A. Valiullina, D.A. Faizullin, R.Kh. Kurbanov, E.A. Ermakova, Spectroscopic, zeta potential and molecular dynamics studies of the interaction of antimicrobial peptides with model bacterial membrane. 2020, *Spectrochim. Acta A Mol. Biomol. Spectrosc.* 242 (2020) 118785.
- [34] E.E. Ambroggio, F. Separovic, J.H. Bowie, G.D. Fidelio, L.A. Bagatolli, Direct visualization of membrane leakage induced by the antibiotic peptides: Maculatin, Citropin, and Aurein, *Biophys. J.* 89 (2005) 1674–1881.
- [35] J. Steink uhler, J. Agudo-Canalejo, R. Lipowsky, R. Dimova, Modulating vesicle adhesion by electric fields, *Biophys. J.* 111 (2016) 1454–1464.
- [36] Y. Tamba, M. Yamazaki, Magainin 2 induced pore formation in the lipid membranes depends on its concentration in the membrane interface, *J. Phys. Chem. B* 113 (2009) 4846–4852.
- [37] H.W. Huang, F.-Yu. Chen, M.-T. Lee, Molecular Mechanism of peptide-induced pores in Membranes. 2004, *Phys. Rev. Lett.* 92 (2004) 198304–198307.
- [38] Y. Chen, M.T. Guarnieri, A.I. Vasil, M.L. Vasil, C.T. Mant, R.S. Hodges, Role of peptide hydrophobicity in the mechanism of action of -helical antimicrobial peptides, *Antimicrob. Agents Chemother.* 51 (2007) 1398–1406.
- [39] M.H. Ali, M. LataShuma, H. Dohra, M. Yamazaki, Translocation of the nonlabeled antimicrobial peptide PGLa across lipid bilayers and its entry into vesicle lumens without pore formation, *Biochim. Biophys. Acta* 1863 (2021), 183680.
- [40] T. Wierprecht, O. Apostolov, M. Beyermann, J. Seelig, Membrane binding and pore formation of the antibacterial peptide PGLa: thermodynamic and mechanistic aspects, *Biochemistry* 39 (2000) 442–452.
- [41] F. Parvez, J.M. Alam, H. Dohra, M. Yamazaki, Elementary processes of antimicrobial peptide PGLa-induced pore formation in lipid bilayers, *Biochim. Biophys. Acta* 1860 (11) (2018) 2262–2271.
- [42] J.P. Ulmschneider, Charged antimicrobial peptides can translocate across membranes without forming channel-like pores, *Biophys. J.* 113 (2021) 73–81.

Animesh Halder
02/06/2022